Waterproofing Details of Connections for Adjacent Precast Concrete Box-beam Bridges

Prepared by:

Anil Patnaik, PhD (Principal Investigator)

Mohamed Habouh, PhD (Former Graduate Student)

Prepared for:
The Ohio Department of Transportation
Office of Statewide Planning & Research

and
Ohio's Research Initiative for Locals

State Job Number 134847 and 2015 ORIL2

October 2018

Final Report

OHIO'S RESEARCH ORIL INITIATIVE *for* LOCALS

U.S. Department of Transportation
Federal Highway Administration

This page is intentionally left blank.

Technical Report Documentation Page

1. Report No.	2. Government Accession No.	3. Recipient's Catalog No.
FHWA/OH-2018/18		

4. Title and Subtitle	5. Report Date
Waterproofing Details of Connections for Adjacent Precast Concrete Box-Beam Bridges	**October 2018**
	6. Performing Organization Code
	The University of Akron

7. Author(s)	8. Performing Organization Report No.
Anil Patnaik (PI)	

9. Performing Organization Name and Address	10. Work Unit No. (TRAIS)
The University of Akron, 402 Butchel Common Akron, OH 44325-2102	
	11. Contract or Grant No.
	SJN 134847 and 2015 ORIL2

12. Sponsoring Agency Name and Address	13. Type of Report and Period Covered
Ohio Department of Transportation 1980 West Broad Street Columbus, Ohio 43223	**Final Report 01/06/2014 to 11/01/2018**
	14. Sponsoring Agency Code

15. Supplementary Notes

16. Abstract

Development of cracks at the longitudinal joints of non-composite box-beam bridges is often a recurring problem that causes water leakage at the joints and corrosion of the embedded prestressing strands. Satisfactory performance of such bridges depends on the effectiveness of the key way, waterproofing membrane, and tie rods, as well as the related construction processes. The primary objective of this study was to identify the sources, causes, and effects of inadequate waterproofing at the joints and to develop prevention measures. The performance of waterproofing membranes and the structural performance of key way joints with the existing and new grout materials were evaluated and correlated with field measurements under traffic loading. Observations of construction practices at a box-beam bridge were also made, and an investigation of a bridge that was in service for 32 years at the time of its demolition was conducted. This study revealed that membrane failure is not the primary cause of water leakage. From the limited site inspections performed in this project, the practices followed at construction sites seem to be flawed and may be largely contributing to water leakage problems in box-beam bridges. In addition, key way joints that use currently specified ODOT geometry and ODOT-approved grouts are incapable of carrying any shear loads in conjunction with out-of-plane moments. Shear transfer strength of key way joints under symmetric loading can be increased through proper selection of grout material, changes to the key way geometry, and proper joint surface preparation. In beam configurations, this strength can increase by a factor of up to 3.5 prior to the occurrence of the first crack. With suitable modifications, it is possible to increase the shear strength of these joints under eccentric loading as well. The new key way geometries and grouts developed and validated in this project, along with modified construction specifications, were successfully implemented in a 55-ft. long new bridge constructed in Shelby, Ohio.

17. Keywords	18. Distribution Statement
Non-composite box-beam bridges, waterproofing membranes for bridges, key way grouts, key way joints in box-beam bridges, shear strength of joints, construction practices.	No restrictions. This document is available to the public through the National Technical Information Service, Springfield, Virginia 22161

19. Security Classification (of this report)	20. Security Classification (of this page)	21. No. of Pages	22. Price
Unclassified	**Unclassified**	**303**	

Form DOT F 1700.7 (8-72) **Reproduction of completed pages authorized**

Waterproofing Details of Connections for Adjacent Precast Concrete Box-Beam Bridges

Prepared by:

Anil Patnaik, PhD

Principal Investigator
Professor, Department of Civil Engineering
The University of Akron, Akron, OH 44325-3905

Phone: 330-972-5226 Email: Patnaik@uakron.edu

Mohamed Habouh, PhD
Former Graduate Student, Department of Civil Engineering
The University of Akron, Akron, OH 44325-3905

October 2018

Prepared in cooperation with the Ohio Department of Transportation,
Ohio's Research Initiative for Locals, and the U.S. Department of Transportation, Federal Highway Administration

ACKNOWLEDGMENTS

Ohio Department of Transportation (ODOT) and Ohio's Research Initiative for Locals (ORIL) provided funding for this project, and the PI is very grateful for this support. The extensive input and timely feedback provided by Dr. Waseem Khalifa and Mr. Jim Welter, the ODOT Subject Matter Experts for this project, and the ORIL TAC (Mr. Steve Luebbe, Mr. Warren Schlatter, and Dr. Eric Steinberg) are gratefully acknowledged. The discussions the research team had on several occasions with Mr. Perry Ricciardi, District Engineer of Tests in ODOT District 3 were critical, and the three bridges he provided helped the research team understand the practical limitations of the problem. The implementation project was also arranged by Mr. Ricciardi. Ms. Vicky Fout has been very helpful in organizing meetings and coordinating the efforts related to the management of the project. Mohamed Habouh was the graduate student who took lead role in conducting the research described in this report. Ali Almonbhi was responsible for the waterproofing membrane evaluation. Several other graduate students at the University of Akron—including Srikanth Marchetty, Abdisa Musa, Mohammed Hafeez, Dheeraj Kondisetti and others—provided assistance in the completion of the experimental work in this project, as and when needed. Dave McVaney, Bill Wenzel and Brett Bell, who are laboratory technicians of the College of Engineering at University of Akron, also provided assistance in completing the experimental work. Sheila Pearson assisted in proofreading and editing the draft reports related to this project.

TABLE OF CONTENTS

LIST OF FIGURES

LIST OF TABLES

EXECUTIVE SUMMARY

Problem Statement

Precast concrete non-composite adjacent box-beam bridges are a common type of bridge deployed by ODOT for short and medium spans (30 to 100 ft.). Box-beams of 36" or 48" width are tied together to form the superstructure of such bridges. Adjacent box-beams need to work together as a single unit for a bridge to function effectively in carrying the applied loads. Structural performance of box-beam bridges is greatly dependent on the shear key, the connection details including the grout, and the waterproofing system attached to the top surface of the box-beams.

Adjacent box-beams are connected using partial or full depth grouted key ways along the sides of the box-beams. Extensive cracking of grout is often a recurring problem leading to failure of the shear key, reflective cracking in the wearing course, and eventually leakage. Severe leakage has often been reported even in some new bridges immediately after construction. Water leakage leads to premature aging and is the primary cause for the corrosion of embedded prestressing strands and non-prestressed steel. Corrosion causes spalling and snapping of strands. Effective functioning of shear key joints becomes critical to the long-term performance of box-beam bridges. Careful and systematic investigation of the problem with particular emphasis on waterproofing materials and the connection details is needed for existing and new box-beam bridges in order to develop potential remedial measures.

The primary goal of this study was to develop an insight into the performance of longitudinal joints with a particular reference to cracking and differential deflection that is believed to cause the waterproofing membrane to fail.

Research Approach and Methods

A systematic study was conducted in this project in order to address the problem and to develop potential solutions. The performance of several waterproofing membranes, some ODOT-approved and others not yet approved, was evaluated in terms of the membrane elongation under in-plane extension and under shear loading. The vertical and horizontal differential deflections due the loading from a fully loaded truck were measured on bridge ASD-42-12.49. The test truck weighed a total of 67.4 kips (including its self weight) and was driven at speeds of 50 or 70 mph on the bridge with predefined travel paths that would maximize the bridge response. A condition assessment was also done on the sheets of membrane extracted from another bridge that was in service for 32 years and was demolished for deck replacement. The extracted membrane was in a very poor condition and did not possess any mechanical strength or stiffness. Some of the deck areas for the bridge did not have membrane, even though the bridge was designed to be provided with a membrane. The common practices employed at a new bridge construction site were observed over the entire duration of its construction. The grout placed in the key way recess was diluted with water to achieve flowability for placement in the key way recess. The construction practices used for bridge construction will need refinement in order to improve the membrane and key way performance.

Structural performance of key way joints was evaluated using several of the commonly used and newly developed grout materials. Shear test specimens were loaded under symmetric loading for this series of tests. New types of high strength concrete grouts were developed to replace the currently used mortar-based grouts. Several large beam assembly tests were also conducted with symmetric and eccentric loading. A substantial increase in shear transfer strength was demonstrated when a revised key way geometry was used in conjunction with high strength concrete grout.

A series of finite element analyses were performed to determine the state of stresses under different loading conditions at the longitudinal joints of typical box-beam bridges. These analyses revealed that deeper key way joints lead to substantial decrease in tensile and shear stresses on the grouted joints, proving that cracking at the longitudinal joints will be reduced by using deeper key ways.

Based on the findings of the study, several recommendations were developed to improve the performance of new box-beam bridges. The implementation was found to be feasible when the changes were limited to the key way geometry and the use of high strength concrete grout that was developed in this study. A set of revised construction specifications were also developed for future use. These recommendations were implemented in a bridge (RIC-CR184-2.17) that was constructed in Shelby, Ohio during the first week of April 2018. No cracks were detected at the time of its initial inspection on May 19, 2018 soon after the bridge was opened to traffic. Subsequent inspections in October 2018 before the final report was submitted also revealed no visible cracks.

The complete details of the research approach and methods are given in the later sections and the appendices of this report.

Research Findings and Summary

The membrane tests revealed that the membranes used on bridge decks are able to accommodate elongations and differential deflections between adjacent box-beams as large as one inch without losing their watertightness properties. With suitable changes to the key way geometry and the use of high strength concrete grout, the cracking potential of the key way joints is expected to be diminished. Substantial reduction in water leakage at the longitudinal joints of adjacent box beams is therefore possible by implementing the recommendations developed in this study. The currently used construction practices were found to be unacceptable from a waterproofing standpoint. Lack of close inspections and noncompliance of ODOT specifications could be the some of the reasons for the poor performance of the longitudinal joints of box-beam bridges. The required watertightness of such bridges can be achieved, as intended, with the use of the revised key way geometry and high strength concrete grout along with strict quality control, careful inspections, and enforcement of the specifications.

Recommendation

It is recommended that the suggested modifications to the key way geometry and the use of the high strength concrete grout developed in this study be used for new adjacent box-beam bridges to be constructed in the future. The implementation of the recommendations are easily achievable and practical as evidenced from the demonstration project that was completed in Shelby, Ohio, as a part of this project.

PROJECT BACKGROUND

Discussion of the Problem

Precast concrete adjacent box-beam bridges are commonly deployed in Ohio for short and medium spans (30 to 100 ft.). Such bridges are popular because of the low depth-to-span ratio, which allows better clearance under the bridge than stringer supported bridge decks. The life-cycle cost of such bridges is relatively low because of the superior performance, rapidness of installation, and ease of construction. It is also possible to quite readily replace an individual box-beam within a bridge (Wood, 2013). Adjacent box-beams are tied together to form the superstructure of such bridges (Fig. 1). These beams need to work together in a bridge to structurally function as a single unit.

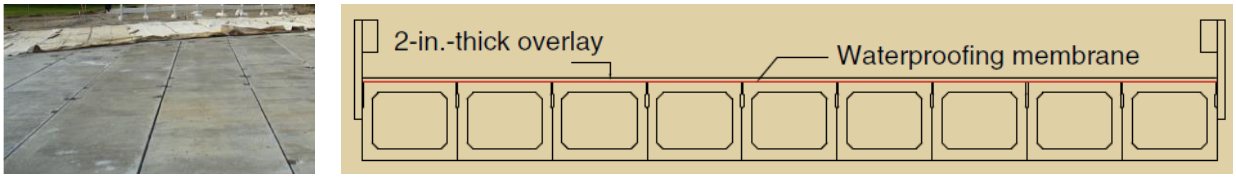

Fig. 1 Longitudinal Joints with Shear Keys Formed Between Adjacent Box-Beams (Bosse and O'Connell, 2010 and Hanna, et al., 2009)

Development of cracks at the interface of the grout and the box-beam key way is a recurring problem that leads to failure of the shear key, reflective cracking in the wearing course, and leakage. Such cracking is common even in some new bridges immediately after construction (Kahl, 2005, Ulku et al., 2010). Water leakage at longitudinal joints is generally believed to be due to the failure of the key ways and waterproofing membranes. Water seepage is one of the primary causes for corrosion of the embedded prestressing strands and non-prestressed steel (Fig. 2), and corrosion leads to spalling and snapping of prestressing strands. Therefore, prevention of water leakage at joints is critical for the durability of box-beams bridges. Any cracking along the joints and differential deflection of adjacent beams is expected to cause the waterproofing membrane to be damaged, which makes water leakage inevitable. Most times, the seeping water is contaminated by deicing chemicals that make the concrete susceptible to corrosion-related damage, such as cracking and spalling.

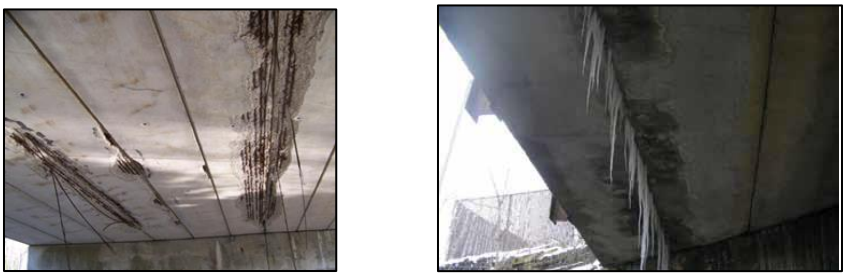

Fig. 2 Severe Deterioration of Underside of ODOT Box-beams at the Longitudinal Joints Due to Corrosion and Spalling (Left) and PennDOT Documentation of Leakage (Right)

In a non-composite box-beam bridge designed to ODOT specifications, the waterproofing of joints comprises a primer coat and a membrane system. An asphalt overlay is placed on top of the membrane system to provide a riding surface. Because of frequent cracking and water leakage problems, ODOT has moved away from non-composite box-beam bridges, and currently the agency uses composite box-beam bridges with reinforced concrete topping for bridges under

its jurisdiction. However, county engineers continue to use non-composite box-beam bridges for local and county bridges.

Key way recesses are formed in precast concrete box-beams at the time of casting. Box-beams are usually installed next to each other and are tied together with mild steel tie rods or post-tensioned strands. The tie rods or prestressing forces from the strands are expected to provide a clamping force normal to the joint. The key ways along the longitudinal joints are then grouted with cement mortar. The hardened grout in the key way enables the transfer of the interacting forces between adjacent box-beams to create a monolithic action of the assembled box-beams. The use of cement-based mortar grouts is a common practice for adjacent box-beam bridges.

The satisfactory performance of non-composite box-beam bridges depends on the shear key geometry and details, the waterproofing membrane, and the tie rods. The joint performance and joint strength can also be affected by other factors such as the properties of grout materials, interface characteristics, amount of transverse force applied to the beams, type of the applied loads, and installation practices during construction.

Research Approach

A systematic study was conducted in this project in order to address the seepage problem and to develop a potential solution. In addition to the literature review, the research program included membrane performance studies, an evaluation of the structural performance of key way joints, study of grout materials and development of a new high-strength high-performance grout, field measurements of vertical differential deflections and separation of beams at longitudinal joints, beam assembly tests with symmetric loading, finite element analysis for eccentric loading and the corresponding structural tests, as well as observation of construction practices and an investigation of a bridge that was in service for 32 years at the time of its demolition. The study also included the development of a basis for implementation and actual implementation of the research results in a newly constructed bridge. These distinct parts of the project are briefly described in this report. The research and findings from all the tasks completed in this project are presented in greater detail in the appendices.

Need for the Research

Watertightness of longitudinal joints is directly affected by cracking and differential deflection at the longitudinal joints, and the effectiveness of shear key joints plays a critical role in the long-term performance of box-beam bridges. Careful and systematic investigation of the problem with a particular emphasis on the waterproofing materials and the connection details, along with the potential remedial measures, was needed for existing and new box-beam bridges.

About one sixth of all bridges built annually in the nation on public roads are adjacent box-beam precast concrete bridges (Huckelbridge, et al., 1997), and there are over 6,000 prestressed box-beam bridges in Ohio (Wood 2008). State DOT's and counties will continue to use box-beam bridges frequently as an economical option under the Federal Highway Administration's "Highways for Life" program (Hanna, et al., 2009). This project provides a basis for preventing corrosion-related deterioration of precast concrete adjacent box-beam bridges and affords an opportunity for improvements in planning, designing, and maintenance of such bridges. With the improved shear key solutions and waterproofing details developed in this study, cracking and leakage can be prevented, and the service life of these bridges can be substantially extended.

RESEARCH CONTEXT

Goals and Objectives of the Study

The broader goal of this study was to develop insight into the performance of longitudinal joints of box-beam bridges with a particular reference to cracking and differential deflection that is believed to cause the waterproofing membrane to fail. The specific objectives of the study were to:

(i) Identify the sources, causes and effects of inadequate waterproofing at the longitudinal joints.
(ii) Develop measures that would assist in the prevention of water leakage by carefully evaluating alternatives.

Specific Tasks Accomplished in the Project

The following tasks were included in the original proposal for this project:

Task 1: Literature review
Task 2: State of practice and potential alternatives
Task 3: Inventory of Ohio adjacent box-beam bridges and selection of bridges for inspection
Task 4: Performance history of ODOT membrane and joint materials and details
Task 5: Joint structural tests
Task 6: Joint watertightness tests
Task 7: Box-beam assembly tests
Task 8: Analysis of research results and recommendations
Task 9: Inspection and maintenance methods
Task 10: Economics of alternatives
Task 11: Preparation of reports

Summary of Literature Review

State of the Current Practice

ODOT drawing PSBD-2-07 provides standardized details of prestressed concrete box-beam bridges for two section widths, 36" and 48". For each width, there are six depths used as standard. The key way depth is 7" if the section depth is less than or equal to 27", while the key way depth is 12" if the section depth is 33" or 44". The opening at the top surface of the beams is ¾", and a wider opening of 1½" is used in the bottom portion of the key way. The box-beams are to be tied together with unbonded transverse tie rods at the diaphragms—typically at a depth of 9" from the top for beams 17" to 27" deep, and 14" from the top for beams 33" or 42" deep. These tie rods are typically 1" diameter steel rods with threads at the ends to receive a plate washer and a nut torqued to 250 ft-lbs (which translates to about 15 kip tension). The transverse through holes for tie rods need to be 2" to 3" in diameter. The key way surface is sandblasted. A non-shrinking mortar or a high early strength grout is placed in the key ways between beams and tie rod recesses after tensioning.

Waterproofing Membranes and Their Effectiveness

Waterproofing membranes are widely used to protect bridge decks from water-induced damage. The waterproofing of joints comprises a primer coat and a membrane system. The membrane consists of asphalt material and waterproofing fabric (Type B), rubberized asphalt and peel-and-stick waterproofing membrane (Type 2), or the preferred high density asphalt mastic between two layers of polymer fabric (Type 3). A 3½-inch-thick asphalt overlay is placed after the waterproofing

treatment is applied to the deck. Appendix A includes details on the use of the waterproofing for bridges in the United States; the types and classifications of waterproofing systems are also explained. The details of each system (primer, membrane and tack coat) are also discussed. This appendix summarizes the specifications and standards related to the waterproofing membrane as well as the design details. The construction details of the waterproofing membrane for both liquid and pre-formed systems are also outlined. The findings from the literature review indicate that waterproofing membrane features and the specifications for waterproofing will ensure satisfactory performance if installed with adequate care. However, research on the performance of waterproofing membranes was found to be limited and lacking, particularly when placed in conjunction with concrete box-beams.

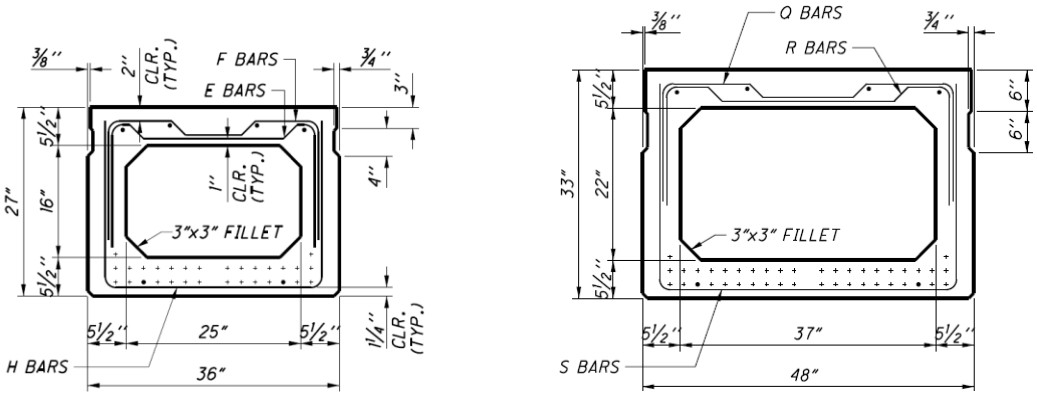

Fig. 3 ODOT Standard Details

The membrane is one component of the waterproofing system. It mainly works as a physical barrier that is typically placed over the top of the concrete surface and, it is covered by a stronger material that functions as the driving surface. Other materials are also used as bonding agents to secure the membrane to the bridge deck. Inadequate implementation of any component can result in poor performance of the system as a whole.

Waterproofing membrane systems are divided into two main categories. First is a construct-in-place system (bituminous and resinous liquid-sprayed systems). The bituminous membrane is the most common material used in practice for this particular system. Second is the preformed membrane system, which is divided into asphalt-impregnated fabric, polymers, elastomers, and asphalt laminated board systems. Asphalt-impregnated fabric is the most common material used in the industry among the preformed membrane systems.

Key Way Joints

The structural performance of a bridge deck in an adjacent box-beam bridge depends on the integrity of adjacent beams, which should function together as a single unit under traffic loading. Shear keys are formed between adjacent beams to provide a connection between the adjacent beams. Key way geometry, grout material, transverse forces, end support connections, and traffic and environmental loads are the main influencing factors for the joint performance. The use of post-tensioning can improve the joint and the shear key performance. However, the tie rods are not as effective as post-tensioning, since the clamping forces developed by tie rods are only distributed over a very small width, which is generally equal to the diaphragm thickness. Eccentric loading can cause out-of-plane moment, creating simultaneous shear and tensile stresses on the joints in adjacent box-beam bridges that can increase the extent and severity of joint cracking.

The complete details of the literature review are provided in Appendix A.

RESEARCH APPROACH

The tasks completed in the project are briefly described in this section. The complete details of the activities for each task are included in the relevant appendices.

Waterproofing Membrane Evaluation

Findings from the evaluation of waterproofing membrane are presented in Appendix B. The test results demonstrate that the tensile strength of membranes is low and remains mostly constant over a temperature range of -4° F to 70° F. The elongation of membranes at failure can be over one inch, but the ability to elongate is reduced when temperature reduces from 70° F to -4° F. The adhesion (peel-off) strength of membranes is also very low for Type II (self-adhesive) and Type III membranes. Direct heat application on binders does not improve the adhesion strength, but the use of sealant in addition to primer improves it. Membranes were found to be capable of accommodating at least one inch of differential (shear) deformation without rupture and are able to provide watertightness even after undergoing shear deformation of over one inch. Membranes subjected to wheel loads over sharp edges do not fail by rupture; punching tests revealed that membranes are susceptible to punching failure when loads are transferred through sharp points such as those of grit, aggregate or beam edges. There is clear evidence from structural tests that membranes will be able to accommodate large elongations and differential deflections between adjacent box-beams without losing their watertightness. This suggests that membrane failures by rupture due to tensile or shear deformations alone may not be the primary cause of water leakage through longitudinal joints of adjacent box-beam bridges as long as the membranes are installed properly and punching of the membranes is prevented during construction. At the onset of the project, there was a general expectation that waterproofing membrane failures may be the sole cause of the problem. However, that line of reasoning was disproved by the membrane tests conducted in this study.

Performance Evaluation of Box-beam Bridges and the Relevant Construction Practices

To understand the state of practice and potential alternatives, an inventory of Ohio's adjacent box-beam bridges was reviewed, and bridges in several ODOT districts were selected for inspection. The performance history of ODOT membranes, joint grout materials and other design details of these bridges are given in Appendix C.

Field Measurements of Vertical Differential Deflections and Separation of Longitudinal Joints

Based on the bridges inspected in various ODOT districts and based on the discussions with ODOT and county engineers, it was noted that the water leakage problem does not appear to have a geographical or statistical trend. Lack of watertightness, cracking at longitudinal joints, and joint failures seem to be a common problem for bridges on highways throughout the state.

Bridge ASD-42-12.49 in Ashland County (ODOT District 3) was selected for the measuring of vertical differential deflections and horizontal beam separation under truck loading. This bridge is a non-composite bridge having a 60-ft. span, thirteen precast-prestressed box-beams tied with one set of three overlapping tie rods in the transverse direction, and an asphalt concrete wearing course. A single set of tie rods was provided at an intermediate location. The maximum recorded vertical differential deflection was determined to be 0.0045 inch. The maximum horizontal separation on the underside of the box-beams was found to be 0.0150 inch.

These measurements provide a basis for defining the extent of stretching and the extent of shear deformation that a waterproofing membrane needs to accommodate without losing its ability to

provide watertightness. The membrane tests presented in earlier sections demonstrate that these membranes are capable of extending axially (in-plane) over one inch (10 to 20% of original length) and deform in shear mode (out-of-plane) by over one inch. Therefore, membranes are able to accommodate the vertical and horizontal differential deflections normally expected in typical box-beam bridges that are known to have cracks at the longitudinal joints and water leakage problems.

Investigation of a Bridge that was in Service for 32 Years at the Time of its Demolition

Bridge RIC-42-12.34, located in Mansfield (Ohio) in ODOT District 3, was constructed in 1983 and scheduled for demolition in August 2015. The width of the bridge was 60 ft. and the span was 34 ft. The primary objective of this task was to evaluate the condition of the waterproofing membrane after the bridge was in service for 32 years. On the day of the demolition, the asphalt concrete overlay was carefully cut to extract waterproofing membrane samples for inspection and watertightness testing.

The lack of watertightness and the corrosion damage at the bottom surface of the box-beams along the longitudinal joints correlated well vertically with the locations where the membrane was missing or severely damaged at the top surface of the bridge. The membrane, where present, was in very poor condition and full of holes that would make it impossible for it to provide any watertightness. The extracted membrane was so brittle and fragile that it could not be tested to determine its mechanical properties.

Observation of Construction Practices at a Bridge Construction Site

To understand bridge construction processes, the sequence of activity, and the time frame for each activity, multiple site visits were made to a construction site in Shreve, Ohio, where a new bridge was under construction. The site observations reported in Appendix C demonstrate a set of unacceptable construction practices followed by contractors. ODOT specifications provide basic guidance and clear protocols on waterproofing membrane installation and grouting of key ways. These specifications and recommendations need to be expanded to include more details to provide a better understanding of the procedures by both contractors and inspectors. Strict adherence to specifications is needed.

Excessive addition of water to grout material needs to be regulated and controlled so as to prevent a diminishing of the structural strength of key way joints. Successful installation of waterproofing membranes requires adequate concrete surface preparation, proper application of the bonding agent, and careful placement of membrane sheets. The waterproofing membrane must be inspected for the presence of any holes before the paving process is started. Driving of heavy equipment must be prohibited before the asphalt concrete overlay is placed so as to prevent damage to the membrane. Strict quality control, careful inspections and stringent enforcement are warranted.

Structural Performance of Key Way Joints

Structural performance of key way joints was studied by testing several joint specimens with and without tie rods as presented in Appendix D. The factors considered were: (i) key way geometries, (ii) grout materials, (iii) commonly used industrial chemical additives or bonding agents, (iv) effects of the use of cement slurry to coat the joint surface, and (v) effects of surface preparation.

The following conclusions were drawn from the joint tests with a tie rod:

(i) A small amount of tie force increases the shear transfer strength of key way joints by a large amount. The tie rod also allows the joint to develop a larger relative slip.

(ii) The shear strength of joints at failure is much larger than the shear strength of the joint at the time of visual appearance of the first crack.

The following conclusions were drawn from the joint tests without ties:

(i) Joint strength can be increased substantially by using deeper and wider key ways.
(ii) Cement slurry and bonding agent does not enhance shear strength.
(iii) Sandblasting the interface can increase the shear strength of the joint significantly.
(iv) Polymer grout has strong bond and shear strength under shear loads.
(v) Magnesium phosphate grouts have poor performance that can get worse when grouts are exposed to humidity and certain other environmental conditions.
(vi) High strength concrete (HSC) grout is a better option compared to ODOT-approved grouts as long as it can be properly placed and compacted adequately within wider key ways.
(vii) Ultra-high performance concrete (UHPC) developed in this study has the highest compressive strength and shear strength of all the grouts tested. A rough interface surface increases the bond and the corresponding shear strength, allowing the key way to utilize the high compressive strength of UHPC. The benefit of high strength is not attainable unless there is adequate bond between the joint surface and the grouted key way.

Shear transfer strength of key way joints can be increased by a factor of up to 5.5 compared to the joints that use the current ODOT-approved grouts with ODOT-recommended key way details through proper selection of grout material, revisions to the key way geometry, and proper surface preparation of the interface.

Study of Grout Materials and the Development of a New High Strength Concrete Grout

As described in Appendix E, the placement of pre-manufactured grouts in the key way using the specified mixing water content is difficult even in laboratory conditions when the opening of the key way is ¾ inch; the workability of the grout is not adequate for placement and consolidation in key ways. The influence of water content on the workability and compressive strength was studied for the three water contents recommended by the manufacturer and three other higher ranges of water content. Test results with different proportions of mixing water showed the effects of higher amounts of mixing water on the strength and the flowability of the grout. The higher the water content, the lower the concrete compressive strength; the reduction can be substantial, by as much as a factor of 2 to 4.

Several high strength and ultra-high strength concrete grouts were developed and are presented in Appendix E. One of the high strength grouts with #8 size coarse aggregate was selected for further joint and beam testing because of its potential for implementation.

Beam Assembly Tests for Symmetric Loading

Joint tests described in Appendix D of this report were conducted with a large number of variables that included a wide range of geometries and grouts. These joint tests provided a basis for selecting the parameters for further testing and evaluation at a larger scale. The symmetric beam assembly tests that were designed and conducted in this project are a simplified representation of three adjacent box-beam units tied together to act as a single unit. The primary objective of the beam assembly tests described in Appendix E was to study the joint strength and behavior under symmetric loading.

The following findings were made based on the laboratory testing of box-beam assemblies:

1. Polymer grout shows superior performance with flowable, self-consolidating properties that do not require vibration or widening of the key way opening to be effective. Polymer grout has three hours of working time after mixing and can be used over a wide range of temperatures, which can provide flexibility in terms of temperature conditions at the time of grouting. Beam assemblies with polymer grout developed 3.2 times the strength of those with the current ODOT-approved cementitious grout using ODOT standard key way geometry. Therefore, polymer grout is a potentially implementable grout for box-beam assemblies.
2. HSC concrete with a maximum #8 aggregate size along with full depth key way is an attractive option to develop higher shear transfer strength at the joint. The strength obtained for beam assemblies with HSC concrete grout was 47% higher compared to those using the current ODOT-specified grout for otherwise identical test specimens.
3. Deeper key ways are able to increase the shear strength by 95% compared to shallow key ways using the same grout material.
4. Sandblasting the key way surface can effectively increase the shear strength by 157% for the same grout material as compared to key ways without sandblasting.
5. Shear failure is local under the applied loads. The effects of joint cracks and tie rods are also local.
6. The failed joints may undergo higher deflections after failure when subjected to further loading beyond the time when the first crack appears. Therefore, the load corresponding to the first crack is considered as the failure load from the standpoint of waterproofing.

Analysis for Eccentric Loading

The interacting forces at the longitudinal joints of adjacent box-beams depend on the joint details, the bond strength between the grout and the box-beam key way recess, and the joint response to the internal forces developed at the interface. It is generally well accepted that the interacting forces can cause shear loading at the longitudinal joints. However, the positioning of wheel loads relative to the joints is expected to cause out-of-plane moments at the joint concurrent with the shear loading. The out-of-plane moments are developed due to the eccentricity of the loading relative to the centerline of individual box-beams. This aspect of longitudinal joint behavior was studied using finite element analyses for three spans and the corresponding beam cross sections. The details of these analyses are included in Appendix G.

Analyses for 90 ft., 65 ft. and 40 ft. simple span bridges were included in the study. The analyses for a 90-ft. simple span bridge with a B42-48 beam cross section was considered because it is the largest cross section used by ODOT. One implementation project was being considered for a bridge with a span of 90 ft. A second set of analyses for a 65 ft. simple span was performed to determine the factors of safety provided by the grouted joint for that span. Factors of safety were determined by comparing the strength obtained from structural tests conducted in the laboratory with the stresses predicted from the finite element analyses for the corresponding loading combinations.

The following conclusions were drawn from the results of the analyses and are presented in Appendix G:

1. Any redistribution of the end reactions between the bearing pads idealized as springs and the anchor dowel bar did not have any effect on the normal stresses or shear stresses on the longitudinal joints as long as all bearing pads have the same stiffness properties. There is no change in the state of stresses in terms of normal stresses and shear stresses at the longitudinal

joints due to the inclusion or exclusion of the end anchor dowel bars in modeling the end supports.

2. The axial spring stiffness representing the bearing pads used in the analyses has no effect on the state of stresses at the longitudinal joints. As long as no differential settlement occurred, no changes were observed in the state of stresses at the joints. Any inaccuracies in assuming the stiffness constants in finite element analyses to represent the bearing pads have no effect on the normal and shear stresses at the longitudinal joints.
3. For box-beams with intermediate diaphragms, most of the out-of-plane moment at the joint is mainly transferred to the adjacent box-beam at the location of the diaphragms. The peak normal stresses occur at the diaphragm locations. However, most of the shear forces are transferred at the locations of the wheel loads.
4. Box-beams with intermediate diaphragms and deeper key ways (a depth of 36 inches) have smaller normal tensile stresses than those with 12-inch-deep key ways by a factor of about 2.0 for normal tensile stresses and a factor of 3 for shear stresses, suggesting that the joints with deeper key ways will have a smaller tendency for cracking to occur at the joint surface.
5. Box-beams without intermediate diaphragms and deeper key ways (depth of 36 inches) also have smaller normal tensile stresses than those with 12-inch-deep key ways, but the reduction of normal stresses is not as much as it is for box-beams with diaphragms.
6. The effectiveness of tie rod clamping force is negligible when the tie rods are tensioned prior to grouting. Therefore, there is no significant contribution of tie rods in controlling the spreading of adjacent box-beams or in the tendency to crack at the joints.
7. Any cracking in the top 3 inches of a joint with a 12-inch-deep key way has a significant effect on the normal stresses in the vicinity of the cracks, suggesting that the crack propagation will be more severe in shallow joints compared to that of beams with deeper key way joints.
8. Overall, the cracking potential is significantly reduced by increasing the depth of the key way joint from 12 inches to 36 inches.

Structural Tests for Eccentric Loads

The strength of the joints under the possible concurrent action of shear loading and the corresponding out-of-plane moment was determined using structural load tests. A study of eccentric load effects at a full or large scale requires larger beams than those used for symmetric loading (described in Appendix F), with comparable cross sections and spans. Such tests are expensive and time consuming. Therefore, simplified smaller-scale test specimens with a length of 42 inches and depth of 21 inches were suitably designed to capture the behavior of full-scale box-beams for select key way geometries, interface conditions, and loading conditions. Structural tests were conducted in order to determine if the key way geometries and grouts developed in this study would satisfy the load carrying requirements at the longitudinal joints of box-beam bridges with typical spans.

The test specimen with the currently used ODOT key way geometry with ODOT-approved grout failed under the self-weight of the test specimen alone without any additional applied load, proving that the current key way with currently used grout is incapable of carrying any shear load in conjunction with out-of-plane tension or moment. For this reason, changes in key way geometry details and grout material specifications are definitely needed. Increasing the key way depth alone without proper surface preparation did not improve the strength of the joint when using ODOT-approved grout. The shear transfer strength of specimens with a sandblasted surface and full-depth key way and with high strength grout or ODOT-approved grout was significantly larger.

The structural tests to determine the joint strength under eccentric loads identified a serious inadequacy of the current key way geometry and ODOT-approved grout. Increasing the depth of the key way to full depth but with no sandblasting was not adequate to improve the joint strength under the simultaneous action of out-of-plane moment and shear. However, the changes made to the key way geometry and the new grout materials were found to improve the joint performance substantially. HSC concrete with #8 coarse aggregate was able to form an excellent bond with the concrete units, resulting in a high tensile strength across the joint.

The test results for the test specimens with eccentric loads and the beam assembly tests presented in Appendix F indicate that the compressive strength of the grout material is not the only measure to qualify the grout for all applications; the bond strength is an equally important factor that might disqualify a high compressive strength grout. In the design process, stress analysis of a bridge is required in order to select the key way geometry for the bridge based on the relevant load combinations and the corresponding joint depth.

The modified geometry of the key way with HSC-grout provides adequate strength to resist the resulting stresses with a factor of safety of about 3.2 for the load cases considered in this study.

Basis for Implementation

Typical finite element models were developed to simulate bridge RIC-TR037-0.21 over Cedar Fork, which is a tributary of the Clear Fork River on Shauck Road in Richland County, Ohio. This bridge was selected for potential implementation of the findings from the project. A finite element model was developed with three-dimensional 8-noded solid elements. The bridge is a box-beam bridge with a total length of 39 ft. with a simply supported span of 38-ft. (center-to-center distance between the end bearings) and a width of 28 ft. Box-beams in this bridge were designed to have the B17-48 cross-section, which is allowed to be used for bridges with spans up to 40 ft (total length of 41 ft) as specified in ODOT standard drawings PSBD-2-07 and PSBDD-2-07.

The details developed for implementation include stresses over the depth of the key ways along the longitudinal joints of adjacent box-beams due to different load cases. Factors considered were: the location of anchor dowel bars at the beam ends, changes to the key way geometry, and stress analysis and design of box-beam sections with the revised key way geometry, as presented in Appendix I.

It was found that substantial changes to the end abutment details are needed if the anchor dowel bar details at the beam ends are to be changed to prevent any longitudinal relative movement between the ends of the box-beams and the end abutments. These changes would have required substantial redesign of the abutments and piles (i.e., the number of piles and the layout of piles). It was therefore decided to retain the original end anchor dowel details so that substantial (and possibly, costly) changes are not incorporated into the abutment and pile details in the design. Changes to the key way geometry and the grout material alone are believed to provide significant improvement in the joint performance, without any changes to the end anchor dowel bar details or the abutment and pile details. Minor changes to the currently used ODOT construction specifications were also recommended, as presented in Appendix I.

However, the implementation of the recommendations did not go forward for bridge RIC-TR037-0.21 due to some miscommunication.

Implementation of Research Results

The details of the successful implementation of the research results are presented in Appendix J. For the implementation, a bridge (RIC-CR184-2.17, SFN 7030013) over Kuhn Road in Shelby, Ohio, was selected. The suggested recommendations and the revised key way details (including the slightly modified grout specifications used in the project) are presented in Appendix J. The bridge was constructed according to the recommended changes during the first week of April 2018, grouted on April 25th, and was inspected soon after it was opened to traffic on May 19, 2018. No cracks were detected during the inspection. The bridge was also inspected in October 2018 in order to evaluate the outcome of the modified specifications and key way details, and no visible cracks were found on the deck surface along the longitudinal joints of the box beams.

Summary

As outlined in this section, research efforts in this project were focused to ensure that the various aspects of preventing water leakage at the longitudinal joints of adjacent box-beam bridges are addressed. The effectiveness of selected membranes in preventing water leakage was evaluated with physical tests. The membranes were found to accommodate at least one inch of vertical shear deformation and at least one inch of extension without losing their waterproofing properties. The structural tests conducted in the study with the revised key way details demonstrate improved performance due to the increased dimensions of the key way geometry and due to the use of high strength (concrete) grout. The implementation of the recommended changes has been documented to demonstrate the improved performance of the bridge design.

RESEARCH FINDINGS AND CONCLUSIONS

Research Findings

Waterproofing Membrane Evaluation

Membranes are capable of accommodating at least one inch of elongation and differential (shear) deformation without rupturing and can provide watertightness even after deformation of over one inch. The differential vertical deflections and horizontal separation of adjacent beams measured under truck loading were about 0.0045 inch and 0.015 inch, respectively. These measurements are much smaller than the capacity of membranes in terms of tensile elongation or shear deformation. The construction practices observed at the site of a new bridge revealed that ODOT specifications need to be enforced more stringently to achieve the intended watertightness of the longitudinal joints of box-beam bridges.

Key Way Joints

The shear transfer strength of key way joints can be increased by a factor of up to 5.5 by using revised key way geometry with a deeper joint and new high strength concrete grout with #8 coarse aggregate as compared to key way joints with the currently used geometry and ODOT-approved cement mortar-based grouts. Good sandblasting and thorough wetting of the joint surface prior to grouting improves the shear transfer strength of the joints. Finite element analysis also confirmed the beneficial effects of deeper key ways on the state of stresses on the joints. Tie rods are ineffective in developing clamping stresses on the joints other than the small clamping stresses achieved at the diaphragm locations.

Key way joints with the currently used ODOT key way geometry and with ODOT-approved grout failed under the self-weight of the test specimens alone without any additional applied load, proving that the key ways with the current geometry and with the currently used type of grout is incapable of carrying any shear load in conjunction with out-of-plane tension or moment. The modified geometry of key ways along with HSC-grouts provides adequate strength to resist the resulting stresses with a factor of safety of over 3 for the load cases considered in this study.

Implementation

The suggested modifications to the key way geometry and the use of the high strength concrete grout developed in this study will be able to reduce cracking and water leakage at the longitudinal joints of adjacent box-beam bridges. Emphasis also needs to be made that the contractor is required to perform the work per the specifications.

Conclusions

The following conclusions are drawn from the findings of the project:

- Membrane failures by rupture due to tensile or shear deformations are not the primary cause of water leakage through the longitudinal joints of adjacent box-beam bridges.
- The currently used ODOT key way geometry with ODOT-approved grouts is incapable of carrying any shear load in conjunction with out-of-plane tension or moment.
- The shear transfer strength of key way joints under loading can be increased substantially by revising the key way geometry to be deeper and wider, using high strength concrete grout, improving the surface preparation for joints, and strictly enforcing ODOT specifications.
- The suggested recommendations and the revised key way details along with the slightly modified ODOT specifications were found to be practical, achievable and easily implementable.

RECOMMENDATIONS FOR IMPLEMENTATION OF RESEARCH FINDINGS

A complete set of recommendations for implementation are given in Appendix J. After considering several factors, it was decided that the recommended implementation be limited to the following three simple changes: (i) revised key way geometry, (ii) type of grout material, and (iii) construction specifications. Therefore, the ODOT specifications relevant to the grouting and waterproofing membrane installation were marginally modified in order to be consistent with the suggested changes as follows. Emphasis also needs to be made that the contractor should perform the work per the specifications.

Recommended Modified Design and Construction Specifications (Valid for a Simple Span of up to 54 ft.)

All the relevant ODOT specifications from (i) Construction Inspection Manual of Procedures, (ii) Construction and Material Specifications, and (iii) standard drawings PSBD-2-07 must be strictly followed in order to minimize the occurrence of water leakage through the longitudinal joints in adjacent box-beam bridges. The following additional recommendations are suggested for implementation.

ODOT Item 515 Prestressed Concrete Bridge Members

Box-beam Grout Installation

1. Key ways should be grouted after the box beams are erected. Generally, plastic rope or jute is installed into the bottom of the key way to block the grout from flowing out. Utmost care shall be taken to seal the bottom edge of the key way to prevent the leakage of wet grout during and after the grouting process.
2. Ensure that the installation is done properly. Box-beam keys have failed because of improper jute installation. However, a suitable foam sealant may be used to seal the key way and make it watertight before the grouting operation begins.
3. The fabricator shall sandblast the key way surface within four days of shipment to the project site as specified in ODOT standard drawings PSBD-2-07. The sandblasting shall yield a visual appearance and texture equal or rougher than 100 grit sandpaper over the entire key way surface. When stains are visible before sandblasting the concrete, use a degreaser to ensure removal of grease, oils and other similar contaminants. The degreaser shall be water soluble so it can be removed before the blasting begins. Before mortaring, remove all dirt, dust, grease, oil and other foreign materials from surfaces using a high pressure wash of at least 1,000 psi at a delivery rate of 4 gal/min.
4. Grout should meet the material requirements of the Office of Structural Engineering's standard box-beam drawings. Additional requirements are to be satisfied for the high performance high strength concrete grout that is recommended to be used in this project. A grout with #8 maximum size aggregate needs to be used in this project with the following specifications:

    - Minimum compressive strength of 10,000 psi needs to be achieved before allowing any construction equipment on the deck.
    - The grout shall be designed to include well graded #8 coarse aggregate suitable for high strength concrete applications.

- The top surface of the grouted joints shall be cured with ODOT-approved curing compound that is to be applied on the surface just after one hour of grouting.
- The grout shall have workability that is adequate to fill the key way.
- Suitable superplasticizers are to be used to adjust the workability of the grout to adequately consolidate the grout in the key way.

5. The manufacturer's mixing instructions are required to be followed and should ensure that the grout is properly mixed, consolidated into the joints, cured, and sampled for testing.
6. Grouting should not be allowed if there is construction traffic or if erection activities are still occurring.
7. The grout can be cracked by the vibration and deflection movements from construction traffic or activities and can make the key ways worthless.
8. The design of the structure depends on the grout used in the shear keys.
9. Do not allow traffic on the deck before the grout has obtained the required strength of 10,000 psi. This includes construction traffic. This specification must be strictly followed.

The mix proportions given in the Table 1 were found to be satisfactory for the high strength grout in a laboratory environment. However, other mixes with better optimized aggregate gradation and supplementary cementitous materials may be used to improve the mix proportions and reduce cement content while maintaining similar minimum strength and performance to achieve very low shrinkage.

Table 1 Possible Mix Proportions for High Strength Concrete Grout for Key Ways

Mix Proportions		
Materials	**Description**	**lbs/yd^3**
Cement	Type I	1100
Coarse aggregate	# 8 limestone	1596
Sand	River sand	1450
Water to Cement Ratio		0.35
Water	Potable water	385
High range water reducing agent 100 ml/100 lb of cement (SIKA 2100)		

Installation of Waterproofing Membrane

The specifications on the preparation of the top surface of box-beams that are given in Section 512.08 should be carefully followed before and after the installation of the membrane. Remove all protrusions more than 0.1 inch in height from the concrete surface at the top of the box-beams. Sweep off dirt and dust, and blow the concrete clean. Fill joints or cracks greater than ⅜ inch (10 mm) wide with Portland cement mortar. In addition to the above, remove oil and grease from surfaces for Type 3 membranes using water and a detergent designed to remove oil and grease from concrete. Flush residual detergent from the surface. Do not allow traffic or construction equipment on the cleaned surface or on the membrane after installation of the membrane and before the asphalt concrete is placed. If any visual damage to the membrane is found after installation of the membrane, suitable repairs must be made to prevent water leakage before placing asphalt concrete. The repair method and acceptance will be determined by qualified inspectors.

Recommendation on Revised Key Way Geometry

As an example, B21-48 beam sections with key way geometry conforming to the details specified in ODOT standard drawing PSBD-2-07 were originally planned to be used for a 54 ft. span bridge. The structural details of the design section are given on sheets 5 and 6 of drawings prepared by Poggemeyer Design Group (attached to Appendix I). Typical sectional details with the prestressing strands but without other nonprestressed reinforcement are reproduced from these drawings and are shown in Fig. 4. The research team developed design calculations as per AASHTO (2012) and determined the required strengths, the design strengths as well as the stresses at the extreme fibers of the section under service load and factored load conditions for the governing load combinations.

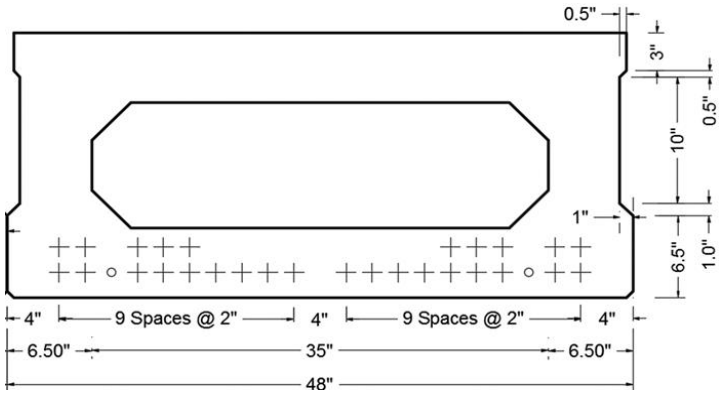

Fig. 4 Revised Cross Section of B21-48 Box Beam that was Used in the Implementation Project

One of the recommendations from this project is to increase the key way dimensions so as to make it easier for placing and compacting grout within the key way recess. However, increasing the width of the key way cuts into the side wall thickness and reduces the total area and moment of inertia of the section compared to a section with the original key way geometry. Therefore, detailed stress checks under service loads and adequacy of design shear and moment strengths under factored load conditions are warranted if any changes to the key way geometry are to be considered. Additional checks are also needed for the prediction of camber and deflection limits specified in PSBD-01-07 for these box-beams.

Steps Needed for Implementation

1. If the suggested implementation is acceptable to ODOT, ODOT's standard drawing PSBD-01-07 needs to be revised by changing the key way geometry and by providing an appropriate number and arrangement for the prestressing strands.
2. The construction specification items to 512.08 and 515.19 on prestressed concrete box beam bridge members needs to be changed as suggested in the above section.
3. Emphasis also needs to be made that the contractor is required to perform the work per the specifications.

Expected Benefits from Implementation

The expected benefits from the implementation of the research results are:

(i) Reduced potential for cracking at the longitudinal joints of adjacent box-beams.
(ii) Improved effectiveness of waterproofing membranes for non-composite box-beam bridges.
(iii) Continued use of non-composite box-beam bridges, which are cost-effective compared to composite box-beam bridges.

Potential Risks and Obstacles to Implementation

A marginal cost increase may occur due to the initial costs of incorporating the revised key way geometries at the precasting plants that normally supply box-beams. This is due to the need for the fabrication of steel forms to match the suggested key way geometries. Not all ready-mix concrete suppliers and contractors in Ohio are conversant with the production and placement of high strength concrete with #8 coarse aggregate. Therefore, there may be a premium to be paid because of the revised material specifications. As bridge contractors will need to pay more attention to the specifications, a lack of stringent quality assurance measures is a potential risk to the successful implementation of the recommendations.

Strategies to Overcome Potential Risks and Obstacles

It is useful to recognize that precasters and concrete suppliers will mark up costs on some of the initial orders to overcome initial premiums associated with the revised key way geometries. Increased awareness of the importance of adherence to the revised specifications will likely reduce the potential risk associated with the implementation.

Potential Users and Other Organizations that may be Affected

Several other bridge owners, such as the Department of Defense, counties in Ohio, and transportation agencies in other states can benefit from the findings of this project.

Suggested Time Frame for Implementation

Implementation is possible immediately.

Cost of Implementation

The cost information provided by ODOT engineers indicates that a change order for $4,500 was needed for the box beam research project keyway modifications. This also includes an additional cost for providing and placing high strength concrete grout (10,000 psi) and modified keyway geometry for the precast box beams for the pilot bridge in Shelby, Ohio. The bridge has six longitudinal joints (seven beams) of 55 ft. length.

Recommendations on How to Evaluate the Ongoing Performance of the Implemented Result

It is recommended that the pilot bridge deck in Shelby, Ohio, where the research results were implemented, be monitored for crack development and performance over the next three to five years so as to verify that the problem of cracking along the longitudinal joints of the non-composite precast concrete box-beams in this bridge has been adequately addressed by the implemented changes.

REFERENCES

A bibliography including a full listing of references is given in Appendix A (Literature Review). The following are the references cited in this summary report only.

List of References

AASHTO, "LRFD Bridge Design Specifications", US Customary Units, Washington, DC, ISBN: 978-1-56051-523-4, 2012.

Bosse, D. and O'Connell, E., "Precast/Prestressed Concrete Beam Production Concepts", Ohio Prestressers Association, Oct. 2010.

Hanna, K.E., Morcous, G., Tadros, M.K., "Transverse Post-tensioning Design and Detailing of Precast, Prestressed Concrete Adjacent Box-girder Bridges", *PCI Journal*, Fall 2009, pp. 160-174.

Huckelbridge, Jr., A.A., and El-Esnawi, H.H. (1997), "Evaluation of Improved Shear Key Designs for Multi-Beam Box Girder Bridges", ODOT Report No. FHWA/OH-97/009, Nov. 1997, 7- pages.

Kahl, S., "Box-Beam Concerns Found Under the Bridge", Research Record, Issue # 102, Sep. 2005, MDOT, 4 pages.

Miller, R.A., Hlavacs, G.M., and Long, T.W., "Testing of Full Scale Prestressed Beams to Evaluate Shear Key Performance", ODOT Report # FHWA/OH-98/019, Dec. 1998, 108 pages.

ODOT Standard Bridge Drawing, "Prestressed Concrete Box-beam Bridge Details", PSBD-2-07, 4 sheets.

PCI Committee on Bridges, "The State of the Art of Precast/Prestressed Adjacent Box-beam Bridges", 2009, 99 pages.

Russell, H.G., "Adjacent Precast Concrete Box-beam Bridges: Connection Details", NCHRP Synthesis 393, 2009, 86 pages.

Russell, H.G., "Adjacent precast concrete box-beam bridges: State of the practice", *PCI Journal*, Winter 2011, pp. 75-91.

Wood, C. (2008), "Rehabilitation of a Prestressed Concrete Box-Beam Bridge", OTEC presentation,http://www.dot.state.oh.us/engineering/OTEC/2008%20Presentations/17A.pdf, 46 pages.

LIST OF APPENDICES

The following reports have been added as appendices:

APPENDIX A: Literature Review
APPENDIX B: Waterproofing Membrane Evaluation
APPENDIX C: Performance Evaluation of Box-beam Bridges and the Relevant Construction Practices
APPENDIX D: Structural Performance of Key Way Joints
APPENDIX E: Study of Grout Materials and the Development of a New Ultra-High Performance Concrete Grout
APPENDIX F: Beam Assembly Tests for Symmetric Loading
APPENDIX G: Analysis for Eccentric Loading
APPENDIX H: Structural Tests for Eccentric Loads
APPENDIX I: Basis for Implementation
APPENDIX J: Implementation of Research Results

Waterproofing Details of Connections for Adjacent Precast Concrete Box-Beam Bridges

Appendix A: Literature Review

Prepared by:

Mohamed Habouh, PhD (Former Graduate Student)
Ali Almonbhi, PhD (Former Graduate Student)
Anil Patnaik, PhD (Principal Investigator)

Prepared for:

The Ohio Department of Transportation
Office of Statewide Planning & Research

State Job Number 134847

07/25/2018

Waterproofing Details of Connections for Adjacent Precast Concrete Box-Beam Bridges

Appendix A: Literature Review

Prepared by:

Mohamed Habouh, PhD and
Ali Almonbhi, PhD
Former Graduate Students, Department of Civil Engineering
The University of Akron, Akron, OH 44325-3905

Dr. Anil Patnaik (PI)

Professor, Department of Civil Engineering
The University of Akron, Akron, OH 44325-3905
Phone: 330-972-5226 Email: Patnaik@uakron.edu

July 2018

Prepared in cooperation with the Ohio Department of Transportation,
Ohio's Research Initiative for Locals, and the U.S. Department of Transportation, Federal Highway Administration

TABLE OF CONTENTS

LIST OF FIGURES

LIST OF TABLES

APPENDIX A: LITERATURE REVIEW

The structural performance of adjacent box-beam bridges depends on the integrity of the joints between adjacent beams. The effectiveness of the grout and the longitudinal joints between the beams will ensure that the box beams act together and share traffic loads. Shear keys are formed in the precast prestressed concrete box beams to accommodate the grout which in turn is believed to transfer vertical and horizontal shear between the beams when they are loaded. When all the box beams in the bridge act as single unit, the traffic loads are well-distributed among the beams. Keyway geometry, grout material, the transverse forces, end support connections, and traffic and environmental loads are the main influencing factors for achieving effectiveness of longitudinal joints. However, cracks often develop at the joints between the box beams and cause leakage of water through these cracks. The seeping water can cause corrosion of the embedded steel reinforcement and prestressing strands.

To prevent leakage of water through the keyway, waterproofing membranes are provided in non-composite box beam bridges. Typical damages are often recorded throughout the longitudinal joints and especially at the abutment locations of the simply supported box beams. The research by others in the past to identify the causes of joint failure and the alternative practices are reported in this appendix.

A.1 Shear Key

Shear key is made up of blockouts on the side of a box beam that is adjacent to another beam. Once the box beams are installed, the longitudinal joint is filled with a filler material that helps to connect the box beams. The longitudinal joints can be of partial or full depth, the depth refers to the keyway depth. These joints are mainly used for two reasons. First, they help to distribute the stresses horizontally between adjacent members so that, differential vertical movement may be prevented. Secondly, they may prevent water from seeping between box beams, which may lead to corrosion related deterioration. In many cases, the transverse reinforcements are used to tie adjacent box beams. Transverse reinforcements usually consist of mild steel bars and/or post-tensioned strand connections (PCI, 2009).

There is no national standard for a shear key configuration; the departments of transportation in various states adopt different types of shear key details. Shear keys are different in geometry, location, and grout depth. Thus, the joint performance is different due to the change in the amount of stresses that each type can resist. The structural behavior of a shear key is very sensitive to the grout practices. There are two types of shear key grouting depth used in the industry: partial and full depth. Partial depth refers to a shear key that is grouted over partial depth and not to the full depth (height) of the box beam. This type of shear key is located near the top of the box beam. Figure A.1 (a) shows the partial depth shear key. The full-depth shear key is a shear key with the grout filling the entire depth of the box beam. Figure A.1 (b) shows the full-depth shear key (Murphy et al., 2010).

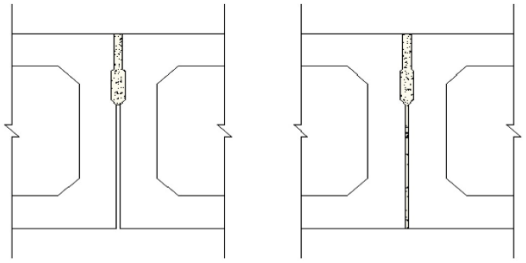

Fig. A.1 (a) Partial length shear key (b) Full length shear key (Murphy et al., 2010)

A.1.1 Shear Key Geometry

A wide variety of shapes, sizes and locations for shear keys is used in practice. These different shear key configurations affect the performance of adjacent box beam bridges. Figure A.2 shows three types of shear key geometries. Finite element analysis and studies show that the performance of joint A in Fig. A.2 is much better than joints B or C when subjected to the similar loading. Additionally, the stresses in joints B and C are larger than those determined for joint A due to height of the keyway. According to a study by Murphy et al. (2010), the geometry of a shear key is very sensitive to the stress magnitude.

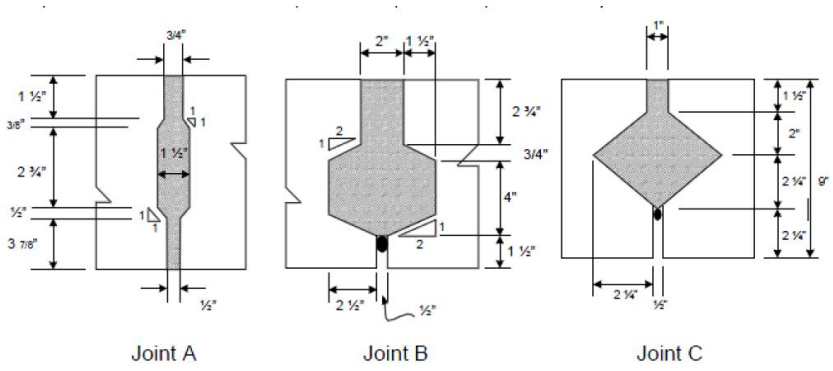

Fig. A.2 Different keyway geometries (Murphy et al., 2010)

The geometries in Fig. A.3 show examples of keyway configurations that were recently employed by Illinois Department of Transportation.

There are no universally accepted design guidelines for keyway configuration or selection. A proper choice of configuration is therefore based on the available strength of the geometry or the stresses imposed on the keyway under the applied loading. The past practice in a particular state DOT can also influence the continued use of a given keyway geometry and design. A survey was conducted by University of Cincinnati researchers to investigate the practices for each state and the design procedure for the used design (Russell, 2011a).

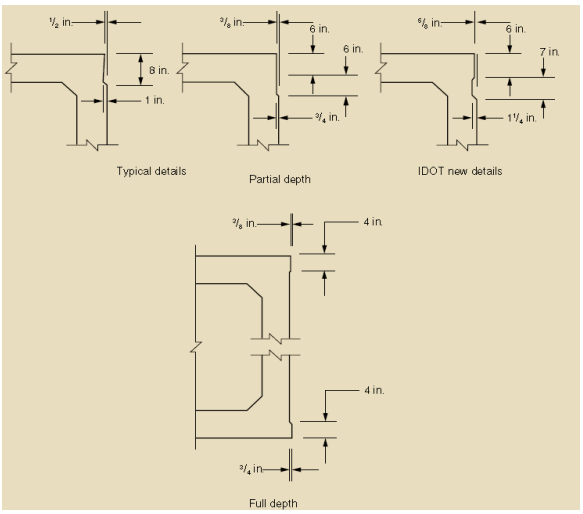

Fig. A.3 Examples of Keyway Configurations (Russell, 2011a)

A.1.2 ODOT Current Practice

Ohio Department of Transportation has standard designs for box beam girders with standard keyway geometry. For all 36" and 48" wide box beams with composite or non-composite beams, when the beam height is 12", 17", 21", and 27", the keyway is 3" deep and 3/4" wide for the top opening to place the grout followed by 4" of depth with 1.5" width. The keyway depth is increased from total of $3 + 4 = 7$" to $6 + 6 = 12$" in case of deeper box beams with a height of 33"or 42", a standard slope of 1: 1 is specified for the chamfers to change width as shown in Fig. A.4.

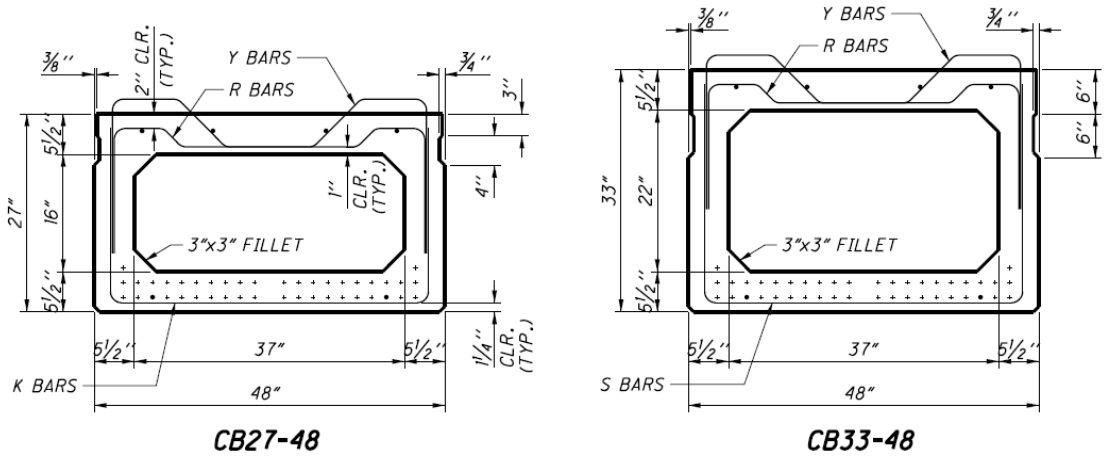

Fig. A.4 Standard ODOT Keyway Geometry

A.2 Grout Material

The most common grout material for joints in precast adjacent box beam bridges is cementitious grout. However other materials such as epoxies have also been used. For shear

key material properties, both tensile and compressive strength are very important due to the types of stresses that the joints are subjected to, such as tension and compression. Moreover, the following characteristics play an important role: shrinkage, bond strength, workability, permeability, and ease of construction. Epoxy based glue material and non-shrinkage grouts are well studied materials and have been widely used. One of the popular materials is "Set-45" magnesium ammonium phosphate ($Mg\text{-}NH_4\text{-}PO_4$) mortar. Set-45 was tested and showed much better results for bond strength and shrinkage compared with conventional non-shrinking grout (Sharpe, 2007).

A.2.1 Evaluation of Grouts

Many small-and large-scale tests were introduced by the researchers to evaluate the grout material as a structural element in addition to the standard tests covered by American Society for Testing and Materials (ASTM).

A.2.1.1 Small-Scale Tests

For the purpose of determining the mechanical properties of the grout, small specimens were tested by several researchers in three different test configurations. These tests were developed to address the tensile strength, compressive strength and shear strength for conventional grout. These tests are: direct tension, direct shear, and four-point flexural. The setup of these three tests is shown in Figs. A.5 to A.7. The direct tension test is shown in Fig. A.5, the direct shear test setup is shown in Fig. A.6, and the four point flexural test setup is shown in Fig. A.7 (Sharpe, 2007).

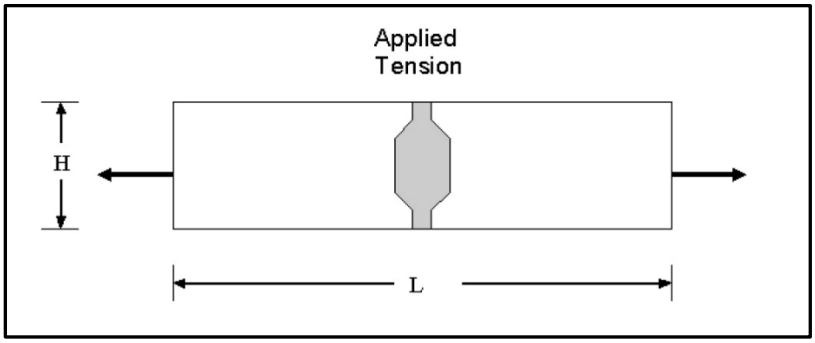

Fig. A.5 Direct Tension Test (Sharpe, 2007)

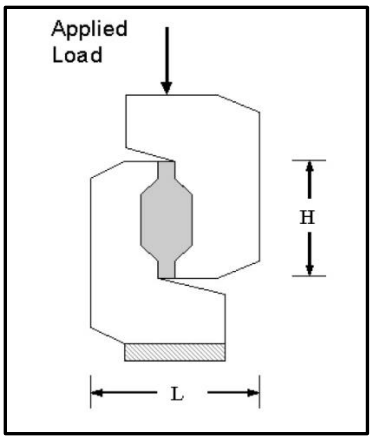

Fig. A.6 Direct Shear Test (Sharpe, 2007)

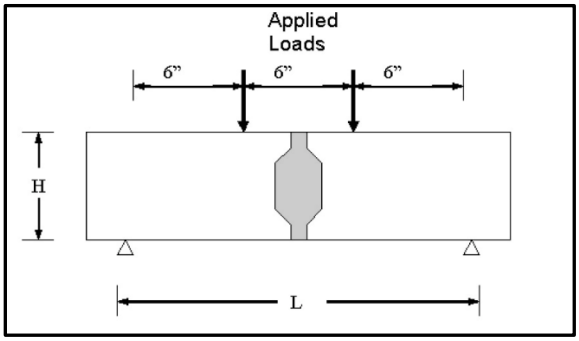

Fig. A.7 Four-Point Flexural Test (Sharpe, 2007)

Test specimens were investigated in several failure modes in the study by Sharpe (2007). These tests represent the full length shear key configuration with a size of 6-8 inches in depth and 5-6 inches in width. The results from these tests showed that the shear key grout has a strength of 223 psi in direct tension, 358 psi in direct shear, and 620 psi in the four-point flexural test (Sharpe, 2007).

In other studies, four types of grouts were subjected to the tests, summarized in Table A.1, which also show the strengths and permeability of those grouts. The materials that were examined are Set-45, Set-45 Hot Weather, Set grout, and polymer concrete. The results of these tests showed the polymer concrete has the highest strength in direct tension, direct shear, four point flexural, and compression tests (Murphy et al., 2010).

Since the main issue with the grout is tensile strength, fiber concrete was suggested to be a good option (Murphy et al., 2010). Fiber is mainly used to increase tensile strength and control cracking. Adding fiber to concrete, which already has a high compressive strength, would produce a material that has reduced shrinkage and cracking potential. Fiber concrete would be a good alternative to the traditional grouts without fiber.

Table A.1: Mechanical Properties for Grouting Materials (Murphy et al., 2010)

Type of Material	Compressive Strength (psi)	Shear Stress (psi)	Tensile Stress (psi)	Flexural (psi)	Permeability
Set 45	5820	301 - 345	176 - 219	267 - 284	very low
Set 45 Hot Weather (Non-shrink Grout)	5658	285 - 306	198 - 215	447 - 531	very low
Set Grout	7700	330 - 402	197 - 246	601 - 634	Moderate
Polymer Concrete	10810	667 - 748	256 - 330	686 - 850	Negligible

A.2.1.2 Large Scale Tests

One of the major advantages of full-scale tests is to simulate the conditions in the field; therefore, the test conditions tend to be closer to the real conditions. Large-scale tests have some drawbacks and usually are very expensive compared to small-scale tests; however, sometimes these are preferable in order to obtain accurate results for complicated problems.

In 1996, New York Department of Transportation studied the measurement and performance of a full-length shear key joint in adjacent box beam bridges. For full-depth shear keys, the study found almost 23% of bridges exhibited longitudinal cracks out of the entire 91 bridges that were inspected. In contrast, there were 54% of partial shear keys that had longitudinal cracks. In addition, only 5.3% of 874 bridges with full-depth shear keys showed deck cracks (Jyotirmeay Lall, 1998). Therefore, the full-depth shear keys were reported as having better performance, which is obvious due to the larger contact area of the grout material. Fig. A.8 shows the categorized frequency of longitudinal deck cracking.

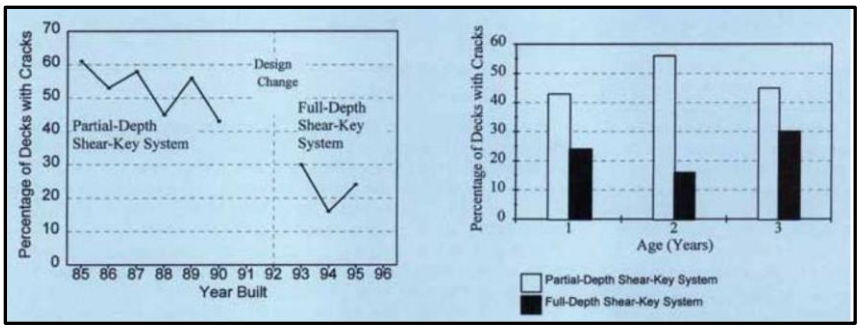

Fig. A.8 Frequency of longitudinal deck cracking (a) By year built (b) By age at the time of inspection (Jyotirmeay Lall, 1998)

In another study, three full-scale adjacent box beams were tested with three different shear key configurations. The first one was the conventional shear key design with grout. The second configuration was the conventional shear key design with epoxy. The third configuration was a new shear key design that was located at mid-depth with non-shrink

grout. These box beams had a length of 75 ft, which is the typical average span length in Ohio bridges. Figure A.9 shows the typical cross section of the tested box beams. Four adjacent box beams were cast, and tests were performed as one unit for each configuration. The loading of each configuration tested was 20 kips, which is equivalent to one wheel of HS20-44 truck plus a 25 percent impact. Hydraulic actuators were used to apply the loading. Figure A.10 shows the schematic of the test configuration and the loading of box beams. (Miller et al., 1998).

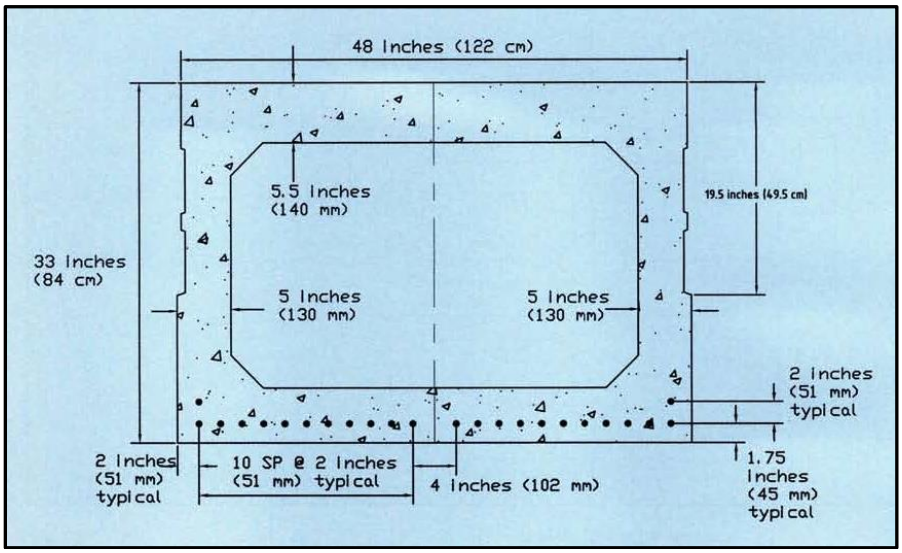

Fig. A.9 The Typical Cross Section for Tested box beams (Miller et al. 1998)

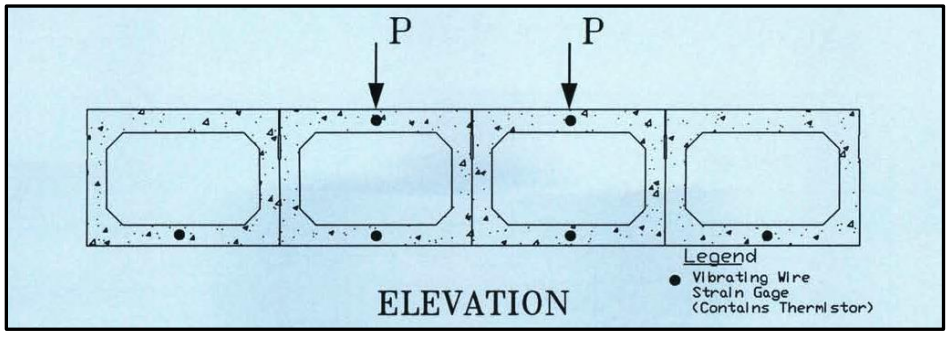

Fig. A.10 Schematic of Test Configuration and Loading of Box Beams (Miller et al. 1998)

Remarkably, the cracks appeared before any physical load was applied to the box beam; and it occurred every time this test was conducted. These cracks were detected by using an ultrasonic pulse velocity technique. The thermal load, due to the change in temperature, was identified as the main reason for initiation of the cracks, and the vehicular loading only propagated these cracks further. A new design with a mid-depth shear key grouted with non-shrinking materials, showed more efficiency in minimizing the cracks under both thermal and physical loading. Another advantage of this design is that the throat was not grouted so it could be wrapped with waterproofing materials to prevent seepage even with cracks

present in the shear key joint. The conventional shear key that was grouted with epoxy exhibited the highest efficiency in this full-scale experiment with no cracks at all under both thermal and physical loadings. Due to the fact that the thermal expansion for epoxy is two to three times that of the thermal expansion of concrete, the shear key resisted the thermal stresses, which were concluded to be the biggest concern. Furthermore, the load distribution data in this full-scale test showed that the load was still distributed horizontally even when cracks were present in the shear key grout. The main concern then is the leakage that reduces the durability of the bridge deck (Miller et al., 1998).

A.2.1.3. ASTM for Grout Material

The compressive strength of the grout material is usually used as an indicator to qualify the grout for the keyway application, and shrinkage and freeze-thaw resistance are also considered for crack control under the severe environmental conditions. A list of ASTM tests related to grouts is shown in Table A.2.

Table A.2: List of ASTM Tests Related to Grouts

#	Test Name	Test #
1	Slant shear bond	ASTM C882
2	Volume change, % expansion	ASTM C 827
3	Volume change	ASTM C-1090
4	Expansion	ASTM C - 157
5	Freeze-thaw resistance	ASTM C666 Procedure A
6	Bond strength, hardened concrete to plastic grout	ASTM C-882 modified
7	Flexure strength - resist vibration	ASTM C-348
8	Bleeding of concrete	ASTM - C232
9	Flexure strength	ASTM - C 78
10	Yield, density, and air content	ASTM - C 138 % C 138M
11	Modulus of elasticity	ASTM C 469, modified
12	splitting tensile	ASTM C 496
13	Punching shear strength	BASF Method

The evaluation of grouts strength was of importance to ODOT to investigate cracks that appear in keyways for the box beam bridges. Current ODOT specification requires that three 3 in. × 6 in. cylinders be made and sent to Office of Materials Management for testing. The minimum required compressive strength of the cylinders is 5,000 psi before allowing construction or vehicular traffic on the structure. However, ASTM specification C1107, "Standard Specification for Packaged Dry, Hydraulic-Cement Grout (non-shrink)" pertains to restrained cube molds. ASTM specification 1107 refers to restrained cube molds. A study was conducted to see if the strength of any of the other methods used is comparable to the strength of restrained cube molds. However, the bond strength between the old concrete

surface and fresh grouts, and the influence of the construction practices was not considered in that study.

A.2.2 Alternative Grouts

A laboratory study by Gulyas (1995) compared component material tests and composite grouted keyway specimens using two different grouting materials: non-shrink grouts and magnesium ammonium phosphate mortars. Comparative composite specimens were tested in vertical shear, longitudinal shear, and direct tension. Results indicate significant differences in performance between the materials. Composite testing of the grouted keyway assemblies, rather than component materials testing, was shown to be a more accurate way to evaluate the performance of the grout material.

The author emphasized that there is no requirement in the specification for important properties of a high quality keyway grout such as the maximum allowable shrinkage and minimum bond strength. The author suggest that polymer modified materials are preferred over cementitious products because of the improved bond to the concrete combined with reduced chloride permeability and the internal self-curing after initial moist curing improved performance in freeze-thaw cycles. The author concluded that composite testing of grouted keyway assemblies provides much more practical information than component testing of the materials. Effects of grouting materials, precast concrete member keyway shapes, curing, substrate exposure, and texture can be evaluated.

A.2.3 ODOT-Approved Grout Material

ODOT requires a non-shrink, non-corrosive, non-metallic cementitious grout material to be used for the application of shear keys. A list of some of the approved grouts and their material properties are shown in Table A.3.

A.3 Transverse Forces

According to Murphy (2010), the enormous amount of live load that bridges carry due to passing vehicles cannot be transferred between box beams through the unreinforced grouted shear key. Transverse reinforcement is needed to transfer such large loads between adjacent box beams. The transverse reinforcement provides compressive normal force in the transverse direction to transfer shear force and moment and to avoid differential deflection between box beams. Figure A.11 shows a typical cross section view of box beams with transverse reinforcement.

A.3.1 Transverse Reinforcement Types

Transverse reinforcement can consist of bonded or unbonded post-tension strands or bars; it can also be bonded or unbonded non-prestressed tie bars. Unbonded post-tension bars are the most commonly type used in the industry.

Table A.3: ODOT QPL Sample Materials

#	Company	Product – Non-shrink, Noncorrosive, Non-metallic Cementitious grout	Flowable Compressive Strength @ 1-7-28 days (psi)	ASTM C827 Early Height Change	Yield per 50 lb (22.7 kg)	Set Time (min)	Expansion - ASTM C-1090 1/7/28 DAYS
1	BASF Building System	Masterflow 928	4,000 / 6,700 / 8,000 flexure 1000 1050 1150	Modulus of elasticity (2.82 / 3.02 / 3.24) * 10E6		180 / 300	0 : 0.3 %
		Construction grout					
2	Bonsal American	Prospec F-77 constrtuction grout	2,500/5,700/7,000			270/450	
3	Chem Master	kemset	4,400 / 7,400 / 8,300	0.90%	0.43	42 / 117	
		Conset grout	2,590 / 5,260 / 6,870	1.20%	0.43	132 / 210	
		Gorilla grout	3,870 / 8,740 / 10,400	1.70%	0.45	165 / 240	
4	Conspec Marketing &Mfg.Co	Endure 50 grout	4500/5800/8000		0.43		
5	Dayton Superior Corp	Sure Grip high performance grout	5,000/8,000/1,0000		0.42		0 : 0.3 %
		Sure Grip utility grout					
		Advantage Grout	2,500 / 6,000 / 8,000		0.43		0 : 0.3
6	Euclid Chemical	N-S Grout	4,500/6,000/8,500		0.45	185 / 287	0.01 , .03 , .05
7	Kaufman Product Inc	Sure Grout - 106	2,400 / 6,400 / 7,600	0.68% (C - 157)	0.45	240 / 300	
8	Kuhlman Construction Products	Kuhlman 1107 grout	3,300 / 6,200 / 7,000				None / none / none
9	L&M Crystex	L&M CRYSTEX	4,600 / 8,160 / 1,0150			300 / ---	0.02%
		Duragrout	2,300/7,000/8,300				
10	Nox Crete Product Groups	NoxCete Construction Grout	3,300/6,200/7,000		0.4		None / none / none
11	Quickrete	Quickrete Non-Shrink Precision Grout	3,000/9,500/12,500	0.40%	0.45		0 : 0.2%
		Non-shrink General Purpose Grout	3,000 / 8,000 / 9,000	0.30%	0.45		0 : 0.2%
12	Sika Corp	Sikagrout 212	3,500 / 5,700 / 6,200			240 / 390	
13	SpecChem	SC PRECISION GROUT	3,500 / 7,600 / 10,275				0.03 , 0.03 , 0.03
14	Vexon Chemical	Certi - Grout 1000	4,025 / 7,700 / 10,250				0.05%
15	W R Meadows, Inc	Sealtight 558-10k	4,500 / 6,500 / 9,200		043 : .64	180 / 300	0.1 : 0.13 : .14
		sealtight CG-86	3,000 / 5,500 / 7,000		0.43		

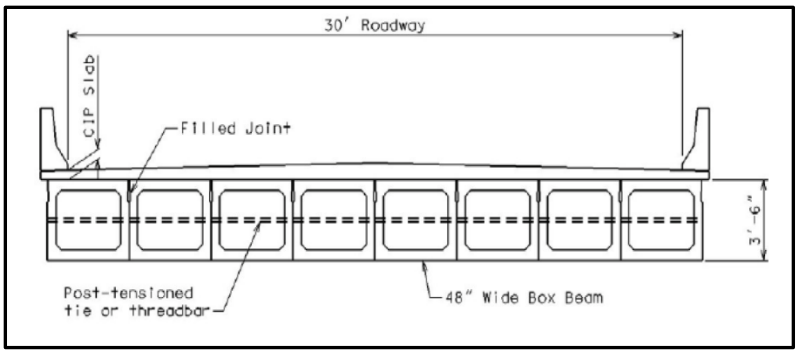

Fig. A.11 Typical Section of Box Beam with Transverse Reinforcement (Murphy et al., 2010)

The location and effective forces in the transverse reinforcement can significantly affect the behavior of the shear key. The shear key may act as a hinge or as a fixed joint that transfers the moment. Some design codes such as Ontario Bridge Design assume that the entire force is carried only by the transverse reinforcement; therefore, the flexural rigidity of shear key is neglected. In the United States, some transportation agencies assume that the shear key carries both shear and moment. One of these agencies is the Michigan Department of Transportation, which uses a structural slab and two layers of transverse post-tension in full-depth shear keys to develop moment-transfer connectors. In Japan, heavy transverse post-tension is used in a very wide and deep shear key and the grout is a regular cast-in-place concrete. This method has been also used in South Korea, but with a partial depth shear key. The idea of using regular cast-in-place concrete is really helpful due to the strength of the concrete, but it needs a wider opening at the top of the shear key and may result in delays in the construction process (Murphy et al., 2010).

A.3.2 Transverse Reinforcement Design

Transverse reinforcements mainly work as diaphragms that transfer the load in the transverse direction. An improper design for transverse reinforcement may lead to cracks in the grouted shear key. The amount of reinforcement suggested by the PCI Bridge Design Manual is shown in Fig. A.12.

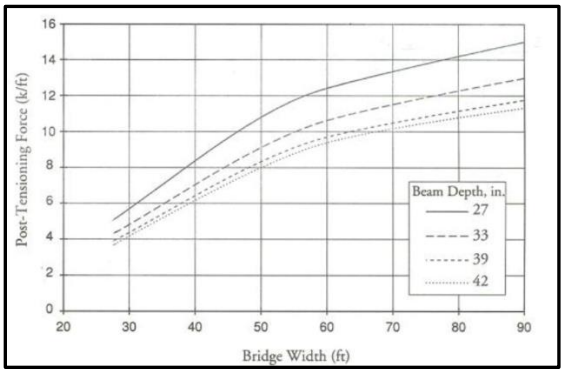

Fig. A.12 PCI Suggested Post-Tension Reinforcement (PCI Committee on Bridges, 2009)

Post-tension reinforcement is common, but it has some disadvantages and limitations. Post-tension reinforcement is difficult to design and construct in skewed bridges. In addition, the post-tension reinforcement is extremely sensitive to corrosion, which is a huge concern because any section loss leads to a severe reduction in strength. As a result, the main function of the transverse reinforcement is affected and the span would not work as one unit. Alternatively, using steel bars for reinforcement is another option, but less efficient even though its use has a lower risk of capacity loss when corroded (PCI Committee on Bridges, 2009). Figure A.13 shows the bar details in shear key between box beams.

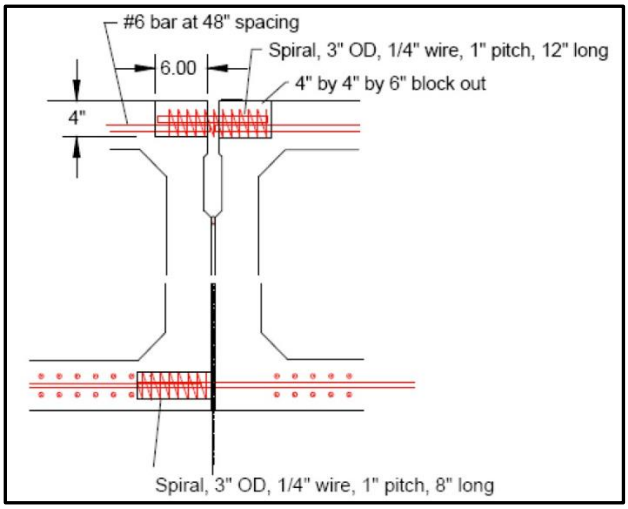

Fig. A.13 Rebar Details in Shear Key Between Box Beams (PCI Committee on Bridges, 2009)

During construction, the transverse reinforcement is installed after the box beams are set on the bearings. Transverse reinforcement passes transversely through adjacent box beams arranged side-by-side for the purpose of locking the beams together. Transverse reinforcement can be placed either before or after the grouting.

A.3.3 State of Practice for Box Beam Bridges (PCI Committee on Bridges, 2009)

Information on the state of practice of the box beam bridges was gathered primarily from a survey of state highway agencies through the AASHTO Highway Subcommittee on Bridges and Structures, and a review of the *AASHTO LRFD Bridge Design Specifications*. The locations for the ties used by various agencies were at the ends, mid-span, quarter-points, and third points, depending on the number of ties. About 70% of the respondents reported that the ties were placed at mid-depth. If two strands or bars were used at one longitudinal location, they were placed at the third points in the depth. Other responses included specific location depths. Figure A.14 shows the relative frequency of use of different types of transverse ties.

In the design criteria for connections reported by Russell (2011a), 81% percent of states and 89% of the respondents to the survey stated that they did not perform any design calculations to determine the number of transverse ties between box beams. Some

respondents provided information about the post-tensioning force used for each transverse tie and the spacing of ties. Based on this information, the average transverse force per unit length along the span for various numbers of ties was calculated. Figure A.15 shows the results for 11 states. Where a single horizontal line is shown in the figure, the value is based on the specified maximum spacing between ties. If the ties are closer than the minimum, the force will be higher than shown in the figure. Some states presented a range of forces as these states used a fixed number of ties for a range of span lengths. These are shown in Figure A.15 as a vertical band of color. A design chart to determine the required effective transverse post-tensioning force is provided in the PCI bridge design manual 4. This chart is based on the work of El-Remaily et al.

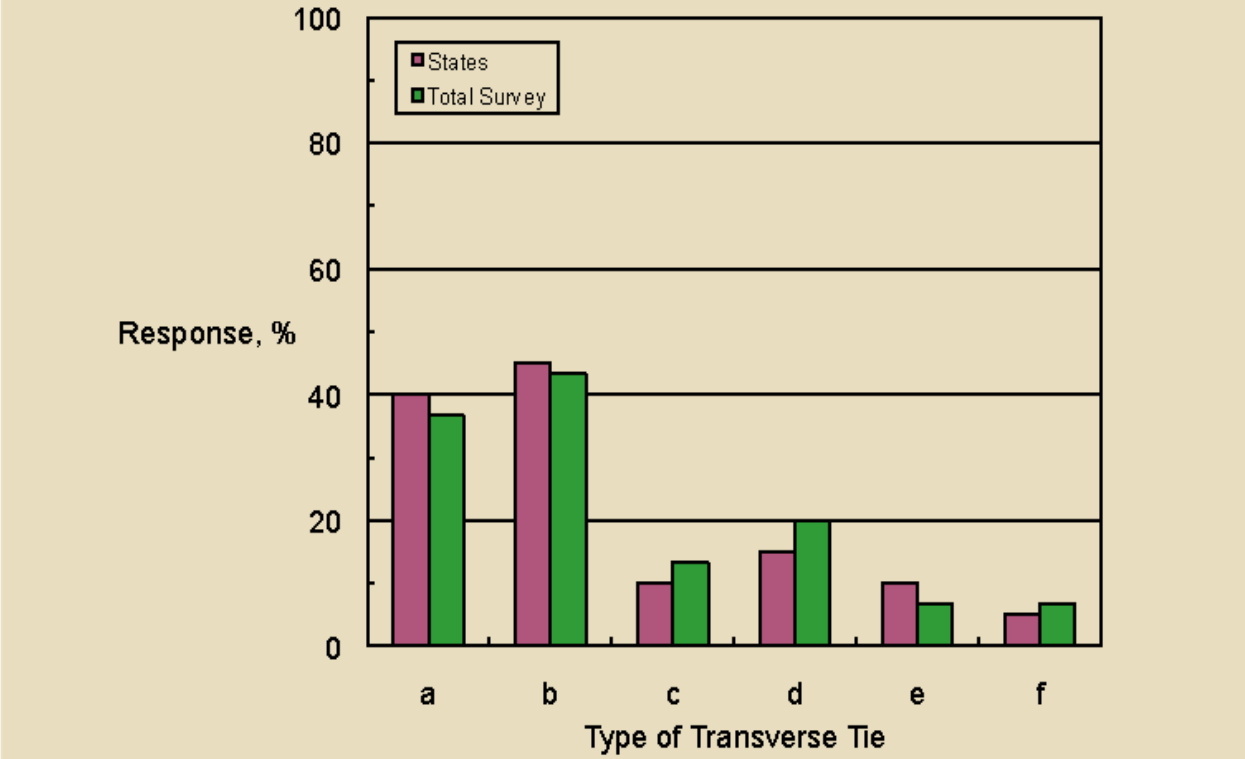

Figure 9. The most common types of transverse ties consist of unbonded post-tensioned strands or bars. Note: a = transverse unbonded post-tensioning strands; b = transverse unbonded post-tensioning bars; c = nonprestressed unbonded reinforcement; d = transverse bonded post-tensioning strands; e = transverse bonded post-tensioning bars; f = nonprestressed bonded reinforcement.

Fig. A.14 The Use of Transverse Ties (Russell, 2011).

A.3.4 ODOT-Standard for Transverse Force

ODOT requires a one-inch-diameter tie-rod through a two-inch hole in the transverse direction through the beams to provide a normal force of 15 Kip, which results from torque of 250 kip-ft. The transverse forces are usually applied to the box beams at the diaphragms after placing the beam assembly on the bearing pads at the bridge location but prior to grouting, the transverse forces do not generate any compression on the grouted joint.

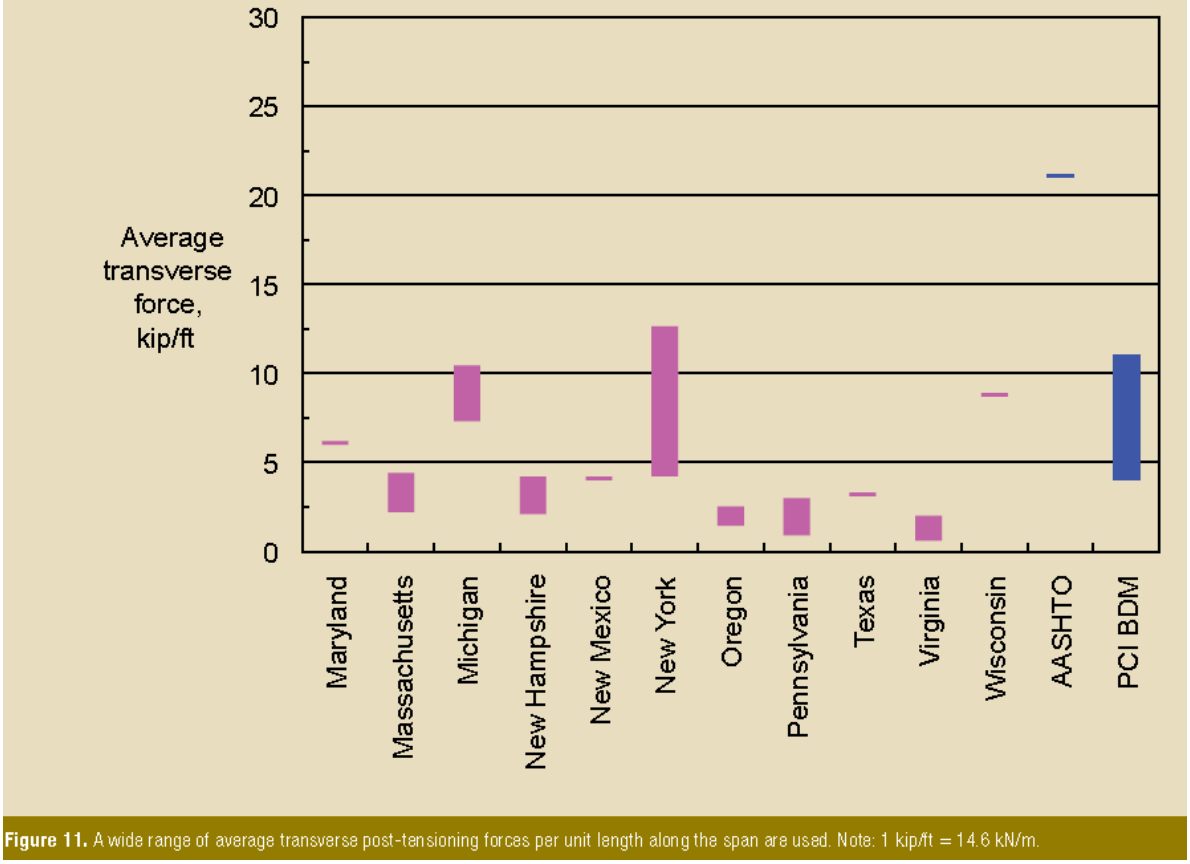

Fig. A.15 Average Transverse Force (Russell, 2011).

A.3.5 Studies of Transverse Forces

Using finite element analysis of three adjacent box beams with two end diaphragms and three intermediate diaphragms, the tie rod forces were applied at each diaphragm location as shown in Fig. A.16. The effect of the transverse forces was found to be very local at the diaphragm locations (Russell, 2011).

The current practice of ODOT requires one tie-rod at the top third of the girder height that might act as a rotational pin. A better application of tie rods is given by PCI (2009) where two tie rods are used to prevent separation under tensile stresses, as shown in Fig. A.17. In "direct" vertical shear, the increase of the load will reduce the friction contribution due to lateral separation and vertical slip, unless the concrete blocks are supported in the horizontal direction to maintain full surface contact. This is common practice in the case of precast-prestressed box beam girders used in bridge design when ties or horizontal prestressing strands are used to provide horizontal support in the case where ties are used or to provide lateral compression in the case where tension prestressed strands are used. The tie elevation and the compressive force applied to the box beams will influence the friction contribution and width of the crack between the units.

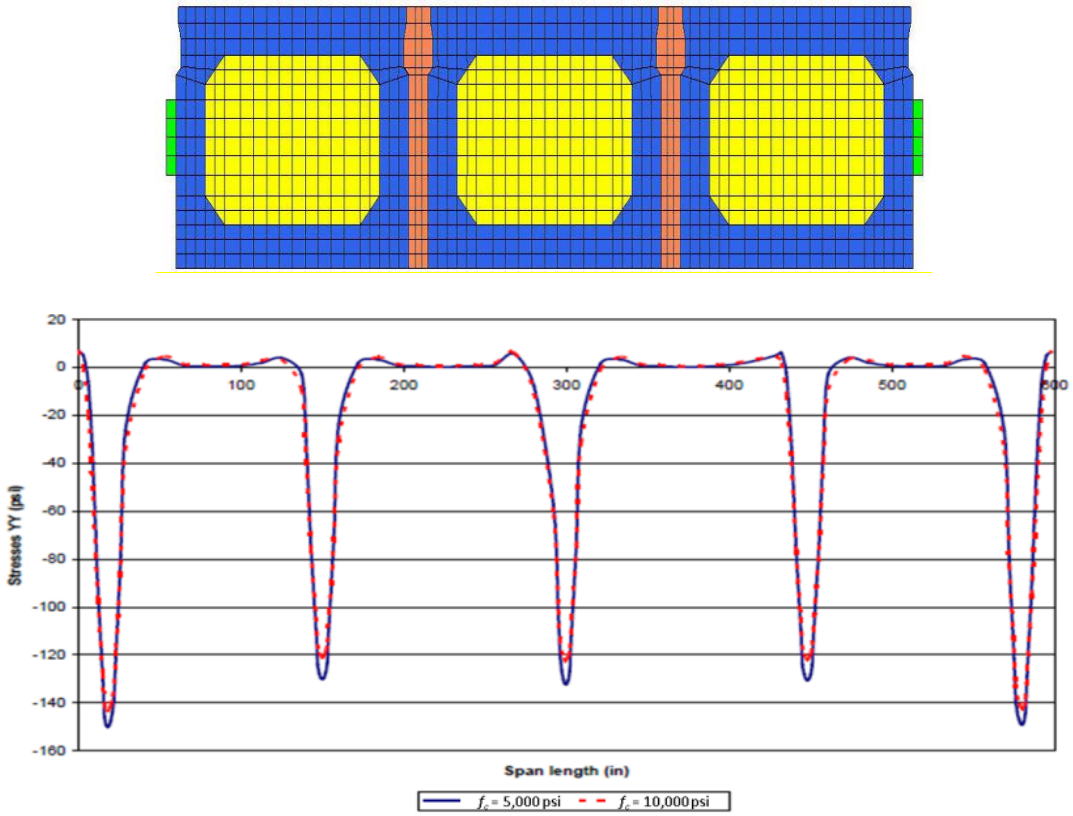

Figure 7-3. Clamping stress along the length of shear key for different grout materials (Note: stresses are taken at mid-depth of the beam)

Fig. A.16 Beam Cross Section (Top), Clamping Stress along the Length of Shear Key (Bottom) (Russell, 2011)

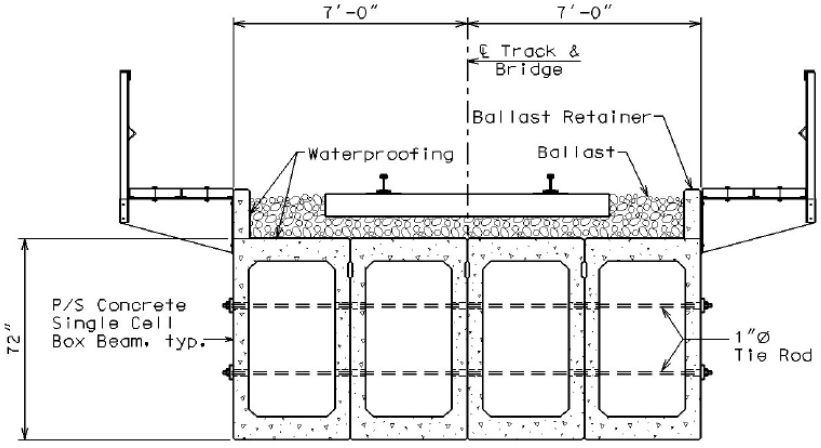

SINGLE CELL BOX GIRDERS

Fig. A.17 Ties in Box Beam Bridges (PCI, 2009)

A.4 Residual Strength of Deteriorated Box Beams

The residual strength of deteriorated box beam bridges is a great concern for public safety and was tested by many researchers. Two 54-ft box beams [36 in. wide × 27 in. deep] were removed and subjected to load tests after being in service for 27 years. The first beam was removed from the center of the bridge with no signs of deterioration, and the second beam showed minor concrete cracking and spalling (Chandu et al., 1991) the measured ultimate flexural strength exceeded the required strength at factored loads. The load-deflection response closely followed the predicted response.

A severely distressed fascia two-cell box beam from the Hawkins Road Bridge in Jackson County, Michigan was removed and tested. The bridge was found to be safe to operate in these conditions (Upul et al., 2005), Figure A.18 shows the underside of the bridge (left) and the top surface of the bridge (right).

Fig. A.18 50-Year-Old Tested Two-Cell Box Beam (Upul et al., 2005)

Fatigue tests were conducted to 27-year-old box beams (Rao et al., 1996) that were removed from a deteriorated multi-beam bridge and subjected to fatigue loading. Visually, the beams appeared to be in good condition but showed signs of water leaking through the longitudinal shear keys and some corrosion of reinforcements. One beam, cycled to a nominal bottom tension stress level of $6\sqrt{f_c'}$ retained excellent performance after 1,500,000 cycles. The other beam was loaded to reach $9\sqrt{f_c'}$; the strength was reduced and fatigue failure occurred after 145,000 load cycles.

Minor signs of deterioration, cracks, water leaking stains, and spalling of concrete cover was noted on the underside of box beams. Testing T-beam girders and I-shaped girders after 27 to 50 years of service showed that the minor deterioration did not affect the flexure strength or the ductility of the girders under service loads, the prestress losses are within the AASHTO predictions for effective prestress forces (Shenoy, 1991; Tabatabi, 1993; Halsey, 1996; Pessiki, 1996; Rao, 1996; Eder, 2005; Czaderski, 2006; Attanayake, 2011). Corroded and snipped strands reduce the load carrying capacity by up to 50 percent (Steinberg, 2011).

A.5 Rehabilitation of Box Beam Girders

It is convenient to replace deteriorated box beam girders at a reasonable cost in a short time as reported by the State of Ohio (Wood, 2008). Two girders were replaced at bridge MOT-35-1.55, located on Route 35 in Jackson township, Montgomery County, Ohio. The visual inspection of the bridge indicated the need for rehabilitation Fig. A.19, the cost for the possible treatments were estimated as shown in Table A.4.

Table A.4: Cost Estimate to Maintain Deteriorated Box-Beam Bridge (Wood 2008)

Cost Estimates		
Option	Preliminary Estimate	Estimate with Inflation
New Non-Composite Superstructure	$174,606	$221,565
New Composite Superstructure	$200,286	$254,151
Replace Beams 5 and 6	$54,433	$69,072
Repair Beams 5 and 6	$55,266	$70,129
Repair and Strengthen Beams 5 and 6 with FRPC	$77,000	$97,709

Fig. A.19 Box Beam Deterioration

In one week and at a $100,000 cost, the two middle girders on the bridge were replaced (as shown in Fig. A.20) and no signs of deterioration appeared in the bridge after one year following replacement (Fig. A.21).

Fig. A.20 Removing the Deteriorated Beam

Fig. A.21 One Year after Replacement

A.6 Dimensional Tolerances and Construction Practices

The poor performance of keyway grout and joint details were of interest to researchers and practitioners. Joint detailing does not usually receive the required attention in bride designs with box beams. This issue was raised by Nottingham (1995) because the intended joint design cannot be achieved due to construction tolerances as shown in Fig. A.22. The author emphasized that the details are as important to construction as they are to the required design performance. Often overlooked, the precast concrete element tolerance can lead to improper joint fit and incomplete grouting. Some of the problems exhibited by joint details can be seen by the illustration; joints are never full strength and can be much weaker than envisioned by the designer.

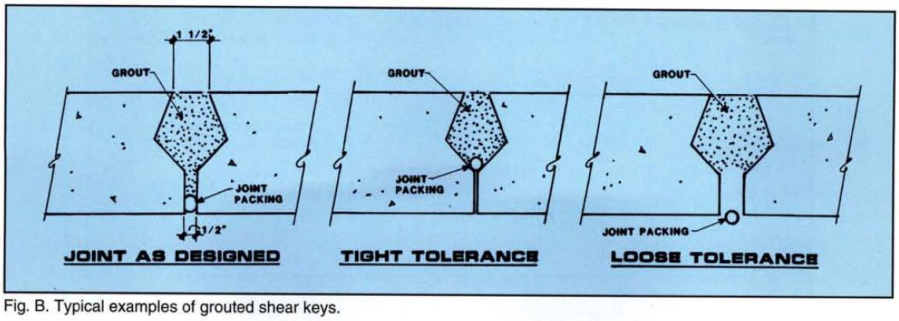

Fig. B. Typical examples of grouted shear keys.

Fig. A.22 Allowable Dimensional Tolerances Effect (Nottingham, 1995)

The author proposed that the joints in Fig. A.23 be sufficiently large to handle panel tolerance and ensure maximum construction speed with full grout-to-panel contact. The author strictly highlighted that the bond capacity of grout will be greatly diminished if the grouting process did not follow strict instructions: the precast surface must be sandblasted and pressure washed just prior to grouting, and the grout should be thoroughly mixed with the minimum required mixing water for placement; otherwise, the delicate grouting operation will turn into a short of controlled chaos.

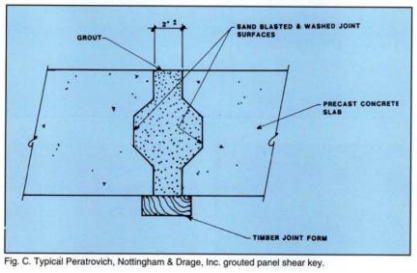

Fig. A.23 Recommended Design (Nottingham, 1995)

A.7 Bearings

For precast prestressed adjacent beam bridges, the bearing is typically made of neoprene pads. Laminated neoprene pads are typically used for long and heavy beams, and plain pads are used for short and light beams (PCI, 2009). In box beam bridges, there are two alternative support configurations: 1) two-point supports where pads are located centrally under the box beam, 2) two box beams share one pad. The main objective of the second alternative is to reduce the relative deflection between two adjacent box beams. Figure A.24 shows the two bearing pad alternatives (Murphy, et al., 2010).

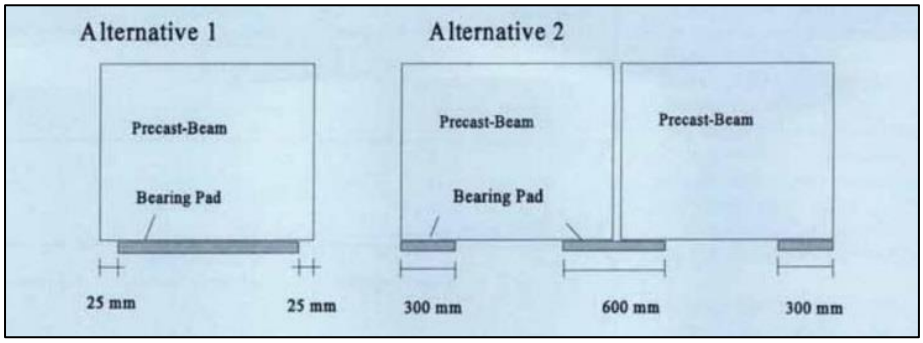

Fig. A.24 Bearing Pads Alternatives (Murphy, et al., 2010)

A.8 PCI Box Beam Design

The widely used PCI adjacent box beam design comes with a full depth shear key. It comes in two standard widths (3 ft and 4 ft) and three standard depths (27 in, 33 in, and 39 in.). Figure A.25 shows a typical PCI box beam section. The PCI adjacent box beam design is used for different span lengths which affects the geometry of the section. The typical span lengths

provided by PCI are showed in Table A.5 PCI adjacent box beam design is adopted by ODOT and has been studied using the finite element method (Sharpe, 2007).

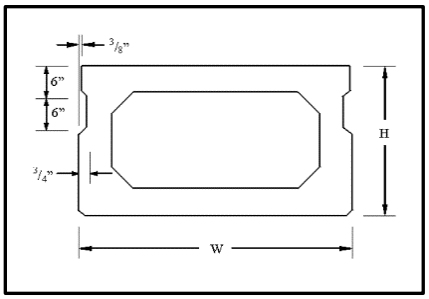

Fig. A.25 Typical PCI Box Beam Section (Sharpe, 2007)

Table A.5: PCI Box Beam Typical Spans (Sharpe, Reflective Cracking of Shear Keys in Multi-Beam Bridges, 2007)

Section Name	Depth	Short	Medium	Long
BI	27	40	60	70
BII	33	50	65	85
BIII	39	60	65	100

A.9 Loading

The moving load applied to a bridge model is generally the HL-93 pattern recommended by the American Association of State Highway and Transportation Officials (AASHTO) for design purposes. The HL-93 pattern represents a heavy tractor-trailer that has three axles with two wheels each. According to the AASHTO specifications, the truck load should be located on the point that causes the maximum stresses to the deck section. The critical positions are at the mid-span and near the supports. Figures A.26 and Fig. A.27 show schematics of critical truck locations on a two-lane bridge (Sharpe, 2007).

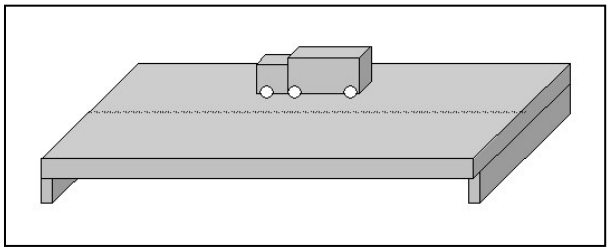

Fig. A.26 Truck at Mid-Span Location (Sharpe, 2007)

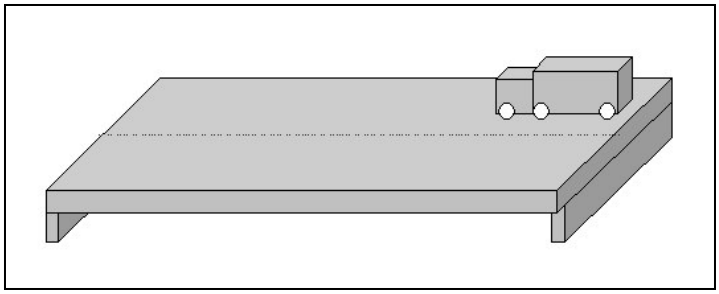

Fig. A.27 Truck at End of Span Location (Sharpe, 2007)

Figure A.28 shows the wheel locations for a two-lane bridge. Figure A.29 and Fig. A.30 show the wheel locations for a three-lane bridge. The locations of the wheel loads were based on AASHTO standards. In order to find the maximum stress locations, the truck axles were moved across the entire length of the bridge. Strangely, the maximum tensile stress was discovered near to the shear key, not directly on top of it. (Sharpe, 2007).

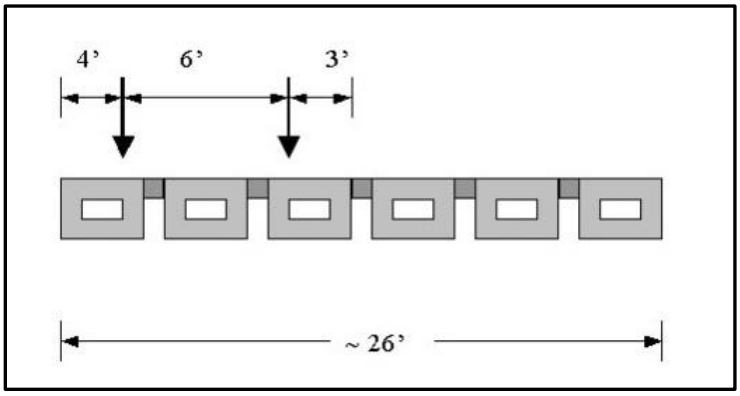

Fig. A.28 Truck Axle Location on a Two-Lane Bridge (Sharpe, 2007)

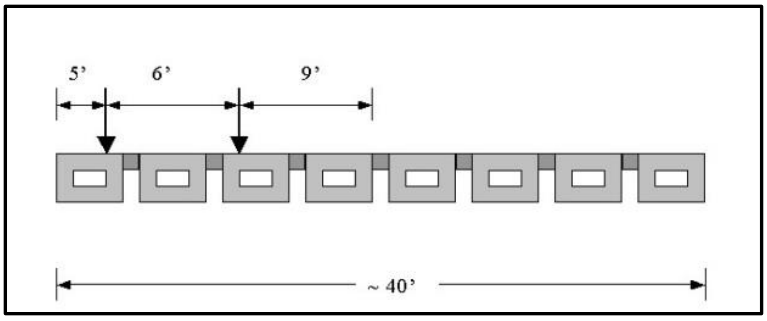

Fig. A.29 Truck Axle Location on a Three-Lane Bridge, Lane 1 (Sharpe, 2007)

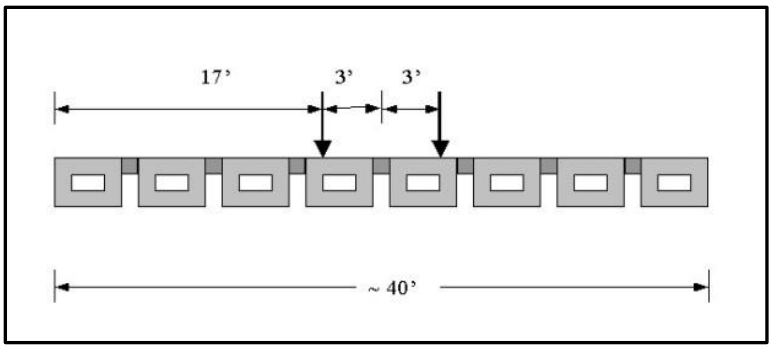

Fig. A.30 Truck Axle Location for a Three-lane bridge, lane 2 (Sharpe, 2007)

A.9.1 Secondary Loading

Initial shrinkage and temperature loading were the secondary loading types that were applied to the model. Shrinkage can occur due to many reasons such as a change in temperature during the curing time, loss of water due to ambient temperatures, and chemical reactions on concrete. Generally, the grout is a non-shrink material. (ASTM) provides the non-shrink grout specifications in ASTM C 157. These specifications can be achieved by incorporating special additives. According to ASTM C 157, the grout can pass the test only if the grout never loses any volume during the specified time. When shrinkage effects are not addressed, the concrete members without reinforcing steel can be subjected to residual stresses. Large tensile stresses can be imposed in a restrained shrinkage condition. Figure A.31 shows a schematic of the effect of restrained shrinkage in a uniaxial specimen (Sharpe, 2007).

The typical shrinkage strain of a non-reinforced concrete member is between 400 and 700 microns. Therefore, the value of shrinkage for the grout that was applied in the model was 500 micron, which is appropriate compared with the value used in other studies conducted on this topic. For box beams, the shrinkage was assumed to be zero since the beams had already reached the ultimate shrinkage before they are installed on the bearing pads. However, the shrinkage strain that was applied to the slab was conservative. Table A.6 shows the values of shrinkage and their converted temperatures (Sharpe, 2007).

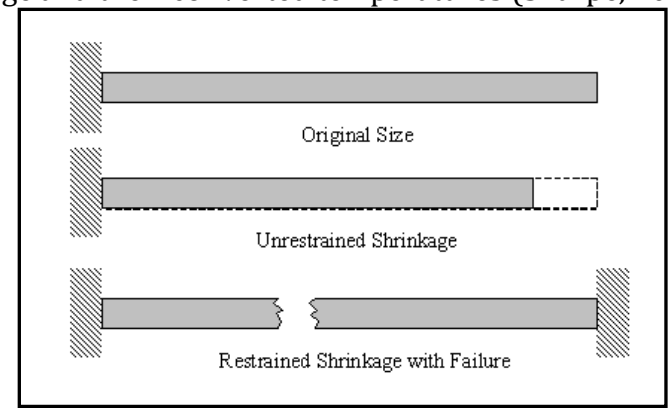

Fig. A.31 Schematic of Shrinkage Effects (Sharpe, 2007).

Table A.6: Shrinkage Loads Applied to Bridges (Sharpe, 2007)

Category	Shrinkage (in/in)	α (in/in/deg F)	Temp (deg F)
Prestressed Box Beam	0	5.5E-06	0
Unreinforced Shear Key	-0.0005	5.5E-06	-91
Reinforced Concrete Slab	-0.0002	5.5E-06	-36

α = thermal expansion coefficient.

The actual shrinkage on the surface of a structural member may be different on the inside the member. The top face may dry faster than the internal locations; therefore, each piece of the shear key may experience different shrinkage rates. Nevertheless, it was assumed that the shrinkage is consistent throughout the entire concrete member (Sharpe, 2007).

According to AASHTO specifications, a thermal gradient load was applied in two cases: a positive thermal profile and a negative thermal profile. Figures A.32 and A.33 show the positive and negative temperature profiles for thermal gradient loads.

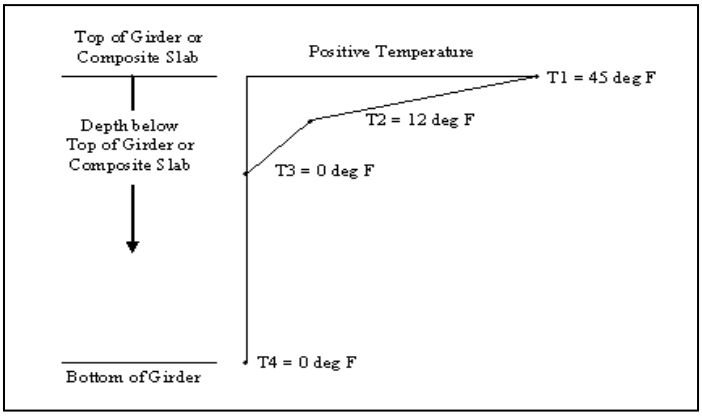

Fig. A.32 Positive Temperature Profile for Thermal Gradient Load (Sharpe, 2007)

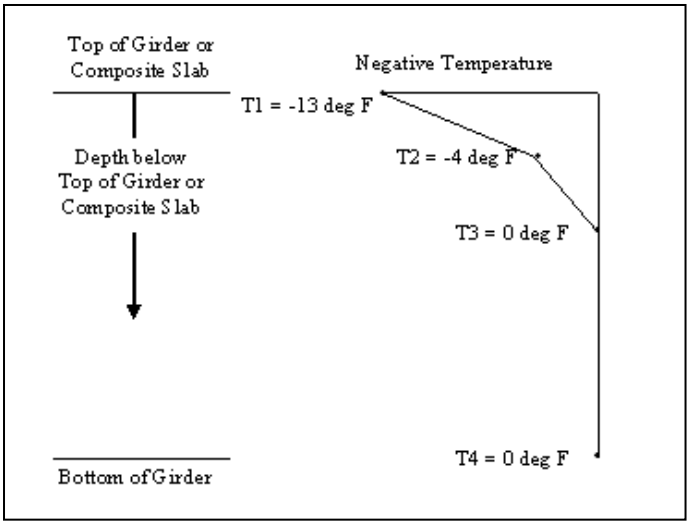

Fig. A.33 Negative Temperature Profile for Thermal Gradient (Sharpe, 2007)

Sharpe's (2007) results showed that PCI adjacent box beam bridges have shear keys that can transfer vehicular loading safely and effectively. The AASHTO HS-25 design truck loading is not producing an amount of stress sufficient to create cracks, especially near the ends of the bridge. In contrast, secondary loading effects, shrinkage and temperature, show much higher stresses than those from vehicular loading. The applied temperature gradient as specified by AASHTO leads to huge tensile stresses that cause cracking in the shear keys. Likewise, shrinkage loading causes cracking to develop in the shear key and the composite slab (Sharpe, 2007).

The results also showed that the most important factors are shear key size and section depth. The number and locations of the bearing pad supports and the presence of a composite slab are also important. The span length is a less important factor for the transverse stresses. The use of post-tensioning shows some improvement for the tensile stresses in the shear key. Also, the full depth shear key exhibits some improvement in tensile stresses. Some of these conclusions are confirmed in the results of other studies that used different methods (Sharpe, 2007).

A.9.2 Eccentric Load Effects

When barriers and curb slabs are assembled with the exterior beams in bridges, an asymmetric cross section should be considered in the box beam design. The effects of this eccentric loading in the transverse direction of the bridge assembly was studied by Kasan and Harries (2013), in which the researchers proposed a relationship to determine the capacity of the facial beams. The possibility of eccentric truck loading on an individual beam suggests out of plane moment and normal stresses on the keyway joint.

A.9.3 Environmental Stresses

Shear key evaluation by testing girders under cyclic loads and environmentally induced loads were performed by Miller (1998) in a three-phase test program as follows: (a) testing of the current keyway details using the currently specified non-shrink grouts, (b) testing the current keyway details using epoxy grout, and (c) testing of modified keyway details using non-shrink grout in which the keyway was moved to the neutral axis of the girder. The author concluded that the epoxy grouts are most resistant to cracking. The keyways experienced some cracking when placed at the neutral axis but were more resistant to cracking than the current ODOT standard grouts, all cracks seems to be thermally induced. A summary of the test plan in by Miller (1998) is presented in Table A.7.

Table A.7: Test Program for Keyway Evaluation (Miller, 1998)

#	Keyway geometry	Grout material	Load (89 kips)	Loading cycles	Grout time	Initial Cracks
1	Currently specified at top	Non shrink grout	(HS20 - 44)	41,000	Late autumn November	• Appeared soon after casting before loads were applied with large changes in strains due to freezing • No new cracking occurred due to loading; cracks caused by temperature propagated
2	Currently specified at top	Epoxy grout	(HS20 - 44)	1,000,000	Summer	Cracked due to heat-induced loading with deformation and transverse strains in the keyway
3	Keyway at neutral axis	Non shrink grout	(HS20 - 44)	1,000,000	Late summer	Thermal stresses caused minimal stresses at the abutment; only one crack propagated with length = 3.25 ft
	Currently specified at top	Epoxy grout	(HS20 - 44)	1,000,000	Early spring April	No cracking occurred in the keyways during the grouting process nor during cyclic or environmental testing

A.10 Summary

The structural performance of the bridge deck in adjacent box-beam bridges depends on the integrity of adjacent beams, which should act together as one unit under traffic loading. Shear keys are formed between adjacent beams to connect these beams to form a bridge deck. Key way geometry, grout material, transverse forces, end support connections, and traffic and environmental loads are the main influencing factors for the joints formed between adjacent beams. The effectiveness of waterproofing of key way joints in adjacent box beam bridges depends on these factors. The use of post-tensioning shows improvement of the joint and the shear key performance. Eccentric loading can cause shear and tensile stresses on the joints in adjacent box beam bridges and can increase joint cracking.

A.11 Waterproofing Systems

A waterproofing membrane is needed for non-composite box beam bridges to prevent water leakage through the longitudinal joints between adjacent box beams. Typical damage is often recorded throughout the longitudinal joints and especially at the abutment locations of simply supported box beams. A summary of the efforts by other researchers in the past focused on waterproofing membranes is reported in this section.

A.11.1 Background

The use of protective membranes at the top of the deck to prevent moisture and chlorides from penetrating the concrete is common for adjacent box beam bridges. When studying the durability of a bridge, the concrete deck is commonly the most susceptible element and can be the restrictive factor affecting the service life. In general, a protective system is often provided to enhance the durability for both new and existing bridge decks. In cold states where deicing salts are used, bridge deck deterioration is a serious concern. Deicing salts are passed along with water through permeable concrete to the reinforcement, which would accelerate the corrosion process. Moreover, chlorides and moisture seeping through cracks, which provide a continual path to the reinforcing steel, can also be destructive. Spalling can occur in the concrete as a result of the increase in the volume of reinforcement steel due to corrosion. The loading capacity of the bridge and riding quality are negatively affected due to this type of deterioration (Frosch, Kreger, & Strandquist, 2013).

A.11.2 Introduction

According to Russell (2011), a waterproofing membrane is defined as a thin impermeable membrane that is used in combination with a hot-mix asphalt wearing surface to protect the deck concrete from penetration of water and deicing salts. Waterproofing membrane systems have been used to protect the concrete on a deck slab from freeze-thaw induced deterioration and essentially to defend the embedded steel reinforcement against corrosion. In several New England states, transportation agencies began using membranes to prevent deterioration of concrete beneath asphalt surfaces. Elsewhere in the United States, waterproofing membrane systems have been used since 1972 as part of the Federal Highway Administration (FHWA) requirements to protect bridge decks against corrosion (Manning, 1995).

Corrosion-related deterioration is one of the most widespread problems that can affect the durability of concrete bridge decks. Concrete itself and steel rebar and/or strands can be damaged in the case of moisture and chloride intrusion. In fact, proper use of waterproofing systems can extend the life of the structure and delay major bridge deck maintenance. The most common types of deterioration that concrete can face are spalling, cracking, and scaling. Spalling is considered a dangerous deficiency due to the high potential for corrosion of the reinforcing steel and/or strand underneath it. Maintaining the durability of concrete bridge decks is still a big challenge due to the nature of steel reinforcement corrosion. One of the primary causes of deterioration is the accumulation of water between the waterproofing materials and the bottom layer of the asphaltic concrete. Other causes of deterioration are the presence of large temperature changes during freezing and thawing, as

well as frequent build-up of hydraulic pressure from cyclic vehicular loads. As a result, the waterproofing material becomes weak and the bond between the asphaltic concrete and the waterproofing material is lost. This leads to water leakage through the joint, and the bridge deck may be exposed to moisture and chloride intrusion that attack the concrete and reinforcement (Russell H. G., 2011).

One of the challenges in terms of protecting bridge decks is the exposure of the horizontal surface of the deck to a large amount of deicing salt during winter seasons. Table 2.1 shows chemicals that might be used by transportation agencies during winter seasons to maintain the operation of roads and highways. Due to the horizontal profile of bridge decks, drainage from the deck becomes difficult and slow. Moreover, bridge decks face very heavy cyclic loading, which aggressively enlarges the cracks that allow seepage of chlorides into the concrete. Furthermore, thermal loading is another cause of initiation and propagation of cracks in asphalt and concrete layers that have unequal thermal behavior.

Table A.8: Chemicals Used Winter Maintenance (Froch, et al., 2013).

	NaCl			CaCl					MgCl	
Agency	NaCl	NaCl Brine	NaCl Inhibited	CaCl	CaCl Inhibited	Complex Cl	CMA	Kac	MgCl	MgCl Inhibited
California DOT	x	x					x			
Connecticut DOT		x								
Idaho TD	x			x	x				x	x
Illinois DOT	x	x		x						
Indiana DOT	x	x			x					x
Maryland State Highway Admin	x	x		x				x	x	x
Minnesota DOT	x	x		x			x	x	x	x
Missouri DOT	x	x		x						
Montana DOT										x
Nebraska DOT	x			x				x	x	x
Nevada DOT	x	x								x
Oregon DOT							x			x
Washington DOT			x		x	x	x			x

A.11.3 Waterproofing Membrane Systems

The membrane is one of the components of the waterproofing system and mainly works as a barrier that is typically located on the top of the concrete surface of the bridge deck and is covered by a strong material that functions as the driving surface. Primers and sealants are used as bonding agents to secure the membrane to the bridge deck. Inadequate implementation of any component can result in poor performance of the system as a whole.

Waterproofing membrane systems are divided into two main categories. First is the construct-in-place system, including bituminous and resinous liquid-sprayed systems. Of these, the bituminous system is the most frequent material used in practice. Second is the preformed membrane system, which is divided into asphalt-impregnated fabric, polymer, elastomer, and asphalt laminated board systems. Asphalt-impregnated fabric has been the most common material used in the industry for preformed membrane systems for the last few decades (Manning, 1995).

A.11.4 The use of waterproofing membrane in US

The use of the waterproofing membrane systems has changed in many highway agencies in recent times. According to a national survey done by Russell (2011), thirty-four out of thirty-five responding agencies stated that they have used waterproofing membranes on concrete bridge decks since 1994. Three departments of transportation have stopped using the waterproofing systems. Four departments of transportation are still using the waterproofing membrane systems, but only on new concrete bridge decks. Eleven departments of transportation use the system only for existing bridges, and sixteen highway agencies have continued using the waterproofing membrane systems for both new and existing bridges. Figure A.33 shows the current use of waterproofing membrane systems. Figure A.34 shows the historical use of waterproofing membrane systems from a 1992 survey of many agencies in the United States.

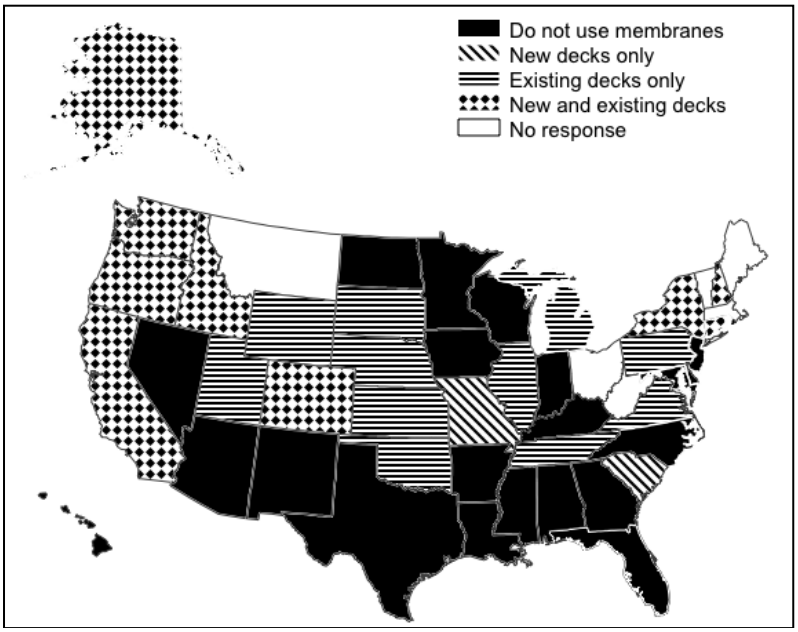

Fig. A.33 Current Use of Waterproofing Membrane Systems (Russell H. G., 2011)

The highway agencies that stopped using waterproofing membrane systems responded to the survey with their reasons for discontinuing. Agencies reported that they had experienced insufficient performance of waterproofing membrane systems, or they began to use some alternative protection strategies such as concrete overlays or full-depth low permeability concrete. Some agencies reported that they do not use waterproofing membrane systems in order to make the inspection easier, since using waterproofing may hinder the inspection of the deck surface. The majority of departments of transportation have continued to use waterproofing membrane systems and have expanded their use in both new and existing bridges for maintenance purposes.

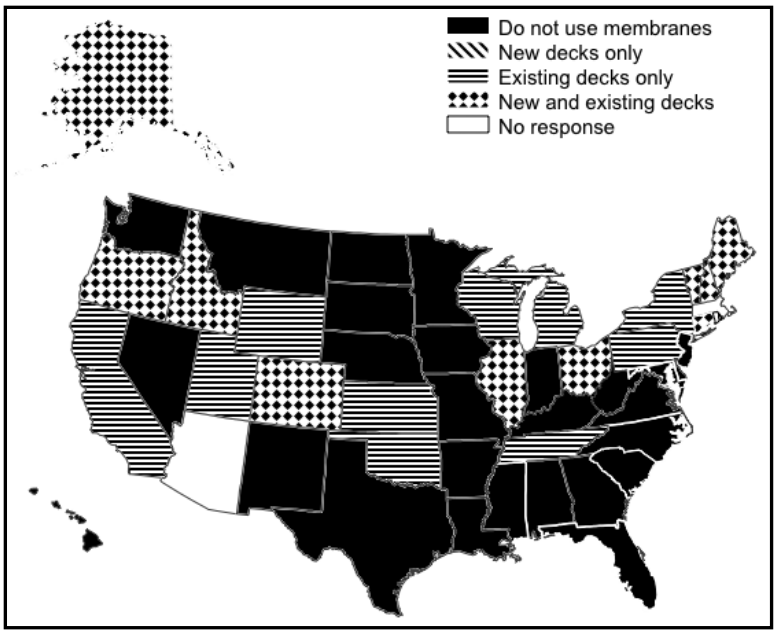

Fig. A.34 Historical Use of Waterproofing Membrane Systems as of 1992 in the United States (Russell H. G., 2011)

A.11.5 Materials

Since 1994, at least 32 different proprietary products from 19 different companies in United States and Canada have been used as waterproofing membrane systems. Based on the nature of the application, the waterproofing membrane system can be classified into two systems: pre-formed sheet systems and liquid systems (Russell H. G., 2011).

The pre-formed sheet systems involve the application of a primer that is applied to clean concrete decks to improve the adhesion of the membrane to the bridge deck. These sheets, which have a self-adhesive face, can be rolled and bonded to the primer-treated deck surface using a simple roller. In other systems, the membrane can be bonded to the deck only by heating the membrane using a machine or a hand torch. Once the membrane is installed, a tack coat can be applied to the top surface to increase the bonding with the overlay asphalt. Manufacturers refer to these systems by various names such as rubberized asphalt, bituminous membrane, polymer-modified asphalt, modified bitumen, polymeric membrane, or bitumen and polymers. Figure A.35 shows the schematic of possible components of a pre-formed system (Russell H. G., 2011).

Liquid systems normally involve the application of a primer to the deck before the membrane is installed. Spray equipment or rollers and squeegees are the main methods to place the membrane. Depending on the manufacturer's specifications, the membranes can be applied cold or hot. Reinforcing fabric may or may not be included in the liquid system. A tack coat is applied prior to replacement of the asphalt overlay. Manufacturers refer to these systems by various names such as rubberized asphalt, two-component polymer, polyurethane, methyl methacrylate, rubber polymer, polymer-modified asphalt, or

rubberized bitumen. Figure A.36 shows a schematic of the possible components of a liquid system (Russell H. G., 2011).

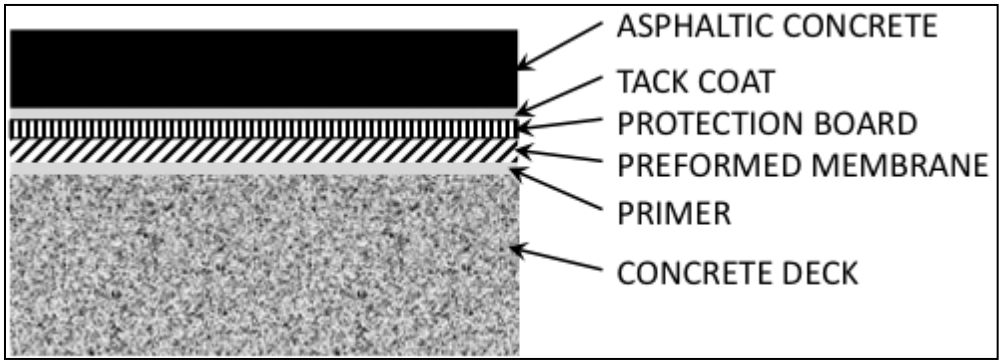

Fig. A.35 Schematic of Components of Preformed Systems (Russell H. G., 2011)

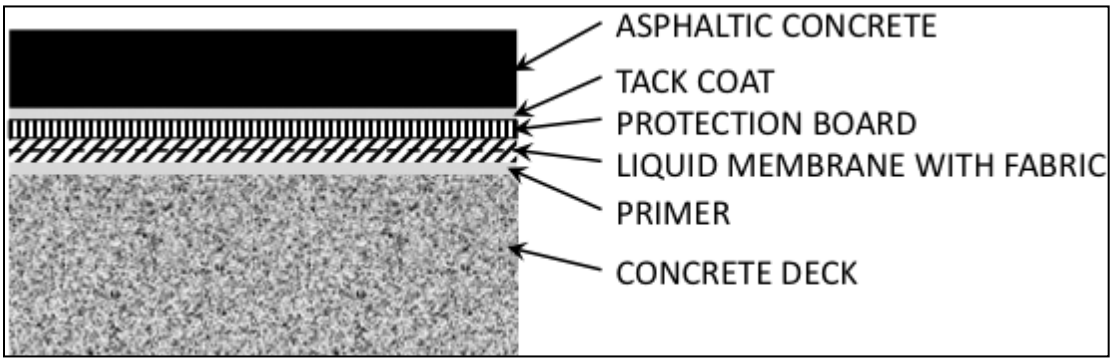

Fig. A.36 Schematic of Possible Components of Liquid Systems (Russell H. G., 2011)

A.11.5.1 Primer

Primers are regularly used to maintain sufficient bond between the concrete and the waterproofing membrane layer. Historically, primers were generally bitumen dissolved in an organic solvent. Due to safety and environmental concerns, these materials were replaced by epoxy. Occasionally, synthetic rubber combined with a resin and dissolved in a solvent is used as a primer. Resinous primers are typically used with resin-based liquid systems (Manning, 1995). Generally, one of the most critical characteristics of a waterproofing membrane system is the bond between the concrete deck and the waterproofing membrane. Primers also provide sealing of small surface cracks in concrete decks. Furthermore, primers need to be flowable to penetrate the textured surface of concrete decks (Strandquist, 2012).

In most cases, a primer can be specified for either liquid application or preformed membrane application. For either type, the primer may be poured and spread by squeegee or sprayed. Figure A.37 shows the application of primer by squeegee.

Fig. A.37 Application of Primer by Squeegeeing (Strandquist, 2012)

A.11.5.2 Membrane

The membrane sheet is the main part of a waterproofing pre-formed system. The key function of the membrane is to act as a physical barrier between the concrete and asphalt layer to prevent moisture and chlorides. Therefore, the membrane must provide a reliable impermeable layer. Membranes are also placed in joint areas; therefore, they must have the ability to elongate extensively. Thermal loading, crack movements, and heavy traffic loading can make bridge beams move vertically and/or horizontally, and the membrane must be able to accommodate all these differential movements.

Manufacturers have produced a variety of waterproofing membrane systems. These systems are classified mainly based on five characteristics: preformed versus applied-in-place; thermoplastic versus thermosetting; unmodified versus modified; reinforced versus un-reinforced; and wearing course versus no wearing course. Another classification is based on the generic type of material (Manning, 1995).

In terms of preformed (often called sheet/membrane systems) versus applied-in-place (often called liquid systems), the classification is very general; these systems are most commonly used in practice. Preformed membranes are typically produced in sheets, usually come in rolls, and are laid on the concrete surface. The membranes are laid on the concrete surface after the application of adhesive materials or the membrane sheets can be self-adhering (often called "peel and stick" membranes). Figure A.38 shows the preformed system. Figure A.39 shows the applied-in-place systems. Both systems have advantages and disadvantages, which are summarized in Table A.9.

Fig. A.38 Preformed System Installation (Strandquist, 2012)

Fig. A.39 Applied-in-Place System (Strandquist, 2012)

The next classification is in terms of thermoplastic versus thermosetting materials. Thermosetting materials are petrochemical materials which, following the initial permanent set through chemical reaction, are not modified noticeably in terms of viscosity with a change of temperature. Thermosetting materials consist of vulcanized rubber sheets and resin-based liquid membranes. The resin-based liquid could be produced from epoxy, polyester, polyurethane, acrylic, or polysulfide resins. However, the viscosity of thermoplastic materials could change with a change in temperature, and the thermoplastic materials do not set permanently through chemical reaction (Manning, 1995).

Regarding the classification between unmodified versus modified membranes, when additive material is added until the point of changing the material properties, the membrane

is considered to be modified. Adding coal tar to resins or using fillers with asphalt membranes are examples of modifications. Conversely, materials added for ease of application or to promote setting (such as emulsifiers or solvents) are not considered to be modifiers; thus, the membranes are considered as unmodified (Manning, 1995).

Table A.9: Comparison of Preformed System versus Liquid System (Manning, 1995)

Preformed Systems	Liquid Systems
•Tend to perform well in laboratory evaluations	•Tend to perform less well in laboratory evaluations
•Quality of material controlled under factory conditions	•Difficult to ensure consistent quality of materials
•Thickness and integrity controlled at the factory	•Difficult to control thickness of membrane and detect presence of pinholes
•Labor-intensive installation, especially if not self adhesive	•Usually applied in one application by spray or squeegee; built-up systems are labor intensive
•Laps required	•Laps not required
•Difficult to install on curved or rough decks	•Application independent of deck geometry. Thin membranes require a smooth deck
•Vulcanized sheets may be difficult to bond to substrate, protection layer and at laps	•Bonding not usually a problem if substrate prepared properly; self adhesive
•Vulnerable to quality of work at critical locations such as curbs, expansion joints and deck drains	•Less vulnerable at critical locations
•Blisters must be repaired by puncturing and patching	•Blisters and blowholes easily repaired in self-sealing materials, but not in thermosetting materials
•Tend to be more expensive	•Tend to be less expensive

In terms of reinforced versus un-reinforced membranes, a membrane can be classified as reinforced when continuous sheets or fibers are used. Examples of reinforcements are glass fiber, polypropylene or nylon fabrics, and polyethylene sheets. Membranes with discontinuous reinforcement are considered un-reinforced as those discontinuous additives could be considered as modifiers or fillers (Manning, 1995).

In laboratory and field investigation of 48 waterproofing membranes in the United Kingdom, an alternative classification system was developed. This classification distinguishes between preformed membrane sheet and liquid systems. Also, this classification offers a secondary classification with respect to material composition. Figures A.40 and A.41 show the details of preformed system and liquid systems, respectively, which were included in that investigation (Manning, 1995).

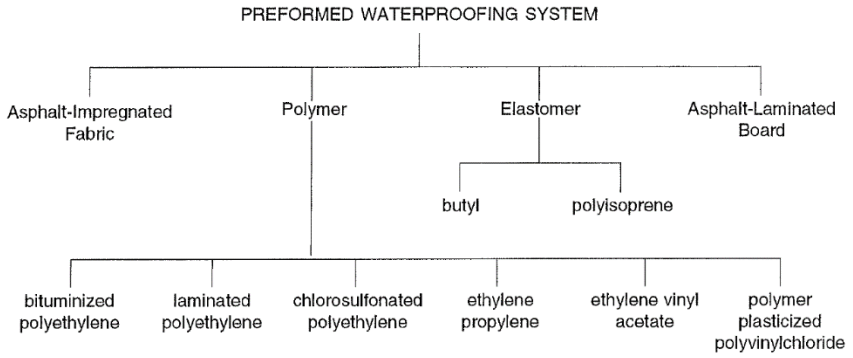

Fig. A.40 Preformed Waterproofing Systems (Manning, 1995)

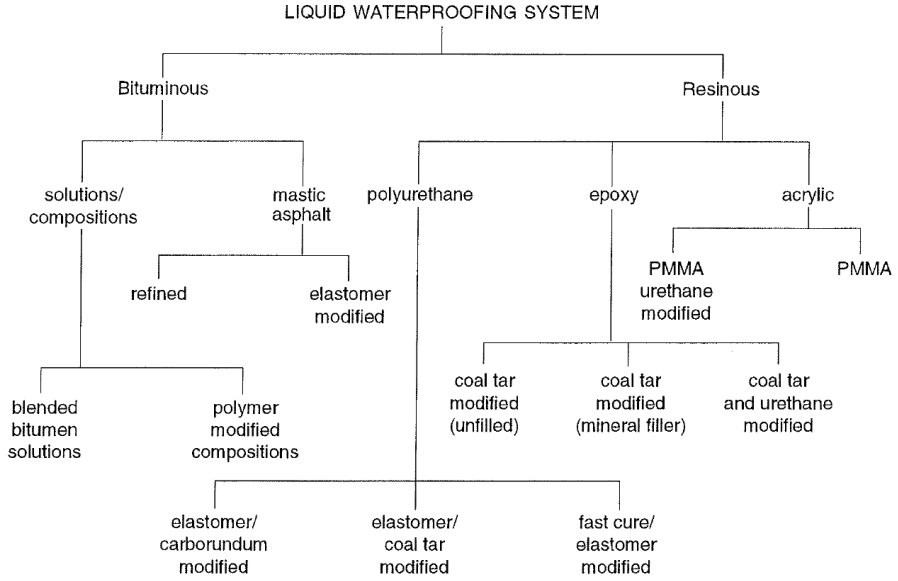

Fig. A.41 Liquid Waterproofing Systems (Manning, 1995)

Preformed systems were divided into four categories: asphalt-impregnated fabric sheets, polymeric sheets, elastomer sheets, and asphalt-laminated boards. Asphalt-impregnated fabric sheets are impregnated absorbent material coated with asphalt cement. The impregnated absorbent material could be either polyester fleece, glass cloth, or woven polypropylene. Polymeric sheets were based on either bituminized, laminated, or chlorosulfonated polyethylene; ethylene propylene; ethylene vinyl acetate; or polymer plasticized polyvinylchloride. The elastomer sheets were based on vulcanized butyl or polyisoprene rubber. With asphalt-saturated felt on the underside, the butyl type became laminated. In North America, other types of elastomeric sheets, such as those made of polychloroprene, ethylene propylene diene monomer, butyl, and Hypalon rubbers, have been used mainly in experimental work in the 1970s. The forth category is asphalt laminated boards, which are made of finely crushed aggregates filled with asphalt cement between

layers of asphalt-saturated felt; this type was used as protection boards for some systems (Manning, 1995).

The liquid systems are categorized into bituminous and resinous systems. Bituminous systems are subcategorized into bituminous solutions or compositions that are blended solutions of various bitumens in hydrocarbon solvents or two-part polymer-modified composition, and mastics. Mastic, a blended solution of refined natural or elastomer-modified mastic asphalts, requires application of heat to be converted into a liquid state. Resinous types were subcategorized into urethane, epoxy, and acrylic resin-based systems. Polyurethanes systems are fast curing elastomer or elastomer-modified, and some are further modified with either carborundum or coal tar. All epoxy resin-based systems are modified with coal tar, minerals or reinforcing polyester fleece. The advantage of these systems is that the concrete does not have to be primed. Acrylic systems are based on polymethylmethacrylate resin (PMMA) and are typically used as a primer; these systems can be modified with urethane (Manning, 1995).

Based on an extensive series of field and laboratory tests, general relationships between material composition and the performance characteristics of primers, adhesives, and membranes were established, these relationships are summarized in Tables A.10 and A.11.

Table A.10: Performance of Generic Primers and Adhesives (Manning, 1995)

Type of Material	Positive Attributes	Negative Attributes
Bituminous primers	Workable over ambient temperature range although some unmodified solvented types increased viscosity at low temperatures.	Drying time was temperature and moisture dependent and took from 1 to 48 hours, depending on composition; limited waterproofing ability and poor long term adhesion.
Resinous primers	Workable over ambient temperature range; moderate waterproofing ability and good resistance to chloride penetration.	Pot life limited at high temperatures.
Oxidized bitumen adhesives	Effective barrier to water and chloride transmission when fully bonded and free from blow holes; minimal water absorption.	Significant increase in stiffness at low temperatures; prone to embrittlement and debonding; generally poor long term bond.
Latex adhesives		Very poor adhesion to concrete; ineffective barrier to water or chloride transmission.
Self-adhesive backing to sheet membranes	Bond generally effective when applied at above 10°C.	Below 10°C, bond progressively weaker and almost non-existent below 5°C; poor bond if laitance or contamination of concrete; prone to debonding in the long term.

Table A.11: Performance of Generic Waterproofing Membrane (Manning, 1995)

Type of Membrane	Positive Attributes	Negative Attributes
Asphalt-impregnated fabrics	-Fabrics not mineral dressed remained flexible. -Not punctured, but deeply indented, by hot aggregate for membranes with a polyester fleece core, a mineral dressing and a thickness of at least 4mm. -Performance improved by using elastomer/polymer modified bitumens to raise softening point and reduce damage. -Resistant to tearing.	-Mineral dressed membranes stiffen and difficult to unroll below 5°C. -Core materials of asphalt impregnated glass cloth or woven polypropylene easily punctured. -Undressed fabrics liable to damage by cold and hot aggregates. -Damaged by prolonged exposure to fuel. -Oxidized bitumen adhesive had poor long term bond.
Polymer sheets	-Bituminized PE, laminated PE and polymer-plasticized PVC sheets generally remained flexible and less liable to recoil and uplift. -Chlorosulfonated PE (>3mm thick) and polymer-plasticized PVC sheets not punctured by hot aggregate. -Extruded and polymer-plasticized PVC sheets not damaged by site activities. -Most had low water absorption, and good resistance to water and chloride transmission provided fully bonded and not punctured.	-Extruded EP, some chlorosulfonated PE and EVA sheets had progressive stiffening at low temperatures with excessive recoil and uplift at the edges. -Most systems punctured by hot aggregate because of low softening point and thin sheets, even when used with mineral dressed protection sheets. -Extruded PVC sheets susceptible to damage from prolonged exposure to fuel. -Bitumen adhesives or pressure sensitive adhesives prone to debonding.
Elastomer sheets	-Butyl and polyisoprene rubber remained flexible over ambient temperature range and were undamaged by site activities. -Polyisoprene unaffected by high temperatures.	-Both systems debonded. -Butyl system damaged by hot aggregates at temperatures above 150°C. -Butyl system damaged by prolonged exposure to fuel.
Asphalt-laminated boards	-Not damaged by site activities. -Thickness of boards contributed to low chloride transmission.	-Stiffened and cracked on flexing at low temperatures . -Severely damaged by hot aggregate above the softening of the bitumen. -Delaminated at very high asphaltic temperatures. -High water absorption. -Self adhesive systems gave a moderately satisfactory bond.
Bituminous liquid membranes	-Polymer modified compositions remained flexible over ambient temperature range. -Must be used in conjunction with asphalt-laminated board; board and membrane penetrated by hot aggregates but self-sealing nature prevented chloride penetration.	-Bitumen-in-solvent solutions were prone to extensive pin and blow holes and blistering during laying; also prone to embrittlement at low temperatures; penetrated by aggregate at low asphalt application temperatures. Water absorption, water and chloride transmission high.
Mastic asphalts	-Indented by hot aggregates but thickness prevented penetration. -Good waterproofing integrity and low water absorption if fully bonded and undamaged.	-Prone to pin and blow holes, partly because of low reflectivity. -Softened considerably at moderate asphalt temperatures. -Embrittled at low temperatures. -Severely affected by exposure to gasoline. -Minimal bond unless primer used.
Urethane resin system	-All systems had good long term adhesion to concrete, but weaker bond to asphalt. -All systems remained flexible and resistant to fuel damage. -Fast cure systems remained flexible, free from damage by site activities, or hot aggregate; these systems also had good waterproofing integrity and low transmission of chlorides, properties which were assisted by the primer.	-Thin coatings (<2mm thick) prone to damage by asphalt surfacing, irrespective of material composition. -Some cold tar and elastomer modified systems prone to pinholing . -Cold tar modified urethanes liable to damage from site activities and hot aggregate; most had moderate to high water absorption; one system attacked by chlorides and fungal growth.
Epoxy resin system	-Chloride transmission low where no pinholes. -Excellent bond to concrete. -Not affected by fuels.	-Thin cold tar modified systems were severely embrittled at low temperatures and under hot asphalt which lead to damage by aggregate; also prone to pinholing . -Water absorption varied between systems. -Epoxy resins modified with urethane and either reinforced with a fabric scrim or mineral filled to form a slurry were very robust but less flexible; good waterproofing integrity and low chloride transmission.
Acrylic resin systems	-Very good bond to concrete and a moderate bond to asphalt via a tack coat. -Fast cure acrylic systems remained flexible and free from damage from site activities or hot aggregate over normal temperature ranges; good chloride resistance and waterproofing integrity which was assisted by the primer.	-Some softening of fast cure systems after prolonged fuel exposure. -Urethane-modified type cracked over existing crack in the concrete.

EP = ethylene propylene, PE = polyethylene, EVA = ethylene vinyl acetate, PVC = polyvinylchloride.

A.11.5.3 Tack Coat

For many waterproofing systems, a tack coat (also called a bond coat) is applied between the waterproofing layer and the layer above (either concrete or asphalt) and is anticipated to improve the bond. In cases where a protective layer is provided, a tack coat can be placed between the membrane and the protective layer; it can also act as the interface between the protective layer and the asphalt or concrete overlay. In the United Kingdom, the thickness of the tack coat is usually specified with regard to the size of the aggregate being used in the asphalt overlay. If large aggregate is used, a thicker tack coat layer is required. For fine aggregate, a thinner tack coat layer is specified to be used as an interface. The aggregate may penetrate the tack coat but may not penetrate the membrane layer, depending on the compaction severity (Strandquist, 2012).

According to Strandquist (2012), the most critical concern regarding a tack coat is its durability against potential damage caused by construction vehicles, which also depends on the thickness of the layers above. The tack coat is at risk of being stripped and damaged during placement and compaction of the asphalt overlay. Some practices may reduce the severity of this problem, such as providing sufficient time for the tack coat to dry until it has

set completely and is tack free. It is also helpful to carefully clean the rubber wheels of the paving vehicle and cover them with a soapy solution. Prior to paving, it is recommended to repair any damage to the tack coat with patches.

A.11.5.4 Protective Layer

The main function of the protective layer is to protect the membrane from damage due to compaction of the wearing surface. Also, the protective layer should protect the membrane sheets from depression caused by angular aggregate or damage from heavy construction equipment. Many departments of transportation agencies in the US and Canada have specifications for this layer. A variety of materials are used for this purpose, such as fiberglass and polystyrene. In the United Kingdom, a layer of sand asphalt (which is simply asphalt concrete that uses fine sand aggregate) is used as an additional layer to the main protective layer (Jordan et al., 2007; Strandquist, 2012).

A.11.6 Specifications and Standards

Many specifications and standards in the United States and other countries specify the use of waterproofing on bridge decks. AASHTO addresses waterproofing in section 21 of LRFD Bridge Construction Specifications (AASHTO, 2010). It covers both types of waterproofing systems, constructed-in-place and preformed membrane systems, and it considers them as protective systems. The concrete surface should be very smooth and free of any holes and projections. Also, the surface should be dry and have a minimum temperature of 35°F. AASHTO provides specific detailed instructions for both asphalt membrane systems and preformed waterproofing membrane systems.

Most transportation agencies in the US have waterproofing membrane specifications that are very comparable to AASHTO specifications. Some differences between state DOTs and AASHTO specifications are documented in Table A.12.

Table A.12: Summary of State Specifications/Requirements versus AASHTO Specifications (Russell H. G., 2011)

Property	AASHTO	States
Minimum thickness for rubberized asphalt, mil.	65	50 and 60
Minimum thickness for modified bitumen, mil.	70	50 and 60
Minimum deck or air temperature, °F	35	40, 45, and 50
Puncture resistance, lb	—	40 and 200
Maximum permeance, perms	—	0.10
Minimum longitudinal overlap, in.	2.0	2.0, 2.5, 3.0, 4.0, and 6.0

— = Not specified.

Both AASHTO and state specifications refer to ASTM standards for material specifications and test methods. These requirements cover both liquid applied waterproofing and

membrane sheets and bonding agents. A list of the related ASTM standard tests is provided in Table A.13.

Table A.13: ASTM Standards Relevant to Waterproofing Membranes (Russell H. G., 2011)

ASTM Designation	Title
D5	Standard Test Method for Penetration of Bituminous Materials
D36/D36M	Standard Test Method for Softening Point of Bitumen (Ring-and-Ball Apparatus)
D41/D41M	Standard Specification for Asphalt Primer Used in Roofing, Dampproofing, and Waterproofing
D146	Standard Test Methods for Sampling and Testing Bitumen-Saturated Felts and Woven Fabrics for Roofing and Waterproofing
D173	Standard Specification for Bitumen-Saturated Cotton Fabrics Used in Roofing and Waterproofing
D449	Standard Specification for Asphalt Used in Dampproofing and Waterproofing
D517	Standard Specification for Asphalt Plank
D882	Standard Test Method for Tensile Properties of Thin Plastic Sheeting
D1228 Withdrawn Standard	Methods of Testing Asphalt Insulating Siding Surfaced with Mineral Granules (Withdrawn 1982)
D1668	Standard Specification for Glass Fabrics (Woven and Treated) for Roofing and Waterproofing
D1777	Standard Test Method for Thickness of Textile Materials
D3236	Standard Test Method for Apparent Viscosity of Hot Melt Adhesives and Coating Materials
D3515 Historical Standard	Standard Specification for Hot-Mixed, Hot-Laid Bituminous Paving Mixtures
D4071	Standard Practice for Use of Portland Cement Concrete Bridge Deck Water Barrier Membrane System
D4541	Standard Test Method for Pull-Off Strength of Coatings Using Portable Adhesion Testers
D4632	Standard Test Method for Grab Breaking Load and Elongation of Geotextiles
D4787	Standard Practice for Continuity Verification of Liquid or Sheet Linings Applied to Concrete Substrates
D6153	Standard Specification for Materials for Bridge Deck Waterproofing Membrane Systems
D6690	Standard Specification for Joint and Crack Sealants, Hot Applied, for Concrete and Asphalt Pavements
E96/E96M	Standard Test Methods for Water Vapor Transmission of Materials
E154	Standard Test Method for Water Vapor Retarders Used in Contact with Earth Under Concrete Slabs, on Walls, or as Ground Cover

A.11.7 Design Details

A survey of all highway agencies in the United States showed that 56% of agencies have no standard design details for waterproofing membrane systems. Figure A.42 shows information on the availability of standard details for the installation of waterproofing membranes in the United States for agencies that responded to the survey. By contrast, only two Canadian highway agencies have no standard design details. Figure A.43 shows examples of standard design details provided in standard drawings of Alberta Transportation, a Canadian highway agency (Russell H. G., 2011).

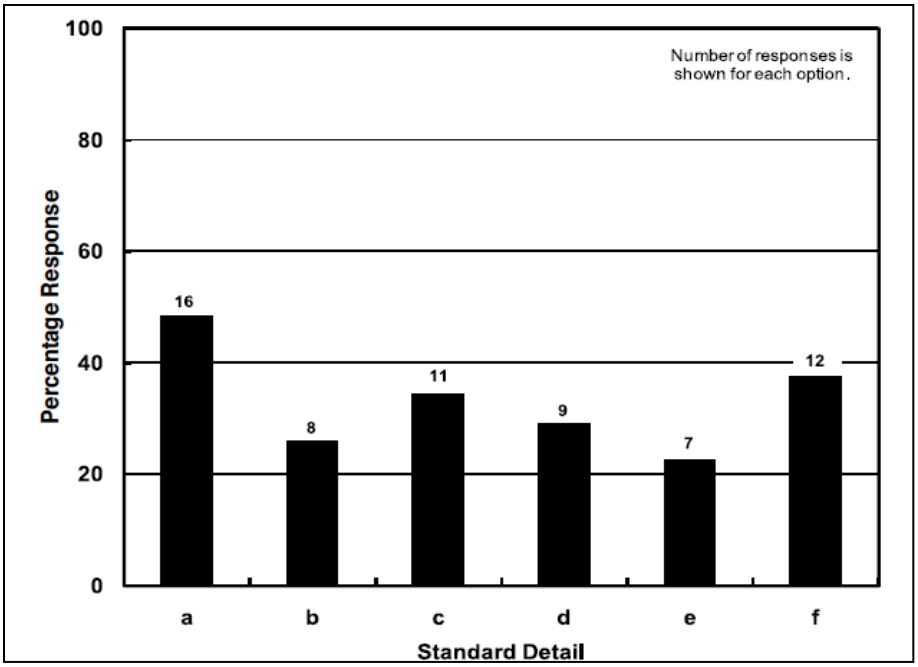

a. Installing waterproofing membranes
b. Terminating edges of membranes
c. Curb details for membranes
d. Concrete barrier details for use with membranes
e. Over construction joints
f. At expansion joints

Fig. A.42 Standard Details Available for the Installation of Waterproofing Membranes (Russell H. G., 2011).

A.11.8 Construction

Most specifications provide some construction procedures, which are given in the following steps:

1. Deck surface preparation,
2. Application of a primer to the concrete,
3. Installation of the waterproofing membrane,
4. Installation of protection board (if used),
5. Repair of unacceptable areas resulting from membrane thickness inadequacies, and
6. Installation of asphaltic concrete riding surface.

Figures A.44 and A.45 show various steps in the construction process for both systems (Russell H. G., 2011).

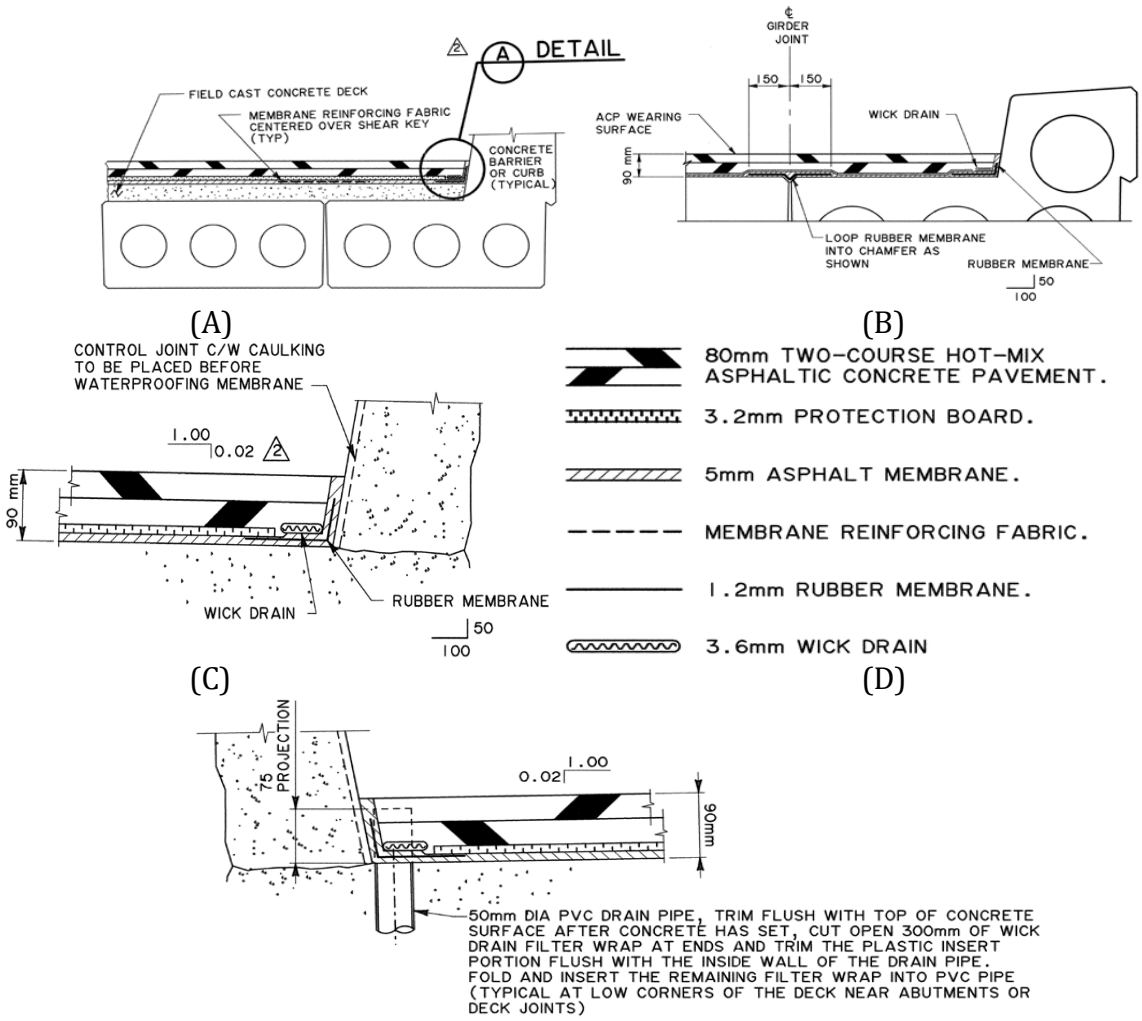

Fig. A.43 Examples of Provided in Standard Drawings (A) Composite Deck, (B) Non-Composite Deck, (C) Detail of Composite Deck, (D) Legend, (E) Drain Pipe Detail (Russell H. G., 2011).

A.11.9 Performance

The waterproofing membrane system has many advantages that encourage engineers to adopt it in their design. A waterproofing membrane system can be constructed rapidly and can cover reflective cracks for most moving loads. Moreover, the waterproofing system is flexible; therefore, it can be applied to almost any deck geometry. On the other hand, the waterproofing membrane system has disadvantages that can limit the performance in some cases. The service life of the membrane depends on the wearing surface life. In addition, the waterproofing membrane system cannot be applied on grades of more than 4% because the bonding capacity is very limited for some systems and debonding can occur (Sohanghpurwala, 2006). Due to the advantages of the waterproofing membrane system, its usage is required by most Canadian and European highway agencies. In contrast, the system is not a requirement for many agencies in the United States.

According to Sohanghpurwala (2006), the ideal waterproofing system should provide a good impermeable layer, adhesion to both concrete and the riding surface, tolerance to rough surfaces, resistance to traffic of heavy equipment during construction, have the ability to span cracks between adjacent members, and have a life span up to 100 years. Additionally, the waterproofing membrane should tolerate high and low temperatures without a change in its performance.

a) Application of Primer to the Concrete

b) Laying out the Sheet Membrane

c) Heating the Sheet Membrane with a Torch

d) Sealing the Overlap Seams by a Hand Roller

(e) Completed Membrane

(f) Compacting the Hot Mix Asphalt

Fig. A.44 Steps in the Installation of a Preformed Sheet Membrane (Russell H. G., 2011).

(a) Hand Spraying

(b) Machine Spraying

Fig. A.45 Application of Liquid Membrane by Spraying (Russell H. G., 2011).

According to Jin-Zhong (2005), a waterproofing membrane can prolong the lifetime of structure if it satisfies the following requirements:

- Impermeable throughout service life
- Strong bond with surfacing layer and bridge deck
- Resistance to damage induced by concrete cracks when paved on bridge decks
- Good durability
- Resistance to shear stresses imposed by braking, accelerating, and cornering vehicle wheels
- Resistance to aggregate breakdown under heavy traffic
- Resistance to water or solution erosion
- Adaptability to changes in temperature

Based on a survey conducted by Russell (2011), transportation agencies were asked for their expectations of service lives of the waterproofing membranes they have used. Most transportation agencies expected 16 to 20 years for new bridge decks and 6 to 20 years for existing bridge decks. Based on that survey, there is not enough evidence to determine whether pre-formed systems or liquids systems have longer life spans. Figure A.46 shows the survey results.

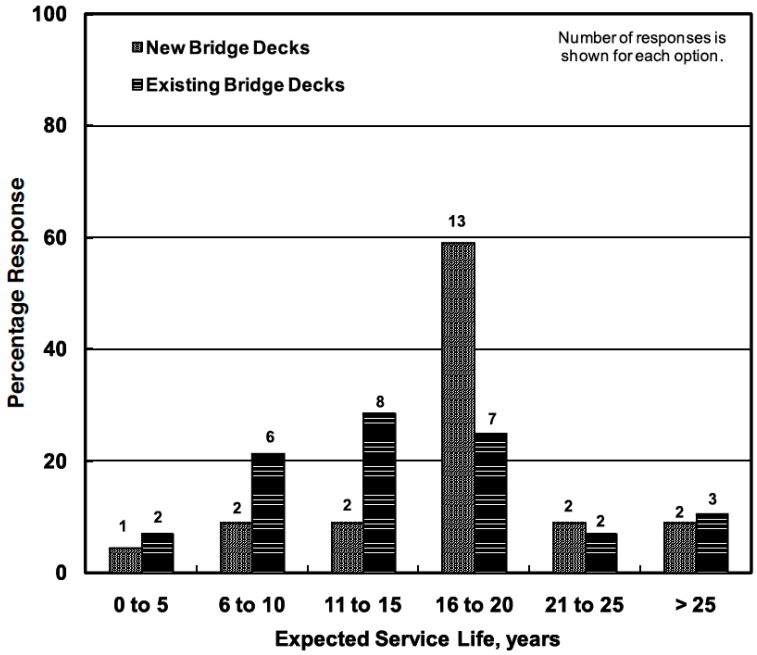

Fig. A.46 Expected Service Life for Waterproofing Membranes (Russell H. G., 2011).

Many types of deficiencies may occur for waterproofing membrane systems used on concrete bridge decks. In service, existing bridges have more deficiencies than new ones. Lack of adhesion between the waterproofing membrane and the concrete deck is the most reported deficiency, reported by more than 60% of transportation agencies. Based on the survey, moisture penetration through the membrane from an unknown source is the second most commonly reported type of defect, mentioned by 55% of the respondents. Figure A.47 displays the response regarding defects that may occur in waterproofing membranes.

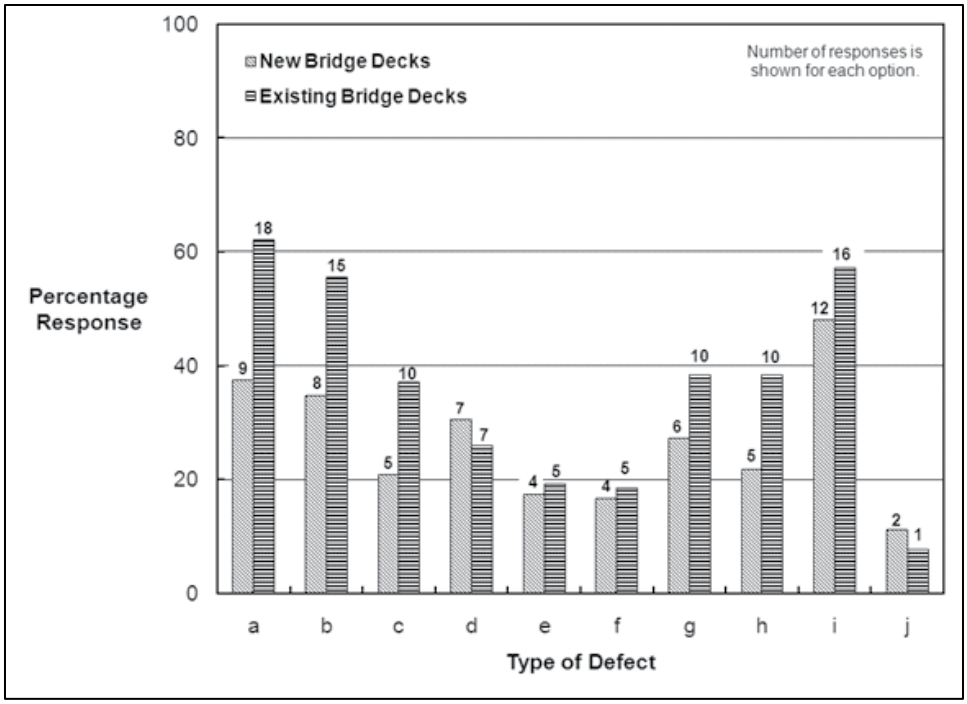

Type of defect:
a. Lack of adhesion between the waterproofing membrane and the concrete deck
b. Lack of adhesion between the waterproofing membrane and the asphalt surface
c. Punctured waterproofing membranes
d. Membrane blistering
e. Horizontal shear failure at the membrane
f. Cracks in the waterproofing membrane
g. Voids under the waterproofing membrane
h. Reinforcement corrosion
i. Moisture penetration through the membrane but cause unknown
j. Other.

Fig. A.47 Types of Defects in Waterproofing Membranes (Russell H. G., 2011)

A.11.10 Summary

Water leakage is a recurring problem that negatively impacts the service life of bridges. Many strategies have been deployed in order to control water leakage. One of them is the use of a waterproofing membrane provided on the top of the deck surfaces as a protective system. Waterproofing membranes are widely used to protect bridge decks from water-induced damage. Common types of damage include steel corrosion and concrete spalling, which can affect the service life of bridges. A protective system is often provided to enhance the durability of both new and existing bridge decks. This appendix includes details on the use of the waterproofing for bridges in the United States. The types and classifications of waterproofing were explained. The details of the materials and the primer, membrane and tack coat were also discussed. Furthermore, this appendix summarizes the specifications and standards related to the waterproofing membrane as well as the design details. The construction details of waterproofing membrane for both liquid and pre-formed systems

were outlined. It is concluded in this chapter that the waterproofing membrane features and the requirements that lead to waterproofing will provide satisfactory performance if installed with adequate care. However, research on the performance of waterproofing membranes was found to be limited and lacking.

Concrete bridge decks can be damaged due to many factors. The corrosion of reinforcing steel is one of the main factors leading to bridge damage. In fact, steel material has low corrosion resistance and needs to be protected from exposure to corrosive solutions, especially those having chloride ions (Cl+). When water containing corrosive chemicals seeps through cracked joints and penetrates the concrete to reach the embedded reinforcing steel, the corrosion process starts and the volume of steel increases. Volume expansion leads to the initiating of concrete cracking that propagates and causes larger cracking and spalling.

The membrane is one of the components of the waterproofing system and mainly works as a physical barrier that is typically located on the top of the concrete surface and is covered by a strong material that functions as the riding surface. Other materials are used as bonding agents to secure the membrane to the bridge deck. Inadequate implementation of any component can result in poor performance of the system as a whole.

Waterproofing membrane systems are divided into two main categories: First is the construct-in-place system, (bituminous and resinous liquid-sprayed systems). The bituminous is the most frequent material used in practice for this particular system. Second is the preformed membrane system, which is divided into asphalt-impregnated fabric, polymer, elastomer, and asphalt laminated board systems. The asphalt-impregnated fabric is the most common material used in the industry among the preformed membrane systems.

REFERENCES

1. ACI. (2011). Building code requirement for reinforced concrete. Detroit: ACI 318-11.

2. Aktan, H., Attanayake, U., Ulku, E., Ahlborn, T. M., & Deshpande, Y. (2009). Condition Assessment and Methods of Abatement of Prestressed Concrete Box-Beam Deterioration Phase II. Western Michigan University and Michigan Technological University, Department of Civil & Construction Engineering and Dept. of Civil & Environmental Engineering. Kalamazoo and Houghton: MDOT.

3. American Association of State Highway and Transportation Officials, AASHTO. (2010). *AASHTO LRFD Bridge Construction Specifications.* Washington, D.C.: AASHTO.

4. Aziz, J. R. (2010). Shear Capacity of Concrete Prizms With Interface Joints. *Journal Of Engineering Volume 16*.

5. Allena, S., & Newtson, C. M. (2011). Ultra-High Strength Concrete Mixtures Using Local Materials. Journal of Civil Engineering and Architecture, 5 (4), 322-330.

6. Attanayake, U., & Aktan, H. (2011). Capacity Evaluation of a Severely Distressed and Deteriorated 50-Year-Old Box Beam with Limited Data. Journal of Performance of Constructed Facilities, 25 (4), 299-308.

7. Attanayake, U., & Aktan, H. (2015). First-Generation ABC System, Evolving Design, and Half a Century of Performance: Michigan Side-by-Side Box-Beam Bridges. Journal of Performance of Constructed Facilities, 29 (3), 04014090(1-14).

8. Bajaj, S., Patnaik, A., Payer, J., Liang, R.Y., Manigandan, K., and Srivatsan, T.S., Extrinsic Influence of Environment on Corrosion Behavior of Enamel Coated Dowel Bars, Emerging Materials Research, Emerging Materials Research, DOI: 10.1680/emr.14.00007, Volume 3, Issue 4, June 2014, pp. 158 –168.

9. Bakht, B., Jaeger, L. G., & Cheung, M. S. (1983). Transverse Shear in Multibeam Bridges. Journal of Structural Engineering, 109 (4), 936-949.

10. Barr, P. J., Parry Osborn, G., Petty, D. A., Halling, M. W., & Brackus, T. R. (2012). Residual Prestress Forces and Shear Capacity of Salvaged Prestressed Concrete Bridge Girders. Journal of Bridge Engineering, 17 (2), 302-309.

11. Bažant, Z. P., Yu, Q., & Li, G.-H. (2012). Excessive Long-Time Deflections of Prestressed Box Girders. I: Record-Span Bridge in Palau and Other Paradigms. Journal of Structural Engineering, 138 (6), 676–686.

12. Birkeland, H. W. (1968). *Precast And Prestressed Concrete.* Class Notes For Course University of British Columbia.

13. Birkeland, P. W., & Birkeland, H. W. (1966). Connections in precast concrete structure. ACI Journal, 63(3):345-68.

14. Bozorgzadeh, A., Megally, S., Restrepo, J. I., & Ashford, S. A. (2006). Capacity Evaluation of Exterior Sacrificial Shear Keys of Bridge Abutments. Journal of Bridge Engineering, 11 (5), 555-565.

15. Brown, K. M. (1998). *Camber Growth Prediction in Precast Prestressed Concrete Bridge Girders.* University of Idaho. Ann Arbor, MI: UMI Microform.

16. Buyukozturk, O., Bakhoum, M. M., & Beattie, S. (1990). Shear Behavior of Joints in Precast Concrete Segmental Bridges. Journal of Structural Engineering, 116 (12), 3380-3401.

17. Carlisle Coatings & Waterproofing Inc. . (2013). *CCW-MIRADRI 860/861 Self-Adhering Waterproofing Membrane.* Wylie: Carlisle Coatings & Waterproofing Inc. .

18. Concrete Sealants Inc. (2013). *ConSeal CS-212 .* Tipp City: Concrete Sealants Inc.

19. Crafco Inc. (2012). *Product Data Sheet Geotac.* Chandler: Crafco Inc.

20. Crafco Inc. (2012). *Product Data Sheet Paveprep.* Chandler: Crafco Inc.

21. Crafco Inc. (2012). *Product Data Sheet Paveprep SA .* Chandler: Crafco Inc.

22. Chynoweth, M. J. (2014). Accelerated Bridge Construction Policy and ABC Slide Technologies. 29th Annual Civil Engineering Professional Development Seminar. MDOT.

23. Czaderski, C., & Motavalli, M. (2006, July-August). Determining the Remaining Tendon Force of a Large- Scale, 38-Year-Old Prestressed Concrete Bridge Girder. PCI Journal, 51(4), 56-68.

24. Dritsos, S. E. (1991). Distortion of Concrete Box Beams Due to Eccentric Transverse Loads. Journal of Structural Engineering, 117 (1), 29-47.

25. Eder, R. W., Millard, R. A., Baseheart, T. M., & Swanson, J. A. (2005). Testing of Two 50 Years Old Precast Post-Tensioned Concrete Bridge Girders. PCI Journal, 50 (3), 90-95.

26. Eduardo, N. J., D, D.-d.-C. a., & Branco b, J. A. (2010). Accuracy of Design Code Expressions for Estimating Longitudinal Shear Strength of Strengthening Concrete Overlays. *Engineering Structures 32*.

27. Eisenbeis, K., Ahlborn, T., Bracewell, D., Chandra, V., Deitz, D., Kaufman, K., et al. (2009). The State of the Art of Precast/Prestressed Adjacent Box Beam Bridges. PCI.

28. El Shahawy, M. (1990). Feasibility Study of Transversely Prestressed Double Tee Bridges. Prestressed Concrete Institute Journal , 35 (5), 56-69.

29. European Asphalt Pavement Association. (2013). *Asphalt pavements on bridge decks.* Belgium: www.eapa.org.

30. Frosch, R. J., Kreger, M. E., & Strandquist, B. V. (2013). *Implementation of Performance-Based Bridge Deck Protective Systems.* Indiana Department of Tranportation and Purdue University, West Lafayette: Joint Transportation Research Program, Indiana Department of Transportation and Purdue University.

31. Grace, N. F. (2014). New Generations of Sustainable CFRP Prestressed Concrete Highway Bridges. 2014 ODOT Bridge Design Conference.

32. Grace, N. F., Jensen, E. A., & Noamesi, D. K. (2011). Flexural Performance of Carbon Fiber-Reinforced Polymer Prestressed Concrete Side-by-Side Box Beam Bridge. Journal of Composites for Construction, 15 (5), 663-671.

33. Gearge M. Hlavacs, T. L. Nondestructive Determination of Response of Shear Keys to Environmental and Structural Cyclic Loading. Committee on Mechanical Properties of Concrete.

34. Grace, N. F., Patki, K. D., Soliman, E. M., & Hanson, J. Q. (2011). Flexural Behavior of Side-by-Side Box-Beam Bridges: A Comparative Study. PCI Journal, 56 (3), 94-112.

35. Grace Construction Products Ltd. (2006). *Bituthene 3000/3000 HC.* Berkshier: Grace Construction Products Ltd.

36. Grace Construction Products Ltd. (2006). *Bituthene 4000.* Berkshine: Grace Construction Products Ltd.

37. Graybeal, B. (2011). Ultra-High Performance Concrete. Iowa and Virginia: Federal Highway Administration Research and Technology.

38. Graybeal, B. (2013). Material Characterization of Field-Cast Connection Grouts. McLean, VA: FHWA.

39. Graybeal, B. Ultra- High Performance Concrete. Turner-Fairbank Highway Research Center, FHWA.

40. Gulyas, R. J., Wirthlin, G. J., & Champa, J. T. (1995). Evaluation of Keyway Grout Test Methods for Precast Concrete Bridges. PCI , 44-57.

41. Habouh, M., Almonbhi, A., and Patnaik, A., Effectiveness of Adjacent Precast Concrete Box-Beam Connections, https://www.dot.state.oh.us/engineering/OTEC/2015_OTEC_Presentations/Tuesda

y_Oct.27/03/OTEC%20Box-Beam%20Presentation%20-%20Habouh%20and%20Patnaik.pdf, OTEC 2015 Conference, Columbus, Ohio, Oct. 2015, visited 12/4/2015, pages 43.

42. Habouh, M. I.. (2015) Shear Transfer Strength of Concrete Placed Against Hardened Concrete. Master Thesis, The University of Akron.

43. Halsey, J. T., & Miller, R. (1996). Destructive Testing of Two Forty-Year-Old Prestressed Concrete Bridge Beams. PCI Journal , 41 (5), 84-93.

44. Hanna, K. M. (2009). Transverse Post-tensioning Design and Detailing of Prescast, Prestressed Concrete Adjacent Box-girder Bridges. PCI Journal , 54 (4), 160-174.

45. Hansen, J., Hanna, K., & Tadros, M. K. (2012). Simplified Transverse Post-Tensioning Construction and Maintenance of Adjacent Box Girders. PCI Journal , 57 (2), 64-79.

46. Harries, K. A. (2009). Structural Testing of Prestressed Concrete Girders from the Lake View Drive Bridge. Journal of Bridge Engineering, 14 (2), 78-92.

47. Henry, R. G. (2011). Adjacent precast concrete box-beam bridges: State of the practice. PCI, 75-91.

48. Hernandez H. D. and Gamble W. L. (1975). *Time-Dependent Prestress Losses in Pretensioned Concrete Construction.* Springfield, Illinois: Illinois Cooperative Highway Research Program.

49. Highways Department of Hong Kong. (2008). *Guidance Notes on the Use of Waterproofing Membranes on Concrete Bridge Decks.* Research & Development Division.

50. Hii, A. K., & Al-Mahaidi, R. (2006). Experimental Investigation on Torsional Behavior of Solid and Box-Section RC Beams Strengthened with CFRP Using Photogrammetry. Journal of Composites for Construction, 10 (4), 321-329.

51. Huckelbridge, A. A., EI-Esnawi, H., & Moses, F. (1995). Shear Key Performance in Multibeam Box Girder Bridges. Journal of Performance of Constructed Facilities, 9 (4), 271-285.

52. Hulkelbridgr, A. (1997). Evaluation of Improved Shear Key Designs for Multibeam Box Girder Bridges. Case Western Reserve University , Departement of Civil Engineering . Columbus : ODOT.

53. Ishac, I. I., & Graves, T. R. (1985). Approximations for Moments in Box Girders. Journal of Structural Engineering , 111 (11), 2333-2342.

54. Issa, M. A., & Abdalla, H. A. (2007). Structural Behavior of Single Key Joints in Precast Concrete Segmental Bridges. Journal of Bridge Engineering, 12 (3), 315-324.

55. Jiang, H., Chen, L., John Ma, Z., & Feng, W. (2015). Shear Behavior of Dry Joints with Castellated Keys in Precast Concrete Segmental Bridges. Journal of Bridge Engineering , 20 (2), 04014062(1-12).

56. Jin-Zhong, P. (2005). Study Of The Road Performance Of Waterproof Materials For Concrete Bridge Decks . *the 24th Southern African Transport Conference (SATC 2005)* (pp. 965-972). Pretoria, South Africa: Document Transformation Technologies cc.

57. Jones, H. (2007). Warm Mix Asphalt Scan Tour. *Ohio Transportation Engineering Conference* (p. 56). Columbus : Ohio Transportation Engineering Conference.

58. Jordan, R. W., Nesnas, K., & Evans, M. G. (2007). *The Performance of Surfacing Overlaying Bridge Deck Waterproofing Systems.* United Kingdom: Transport Research Laboratory.

59. Jyotirmeay Lall, S. A. (1998). Performance of Full-Depth Shear Keys in Adjacent Prestressed Box Beam Bridges. PCI Journal , 43 (2), 72-78.

60. Kahl, S. (2005). Box-Beam Concerns Found under the Bridge. (J. R. Terry McNinch, Ed.) Research Record (102), 1-4.

61. Kaneko, Y., Connor, J. J., Triantafillou, T. C., & Leung, C. K. (1993). Fracture Mechanics Approache for Failure of Concrete Shear Key. I: Theory. Journal of Engineering Mechanics, 119 (4), 681-700.

62. Kasan, J. L., & Harries, K. A. (2013). Analysis of Eccentrically Loaded Adjacent Box Girders. Journal of Bridge Engineering, 18 (1), 15-25.

63. Kesse, G., & Lees, J. M. (2007). Experimental Behavior of Reinforced Concrete Beams Strengthened with Prestressed CFRP Shear Straps. Journal of Composites for Construction, 11 (4), 375-383.

64. Korhonen, C. J., Buska, J. S., Cortez, E. R., & Greatorex, A. R. (1999). *Procedures for the Evaluation of Sheet Membrane Waterproofing.* U.S. Army Cold Regions Research and Engineering Laboratory. Storrs: New England Transportation Consortium.

65. Lall, J., Alampalli, S., & DiCocco, E. F. (1998). Performance of Full-Depth Shear Keys in Adjacent Prestressed Box Beam Bridges. PCI Journal , 43 (2), 72-79.

66. Larson, K. H., Peterman, R. J., & Esmaeily, A. (2007). Bond Characteristics of Self-consolidating Concrete for Prestressed Bridge Girders. PCI JOURNAL, 52 (4), 44-57.

67. Larsen, K.R. and Patnaik, A.K., New Materials Minimize Effects of Steel Corrosion in Reinforced Concrete, Materials Performance, Vol. 52, No. 12, Dec. 2013, pp. 21-24.

68. Larson, M. B. (2005). Box-Beam Concerns Found under the Bridge. Michigan Technological University. ODOT.

69. Li, G. L., Yang, D. Y., & Lei, Y. L. (2013). Combined Shear and Bending Behavior of Joints in Precast Concrete Segmental Beams with External Tendons. Journal of Bridge Engineering, 18 (10), 1042-1052.

70. Loov, R.E. and Patnaik, A.K., Authors' Closure of Reader Comments on Horizontal Shear Strength of Composite Concrete beams, The PCI Journal, Chicago IL, Sep-Oct. 1994, pp. 106-109.

71. Loov, R.E. and Patnaik, A.K., Horizontal Shear Strength of Composite Concrete beams, The PCI Journal, Chicago IL, Jan-Feb. 1994, pp. 48-69: This paper received the Martin P. Korn award of the PCI.

72. Lundqvist, P., & Riihimäki, J. (2010). Testing of Five 30-Year-Old Prestressed Concrete Beams. PCI Journal, 55 (4), 50-58.

73. Mahmoud et al., M. (2013). Interfacial shear behavior of composite flanged concrete beams,. HBRC , 10 (2), pp. 206-214.

74. Manning, D. G. (1995). *Synthesis of Highway Practice 220.* Transportation Research Board, National Research Councíl. Washington, D.C.: National Academy Press.

75. Mansur, M. A., Vinayagam, T., & Tan, K. H. (2008). Shear transfer across a crack in reinforced high strength concrete. *ACES J Material*, pp. 20(4):294–302.

76. Maria Murphy, J. K. (2010). Determining More Effective Approaches for Grouting Sear Keys of Adjacent Box Beams. University Park: The Tomas D. Larson Pennsylvania Transportation Institute.

77. Mattock, A. H. (2001). Shear friction and high strength concrete. ACI Structural journal.

78. McGhee, C. L., & Ng, D. (2011). Innovative Construction Methods for Prestressed Concrete Box Beam Replacement. GPD Group. ODOT.

79. Mitchell, G. (2002). Horizontal Shear Transfer Across a Roughenen Surface. *Cement & Concrete Composites*, 25 (2003) 379–385.

80. Miller, R. A., Hlavacs, G., & Long, T. (1998). Testing of Full Scale Pre-Stressed Beams to Evaluate Shear Key Performance. University of Cincinnati , Departemnet of Civil And Environmental Engineering . Cincinnati: FHWA.

81. Miller, R. H. (1998). Testing of Full Scale Prestressed Beams to Evaluate Shear Key Performance. Cincinnati: PCI Journal.

82. Mohammed, H. (2015). Mechanical Properties Of Ultra High Strength Fiber Reinforced Concrete. 196.

83. Murphy, M., Kim, J., Sang, Z., & Xiao, C. (2010). Determining More Effective Approaches For Grouting Shear Keys of Adjacent Box Beams. Commonwealth Of Pennsylvania, Departement Of Transportation, Harrisburg.

84. Naito,, C. J. (n.d.). Retrieved from Google: http://www.google.com/imgres?newwindow=1&safe=off&hl=en&biw=1242&bih=545&tbm=isch&tbnid=BghQeccoJdC1iM%3A&imgrefurl=http%3A%2F%2Fwww.lehigh.edu%2F~cjn3%2Fpenndot.shtml&docid=dfi2nZhB6zCxFM&imgurl=http%3A%2F%2Fwww.lehigh.edu%2F~cjn3%2Fcorr.jpg&w=800&h=600&

85. Naito, C., & Warncke, J. (2008). Inspection Methods & Techniques to Determine Non Visible Corrosion of Prestressing Strands in Concrete Bridge Components. Leigh University, Pennsylvania Department of Transportation. Bethlehem: ATLASS.

86. Naito, C., Jones, L., & Hodgson, I. (2011). Development of Flexural Strength Rating Procedures for Adjacent Prestressed Concrete Box Girder Bridges. Journal of Bridge Engineering, 16 (5), 662-670.

87. Naito, C., Sause, R., & Thompson, B. (2008). Investigation of Damaged 12-Year Old Prestressed Concrete Box Beams. Journal of Bridge Engineering, 13 (2), 139-148.

88. Naito, C., Sause, R., Hodgson, I., Pessiki, S., & Macioce, T. (2010). Forensic Examination of a Noncomposite Adjacent Precast Prestressed Concrete Box Beam Bridge. Journal of Bridge Engineering, 15 (4), 408-418.

89. Naito, C., Sause, R., Hodgson, I., Pessiki, S., & Macioce, T. (2010). Forensic Examination of a Noncomposite Adjacent Precast Prestressed Concrete Box Beam Bridge. Journal of Brdige Engineering, 15 (4), 408-418.

90. Nawy, E. G. (2009). *Prestressed concrete a fundamental approach.* Ruters, New Jersey: Prentice Hall.

91. Nottingham, D. (1995, July-August). Reader Comments on Evaluation of Keyway Grout Test Methods for Precast Concrete Bridges. PCI, pp. 98-103.

92. ODOT Office of Structural Engineering. (2011, 01 21). *Standard Bridge Drawings*. Retrieved from The Ohio Department of Transportation: https://www.dot.state.oh.us/Divisions/Engineering/Structures/standard/Bridges/Standard%20Drawings/PSBD-2-07.pdf

93. ODOT. Study of Non-Shrink Keyway Grout for Strength. Ohio Department of Transportation.

94. Ohio Department of Transportation . (2013). *Construction and Material Specifications.* Columbus, Ohio: Ohio Department of Transportation .

95. Pagán-Ortiz, J. (2013). Ultra-High Performance Concrete :A State-of-the-Art Report for the Bridge Community. FHWA.

96. Patnaik, A.K. and Ramakrishnan, V., Research Needs for High Volume Fly Ash Concrete, ICI Journal, Vol. 5, No. 3, Nov.-Dec. 2004, pp. 13-18.

97. Patnaik, A.K. and Patnaikuni, I., Correlation of Strength of 75mm Diameter and 100mm Diameter Cylinders for High Strength Concrete, Cement and Concrete Research International Journal, Vol. 32, Issue 4, April 2002, pp. 607-613.

98. Patnaik, A.K., Discussion for Evaluation of ACI 318-95 Shear-Friction Provisions, Paper by R. Valluvan, M.E. Kreger, and J.O. Jirsa, ACI Structural Journal, American Concrete Institute, May-June 2000, 97(3):525-526.

99. Patnaik, A.K., Discussion for Horizontal Shear Strength of Indirectly Loaded Composite Concrete Beams, Paper by K.H. Tan, L.W. Guan, X. Lu, and T.Y. Lim, ACI Structural Journal, American Concrete Institute, May-June 2000, 97(3):529.

100. Patnaik, A. H. (2001). Behavior of composite concrete beams with smooth interface. ASCE J Struct Eng.

101. Patnaik, A., Habouh, M., & Almonbhi, A. (2015). Effectiveness of Adjacent Precast Concrete Box-Beam Connections. *Ohio Transportation Engineering Conference* (p. 43). Columbus: The Ohio Department of Transportation.

102. Patnaik, A.K., Ramakrishnan, V. and Ganesh babu, K., (Editors), Use of High Volume Fly Ash Concrete and the Related Environmental Effects, Proceedings of the National Science Foundation (NSF) sponsored US-India Workshop – January 2004, Chennai, India. 215 pages.

103. Patnaik, A., Baah, P., Ricciardi, P., and Khalifa, W., Cracking Behavior of Three Span Structural Slab Bridge Decks, Paper # 15-3445, TRB Annual Meeting 2015, Washington DC, Compendium of Papers, Jan. 2015, 16 pages.

104. Patnaik, A., Musa, A., Marchetty, S., and Liang, R., Full-Scale Testing and Performance Evaluation of Rockfall Concrete Barriers, Paper # 15-3464, TRB Annual Meeting 2015, Washington DC, Compendium of Papers, Jan. 2015, 15 pages.

105. Patnaik, A., Miller, L., and Standal, PC., Fiber Reinforced Concrete Made from Basalt FRP Minibar, Concrete Innovation Conference 2014 - CIC 2014, June 11-13, 2014, Oslo, Norway, 10 pages.

106. Patnaik, A., Bajaj, S., Lewis, J., Payer, J., and Liang, R., Retardation of Strength Degradation of Reinforced Concrete due to Steel Bar Corrosion with Fiber Additions, DoD Corrosion Conference 2013, NACE International, Sept. 16-17, 2013, 14 pages.

107. Patnaik, A., Miller, L., Adhikari, S., and Standal, PC., Basalt FRP MiniBar Reinforced Concrete, Fibre Concrete 2013, Sep. 12-13, 2013, Prague, Czech Republic, 10 pages.

108. Patnaik, A., Payer, J., Liang, R., Xia, N., Shan, X., Bajaj, S., Lewis, J., and Yousif, H., Experimental Evaluation and Computation Modeling of Non-Uniform Corrosion of Steel Reinforcement in Concrete, 2011 DoD Corrosion Conference, NACE International, Palm Springs, CA July-Aug. 2011, 12 pages.

109. Patnaik, A.K., Behavior of Composite Concrete Beams with a Smooth Interface, Journal of Structural Engineering, American Society of Civil Engineers, April 2001, Vol. 127 No. 4, pp. 359-366.

110. Patnaik, A.K., Longitudinal Shear Strength of Composite Concrete Beams with a Rough Interface and no ties, Australian Journal of Structural Engineering, IEAust, 1999 V1(3): pp. 157-166.

111. Patnaik, A., Musa, A., Marchetty, S., and Liang, R., Full-Scale Testing and Performance Evaluation of Rockfall Concrete Barriers, Transportation Research Record: Journal of the Transportation Research Board, No. 2522-03, 2015, DOI 10.3141/2522-03, pp. 27-36.

112. Patnaik, A., Habouh, M., and Almonbhi, A., "Waterproofing Details of Connections for Adjacent Precast Concrete Box-Beam Bridges", Draft Final Report, Ohio DOT/FHWA ORIL project, SJN 134847, September 2015, 108 pages.

113. Patnaik, A., and Baah, P., "Cracking Behavior of Structural Slab Bridge Decks", Final Report, ODOT/FHWA SJN 134708, January 2015, 214 pages.

114. PCI Committee on Bridges. (2009). The State of the Art of Precast/Prestressed Adjacent Box Beam Bridges. chicago: Precast/Prestressed Concrete Institute.

115. PCI. (2009). The State of the Art of Precast/Prestressed Adjacent Box Beam Bridges.

116. Pedro, M. S., & Eduardo, N. B. (2011). Factors Affecting Bond Between Old And New Concrete. ACI Material Journal , 108 (4), 449-456.

117. Pedro, M. S., & Eduardo, N. J. (2012). A state-of-the art review on shear friction. Engineering Structures , 45, 435–448.

118. pedro, M. S., & Eduardo, N. J. (2013). A State of The Art Reviw on Roughness Quantification Method for Concrete Surfaces. Construction and Building Materials 38 912-923 .

119. Pessiki, S., Kaczinski, M., & Wescott, H. H. (1996, November-December). Evaluation of Effective Prestress Force in 28-Year-Old Prestressed Concrete Bridge Beams. PCI journal, 41(6), 78-89. Retrieved from http://www.pci.org/uploadedFiles/Siteroot/Publications/PCI_Journal/1996/DOI_Articles/jl-96-november-december-6.pdf

120. Polyguard Products Inc. (2010). *Polyguard 1100 Membrane Data Sheet .* Ennis: Polyguard Products Inc.

121. Polyguard Products Inc. (2013). *NW-75 Membrane data sheet.* Ennis: Polyguard Products Inc.

122. Poston, R. W., Phipps, A. R., Almustafa, R. A., Breen, J. E., & Carrasquillo, R. L. (1988). Effect of Transverese Prestressing in Bridge Decks. Journal of Structural Engineering , 114 (4), 743-764.

123. Propex Operating Company LLC. (2011). *Product Data Petrotac 4591 .* Chattanooga: Propex Operating Company LLC.

124. Ramakrishnan, V., and Patnaik, A.K., Implementation of High Performance Concrete with Optimized Aggregate Gradation And Flyash in Bridge Decks, the proceedings of the international conference on Recent Advances in Concrete Technology (RAC07), Baltimore, MD, Sep. 2007, 20 pages.

125. Ramakrishnan, V., Zellar, R., and Patnaik, A.K., A High Performance Fiber for Reducing Plastic Shrinkage Cracks in Concrete, Proceedings of Recent Advances in Engineering Mechanics Conference (RAEM 2006): Editors – J. Kreiner, and C. Putcha, Fullerton, CA, Jan. 2006, pp. 19-25.

126. Ramakrishnan, V., Zellar, R., and Patnaik, A.K., Plastic Shrinkage Reduction Potential of a new High Tenacity Monofilament Polypropylene Fiber, in American Concrete Institute ACI/CANMET Special Publication SP243 on Recent Advances in Concrete Technology - Editor: V.M. Malhotra, May 2007, pp. 49-62.

127. Rangan, B. V. and Patnaik, A. K. (Editors), High Performance High Strength Concrete, the Proceedings of the International Conference, Perth, Australia, August, 1998, ISBN: 1 863 42 2846, 739 pages.

128. Rangaraju, P. R., Kizhakommudom, H., Li, Z., & Schiff, S. D. (2014). Development of High-Strength/High Performance Concrete/Grout Mixtures for Application in Shear

Keys in Precast Bridges. Clemson University, Glenn Department of Civil Engineering. SOUTH CAROLINA: South Carolina Department of Transportation.

129. Rao, C., & Frantz, G. C. (1996). Fatigue Tests of 27-Year-Old Prestressed Concrete Bridge Box Beams. PCI Journal , 41 (5), 74-83.

130. Raths, C. H. (1977). Reader comments of paper "Design proposals for reinforced concrete corbels" May-June 1976;21(3):18-42, by Mattock A PCI. PCI .

131. Roberts, S. E. (2010). Influence Of Shear Key Performance On The Fatigue Life Of Adjacent Beam Bridges. Master Thesis, Clemson University, Civil Engineering Departement , Clemson.

132. Russell, H. G. (2009). Adjacent Precast Concrete Box Beam Bridges :Connection Details. The National Academies of Sciences, Engineering, and Medicine. Glenview: NCHRP.

133. Russell, H. G. (2011). Adjacent precast concrete box-beam bridges:State of the practice. 56 (1), 75-91.

134. Russell, H. G. (2011). Waterproofing Memberannes for Concrete Bridge Decks. A Synthesis of Highway Practice (425), 32.

135. Russell, H. G. (2012). Discussion , Adjacent box-beam bridges. PCI Journal , 57 (4), 134-137.

136. Saibabu, S., Lakshmanan, N., Rama, A., Chitra, S., Jayaraman, R., & Senthil, R. (2009). External Prestressing Technique for Strengthening of Prestressed Concrete Structural Components. Practice Periodical on Structural Design and Construction, 14 (2), 90-98.

137. Scianna, A., Prusaczyk, S., Jiang, Z., Christenson, R. E., DeWolf, J. T., & Kim, J.-H. (2014). Monitoring of Curved Post-Tensioned Concrete Box-Girder Bridge – I-384 WB Over I-84 in East Hartford (Bridge #5686). Connecticut Transportation Institute, Connecticut Department of Transportation. Storrs: University of Connecticut.

138. Sennah, K. M., & Kennedy, J. B. (2002). Literature Review in Analysis of Box-Girder Bridges. Journal of Bridge Engineering, 7 (2), 134-143.

139. Shamass, R., Zhou, X., & Alfano, G. (2015). Finite-Element Analysis of Shear-Off Failure of Keyed Dry Joints in Precast Concrete Segmental Bridges. Journal of Bridge Engineering, 20 (6), 04014084(1-12).

140. Shann, S. V. (2012). Application of ultra high performance concrete (UHPC) as a thin-bonded overlay for concrete bridge decks. Department of Civil and Environmental Engineering. Houghton: Michigan Technological University.

141. Sharpe, G. P. (2007). Reflective Cracking of Shear Keys in Multi-Beam Bridges. Huston: Texas A&M University.

142. Shushkewich, K. W. (2006, January). Transverse Analysis of Strutted Box Girder Bridges. Journal of Bridge Engineering, 11(1), 33-47. Retrieved from http://dx.doi.org/10.1061/(ASCE)1084-0702(2006)11:1(33)

143. Sohanghpurwala, A. A. (2006). *NCHRP Report 558: Manual on Service Life of Corrosion-Damaged Reinforced Concrete Bridge Superstructure Elements.* Transportation Research Board of the National Academies. Washington, D.C.: NCHRP.

144. Steinberg, E., & Miller, R. A. (2011). Assessment of Deteriorated PrestressedConcrete Bridge Box Beams. Ohio University , University of Cincinnati, Department of Civil Engineering. Columbus : The Ohio Department of Transportation.

145. Strandquist, B. V. (2012). *Assessment of Bridge Deck Protective Systems.* Purdue University, www.docs.lib.purdue.edu/dissertations/AAI1535165/.

146. Tabatabai, H., & Dickson, T. J. (1993, September-October). Structural Evaluation of a 34-Year-Old Precast PostTensioned Concrete Girder. PCI journal, 38(5), 50-63. Retrieved from http://www.pci.org/uploadedFiles/Siteroot/Publications/PCI_Journal/1993/DOI_Articles/jl-93-september-october-6.pdf

147. Tadros, M. K., & Morcous, G. (2009). Application of Ultra-High Performance Concrete to Bridge Girders. University of Nebraska-Lincoln, Departement Of Civil Engneering. Lincolin: Nebraska Department of Roads.

148. Tapan, M. (2006, August). Strength Evaluation of Deteriorated Reinforced Concrete Bridge Columns. Dissertation, Graduate School of Syracuse University.

149. Ubbing, J. L. (2014). Analytical Investigation of Adjacent Box Beam Ultra-High Performance Concrete Connections. 1-111.

150. Ulku, E., Attanayake, U., & Aktan, H. M. (2010). Rationally Designed Staged Posttensioning to Abate Reflective Cracking on Side-by-Side Box-Beam Bridge Decks. Journal of the Transportation Research Board, 2172 (10), 87–95.

151. United Kingdom Department for Transport (UKDOT). (1999). *Design Manual for Roads and Bridges, Volume 2.* London: UKDOT.

152. W. R. Meadows Inc. (2013). *Product Data of MEL-ROL Rolled, Self-Adhering Waterproofing Membrane.* Hampshire: W. R. Meadows Inc.

153. Wall, J. S., & Shrive, N. G. (1988). Factors Affecting Bond Between Old and New Concrete. ACI Material Journal , 85-M15.

154. Weldon, B. D., Jáuregui, D. V., Newtson, C. M., Taylor, C. W., Allena, S., Montoya, K. F., et al. (2012). Feasibility Analysis of Ultra High Performance Concrete for Prestressed Concrete Bridge Applications . New Mexico State University , Department of Civil Engineering . Las Cruces, NM : New Mexico City Department of Tranportation.

155. Wille, K. (2013). Development of Non-Proprietary Ultra-High Performance Concrete for Use in the Highway Bridge Sector. McLean, VA: Federal Highway Administration.

156. Wong, R., Ma, S., Wong, R., & Chau, K. T. (2007). Shear strength components of concrete under direct shearing (Vol. 37). Cement and Concrete Research.

157. Wood, C. (2008). Rehabilitation of a Prestressed Concrete Box Beam Bridge. Montgomery County, Ohio: ODOT.

158. Xia, N., Liang, R.Y., Payer, J., Patnaik, A., Probabilistic modeling of the bond deterioration of fully-grouted rock bolts subject to spatiotemporally stochastic corrosion, Structure and Infrastructure Engineering, Vol. 9, No. 11, Nov. 2013, pp. 1161-1176.

159. Xia, N., Qingwen R., Liang, R.Y., Payer, J., Patnaik, A., Non-Uniform Corrosion Induced Stresses in Steel Reinforced Concrete, ASCE Journal of Engineering Mechanics, Vol. 138, No. 4, April 2012, pp. 338-346.

160. Xia, J. (2011). Ultra-High Performance Fiber Reinforced Concrete in Bridge Deck Applications.

161. Ya-dong, Z., & Xu-dong, S. (2015). Research on Twice-prestressed Composite Beam and Its Application in Highway Bridges. Journal of Highway and Transportation Research and Development, 9 (2), 47-53.

162. Yamane, T., Tadros, M. K., & Arumugasaamy, P. (1994). Short to Medium Span Precast Prestressed Concrete Bridges in Japan. PCI Journal, 39 (2), 74-100.

163. Yuan, A., Qian, S., He, Y., & Zhu, X. (2015). Capacity Evaluation of a Prestressed Concrete Adjacent Box Girder with Longitudinal Cracks in the Web. Journal of Performance of Constructed Facilities, 29 (1), 04014028(1-9).

164. Zhou, S.-J. (2011). Shear Lag Analysis in Prestressed Concrete Box Girders. Journal of Bridge Engineering, 16 (4), 500-512.

165. Xia, N., Liang, R., Payer, J., and Patnaik, A., A Study of Concrete Behavior Due to Non-Uniform Corrosion of Reinforcing Bars, 2011 DoD Corrosion Conference, NACE International, Palm Springs, CA July-Aug. 2011, 12 pages.

Waterproofing Details of Connections for Adjacent Precast Concrete Box-Beam Bridges

Appendix B: Waterproofing Membrane Evaluation

Prepared by:

Ali Almonbhi, PhD (Former Graduate Student)
Mohamed Habouh, PhD (Former Graduate Student)
Anil Patnaik, PhD (Principal Investigator)

Prepared for:

The Ohio Department of Transportation
Office of Statewide Planning & Research

State Job Number 134847

07/25/2018

Waterproofing Details of Connections for Adjacent Precast Concrete Box-Beam Bridges

Appendix B: Waterproofing Membrane Evaluation

Prepared by:
Ali Almonbhi, PhD and
Mohamed Habouh, PhD
Former Graduate Students, Department of Civil Engineering
The University of Akron, Akron, OH 44325-3905

Dr. Anil Patnaik (PI)
Professor, Department of Civil Engineering
The University of Akron, Akron, OH 44325-3905
Phone: 330-972-5226 Email: Patnaik@uakron.edu

July 2018

Prepared in cooperation with the Ohio Department of Transportation,
Ohio's Research Initiative for Locals, and the U.S. Department of Transportation, Federal Highway Administration

TABLE OF CONTENTS

LIST OF FIGURES

LIST OF TABLES

APPENDIX B: WATERPROOFING MEMBRANE EVALUATION

B.1 Introduction

Waterproofing membranes are widely used as a protective system for concrete members that are exposed to rainwater and moist conditions. In this appendix, the testing methods and evaluation of the waterproofing systems that are normally used for adjacent box beam bridges are briefly described and the performance of some of the typical membranes evaluated. Most of the earlier research studies on membranes emphasized the evaluation of the membrane sheets alone. Membrane performance by itself is an important part of the system in providing watertightness, but the performance of the waterproofing membrane as a system in conjunction with concrete substrate is equally important. In this project, the evaluation of waterproofing systems was done under two conditions, i.e., (i) membrane performance in isolation and (ii) performance when the membrane was adhered to a concrete substrate. The primary objective in this task was to evaluate sheet membranes based on their ability to accommodate stretching, adhere to concrete, and resist punching while providing an adequate water barrier in a box beam bridge configuration. The following tests were conducted for the evaluation of typical waterproofing membranes:

1. Tensile tests at different temperatures
2. Adhesion tests
3. Differential deflection tests
4. Punching tests
5. Tests to detect initiation of leakage
6. Membrane performance under passenger car wheel load

Laboratory testing of membrane sheets provide good insight into the sheet behavior and was a good starting point to understand the waterproofing membrane system. Mechanical properties such as tensile strength and elongation were evaluated first. More complexities such as the effects of concrete surface condition and adhesion, sharp edges within joints and tearing potential, wheel load condition and the directionality of wheel loads were also studied. Tensile tests were used to determine the elongation characteristics. The bond between a waterproofing membrane and the adjoining concrete surface was studied using adhesion tests. After the adhesion test, the potential for leakage of water during extension of membrane was established using a new type of leakage initiation test. Waterproofing membranes were also tested for punching resistance to address the effects of sharp edges and pointed surfaces caused by debris and loose aggregates present on concrete surfaces.

The ODOT Qualified Product List (QPL) of waterproofing membranes for both Type II and Type III membranes was considered in developing a test plan. Type II membranes are “peel and stick” membranes that are normally used on vertical surfaces. ODOT mostly does not use this type of membrane for waterproofing bridge decks which are mostly horizontal surfaces. Type III membranes are commonly used on flat horizontal surfaces with just primer or with primer and sealant. All waterproofing membranes are standardized based on ASTM tests and need to meet the ODOT requirements before these membranes are approved for use. The required ASTM tests for the prequalification of membranes were reviewed from the existing

literature. Table B.1 shows the requirements for ODOT Type III membranes and Table B.2 shows the requirements for Type II membranes (Ohio Department of Transportation , 2013). Moreover, the entire list of waterproofing membrane test results was reviewed based on the data sheets provided by manufacturers.

Table B.1: Type III Waterproofing Membrane Requirements

Physical Properties	**Requirements**	**ASTM Test**
Thickness	0.135 inches (3.43 mm) min.	-
Width	36 inches (914 mm) min.	-
Weight	0.8 lb/ft^2 (3.875 kg/mm^2) min.	-
Tensile strength (machine direction)	275 lb/in (48.1 N/mm)	ASTM D 882 Modified [1]
	200 psi (13.8 MPa)	
Tensile strength	150 lb/in (26.2 N/mm)	ASTM D 882 (90° machine direction) Modified [1]
	1000 psi (6.9 MPa)	
Elongation at break	100%	ASTM D 882 Modified [1]
Brittleness	Pass	ASTM D 517
Softening point (mastic)	200°F (93°C) min.	ASTM D 36
Peel adhesion	2.0 lb/in (0.35 N/mm)	ASTM D 413 [1]
Cold flex ASTM D 146 2X5 inch (50x125 mm) specimen-180° bend over 2 inch (50 mm) mandrel	No cracking	-
Heat stability 2x5 in. (50 x125 mm) specimen vertically suspended in a mechanical convection oven 2 hr @ 190 °F (88 °C)	No dripping or delamination	-

Source: (Ohio Department of Transportation , 2013)

[1] Measured at a test speed of 12 inches/minute (300 mm/minute) with 1 inch (25 mm) initial distance between the grips.

Table B.2: Type II Waterproofing Membrane Requirements

Physical Properties	ODOT Requirements	ODOT/ASTM Tests
Thickness	60 mils (1.5 mm) min.	ASTM D 1777
Width	36 inches (914 mm) min.	-
Pliability	No Effect	ASTM D 146 [1]
Elongation	300% min	ASTM D 412 (Die C)
Puncture Resistance-Membrane	40 lb (18 kg) min.	ASTM E 154
Permeance (Grains/ft2/hr/in Hg)	0.1 max.	ASTM E 96 (Method B)
Water Absorption (% by Weight)	0.2 max.	ASTM D 570
Adhesion to concrete	5.0 min.	ASTM D 903

Source: (Ohio Department of Transportation , 2013)
[1] Tests conducted using a 180° bend over a ¼ inch (6 mm) mandrel @ -25° F (-32° C)

Five different representative waterproofing membranes were selected for the evaluation in this study as listed in Table B.3. Some of the waterproofing membranes tested were selected from ODOT's Qualified Product List (QPL), and the remaining membranes were not included in the approved list. Both self-adhesive (SA) type and traditional, non-adhesive type membranes were tested. These five membranes are considered to be representative of the membrane types commonly used in the industry.

Table B.3: Waterproofing Membranes Evaluated in This Study

#	Brand Name	Type	Manufacturer
1	Polyguard 1100	Type III	Polyguard Products, Inc
2	665 Membrane	SA, Not in ODOT QPL (Type II)	Polyguard Products, Inc
3	Coldflex 2000 SA	SA, Not in ODOT QPL (Type II)	Polyguard Products, Inc
4	PavePrep	Type III	Crafco, Inc.
5	PavePrep SA	Type II	Crafco, Inc.

SA = Self-adhesive

B.2 Evaluation Tests for Waterproofing Membrane

B.2.1 Tensile Strength at Different Temperatures

B.2.1.1 Test Setup

Ideally, waterproofing membranes must be able to bridge the cracks at the longitudinal joints between adjacent box beams mostly by stretching without losing its waterproofing property. The cracks at such longitudinal joints widen the most at low temperatures. Waterproofing membranes are generally not strong enough to resist the forces caused by vertical and horizontal movements at a crack. However, membranes need to stretch adequately to accommodate crack widening without losing the watertightness property.

In addition, membranes need to stretch in such a way that the differential deflections between adjacent box beams can be accommodated without losing watertightness. Tensile and elongation tests are useful to measure the capacity of the waterproofing membranes to elongate under tensile forces. Furthermore, the effects of temperature changes were also included in this test. Each type of membrane was tested at five different temperatures: 70°, 40°, 23°, 14° and -4° F. Each sample was conditioned in an environmental chamber at the desired temperature for at least one hour before testing. Tensile tests were based on the test procedures specified in ASTM standards D412, D638, D882, D2523, and D4885. The specimens were dog-bone shaped with a total length of 10 inches. Figure B.1 shows the shape and dimensions of typical tensile test specimens. Steel plates were glued to the membrane specimens at the ends using an epoxy having 3,300 psi bond strength.

Fig. B.1 Typical Tensile and Elongation Test Specimen Dimensions (inches)

In this test, two important parameters were determined: the maximum load the specimen can carry and the corresponding maximum elongation. The typical load versus elongation curves for the five types of membranes at room temperature are shown in Fig. B.2. As seen in this figure, specimens elongated even after the maximum load was reached, after which point, the specimens started to lose their ability to resist load. The failure mode (Fig. B.3) for the test specimens was mostly identical.

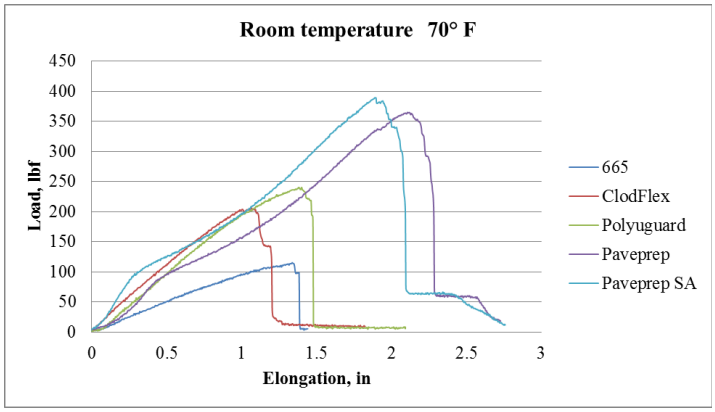

Fig. B.2 Typical Load-Elongation Curves for Five Membranes at 70° F

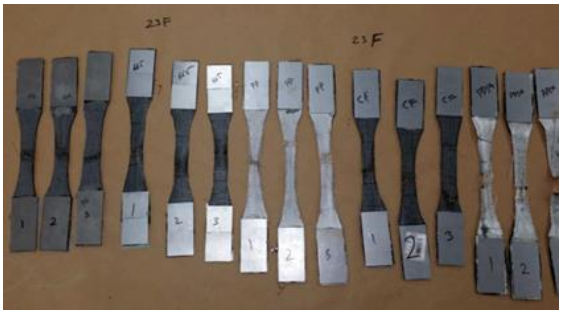

Fig. B.3 Specimen Failure Mode

B.2.1.2 Test Results and Discussion

The tensile strengths of the waterproofing membranes were found to be very low and, thus, the membranes cannot be expected to resist much load at the longitudinal joints of box-beam bridges. Therefore, these membranes may be considered as nonstructural. Low tensile strengths of the membrane become less important than their ability to elongate. Nevertheless, all five membranes showed relatively constant tensile strengths at all temperatures (Fig. B.4). The reduction in the capacity to elongate was, however, more prominent with up to 40% loss in elongation compared the elongation at room temperature when specimen temperature was reduced to -4° F (Fig. B.5). This translates to about 5% reduction in actual elongation. Tensile tests showed that Paveprep and Paveprep SA were superior in both elongation and tensile strength compared to other membranes. For all membranes, the elongation of over one inch is much larger than what can be expected at the longitudinal joints of adjacent box beams.

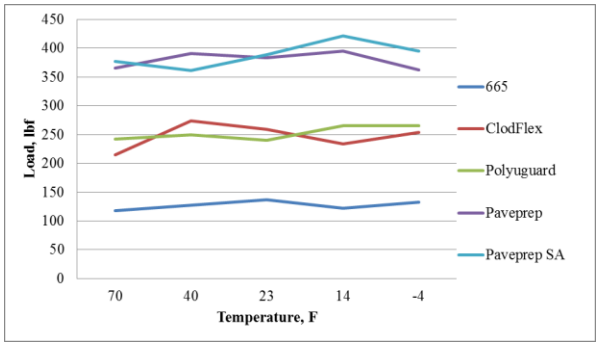

Fig. B.4 Tensile Strength Curves for Five Membranes at Five Temperatures

B.2.2 Adhesion Test

B.2.2.1 Test Setup

Adhesion failure between a waterproofing membrane and the concrete bridge deck is one of the most common problems in the waterproofing industry (Fig. A.47 in Appendix A). This failure causes water to seep from underneath the membrane sheets; and debonding between

a waterproofing membrane and the adjacent concrete surface can occur due to blistering (Fig. A.47 in Appendix A). This was also reported by Frosch, et al. (2013). Both Type II "peel-and stick" and Type III membranes suffer from membrane blistering.

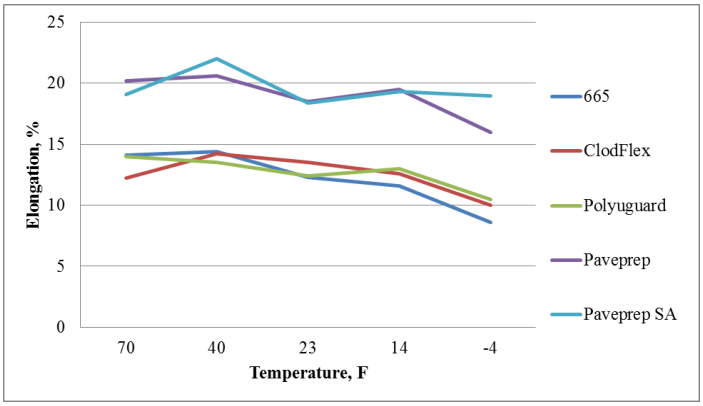

Fig. B.5 Percentage Elongation Curves for Five Membranes at Five Temperatures

For Type III membranes, it is a common practice to use a bonding agent between the membrane and the primed concrete surface. In Type II membranes, the bonding agent is part of the membrane sheet and in some cases an extra bonding agent may also be needed. According to ODOT CMS 2013, the requirements for using a primer coat seem to be general for all cases (Types II and III). However, for Type II the requirement is to use primer if substrate temperature is below 50° F. Some manufacturers require primer to be used for Type II membranes when the pavement surface temperature is low. For example, if the deck temperature is below 70°F (21°C), primer is required prior to the installation of Paveprep SA (Type II).

Adhesive strength between waterproofing membranes and concrete surfaces was measured by peeling membrane sheet strips from hardened cement mortar blocks at an angle of 180°. Tensile load was applied at a constant rate of 0.4 inch per minute until each strip was peeled off from the specimen's mortar block completely. The mortar blocks were prepared in sizes of 4"×4"×14" and cut into 4"×4"×2" blocks. Only saw-cut faces were used to attach waterproofing membranes so as to reduce any variation due to different surface roughness of as-cast surfaces and to ensure repeatability of the tests. The manufacturers' instructions were followed to apply the primer and the sealant. Fig. B.6 shows the test setup for adhesion tests and the failure mode of the test specimens. A wooden frame was used to stabilize the test specimens during testing.

Direct heat application with a gas torch is used in some countries to increase the bond strength between the membrane and the substrate (Frosch et al., 2013). There is no mention of heat application in the manufacturers' data sheets for the waterproofing membranes that were used in this study. The sealant used in this study was "Hot-Applied Modified Asphalt Sealant" made by Crafco. The primer was 33140 Crafco Asphalt Primer.

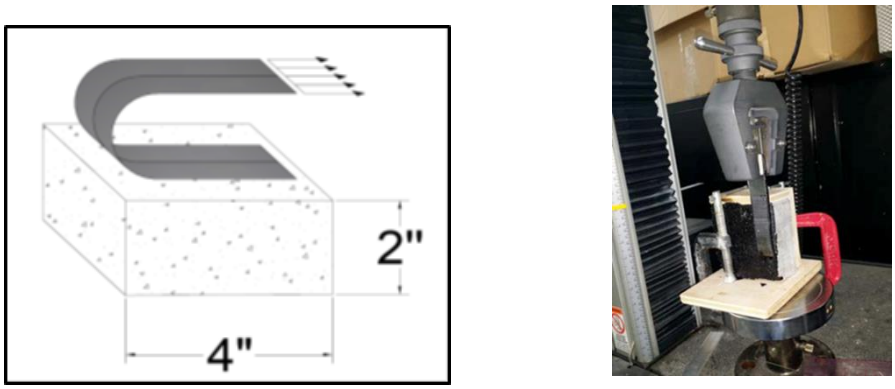

Fig. B.6 Adhesion Test Details

In order to comply with the relevant ODOT and membrane supplier requirements, primer was used on all the specimens in this test (i.e., for both Type II and Type III membranes). Three samples (strips) were tested to measure the potential improvement of adhesion strength due to the application of heat to Type II membranes. A sealant is normally applied to Type III membranes at 380°F as a common practice. The following three combinations were tested:

1. Samples with the use of direct heat and the use of primer and sealant together as bonding agent.
2. Samples with no heat application and with the use of primer and sealant together as bonding agent.
3. Samples with the use of direct heat and the use of only primer as the bonding agent, but no sealant.

B.2.2.2 Test Results and Discussion

Remarkably, all waterproofing membranes that were tested (both Type II and Type III) showed very little peel-off or adhesive strength. For the first set of test specimens that were subjected to direct heat with the use of primer and sealant as the bonding agent, the average peel forces were between 15 to 18 lb per one-inch width. For the second set of specimens, which were prepared similar to the first set but without any application of direct heat, the peel-off strengths were between 13 to 20 lb per inch width. For the third set, when only primer was used as the bonding agent without any sealant, the peel-off strengths were less than 15 lb per one-inch width.

Fig. B.7 shows typical trend lines for three load-extension curves corresponding to the three conditions. The adhesive strength between the membrane and concrete seems to be negligible and may need to be enhanced for improved waterproofing performance. The improvement in adhesive strength due to the use of direct heat is very limited. Also, tests suggest that the primer and sealant together (#1) perform better than when primer alone (#3) is used as the bonding agent.

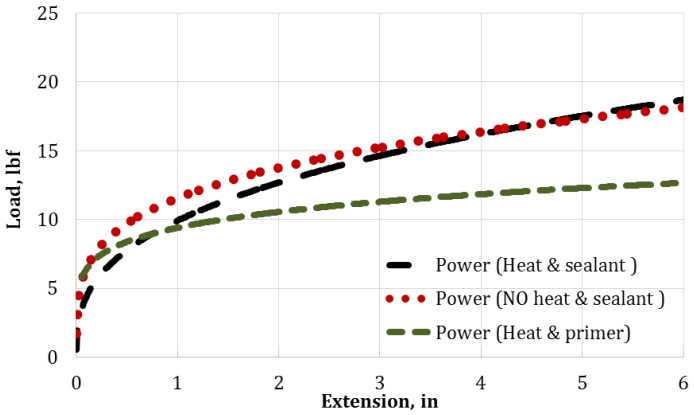

Fig. B.7 Comparisons of Three Sets of Adhesion Tests

B.2.3 Ultimate Differential Deflection Test

The ultimate differential deflection test is a new type of test intended to simulate a realistic and extreme condition that a membrane may face during its service life. This test was designed to determine the maximum differential deflection that a membrane can accommodate under shear loading. The loading direction in a tensile test is parallel to the specimen in the plane of the membrane. Differential deflection of adjacent box beams in a bridge would cause a shear type of deformation of the membrane which is out-of-plane of the membrane when adjacent box beams deflect unequally. The objective of this test was to determine the ultimate elongation capacity of waterproofing membranes subjected to shear loading in the presence of differential movement under the asphalt concrete overlay next to the sharp edges of the box beams in a bridge.

B.2.3.1 Test Setup

In order to simulate the longitudinal joints in a precast box-beam bridge, four mortar blocks of 2”×4”×4” were carefully cut. The lower two blocks were placed close to each other with very little gap between the blocks at the joint. The waterproofing membrane was applied to these two adjacent mortar blocks. Manufacturer’s instructions were followed for installation of the different membranes. For both Type II and Type III membranes, sealant was applied to enhance bonding. The membrane was wrapped around the lower two mortar blocks to be well anchored under the clamps. The upper two mortar blocks were placed on the top of the lower blocks without bonding agent to simulate placement of an asphalt/concrete overlay over the membrane without a binder between these two layers. Fig. B.8 shows a typical setup for these tests.

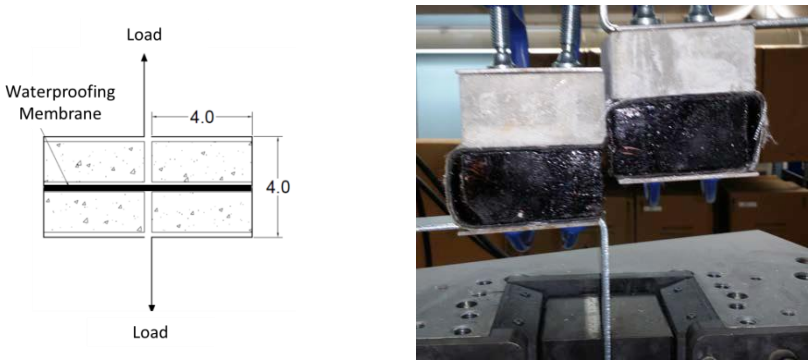

Fig. B.8 Ultimate Differential Deflection Test Details

B.2.3.2 Test Results and Discussion

Fig. B.9 shows typical load-elongation curves for the five membranes that were tested. The specimens were four inches in width. However, for a comparison of loads and elongations, these curves were normalized to a one-inch width. Large differential elongations of at least 1.0 inch were recorded for each of the five test membranes. Most samples of Polyguard, ColdFlex, and 665 membranes failed partially; others failed by full rupture. Almost all the samples of Paveprep and Paveprep SA failed by full rupture. Fig. B.10 shows the typical failure modes of the test specimens.

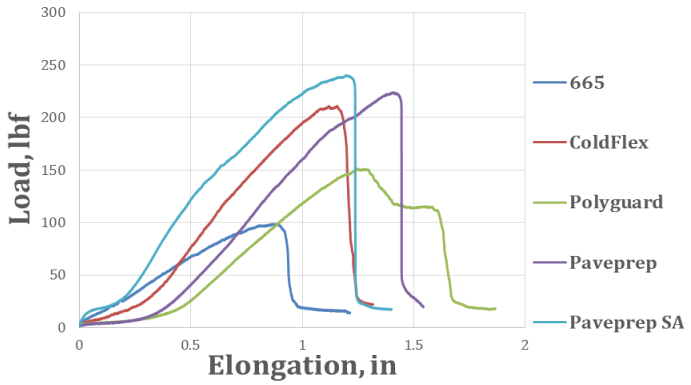

Fig. B.9 Typical Differential Deflections for 1-inch-wide Specimens

Fig. B.10 Ultimate Differential Deflection Failure Modes: Full Rupture (*left*) and Partial Rupture (*right*)

B.2.4 Leakage Initiation Detection

From previous tests (tensile tests and differential deflection tests), the capacity of a membrane to stretch was found to be large. The question to be answered in this test was if the waterproofing membrane can prevent leakage while it stretches by as much as one inch. After many unsuccessful trials, the test plan was repeatedly revised and improved to develop a suitable water leakage test.

The primary intent of the leakage tests was to investigate if there is any leakage before the membrane reaches its deformation limits. It was important to determine if the membrane can retain its waterproofing property over the entire time of its deformation.

For this test, a one-inch differential deflection limit was assumed to be satisfactory. Furthermore, one inch of elongation is fairly large and was considered adequate to accommodate typical differential deflections in box-beam bridges. These tests were done under extension control of 0.2 inch per minute, which is slow enough to detect with the naked eye any leakage over the blotting paper attached to the membrane.

B.2.4.1 Test Setup

The first test setup tried in this study used a square-shaped specimen and a square-shaped frame loaded with a square-shaped loading plate. The sharp corners of the loading plate damaged the membrane specimen during the trial tests. Therefore, the test results with square specimens were disregarded. The revised test setup comprised a circular transparent plexiglass hollow tube and a circular loading plate. Dyed water was used to fill around the loading plate in the deflected region of the membrane while the loading plate was being plunged into the membrane, which was firmly attached to the top of the tube. Blotting paper was attached to the plexiglass tube on the inside of the tube to detect any dripping of dyed water. The frame for the leakage initiation detection test is shown in Figs. B.11 and B.12. A four-inch-diameter loading plate was used to plunge into the membrane. An Instron HDX loading machine was used in this test.

B.2.4.2 Test Results and Discussion

All five types of waterproofing membranes were subject to the detection of leakage initiation test. In this test, loading was continued until a one-inch depression of the membrane was achieved relative to the rim of the hollow tube. All five membranes passed the one-inch deflection criterion used in this test without any indications of water leakage. Figure B.13 shows top and bottom views of a typical specimen after the test. These tests demonstrated that there can be no leakage through the membrane for at least about 1.0 inch of differential deformation. Figure B.14 shows a typical load-elongation curve. This test confirmed that waterproofing membranes were able to maintain watertightness even after deforming one inch, which is significant.

Fig. B.11 Hollow Tube Used in the Test

Fig. B.12 Detection of Leakage Initiation Test Setup

Fig. B.13 Top (*left*) and Bottom (*right*) Views of a Typical Test Specimen after the Test, Showing no Leakage at the Bottom

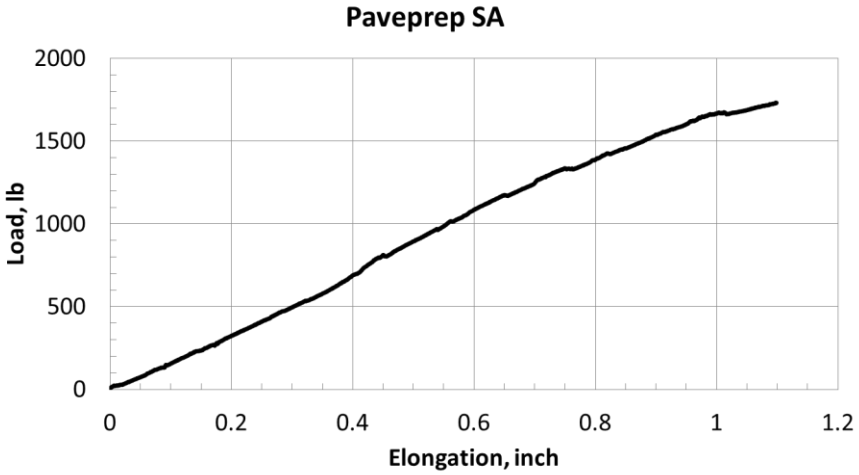

Fig. B.14 Load vs. Elongation for a Typical Detection of Leakage Initiation Test

B.2.5 Punching Test

A waterproofing membrane can tear or be punched through during construction. For example, loose aggregate or debris with sharp corners that exist on the top surface of bridge decks when the waterproofing membrane is laid may punch through the membrane if any wheel load is applied to the bare membrane before the asphalt concrete overlay is placed. Furthermore, asphalt concrete generally contains (over 85% by volume) crushed aggregate with a variety of angularity and sharpness characteristics, and those sharp corners may be a source for punching failures. This test was designed and conducted to determine the punching resistance of waterproofing membranes.

The main objective of this test is to purely determine the punching resistance of membranes. Punching resistance is one of the key factors for membrane classification in terms of watertightness. There is currently no standardized method to perform this test and therefore a new test was designed and used in this study.

B.2.5.1 Test Setup

An Acme laboratory penetrometer was used for the punching tests. This penetrometer is equipped with an arm to apply loads manually and has a load cell to measure the applied load during the test. As a modification to this equipment, an ohmmeter was attached to detect when punching occurred. The ohmmeter terminal wires were connected to the plunging tip on one side and to a steel plate under the membrane test specimen on the other end. The ohmmeter provides an indication of punching by making a beeping sound and changing the digital reading when the circuit becomes closed, i.e., the tip of the plunger penetrates the membrane and touches the steel plate below the membrane. The load was recorded for each punching occurrence. Figs. B.15 and B.16 show the punching test setup used in this study.

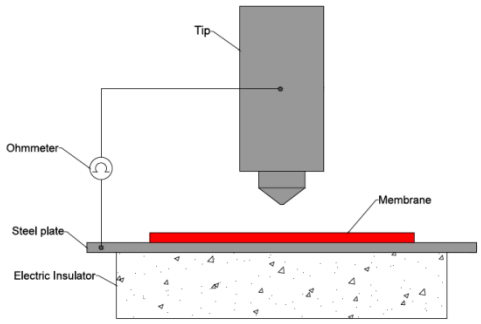

Fig. B.15 Schematic of the Punching Test

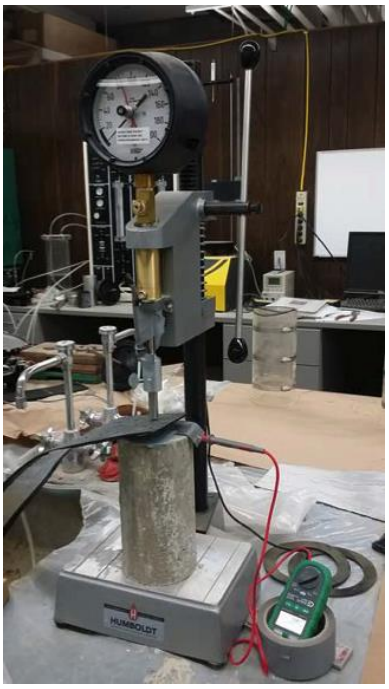

Fig. B.16 Punching Test Setup

The tip shown in Fig. B.15 was made from a low carbon steel bar, that provides good electrical conductivity. The tip was designed to simulate the effect of sharp corners of grit, aggregate, or beam corners. A 37.5° angle was used. The schematic details of the setup are shown in Fig. B.15. Membrane test specimens were cut into 4" wide strips before testing.

Type II membranes, which are self-adhering, are supplied with a non-conductive protective sheet on the surface with the adhesive coating. Type III membranes do not come with such protective sheets. For test specimens made from Type II membranes, the protective sheets were removed before placing the specimen on the bottom steel plate. Aluminum foil was attached to the sticky surface of the membrane so that the membrane would not stick to the steel plate below the specimen. The aluminum foil attached underneath the membrane specimens allowed the current to pass through to the steel plate upon penetration of the plunger. All punching tests were conducted at room temperature.

B.2.5.2 Test Results and Discussion

In this test, five different waterproofing membranes selected in the study were subjected to punching loads. More than forty specimens were tested for each membrane type, and the test results were statistically analyzed after excluding outliers. This test showed superior punching resistance of both PavePrep and PavePrep SA with an average resistance of over 144 lb. Polyguard 665 had the lowest punching resistance with an average of 91 lb.

The punching test results show that waterproofing membranes will be punched through at about 120 lb. For all types of membrane tested in this study, the punching resistance was very low. These membranes have a high risk of getting punched through during construction if they are not properly protected. The movement of heavy construction equipment directly above the membrane will cause such punching type of damage to waterproofing membranes.

B.2.6 Membrane Performance under Passenger Car Wheel Load

A simple test was devised to evaluate the waterproofing membrane performance under a passenger car wheel load of about 1,200 lb. A metal plate assembly was used to test the membrane as shown in Fig. B.17. A car was driven many times on the top of the membrane installed over a plate assembly in directions parallel and transverse to the sharp edge as shown in Fig. B.18. After the wheel load application in each test, the test membrane was separated from the plate assembly and visually inspected. It was observed that there was no shearing or tearing of the membrane after the application of the wheel loading several times. Each membrane was then tested for watertightness. No water leakage was detected, suggesting that the membrane retained its waterproofing property even after wheel loading.

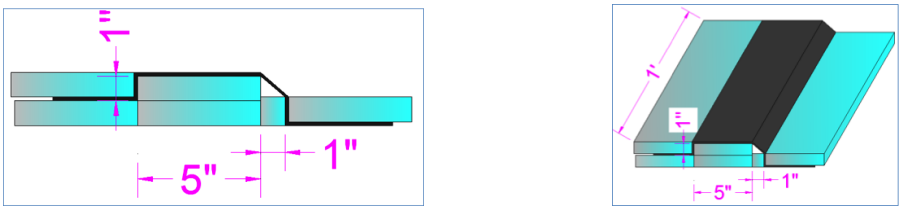

Fig. B.17 Setup for Waterproofing Membrane Test Under Wheel Loads

Fig. B.18 Membrane Subjected to Wheel Loading (1,200 lb)

B.3 Tests on the Aged Membrane Extracted from the RIC-42 Bridge Deck

Pieces of membrane were extracted from the RIC-42 bridge deck before the removal of the box beams that were in service for more than 30 years. The box beams for the bridge were being replaced for the bridge and therefore, sample of membranes were extracted from the bridge as described in Appendix C. However, the membrane samples were full of holes and brittle to the extent that it was possible to break/tear the sample with bare hands. Therefore no membrane tests were possible on the extracted pieces of the membrane from the demolished bridge.

B.4 Summary

The test results presented in this chapter demonstrate that the tensile strength of membranes is low and remains mostly constant over a temperature range of -4° F to 70° F. The elongation of membranes at failure can be over one inch, but the ability to elongate is reduced when temperature reduces from 70° F to -4° F. The adhesion (peel-off) strength of membranes is very low for Type II (self-adhesive) and Type III membranes. Direct heat application on binders does not improve adhesion strength, but use of sealant in addition to primer improves adhesion strength. Membranes are capable of accommodating at least one inch of differential (shear) deformation without rupture. Membranes can provide watertightness even after shear deformation of over one inch. Membranes subjected to wheel loads over sharp edges did not fail by rupture. However, punching tests revealed that membranes are susceptible to punching failure when loads are transferred through sharp points similar to corners of grit, aggregate or beam edges. Based on the results developed from the tests described in this appendix, there is clear evidence that membranes will be able to accommodate large elongations and differential deflections between adjacent box beams without losing watertightness property. This suggests that membrane failures by rupture due to tensile or shear deformations may not be the primary cause of water leakage through the longitudinal joints in adjacent box beam bridges as long as membrane is installed properly and punching of the membranes do not occur during construction. At the onset of this project, there was a general feeling that failure of waterproofing membranes may be the sole cause of the problem. However, that school of thought was disproved from the membrane tests conducted in this study.

Waterproofing Details of Connections for Adjacent Precast Concrete Box-Beam Bridges

Appendix C: Performance Evaluation of Box-Beam Bridges and the Relevant Construction Practices

Prepared by:

Mohamed Habouh, PhD (Former Graduate Student)
Ali Almonbhi, PhD (Former Graduate Student)
Anil Patnaik, PhD (Principal Investigator)

Prepared for:

The Ohio Department of Transportation
Office of Statewide Planning & Research

State Job Number 134847
07/25/2018

Waterproofing Details of Connections for Adjacent Precast Concrete Box-Beam Bridges

Appendix C: Performance Evaluation of Box-Beam Bridges and the Relevant Construction Practices

Prepared by:

Mohamed Habouh, PhD
Ali Almonbhi, PhD

Former Graduate Students, Department of Civil Engineering
The University of Akron, Akron, OH 44325-3905

Dr. Anil Patnaik (PI)
Professor, Department of Civil Engineering
The University of Akron, Akron, OH 44325-3905
Phone: 330-972-5226 Email: Patnaik@uakron.edu

July 2018

Prepared in cooperation with the Ohio Department of Transportation, Ohio's Research Initiative for Locals, and the U.S. Department of Transportation, Federal Highway Administration

TABLE OF CONTENTS

LIST OF FIGURES

LIST OF TABLES

APPENDIX C: PERFORMANCE EVALUATION OF BOX-BEAM BRIDGES AND THE RELEVANT CONSTRUCTION PRACTICES

C.1 FIELD MEASUREMENTS OF VERTICAL DIFFERENTIAL DEFLECTIONS AND SEPARATION OF LONGITUDINAL JOINTS UNDER TRUCK LOADING

C.1.1 Objective

The objective of measuring differential vertical deflections and horizontal separation at the longitudinal joints of typical box beam bridges was to determine the movements that can be expected in an actual bridge when subjected to traffic loading. The magnitude and nature of these movements were needed to determine if the waterproofing membrane has adequate capacity to bridge between the cracks at longitudinal joints, as the membrane needs to accommodate these vertical and horizontal movements while maintaining the waterproofing property. Such measurements were also needed to help evaluate key ways and to understand the load paths and the state of stresses within the longitudinal joints. The measured differential deflections and separations provide a basis to define failure for these joints in actual bridges. The differential deflections and the horizontal movements of the laboratory test specimens were correlated with the actual site measurements in order to define "failure" in the laboratory test specimens and develop strategies to minimize failures.

C.1.2 Methodology

C.1.2.1 Bridge Selection

The database provided by ODOT for the entire state was reviewed and several bridges in various parts of the state were physically inspected to select a suitable bridge for detailed measurements of differential vertical deflections and horizontal movements. Some of the inspected bridges were found to be unsuitable for obtaining detailed measurements.

Based on the bridges inspected in various ODOT districts and based on the discussions with ODOT and county engineers, it is noted that the water leakage problem does not appear to have a geographical or statistical trend. Lack of watertightness, cracking at longitudinal joints, and joint failures seem to be common problems in the bridges on highways throughout the state and on many county roads.

Bridge ASD-42-12.49 in Ashland County (ODOT District 3) was selected for measuring vertical differential deflections and horizontal differential movements under truck loading. This bridge is a non-composite bridge having a 60-ft. span, thirteen precast-prestressed box beams tied with one set of three overlapping tie rods in the transverse direction, and an asphalt concrete wearing course. A single set of tie rods was provided at an intermediate location as shown in Fig. C.1. The current ODOT standard PSBD-2-07 requires two intermediate diaphragms (and two sets of tie rods) to be provided for spans greater than 50'-0" but less than 75'-0". Therefore, a single set of tie rods provided in this bridge at an intermediate location does not satisfy these requirements. The bridge otherwise met the following selection criteria:

- It had around 12 ft of clear height under the bridge, which was suitable height for installing dial gages at the bottom of the girders.
- The bridge was located on a straight highway to allow the loaded test truck to pick up speed (up to 70 mph) before reaching the bridge and to slow down after driving over the bridge without the need for traffic control.
- There was easy access to the area below the bridge to allow working under the bridge, i.e., no dense vegetation, deep water in the stream, or steep side slopes.

Bridge ASD-42-12.49 was recognized by ODOT bridge engineers to be defective, and the key way joints between adjacent box beams were documented to have longitudinal cracks and known water leakage problem. Longitudinal cracks appeared on the surface of the asphalt concrete layer as seen in Fig. C.2. Cover spalling and corrosion for the reinforcement was observed at the underside of the box beams of the bridge.

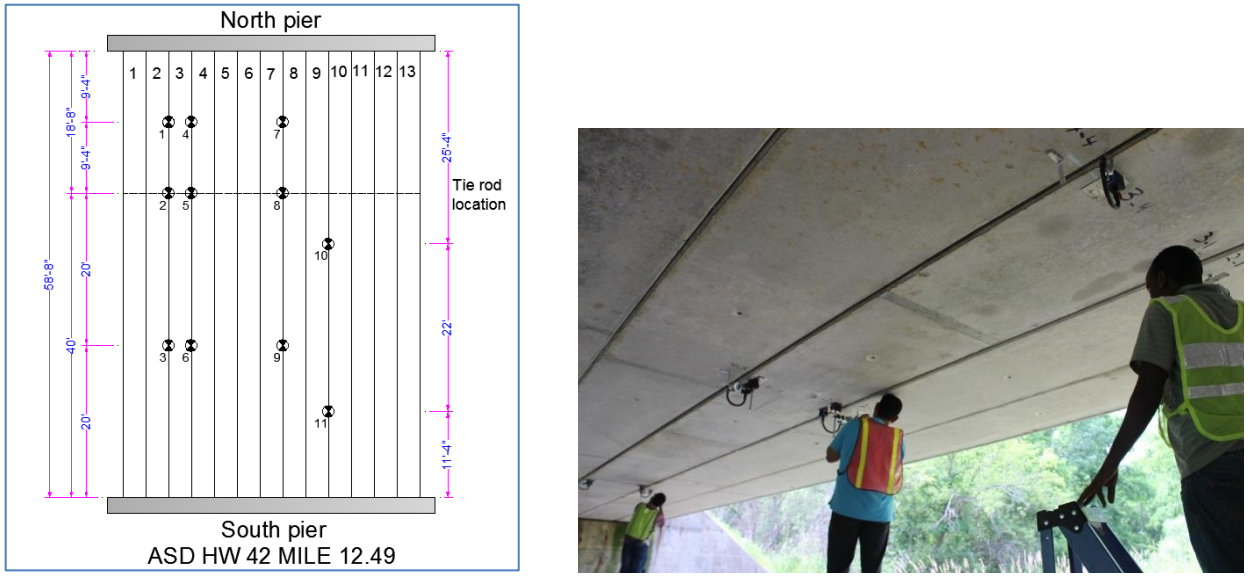

Fig. C.1 Plan Dimensions and View of the Underside of Bridge ASD-42-12.49

C.1.2.2 Measurements

The locations of interest for recording deflections were carefully selected based on the visual inspection of the bottom of the bridge to identify the locations where the water leakage damage had occurred and where cracks were clearly visible on the surface of the asphalt concrete overlay. Four longitudinal joints were selected out of the twelve joints between the thirteen box beams. Dial gages were installed on the underside of the beams to measure the relative movements at 11 locations as shown in Fig. C.1.

The locations of the joints between the box beams were located and measured at the bottom of the bridge and marked on the top on the asphalt concrete surface by carefully transferring the corresponding points from the bottom of the bridge. A truck was loaded to a total load of 67.4 kips (including the self-weight of the truck) and was driven over the bridge at speeds of

50 or 70 mph following specifically marked paths. The loaded truck was guided to drive on the beam next to the longitudinal joint where the gage readings were taken. The differential deflections and the lateral spread were videotaped and later analyzed to obtain measurements of the maximum movements.

Fig. C.2 Surface Cracks and Path of Truck Wheels (*left*) and Typical Cover Spalling on Bottom Surface (*right*)

An intermediate tie rod was located at 40 ft from the south pier and 18ft-8in from the north pier. No tie rods were present at the supports. Measurements were obtained from gages at Points 2, 5, and 8 at the tie rod location. Points 1, 4, and 7 were located at half the distance between the tie rod and the north pier. Points 3, 6, and 9 were located at half the distance between the tie rod and the south pier to monitor the effects of the clamping forces provided by the tie rod and the effects of the spacing between tie rods and the end supports. Points 10 and 11 were located where severe cracks were visible. The accuracy of the dial gages was 0.0005 in.

C.1.3 Test Results and Discussion

The measured vertical differential deflection and lateral relative spread between the adjacent girders were the least at the middle tie rod location, with values equal to 0, 0 for Point 2, 0.0020", 0.0018" for Point 5, and 0.0010", 0.0010" for Point 8 (Table C.1). The maximum vertical differential deflection was recorded at the center of the length between the middle tie rod and the south pier with 40 ft spacing between the tie rods. Fig. C.3 shows typical vertical differential deflections at three locations. The maximum recorded vertical differential deflection was 0.0045 inch. The maximum horizontal separation at the underside of the box beams was measured to be 0.0150 inch. Fig. C.3 shows the vertical differential deflection at Points 7, 8, and 9. For all locations, the movements were the largest at the time when the truck was directly above the measured point.

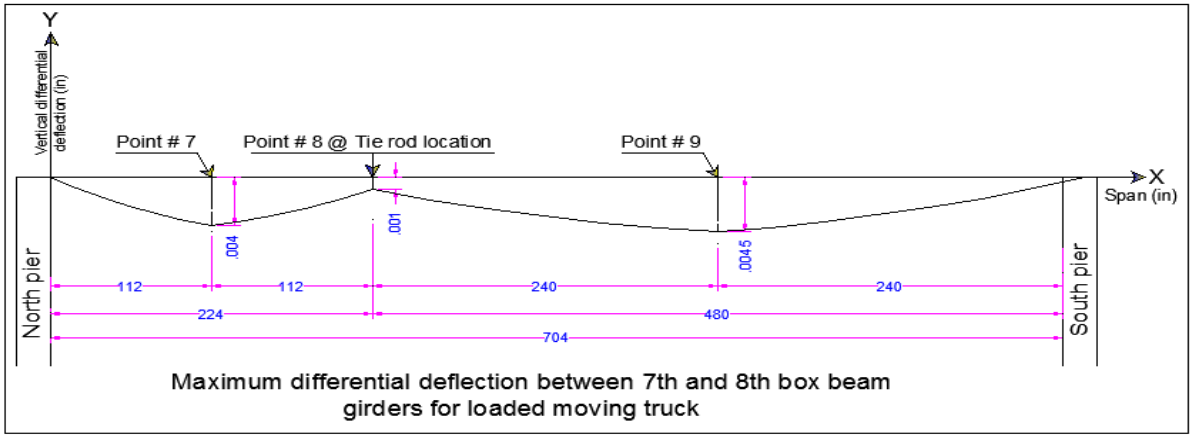

Fig. C.3 Differential Vertical Deflections in Inches at Points 7, 8, and 9

Table C.1: Significance of Test Points and Measured Values

Test point	Point significance	Vertical differential deflection (in)	Horizontal differential deflection (in)	Truck speed (mph)	Truck load (kips)
1	At middle distance between the north pier and the middle tie rod	0.0010	---	50	
1	At middle distance between the north pier and the tie middle rod	0.0020	---	50	
2	At the middle tie rod location	0.0000	0.0000	50	
3	At middle distance between the south pier and the tie middle rod	0.0010	0.0000	50	
4	At middle distance between the north pier and the middle tie rod	0.0015	---	50	
4	At middle distance between the north pier and the middle tie rod	0.0025	---	50	
5	At the middle tie rod location	0.0020	0.0018	50	67.4
6	At middle distance between the south pier and the middle tie rod	0.0030	0.0150	50	
7	At middle distance between the north pier and the middle tie rod	0.0040	0.0000	70	
8	At the middle tie rod location	0.0010	0.0010	70	
9	At middle distance between the south pier and the middle tie rod	0.0045	0.0095	70	
10	Cracks on the surface aligned with the joint location	0.0010	0.0015	70	
11	Cracks on the surface aligned with the joint location	0.0015	0.0010	70	

C.1.4 Summary of Findings

Based on the field measurements obtained for bridge ASD-42-12.49, the following findings were noted:

- These measurements provide a basis for defining the extent of stretching and the extent of shear deformation that a waterproofing membrane needs to accommodate without losing its ability to provide watertightness. The membrane tests presented in earlier sections demonstrate that these membranes are capable of extending axially (in-plane) over one inch (10 to 20% of original length) and deform in shear mode (differential deflection out-of-plane) by over one inch. These field measurements and laboratory tests lead to the conclusion that membranes can accommodate the vertical and horizontal differential deflections that can be normally expected in typical box beam bridges known to have cracks at the longitudinal joints and water leakage problems.
- Tie rod clamping-force reduces the relative movements between the adjacent box beams at the location of the tie rods.
- The greater the distance between the tie rod locations, the larger the relative movements between the adjacent box beams in a bridge.

C.2 INVESTIGATION OF A BRIDGE THAT WAS IN SERVICE FOR 32 YEARS AT THE TIME OF ITS DEMOLITION

Bridge RIC-42-12.34, located in Mansfield, Ohio, in ODOT District 3, was constructed in 1983 and scheduled for demolition in August 2015. The width of the bridge was 60 ft. and the span was 34 ft. The primary objective of this task was to evaluate the condition of the waterproofing membrane after the bridge was in service for 32 years. On the day of the demolition, the asphalt concrete overlay was carefully cut to extract waterproofing membrane samples for inspection and watertightness testing. The underside of the bridge was found to have several locations of severe corrosion of strands, spalling and deterioration as shown in Fig. C.4. Suitable locations to remove the asphalt concrete overlay were selected to expose the membrane on the deck surface based on the amount of corrosion, spalling and cracking on the underside of the box beams.

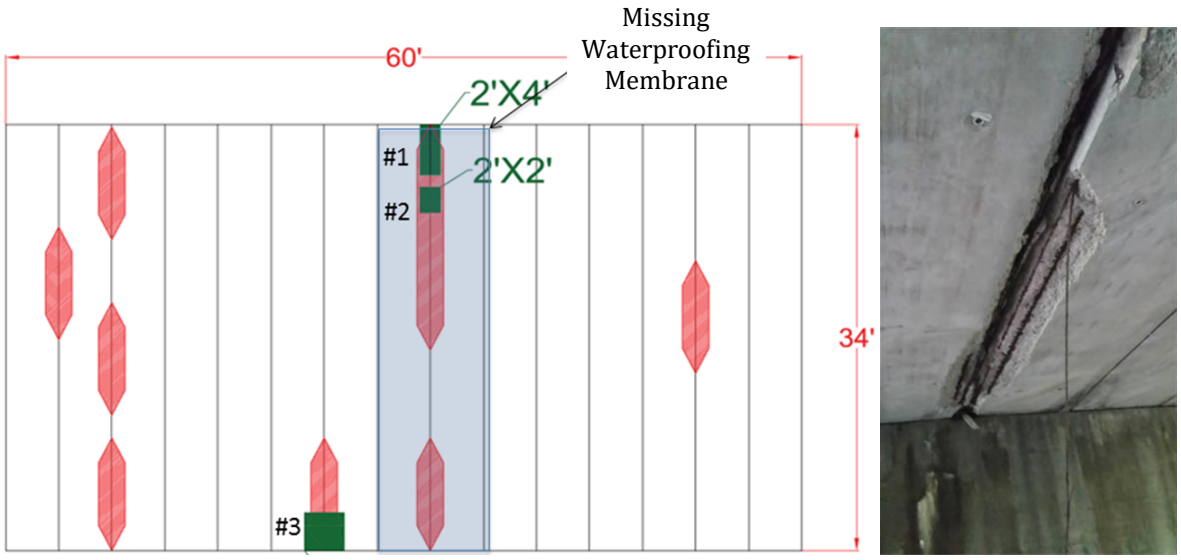

Fig. C.4 Corrosion Damage on the Underside of Box Beams

On the removal of asphalt concrete on the deck top surface, a large area (about 250 to 300 ft^2) on the bridge deck was found to have no waterproofing membrane at all. Three membrane specimens were extracted from other locations on the bridge deck. Two of these specimens were full of visible holes. A watertightness test was performed for the remaining membrane specimen, which seemed to be in good condition by visual inspection but miserably failed to prevent leakage.

The most severe corrosion and spalling were found at locations where no waterproofing membrane was present. The waterproofing membrane specimens collected from the locations corresponding to severe corrosion were fully damaged and were not watertight. The bond between the waterproofing membrane and box beams was lacking, even though there was some bonding of the membrane with the asphalt overlay. The box beam surface at the key way interface was not sandblasted. Longitudinal cracks between the grout and the

box beams were wide and were visible throughout the bridge deck (Fig. C.5). Where provided, the membrane was in very poor condition.

Fig. C.5 Condition of a Typical Joint and Deck Surface

Small pieces of the membrane that were retrieved from the locations where the membrane was exposed with a jack hammer (Fig. E.2) were too fragile to perform any laboratory mechanical tests. Therefore, no tensile tests or other tests were performed on these retrieved membranes.

In summary, the lack of watertightness and the corrosion damage at the bottom surface of the box beams along the longitudinal joints correlated well vertically with the locations where the membrane was missing or severely damaged at the top surface of the bridge. The membrane, where present, was in very poor condition and full of holes that would make it impossible for the membrane to provide any watertightness.

C.3 OBSERVATION OF CONSTRUCTION PRACTICES AT A BRIDGE CONSTRUCTION SITE

To understand the construction processes, the sequence of the activity, and the time frame for each activity, multiple site visits were made to a construction site where a new bridge was under construction in Shreve, Ohio. The construction process was discretely observed so as not to interfere with the normal course of construction. On the first working day, seven box beams were delivered to the site. Within 3 hours of the delivery, the beams were installed in position and tied together with tie rods tensioned to the specified torque to provide the transverse clamping force of 15 kips at each tie rod location. During the second working day, the six longitudinal joints were grouted by noon. The bridge was ready for the waterproofing membrane to be laid within two days.

The box beams for this bridge were B17"-48" with 17 inches of height and 48 inches of width having a 7-inch key way which was sandblasted according to ODOT specifications. The girders were a little out of sweep but within the allowable tolerance of one inch. Oakum (ropes) of one inch diameter was used to fill the gaps between the box beams with the intent of preventing grout from leaking from the bottom of the beams into the stream below.

The grouting process proceeded rapidly. After blowing the dust from the bridge deck and the joints, the grout was mixed in a grout mixer that was placed on the top of the bridge deck. Immediately after mixing, wet grout was transported to the joints in trolleys. An approved grout material from ODOT's QPL was used. The mixing water was around 5 quarts per 50 lb bag to obtain a flowable consistency and to accomplish the filling of the key way with wet grout in a reasonably short period of time. However, the amount of water added seemed excessive, and much more than what would be required to allow the development of the compressive strength to the specified level.

During the installation of the waterproofing membrane, the deck surface preparation was very poor. Many concrete protrusions, grit, debris, and nails (used for nailing the drip strips at the edges of the bridge) remained on the deck surface. A heavy asphalt pavement roller was driven on the deck surface several times, likely perforating the membrane even before the asphalt concrete overlay was placed. Fig. C.6 shows concrete protrusions and nails on the deck surface after the concrete surface was prepared and just before the membrane was installed. Fig. C.7 shows the use of a compaction roller and a paver over the unprotected waterproofing membrane after its installation.

The site observations reported in this appendix demonstrate a set of unacceptable construction practices followed by contractors. ODOT specifications provide basic guidance and clear protocols on waterproofing membrane installation and grouting of key ways. These specifications and recommendations need to be expanded to include more details to provide a better understanding of the procedures by both contractors and inspectors. Excessive addition of water to grout material needs to be regulated and controlled so as to prevent the diminishing structural strength of key way joints. Successful implementation for a waterproofing membrane needs careful concrete surface preparation, proper installation of the bonding agent, and laying of membrane sheets. The waterproofing membrane must be inspected before the paving process is started. Driving of heavy equipment needs to be

prohibited before the asphalt concrete overlay is placed so as to prevent damage to the membrane.

Fig. C.6 Protrusions Documented Just Prior to Laying the Waterproofing Membrane

Fig. C.7 Heavy Equipment Being Driven over an Unprotected Membrane

Waterproofing Details of Connections for Adjacent Precast Concrete Box-Beam Bridges

Appendix D: Structural Performance of Key Way Joints

Prepared by:

Mohamed Habouh, PhD (Former Graduate Student)
Anil Patnaik, PhD (Principal Investigator)

Prepared for:

The Ohio Department of Transportation
Office of Statewide Planning & Research

State Job Number 134847
07/25/2018

Waterproofing Details of Connections for Adjacent Precast Concrete Box-Beam Bridges

Appendix D: Structural Performance of Key Way Joints

Prepared by:
Mohamed Habouh, PhD
Former Graduate Student, Department of Civil Engineering
The University of Akron, Akron, OH 44325-3905

Dr. Anil Patnaik (PI)
Professor, Department of Civil Engineering
The University of Akron, Akron, OH 44325-3905
Phone: 330-972-5226 Email: Patnaik@uakron.edu

July 2018

Prepared in cooperation with the Ohio Department of Transportation,
Ohio's Research Initiative for Locals, and the U.S. Department of Transportation, Federal Highway Administration

TABLE OF CONTENTS

LIST OF FIGURES

LIST OF TABLES

APPENDIX D: STRUCTURAL PERFORMANCE OF KEY WAY JOINTS

D.1 Structural Tests of Joints with Tie Rods

D.1.1 Introduction and Objectives

Ties or prestressing strands are used to provide clamping force in the transverse direction of adjacent precast prestressed box-beam bridges to ensure the integrity of the bridge in transferring the loads between the adjacent beams. The amount of transverse force applied to the adjacent box beams is believed to increase the shear transfer strength and to provide lateral stability for the bridge assembly.

The objective of the structural tests is to determine (i) the effects of clamping forces provided by the transverse ties on the joint assemblies, and (ii) the vertical differential deflection between the concrete units.

D.1.3 Test Procedure for Structural Tests

The test specimens comprised three small units with two key way joints having geometry similar to the one specified in ODOT standard drawings as shown in Fig. D.1. The three units in each specimen were tied together with a tie rod with three different levels of tie forces. The grout was ODOT-approved Kuhlman 1107 grout with a compressive strength on the day of testing of 7,500 psi.

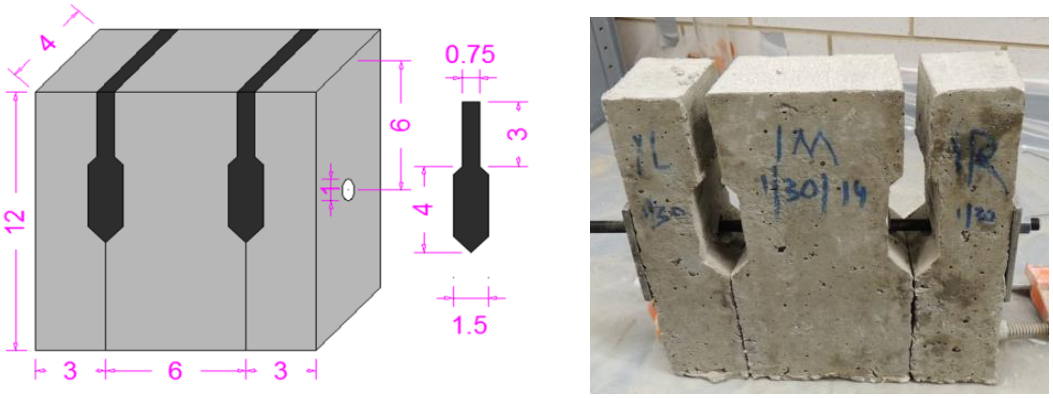

Fig. D.1 Details of Joint Tests Specimen with a Tie Rod

ODOT requires a one-inch-diameter tie-rod inserted in a two-inch-diameter hole in the transverse direction through the adjacent box beams to provide a normal force of 15 kips that would result from a torque of 250 lb-ft. In this test program, Grade B7 alloy steel threaded rods with ½" diameter and 20 threads per inch were used. The diameter of the hole in the concrete units for the tie rod was 1 inch, and different levels of torque (100 lb-in, 200 lb-in, and 230 lb-in) were applied prior to the placement of grout (which is the common practice for ODOT box beam bridges). The tie rod was placed at six inches from the top of the girder.

Seven specimens were tested under static axial symmetric loading, which is achieved by supporting the external concrete units against vertical movements with roller supports and

loading the middle concrete unit. Two specimens without a tie rod were tested as control specimens and five specimens had a tie rod each with different levels of torque as given in Table D.1. Fig. D.2 shows the vertical displacement versus first crack load and failure load for each specimen.

D.1.4 Test Results for Joints with Tie Rods

The results developed from the testing of the seven specimens and descriptions of the failure condition are shown in Table D.1. First crack load is shown in Table D.2.

Table D.1: Test Data at Failure for Joints with Tie Rods

#	Concrete compressive strength (psi)	Grout compressive strength (psi)	Tie rod torque	Failure load (lb)	Vertical displacement (in)	Top lateral displacement (in)	Bottom lateral displacement (in)
S1	8,615	7,477	0	4,940	0.0395	Not measured	0.004
S2	8,615	7,477	0	8,530	0.03925	Not measured	0.014
S3	8,615	7,477	230	23,050	0.1425	0.0425	0.092
S4	8,686	7,477	230	23,068	0.13075	Not measured	0.055
S5	8,686	7,477	200	23,838	0.11275	0.0315	0.07
S6	8,686	7,477	200	29,133	0.13225	0.0165	0.078
S7	8,615	7,477	100	25,691	0.09375	0.06	0.0445

Table D.2: Test Data at First Crack for Joints with Tie Rods

#	Concrete compressive strength (psi)	Grout compressive strength (psi)	Tie rod torque	First crack load (lb)	Vertical displacement (in)	Top lateral displacement (in)	Bottom lateral displacement (in)
S1	8,615	7,477	0	2,800	0.013	Not measured	0.0023
S2	8,615	7,477	0	7,800	0.0245	Not measured	0.0055
S3	8,615	7,477	230	18,000	0.0646	0.0045	0.0065
S4	8,686	7,477	230	18,000	0.0635	Not measured	0.0065
S5	8,686	7,477	200	18,000	0.05525	0.012	0.012
S6	8,686	7,477	200	11,500	0.0555	0.0055	0.0055
S7	8,615	7,477	100	13,500	0.033	0.017	0.003

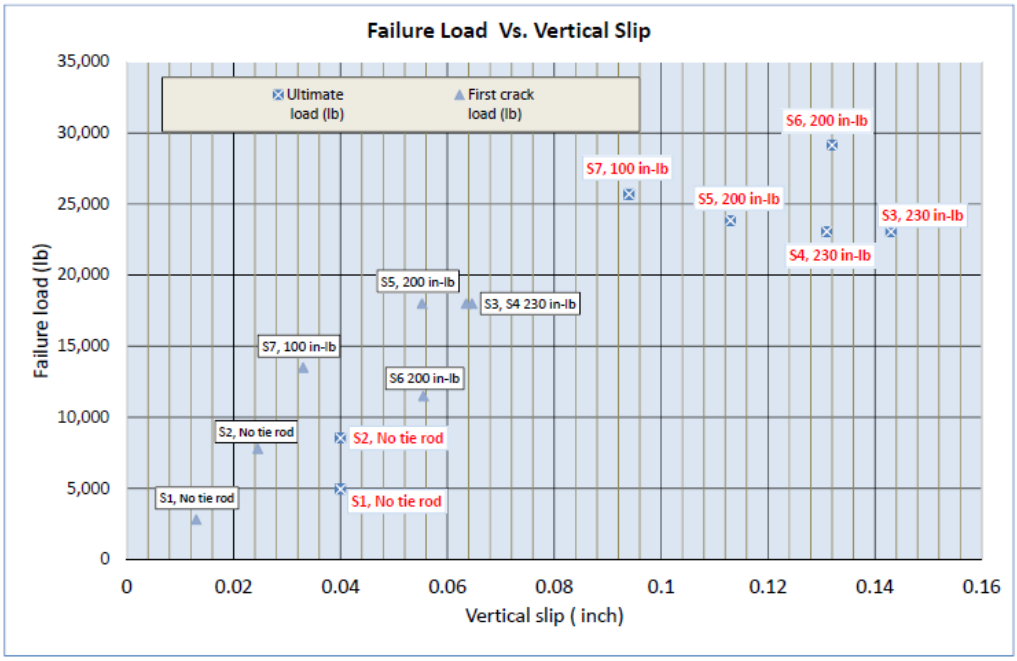

Fig. D.2 Summary of Test Result

D.1.5 Discussion

D.1.5.1 Failure Modes

A sudden failure took place at the shear interface between the grout material and the concrete unit for the specimens without a tie rod; concrete units and grout were not damaged or cracked. For specimens with a tie rod, the specimens could be loaded until the concrete units were cracked or the tie rod yielded. For the specimen size used in this study, the concrete failed before the tie rod failed, as shown in Fig. D.3.

Fig. D.3 Typical Failure Mode, Specimens without Ties (left)
Specimen with Tie Rod (right)

D.1.5.2 First Crack Load and Reserve Strength

A larger first crack load was recorded for the specimens with a tie rod compared to those without a tie rod. A load equal to 11,500 lb to 18,000 lb for specimens with tie rods was recorded as compared to 2,800 lb and 7,800 lb for the specimens without tie rod. The resulting higher load carrying capacity may be due to the contribution of the steel area of the tie rod crossing the two interfaces and larger frictional resistance at the interface due to the clamping force resulting from the tie rod torque. The reserve strength or the "post-cracking load" was larger for the specimens with a tie rod. ~~because the tie rod provides~~ This is due to the lateral stability, provided by the tie rod, thereby preventing the excessive lateral spread of the units at the bottom.

D.1.5.3 Vertical Displacement

Using a tie rod with the resulting clamping force allows a larger vertical slip at first crack load. There was a trend of increasing vertical slip as the clamping force increased in all specimens. A vertical slip of 0.025 inch was the maximum slip recorded for specimens without a tie rod, and the slip increased to 0.033 inch for specimen S7, which had a 100 in-lb torque. Specimens S5 and S6, with torque equal to 200 in-lb, had the same amount of slip (0.055"). For specimens S3 and S4 with 230 in-lb torque, vertical slips equal to 0.063" and 0.064" were recorded. Increasing the clamping force allowed a larger vertical slip at first crack load.

D.2 Structural Tests of Joints without Tie Rods

D.2.1 Introduction

Based on finite element analyses of box-beam bridges from a Michigan DOT research project (Russell, 2011) mentioned that the clamping effects of tie rods are mostly limited to a length equal to the diaphragm thickness when the tie rods are used at the locations of the diaphragms. This means that ~~no~~ clamping stresses are not available in the remaining length of the box beams between diaphragms (which can be as much as 24 to 50 ft.). Therefore, the small joint test specimens were subsequently modified in later work to exclude the tie rod and any clamping force.

D.2.2 Objective

There are many factors that might affect the shear strength of key ways. Simplified test specimens were designed to determine the effects of these factors on shear strength of key way joints and to observe the associated failure modes, differential deflection, and lateral spread of the joints to down select the tentative characteristics for a larger scale test plan.

D.2.3 Test procedure

Three concrete units were cast separately and then joined together by filling the key ways with grout. The external units were 4"x4"12" with key way formed on the inner side, and the middle unit was 6"x4"x12" with two key ways formed on the two outer sides as shown in Fig. D.4. The 28-day compressive strength of the concrete units was 6,800 psi.

In the test setup, the middle unit was supported against vertical movement, and the load was applied upward on the two external units resulting in symmetric shear loading on the key way joints. Six dial gages were installed to measure the vertical differential deflections and lateral spread. Roller supports were used in order to allow lateral spread.

D.2.3.1 Shear Test Setup and Procedure

The instrument used for the test was a hydraulic test machine with a capacity of 300 kips, whereas the maximum applied load to the specimens was 60 kips. A loading rate of 70 lb/sec was used in the static loading.

Dial gages were fixed at the top of the moving (left and right) concrete units to measure the upward slip relative to the middle fixed block and the corresponding applied load. The load and the corresponding vertical slip were recorded to develop a load-slip diagram by calculating average slip from the two gages. The test machine and the test setup are shown in Fig. D.4.

Fig. D.4 Hydraulic Test Machine (left) – Test Specimen and Setup (right)

D.2.4 Factors Studied

The factors considered in this study were:

(i)	Key way geometries	(4 geometries)
(ii)	Grout material	(7 grouts)
(iii)	Commonly used industrial chemical additives	(bonding agents)
(iv)	Cement slurry	(use of slurry)
(v)	Surface preparation	(sandblasting)

D.2.4.1 Key way geometry

A test specimen prepared according to the current ODOT practice was considered as the control specimen and is referred to as "partial depth, narrow key way". Three tentative geometries were investigated with combinations of wider and deeper key ways as shown in Fig. D.5. Set # 1 had a key way conforming to the current practice of ODOT with ¾" opening at the top for the top 3 inches of depth, then 1.5" width for 4 inches of depth. Set # 3 had a 1.5" top opening width followed by 3" of width with same height of key way as Set #1. Set # 2 had the same width of the standard geometry and the same 3" of height for the top portion as Set #1 and #2, but the key way extended to the bottom of the concrete units, except for the last inch at the bottom to contain the grout material during casting. Set # 4 had the height of the top opening that was the same as specified for the standard geometry, but it had a deeper and wider key way as shown in Fig. D.5.

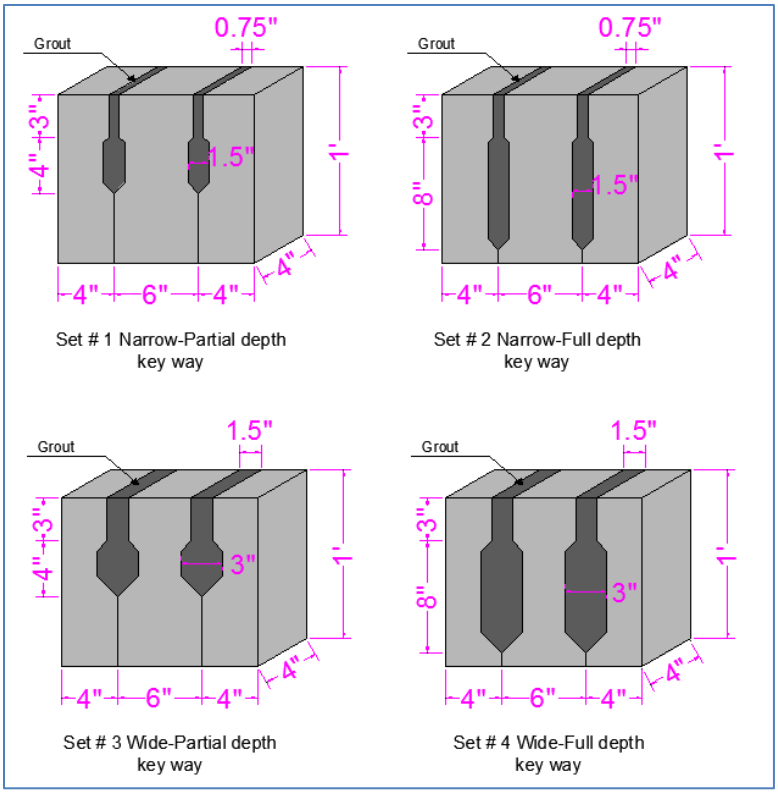

Fig. D.5 Key Way Geometries Used in Joint Tests without Tie Rods

D.2.4.2 Grout types

Cement-based grout: Kuhlman 1107

This grout is a non-shrink, noncorrosive, non-metallic cementitious grout, with controlled aggregates, admixtures and Portland cement. It is a ready-to-use grout that can be mixed by adding water. It has a setting time of 15 minutes as suggested by the manufacturer, and the mixing time is three to five minutes depending on the amount of mixing water.

Cement-based grout - Normal strength concrete (5,400 psi)

Normal strength concrete was made by using traditional concrete with maximum #8 coarse aggregates and Type 1 Portland cement (Table D.3). This grout is a ~~cheaper~~less expensive option with adequate strength, and it achieved proper compaction. The top opening of the key way ~~was~~ needs to be wider, preferably at least one inch, to allow for the insertion of a small vibrator.

Table D.3: Mix Design for Normal Strength Concrete Used as Grout Material

Mix Proportion		
Materials	Description	lbs/yd^3
Cement	Type I	725
Coarse aggregate	# 8 milestone	1523
Sand	River sand	1523
W/C		0.4
Water	Potable water	290

The setting time for normal strength concrete is around thirty minutes, and the average 28-day compressive strength was 5,400 psi.

Cement-based grout – High-strength concrete (9,800 psi)

This grout was made using traditional concrete with maximum #8 coarse aggregates and Type 1 Portland cement. Compaction was provided to the grout with a vibrator. The opening at the top of the key way was at least one inch to allow for vibration. The relevant mix design is shown in ~~Fig.~~ Table D.4.

Table D.4: Mix Design for High-Strength Concrete Used as a Grout Material

Mix Proportions		
Materials	Description	lbs/yd^3
Cement	Type I	1100
Coarse aggregate	# 8 milestone	1596
Sand	River sand	1450
W/C		0.35
Water	Potable water	385
High range water reducing agent 100ml/100 lb of cement (SIKA 2100)		

Cement-based grout: Ultra-high strength concrete (19,000 psi)

The main objective of this task was to use economical and readily available materials for developing a high-performance grout based on UHPC (ultra-high performance concrete). Sand used in the trials was conventional sieved siliceous river sand with sub-rounded grains

with the ~~least amount of~~no clay or silt-particle contamination. Details regarding the mix design and mixing procedure are discussed later in this report.

Polymer-based grout: Master Flow 4316

This is a polymer-based grout consisting of hydraulic binder with applied nanotechnology and premium mineral aggregates as per manufacturer's description. This grout material is pre-manufactured; only the mixing water needs to be added to the dry grout. Mixing water is around 5.75 to 6.25 pound of water per 50 pounds of grout. Mixing time is three minutes, and setting time is 180 minutes with flowable, self-consolidating consistency that requires no vibration, and no curing at the wide range of operating temperatures from 35 to 100° F (2 to 38° C). Polymer-based grout can also be used in cold weather. Proper sealing of the key way is required to prevent leakage of the grout during casting ~~considering~~ due to the high flowability. The compressive strength exceeded 16,000 psi after twenty eight days.

Magnesium-phosphate grout: Master Emaco T 545 and Master Emaco T 545 HT

Two formulations of magnesium-phosphate based grouts were also tested. It is a one-component magnesium-phosphate based mortar; the operating temperature of this grout is from 85 to 100° F (29 to 38° C) which ~~might be~~is a limitation in cold weather applications. The setting and workable time is ten minutes. One and a half minutes of mixing ~~was~~ is recommended with mixing water of a maximum of 4.18 pounds per fifty pounds of grout. The manufacturer recommends no wet curing (air cure only) for these two components except for some protection from rain immediately after placing, if required. Liquid-membrane curing compounds or plastic sheeting may be used to only protect the early surface from precipitation.

D.2.4.3 Surface preparation

The surface roughness effects on key way joints was studied by sandblasting the concrete surface using 120 psi air pressure mixed with sand passing a #30 mesh as shown in Fig. D.6. Test specimens were tested for sandblasted surface with UHPG, HSC grout, with and without bonding agent, and with and without cement slurry. The key way surfaces were wetted prior to the placement of the grouts.

D.2.4.4 Shrinkage Cracks

The heat of hydration and/or hot weather might cause the mixing water to evaporate soon after placing the grout, leading to shrinkage cracks at the surface that will propagate when the service loads are applied (Miller R. H., 1998). Proper curing and protection of the exposed surface can reduce shrinkage cracks by preventing the mixing water from evaporation in the early age of the grout material. No curing, wet curing and curing compound were used separately in this study to monitor their effect on shrinkage cracks.

D.2.4.4 Cement Slurry Effect

~~The f~~Free water is required at the interface ~~is required~~ to develop bond strength between the fresh cementitious grout and the hardened concrete surface of the box beam girder ~~at the interface~~. Cement slurry can help to increase bonding and shear strength at the interface. Cement slurry mix was three parts by weight of cement mixed with two parts of water. It was poured from the top opening of the joint to flow onto the key way surface immediately before placing the grout material, as shown in Fig. D.7.

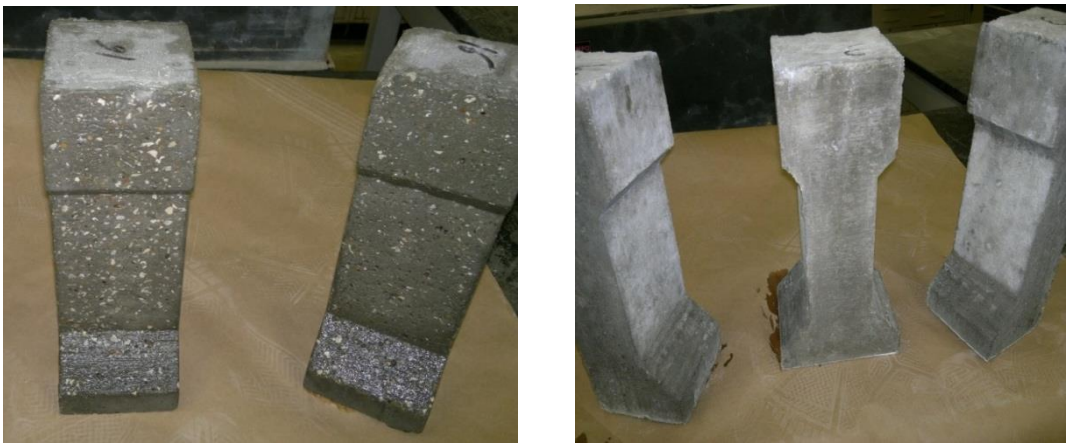

Fig. D.6 Sandblasted Surface (Left) vs. As-Cast Concrete Surface (Right)

Fig. D.7 Application of Cement Slurry (See on the Left Facing Side)

D.2.4.5 Bonding agent effect

Two types of bonding agent products are currently available and are commonly used in the construction industry. Type I is a liquid compound that should be applied by ~~painting~~ coating the surface prior to pouring the grout~~;~~; this type of compound is not practical for the key way applications because of the small width of the key way and the narrow top opening. Type II is a liquid compound that should be mixed with the grout. WeldeCrete Type II bonding agent was used in order to evaluate its effect on bond and shear strength of the joint.

D.2.5 Results and Discussion

D.2.5.1 Definition of failure

The specimens were considered to have failed at the first crack load; further load was applied after the first crack until the specimens fell apart. Specimens were able to carry load after the first crack because of the bearing strength at the bottom flange that results from the key way shape.

D.2.5.2 Shear strength

The average strength of the three test specimens that were grouted with the ODOT-approved grout material and with the standard ODOT geometry was considered as a control strength. The average strength for each of the tested grouts and geometries were compared with the strength of the control test specimens. The average shear strength of the approved ODOT grout with standard key way geometry was 5,700 lb. The failure mode for this grout material was shear failure by debonding at the interface between the concrete units and the grout material.

The maximum average shear strength was 37,000 lb, which was obtained from the specimens grouted with polymer grout and narrow/full depth key way. The failure of these specimens was through the concrete units and not at the joint between the concrete and the grout. All test results are presented in Table D.5 and Fig. D.8.

Table D.5 : Percent Average Change in First Crack Load

Key Way Geometry	Grout Material	Cracking load (lb)	% Average change in first crack load
Partial / Narrow key way	ODOT-Approved Grout	5,700	100
	Magnesium Phosphate (1)	4,767	84
	Magnesium Phosphate (2)	5,033	88
	Polymer Grout	14,833	260
Full / Narrow key way	ODOT-Approved Grout	15,950	280
	Magnesium Phosphate (1)	5200	91
	Magnesium Phosphate (2)	6,167	108
	Polymer Grout	37,000	649
Partial / Wide key way	ODOT-Approved Grout	8,800	154
	Magnesium Phosphate (1)	5,800	102
	Magnesium Phosphate (2)	4850	85
	Polymer Grout	17,167	301
	Concrete (5,400 psi)	12,500	219
Full / Wide key way	ODOT-Approved Grout	14,550	255
	Magnesium Phosphate (1)	6,400	112
	Magnesium Phosphate (2)	8,333	146
	Polymer Grout	29,667	520
	Concrete (5,400 psi)	16,500	289
	HSC (9786 psi)	17,200	302
	HSC (4282 psi) with bonding agent	17,439	306
	HSC (4282 psi) with bonding agent and sand blasted surface	23,703	416
	HSC (9786 psi) with sand blasted surface	29,367	515
	UHPC - sand blast	34,700	609
	UHPC - cement slurry	5,300	93
	UHPC - sand blast + cement slurry	24,067	422
	UHPC - no Sand blast - no cement Slurry	8,100	142

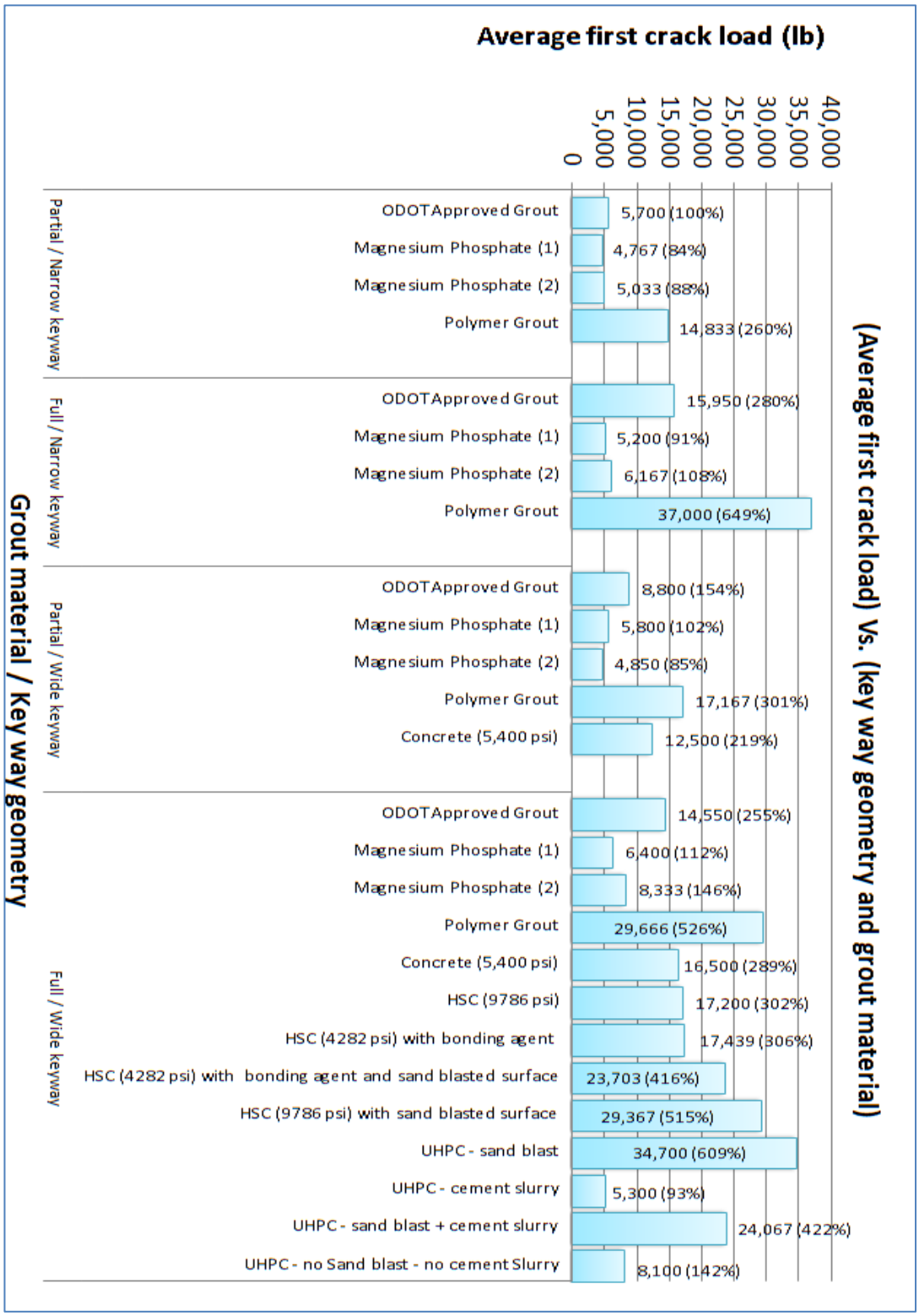

Fig. D.8 Summary of Test Results for Joint Test without Tie Rod

D.2.5.3 Failure modes

D.2.5.3.1 Failure Mode A

The first type of failure (Failure Mode A) occurs at the interface between the grout and the concrete unit. Failure occurs by large horizontal and/or vertical spread before cracking at the joint. This type of failure was observed in all test specimens with ODOT-approved grout material, normal strength concrete grout, magnesium-phosphate based grout, UHP Grout without the application of either the cement slurry or sandblasting, and UHP Grout with cement slurry without sandblasting. Failure Mode is shown in Fig. D.9.

Fig. D.9 Failure Mode A

D.2.5.3.2 Failure Mode B

One specimen failed by the second type of failure mode (Failure Mode B). In this mode, failure occurs by shear failure through the grout at 17,167 lb for wide-partial depth key way and polymer grout. This failure mode, shown in Fig. D.10, can be avoided by increasing the depth of the key way. However, it should be noted that the load carried by the specimen before this mode of failure is high.

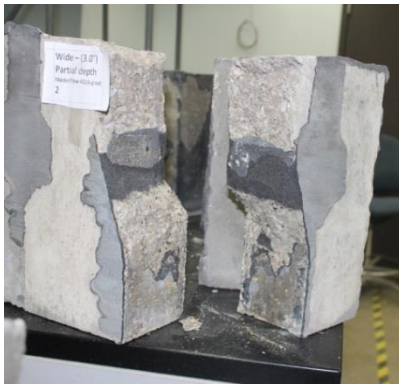

Fig. D.10 Failure Mode B in Polymer Grout, Wide-Partial Depth Key Way

D.2.5.3.3 Failure Mode C

Failure Mode C occurs by diagonal cracking in the middle (loaded) concrete unit. This failure was observed for 12 specimens with HSC grout, 11 specimens out of 12 with the polymer-based grout material, and six specimens with the UHPG with sandblasting with or without cement slurry. Details for each are as follows:

- Failure in HSC grout without bonding agent or sandblasting: Typical failure occurred by de-bonding and diagonal shear in the middle concrete unit for specimens with HSC grout with average cracking load of 17,200 lb with failure mode as shown in Fig. D.11.

- Failure in HSC grout with bonding agent: Typical failure occurred by de-bonding and diagonal shear in the middle concrete unit for specimens with HSC grout with bonding agent. Average cracking load was 17,439 lb with the failure mode as shown in Fig. D.11.

Fig. D.11 Failure Mode C - Failure in HSC Grout (Left); Failure in HSC Grout with Bonding Agent (Right)

- Failure in HSC grout with bonding agent and sandblasted surface: Typical failure occurred by de-bonding and diagonal shear in the middle concrete unit for specimens with HSC grout with bonding agent and sandblasted surface. Average cracking load was 23,703 lb with failure mode as shown in Fig. D.12.

- Failure in HSC grout without bonding agent and with sandblasted surface: Typical failure by de-bonding and diagonal shear in the middle concrete unit for specimens with HSC grout with sandblasted surface. Average cracking load = 29,367 lb as shown in Fig. D.12.

-

Fig. D.12 Failure Mode C - Failure in HSC Grout with Bonding Agent and Sandblasted Surface (Left); Failure in HSC Grout without Bonding Agent and With Sandblasted Surface (Right)

- Failure in UHPG with cement slurry and sandblasted surface: Typical failure occurred by de-bonding and diagonal shear in the middle concrete unit for specimens with UHP grout with cement slurry and sandblasted surface. Average cracking load was 24,067 lb with failure mode as shown in Fig. D.13.

Fig. D.13 Failure Mode C - Failure in UHPG with Cement Slurry and Sandblasted Surface through Concrete and Grout Interface

- Failure in UHPG with sandblasted surface: Typical failure for specimens with UHP grout with sandblasted surface. Failure occurred in the middle concrete unit, but not in the grout material. Average cracking load was 34,700 lb. The failure load was limited by the strength of the concrete units, and not the strength of the grout with failure mode as shown in Fig. D.14.

Fig. D.14 Failure Mode C - Failure through Concrete in Specimens with UHP Grout with Sandblasted Surface

- Polymer Grout For partial depth key way, the shear failure plane extended from the middle concrete unit to the bottom slope of the key way. The failure plane showed different slopes depends on the key way depth as seen in Fig. D.15. For the case of partial depth, and in this figure, for full depth key way. The deeper the key way, the larger the ultimate load.

Fig. D.15 Failure Mode C - Failure in Polymer Grout: Narrow-Partial Depth Key Way (Left), Full Depth Key Way (Right)

D.2.6 Discussion

D.2.6.1 Effect of Key Way Geometry on Vertical Shear Strength

Tests results indicated that joints with deeper key ways have larger strength in resisting shear loads. Load transfer between the middle-loaded concrete unit to the external supported concrete units through the grout consists of two main components: shear resistance at the interface and bearing on the bottom flange. No failure was observed in the bottom flange in any of the test specimens (see Fig. D.16 and also Table D.6).

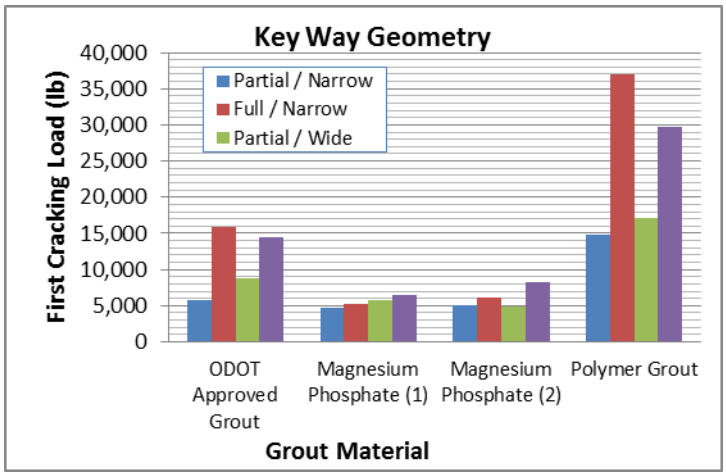

Fig. D.16 Key Way Geometry vs. Shear Strength

Table D.6: Key Way Geometry vs. Shear Strength

Grout Material	First Cracking Load			
	Key Way			
	Partial / Narrow	Full / Narrow	Partial / Wide	Full / Wide
ODOT-approved grout	5,700	15,950	8,800	14,550
Magnesium Phosphate #1	4,767	5,200	5,800	6,400
Magnesium Phosphate #2	5,033	6,167	4,850	8,333
Polymer grout	14,833	37,000	17,167	2,9667

D.2.6.2 Increased shear strength when contact area was increased at the interface

When Narrow/Partial depth key way was compared to Narrow/Full depth key way, the bearing area is constant with a width of 1.5 inches and the interface area was increased from 4" × 7" to 4" × 11". The same trend was observed when Wide/Partial depth key way was compared to Wide/Full depth key way, with a constant bearing length of 3 inches and interface area increased from 4" × 7" to 4" × 11" as shown in Fig. D.17.

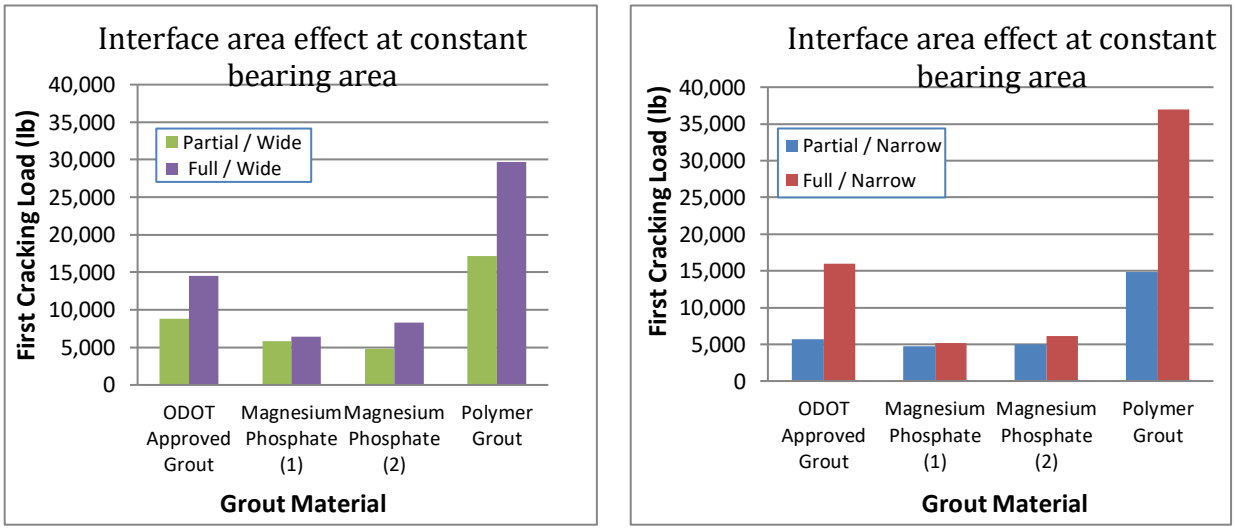

Fig. D.17 Key Way Depth vs. Shear Strength

D.2.6.3 Increased shear strength when bearing area was increased at the bottom flange

When Narrow/Partial depth key way was compared to Wide/Partial depth key way, the interface shear area is constant 4" × 7" with the bearing width increased from 1.5" to 3". The same trend was observed when Narrow/Full depth key way was compared to Wide/Full depth key way, the interface shear area is constant 4" × 11" with the bearing area increased from 1.5" to 3" as shown in Fig. D.18 resulting in a marginal increase in the shear strength.

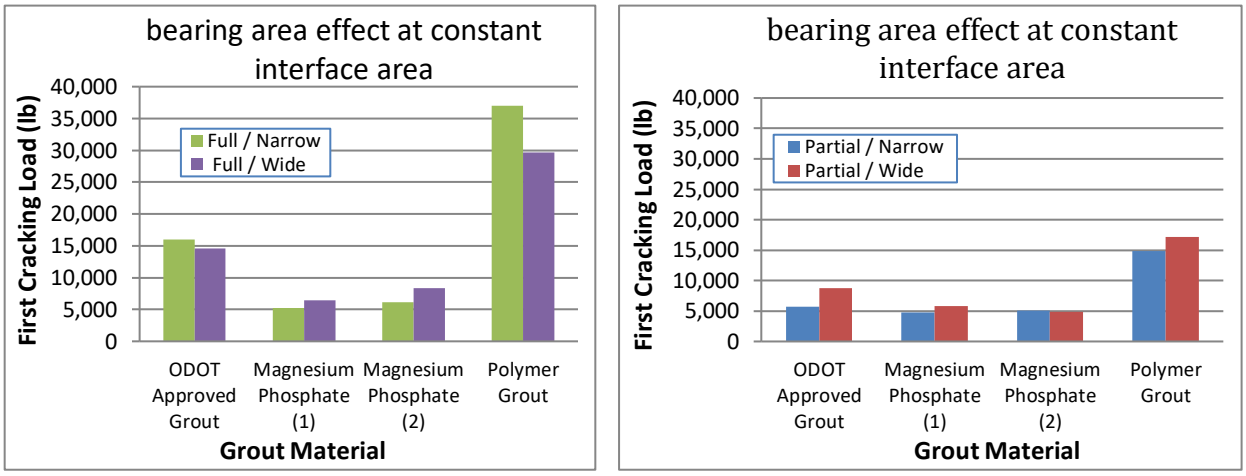

Fig. D.18 Key Way Width vs. Shear Strength

D.2.6.4 Bonding agent, cement slurry, and sandblasting vs. shear strength

Bonding agent reduced the strength for all test specimens with HSC grout. The maximum strength was obtained with sandblasted surface and without bonding agent. Cement slurry reduced the strength for all test specimens with UHP grout. The maximum strength was obtained with sandblasted surface without cement slurry as shown in Fig. D.19.

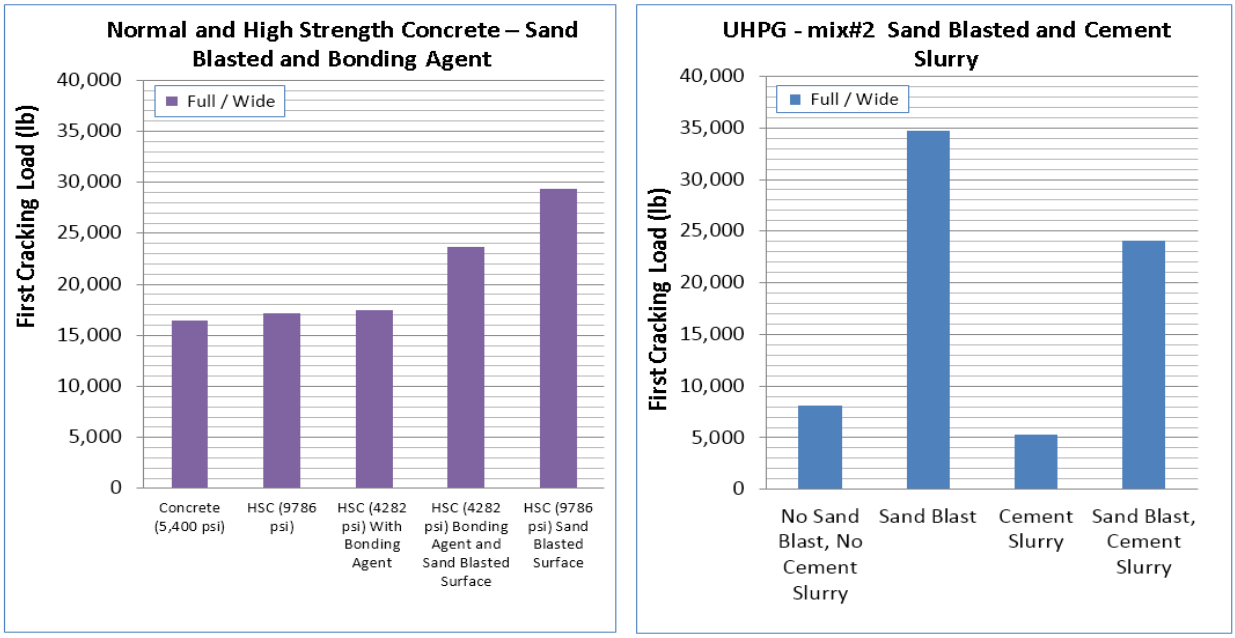

Fig. D.19 Shear Strength vs. Surface Condition for UHPG

D.2.6.5 Grout material

Kuhlman 1107

For the specimens grouted with Kuhlman 1107 (an ODOT-approved grout) with the current practice for the key way geometry, strength can be increased by increasing the key way depth or increasing key way depth and width.

Normal strength concrete

Even though surface cracks appeared at the interface for normal strength concrete and the 28-day compressive strength of the concrete used as a key way grout was 5,400 psi, the strength was higher than what was obtained with Kuhlman 1107 grout material. For Wide/Partial depth key way, the average strength was 42% higher than the strength obtained for specimens grouted with Kuhlman 1107 grout.

For Wide/Full depth key way, the average strength was 13.4% higher than the specimens grouted with Kuhlman 1107 grout.

High strength concrete

For Wide/Full depth key way, the average strength for HDS was 18.2% higher than the specimens grouted with Kuhlman 1107 grout.
For Wide/Full depth key way, with sandblasted surface, the average strength was 102% higher than the specimens grouted with Kuhlman 1107 grout.

This grout is a very good alternative to Kuhlman 1107 grout.

Master flow 4316 (Polymer grout)

This grout material is the best option to avoid shear failure and de-bonding failure at the interface because of good bond with concrete units.

Master Emaco T 545 - Master Emaco T 545 HT

This grout material has specific requirements that can be difficult to satisfy in practical conditions. These specifications are:

- Must be mixed, placed, and finished within 10 minutes under normal temperatures (71°F or 21°C).
- No curing is required, but it must be protected from rain immediately after placing.
- Liquid-membrane curing compounds or plastic sheeting may be used to protect the early surface from precipitation, but wet curing should never be done.

UHPC Grout

For wide/full depth key way and without sandblast or cement slurry, the average strength of UHPC grout was 44% lower than the specimens grouted with Kuhlman 1107 grout. UHPC does not develop shear strength if it is not properly bonded to the key way surface. However, ~~F~~for wide/full depth key way and with sandblasted surface, the average strength of UHPC grout was 140% higher than the specimens grouted with Kuhlman 1107 grout. This grout is also a great alternative to Kuhlman 1107 if the surface is sandblasted and coated with cement slurry.

D.3 Summary and Conclusions

The following conclusions were drawn from the joint tests with a tie rod:

Small amount of tie force increases the shear transfer strength of key way joints by a large amount. The tie rod also allows the joint to develop a larger relative slip. The shear strength of joints at failure is much more than the shear strength of the joint at the time of visual appearance of the first crack for the same joint.

The following conclusions were drawn from the joint tests without ties:

(i) Joint strength can be increased using deeper and~~/or~~ wider key way.
(ii) Cement slurry and bonding agent does not enhance shear strength.
(iii) Sandblasting the interface can increase the shear strength of the joint significantly.
(iv) Polymer grout has a strong bond and shear strength under shear loads.
(v) Magnesium phosphate grouts have poor performance that can get worse if exposed to humidity and environmental conditions.
(vi) HSC grout is a better option compared to ODOT-approved grouts as long as it can be properly placed and compacted adequately within the wider key way.
(vii) UHPC has the highest compressive strength and shear strength. Rough interface surface increases the bond and the corresponding shear strength allowing the key way to utilize the high compressive strength of UHPC.

Shear transfer strength of key way joints can be increased by a factor of up to 5.5 compared to the joints that use the current ODOT-approved grouts and ODOT-recommended key way details through proper selection of grout material, ~~adjustment~~ revisions to the key way geometry, and surface preparation of the interface.

Waterproofing Details of Connections for Adjacent Precast Concrete Box-Beam Bridges

Appendix E: Study of Grout Materials and the Development of a New Ultra-High Performance Concrete Grout

Prepared by:

Mohamed Habouh, PhD (Former Graduate Student)
Anil Patnaik, PhD (Principal Investigator)

Prepared for:

The Ohio Department of Transportation
Office of Statewide Planning & Research

State Job Number 134847
07/25/2018

Waterproofing Details of Connections for Adjacent Precast Concrete Box-Beam Bridges

Appendix E: Study of Grout Materials and the Development of a New Ultra-High Performance Concrete Grout

Prepared by:
Mohamed Habouh, PhD
Former Graduate Student, Department of Civil Engineering
The University of Akron, Akron, OH 44325-3905

Dr. Anil Patnaik (PI)
Professor, Department of Civil Engineering
The University of Akron, Akron, OH 44325-3905
Phone: 330-972-5226 Email: Patnaik@uakron.edu

July 2018

Prepared in cooperation with the Ohio Department of Transportation, Ohio's Research Initiative for Locals, and the U.S. Department of Transportation, Federal Highway Administration

TABLE OF CONTENTS

LIST OF FIGURES

LIST OF TABLES

APPENDIX E: STUDY OF GROUT MATERIALS AND THE DEVELOPMENT OF A NEW ULTRA-HIGH PERFORMANCE CONCRETE GROUT

E.1 Evaluation of Approved Grout Materials

One of the ODOT-approved commercially available grouts is Kuhlman 1107. In this appendix, the influence of water content on the workability and compressive strength of this grout is presented, and the results are shown in Fig. E.1. The manufacturer recommends three ranges of water content:

- Three quarts of water per 50 lb of grout: the manufacturer describes the consistency as “plastic”.
- Three and one-fifth quarts of water per 50 lb of grout: the manufacturer describes the consistency as “flow-able”.
- Three and a half quarts of water per 50 lb of grout: the manufacturer describes the consistency as “pump-able”.

The placing of pre-manufactured grouts in the key way with the specified mixing water content was difficult even in laboratory conditions for a ¾-inch opening of the key way; the workability of grout was simply not adequate for placement and consolidation in key ways. Longer working time and more flowability are preferred to ensure that grout can be placed through the ¾-inch opening and the grout flows to the bottom to completely fill the key way. In controlled laboratory tests, the grout for small joint tests was wet cured at room temperature for 28 days, with no load application on the joints before testing. Even the highest recommended water content (3.5 qt/50 lb) was not adequate for the narrow opening of ¾ inch. Vibration was needed to ensure proper compaction of the grout material in the key way in laboratory conditions. However, construction sites do not allow such ideal conditions. Pavers and rollers driving over a newly constructed bridge before 28 days while the grout is still curing can load the grouted joint prematurely. Actual compressive strengths of grouts at early ages and the effect of increased mixing water were therefore studied in this project.

The influence of water content on the workability and compressive strength was studied for the three water contents recommended by the manufacturer and three higher ranges of water content: 4, 4.5, and 5 quarts per 50 lb bag of grout. Twelve standard test cubes were made for each of the six water content ratios and tested at one, three, seven, and 28 days to develop the relation between the water content and the compressive strength. The reduction in compressive strength of grouts is significant with the addition of water during the entire curing time of the grout. Testing 2”cubes as per ASTM C-109 for 1, 3, 7, and 28 days with different proportions of mixing water showed the effect of higher amounts of mixing water on the strength to the flowability obtained, as shown in Fig. E.1.

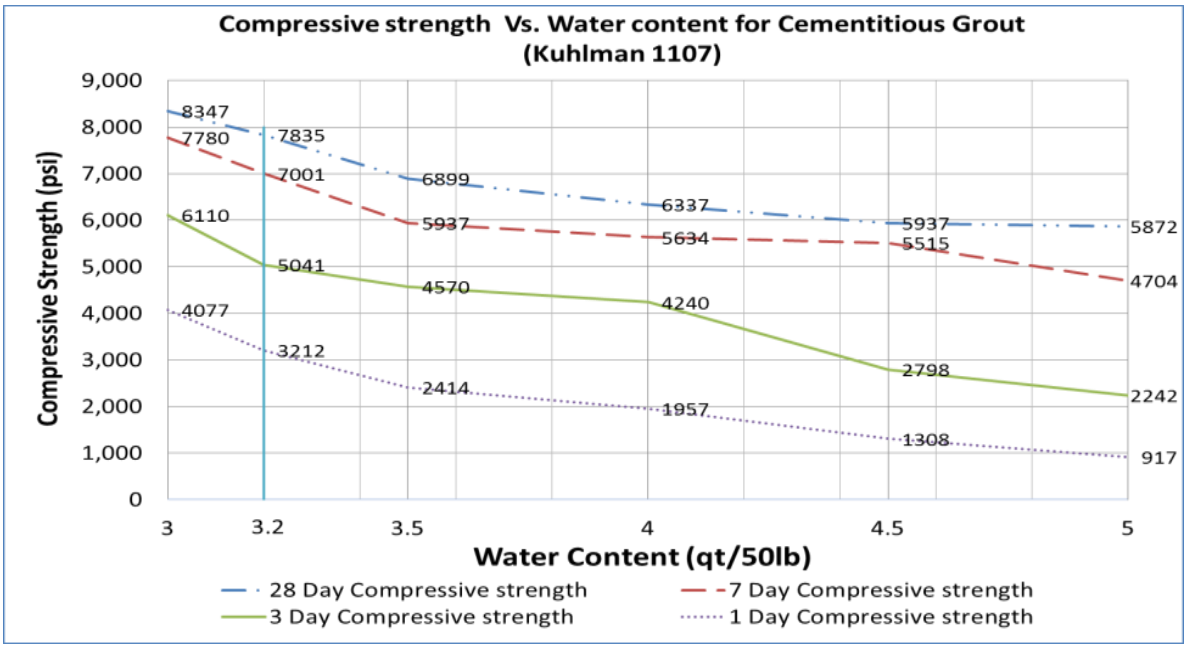

Fig. E.1 Influence of Water Content in a Grout on Compressive Strength

E.2 Performance Improvement of Approved Grout Material

A high-range water reducing agent "SIKA 2100" was used to improve the workability and the compressive strength of grout materials to achieve the desired workability. A slump cone of 2"×4"×6" size was used to measure the spread. With 3 quarts per 50 lb grout, the spread was limited to the diameter of the test cone. The spread could be increased to 7.5 inches using a larger amount of mixing water of 4.5 quarts per 50 lb grout.

Three mixes were made with a superplasticizer dosage equal to 40, 80, 160 ml per 50 lb grout and three quarts of mixing water per 50 lb grout~~,~~. ~~and t~~The spread was increased to 14, 15.5, and 17 inches as shown in Table E.1. These tests provide a solution to the problem of low workability for key way joint application, which can be improved with a suitable dosage of superplasticizers.

Table E.1: Increasing Mixing Water vs. the Use of Superplasticizer

Mix #	Superplasticizer dose (ml/50 lb grout)	Water content (quarts)	Spread (in)
1	0	3	2
2	0	4.5	7.5
3	40	3	14
4	80	3	15.5
5	160	3	17

Fig. E.2 Inadequate Workability with 3 Quarts Water per 50 lb of Grout (Left); Improved Workability with 3 Quarts Water and 40 ml Superplasticizer per 50 lb Grout (Right)

E.3 Development of High Strength Grouts

It was determined from the joint tests that the higher the compressive strength of the grout, the higher the shear transfer strength of the joint. Therefore, two high compressive strength grouts were developed. Suitable mix designs with and without coarse aggregate were developed after a number of trials and design optimization of the mixture proportions.

E.3.1 Mix Proportion for High Strength Grout with and without Coarse Aggregate

A grout mix design was developed through trials to achieve flowable high strength mixes with at least 10,000 psi compressive strength. The mix proportions given in Table E.2 are for high strength grout without coarse aggregate. Similarly, a high strength (concrete) grout with #8 aggregate was also developed with mixture proportions as given in Table E.3

Table E.2: Mix design for High Strength Grout without Coarse Aggregate

UHP Grout	Cement	Silica fume	Sand	Water W/C = 0.23	S.P.	Steel fiber
Mix proportion by weight	1	0.15	1.25	0.23	0.03	2% by volume
lb/ft^3	56	8.4	70	12.9	1.7	10
lb/yd^3	1512	227	1890	348	46	270
kg/m^3	900	135	1125	207	27	160

Table E.3: Mix Proportions for High Strength (Concrete) Grout with #8 Aggregate

HSC Grout	Cement	Sand	Aggregates	Water W/C = 0.35	S.P.
Mix proportion by weight	1	1.32	1.45	0.35	0.03
lb/ft^3	41	54	59	14.5	1.7
lb/yd^3	1100	1450	1596	385	46

Both these grouts with and without coarse aggregate performed much better than Kuhlman 1107 grout both in terms of workability and compressive strength. However, the high strength (concrete) grout with #8 coarse aggregate presented in this section was later found to be the most suitable grout based on the structural tests.

E.3.2 Development of Ultra-High Performance Grout

The existing options for ultra-high performance concrete (UHPC) are limited due to the need to use silica sand and quartz powder, which are both expensive. Traditionally, UHPC is produced with Ottawa sand having a pre-defined particle size distribution. The main reason for considering Ottawa sand is due to its mineralogy, particle shape and size distribution. Ottawa sand is siliceous almost with rounded to sub-rounded grains, and it has a smooth surface. The inherent properties of Ottawa sand are favorable when working with low water-to-cement ratios and when enhanced workability is needed. The use of standard Ottawa sand and quartz powder in UHPC production is restrictive where availability of these materials is limited.

The main objective of this trial was to use economical and readily available materials for developing a high performance grout based on UHPC. Consequently, the sand used in ~~our~~ these trials is conventional siliceous river sand with sub-rounded grains.

E.3.2.1 Findings from Trial Mixes

- Optimization of silica fume content: dosage of 15% was better than 20%
- Water to total binder ratio (W/B) = 0.2 is adequate for self-compacting; W/B = 0.17 needs vibration
- Grout with Type III cement ~~gives~~ provides higher early strength than grout with Type I cement
- ½ inch steel fiber content and superplasticizer dosage were kept constant
- Standard deviation of 6 cube samples with Type I cement was about 200 psi, and Type III cement was about 250 psi, with good repeatability
- Heat curing was done using 112° F or 50° C (water cured) for 5 days followed by 392° F or 200° C (oven curing) for 2 days; Type I cement was used
- Normal curing was done in a fog room with 98% humidity at 70° F or 21° C

- Heat cured specimens gained strength of 26,870 psi in 7 days (Table E.4), while water cured specimens gained strengths of 16,300 psi with Type III cement and 13,100 psi with Type I cement in 7 days

Table E.4: Cement Type vs. Curing Conditions

	Heat cured 112° F (50° C) for 5 days 392° F (200° C) for 2 days	Normal cured 70° F (21° C)
Type I cement	26,870 psi	13,100 psi
Type III cement	---	16,300 psi

E.3.2.2 Mixing Procedure

Acceptable mixing was achieved in an Imer Mortarman 120 plus mixer by using the following steps:

1. Add 40% of the superplasticizer to water before mixing
2. Place all the dry materials in the mixer (cement, silica fume, sand, fibers) and mix for 3 minutes to ensure proper mixing
3. Add water (with 40% superplasticizer) to the dry materials and mix slowly for 2 minutes
4. Wait for 1 minute and add the remaining superplasticizer and mix for 30 seconds
5. Continue mixing until the mix changes from dry powder to a thick paste
6. The casting of all the cube specimens was done within 20 minutes of mixing. All the specimens were cast and covered with a plastic sheet to avoid evaporation of water.

E.3.2.3 Mix Ingredients

The use of large size gravel was not found to be suitable for ultra-high performance grout. Different types of cements, undensified silica fume, water content, high-range water reducing agents, and steel fibers were used in the trials.

Fig E.3 Mix Ingredient and High Shear Mixer

The sand used in the mix needed to be very clean, since contamination with clay and silt particles reduced the cement-aggregate bond strength. Also, presence of clay and silt particles increased the water demand. The primary concern regarding the aggregate in the mix design for ultra-high performance grout is gradation, maximum particle size and strength. Large size particles are preferable, if workability can be achieved. The nominal size of sand ranged from 0.15 to 0.6 mm (0.006 inch to 0.024 inch). Sand was sieved, and a typical particle size distribution is shown in Fig. E.4.

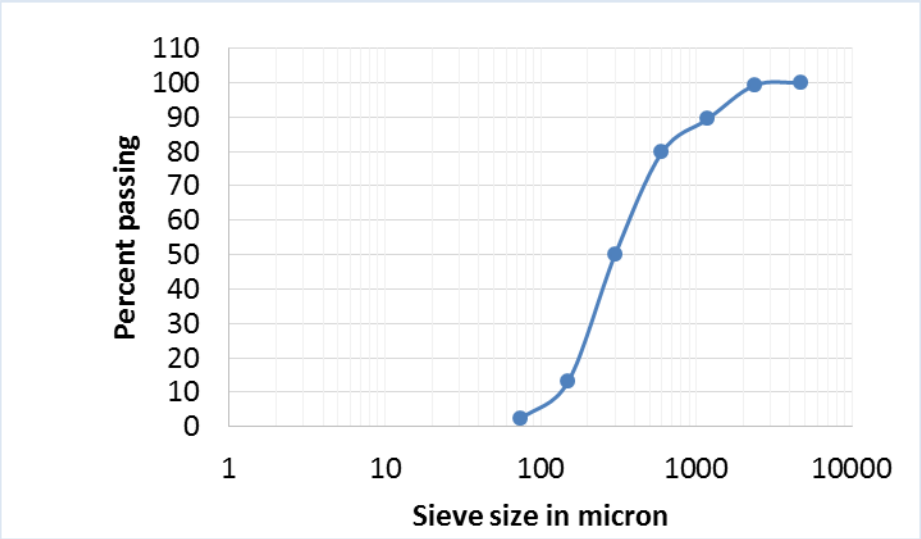

Fig. E.4 Typical particle size distribution

E.3.2.5 High-Range Water Reducing Agent

To obtain a mix with good workability, Sika Viscocrete 2100 high range water reducer was used. It can achieve water reduction up to 45% at higher dosages. Sika Viscocrete 2100 meets the requirements of ASTM C-494 Types A and F. It is suitable for making self-compacting concrete, and it improves the properties of fresh and hardened concrete.

E.3.2.6 Cement Type versus Compressive Strength

The use of Type III cement allows early high compressive strength compared to Type I cement. The seven-day compressive strength of concrete grout with Type III cement was 16,350 psi~~, when Type I cement could develop~~ compared to 13,100 psi with Type I cement.

E.3.2.7 Steel fiber

Steel fiber with aspect ratio of 62 was used to reduce the shrinkage cracks and improve the compressive strength. The properties of the steel fibers are shown in Fig. E.5.

Description	Steel fibers	
Length	½ 13	in. mm
Diameter	0.008 0.2	in. mm
Density	490 7.8 – 8.0	lb/ft^3 gm/cm^3
Tensile Strength	145 1,000	ksi MPa

Fig. E.5 Steel Fiber Characteristics

After many trials, the final mix design to be used for key way applications was developed and optimized with mixture proportions as given in Table E.5.

Table E.5: Mix Design for Ultra High Performance Grout without Coarse Aggregate

UHP Grout	Cement	Silica fume	Sand	Water W/C = 0.23	S.P.	Steel fiber
Mix proportion by weight	1	0.15	1.25	0.23	0.03	2% by volume
lb/ft^3	56	8.4	70	12.9	1.7	10
lb/yd^3	1512	227	1890	348	46	270
kg/m^3	900	135	1125	207	27	160

S.P. stands for superplasticizer (high-range water reducer)

Waterproofing Details of Connections for Adjacent Precast Concrete Box-Beam Bridges

Appendix F: Beam Assembly Tests for Symmetric Loading

Prepared by:

Mohamed Habouh, PhD (Former Graduate Student)
Anil Patnaik, PhD (Principal Investigator)

Prepared for:

The Ohio Department of Transportation,
Office of Statewide Planning & Research

State Job Number 134847
07/25/2018

Waterproofing Details of Connections for Adjacent Precast Concrete Box-Beam Bridges

Appendix F: Beam Assembly Tests for Symmetric Loading

Prepared by:

Mohamed Habouh, PhD
Former Graduate Student, Department of Civil Engineering
The University of Akron, Akron, OH 44325-3905

Dr. Anil Patnaik (PI)
Professor, Department of Civil Engineering
The University of Akron, Akron, OH 44325-3905
Phone: 330-972-5226 Email: Patnaik@uakron.edu

July 2018

Prepared in cooperation with the Ohio Department of Transportation, Ohio's Research Initiative for Locals, and the U.S. Department of Transportation, Federal Highway Administration

TABLE OF CONTENTS

LIST OF FIGURES

LIST OF TABLES

APPENDIX F: BEAM ASSEMBLY TESTS FOR SYMMETRIC LOADING

F.1 Objective

Joint tests described in Appendix E of this report were conducted with a large number of variables that included a wide range of geometries and grouts. The joint tests provided a basis for selecting the parameters for further testing and evaluation at a larger scale. The symmetric beam assembly tests conducted in the laboratory in this project are a simplified representation of three adjacent box beam units tied together to act as a single unit. The primary objective of the beam assembly tests was to study the joint strength and behavior under symmetric loading.

F.2 Test Procedure

Each beam assembly comprised three concrete beam units with two longitudinal key ways (Fig. F.1). Load was applied downward to the middle unsupported beam unit at the midspan, and the two external beam units were symmetrically supported upward at the ends. The middle beam unit was not supported at the ends and the external units were not directly loaded. This support condition ensured that the load applied to the middle beam unit at the midspan is transferred to the end supports through the two longitudinal joints symmetrically. The current ODOT practice in terms of key way geometry and grout material was used to develop the baseline test results as a starting point.

F.3 Test Specimen Configurations

Seven sets of beam assembly tests were conducted to include variables such as the types of grout material, key way geometry, and the effects of previously induced failure.

- Sets # 1 and 2 had standard key way geometry with ODOT-approved grout and as-cast concrete surface at the interface (new, unused assemblies)
- Set # 3 had standard key way geometry with polymer grout and as-cast concrete surface at the interface (re-grouted assembly). This set was a remanufactured assembly; after testing Set # 1, the assembly was taken apart, the old grout removed from the joints, and the key way was re-grouted.
- Set # 4 had full depth–wide key way with ODOT-approved grout and as-cast concrete surface at the interface (new, unused assembly)
- Set # 5 had full depth–wide key way with HSC grout and as-cast concrete surface at the interface (new, unused assembly)
- Set # 6 had full depth–standard width key way with polymer grout and as-cast concrete surface at the interface (new, unused assembly)
- Set # 7 had full depth–wide keyway with HSC grout and sandblasted concrete surface at the interface (re-grouted assembly). This set was a remanufactured assembly. After testing Set # 4, the assembly was taken apart, the old grout was removed from the joints, and the keyway was re-grouted.

Typical details of the beam assembly test specimens are shown in Figs. F.1 to F.3. The complete details for each test specimens are presented in the next section.

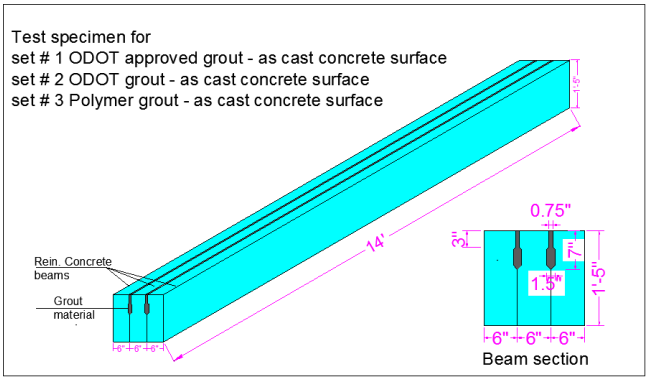

Fig. F.1 Test Specimen Details for Sets # 1, 2, and 3

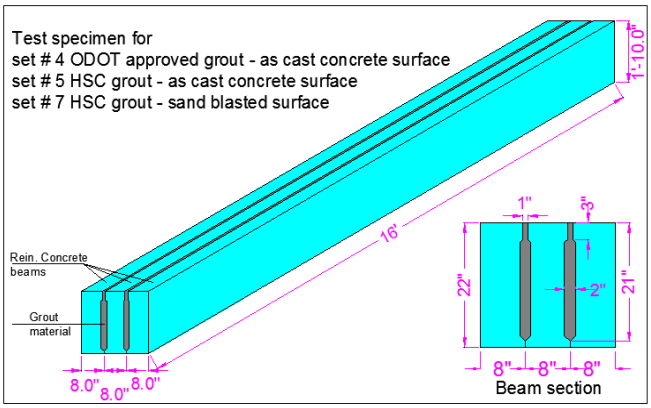

Fig. F.2 Test Specimen Details for Sets # 4, 5 and 7

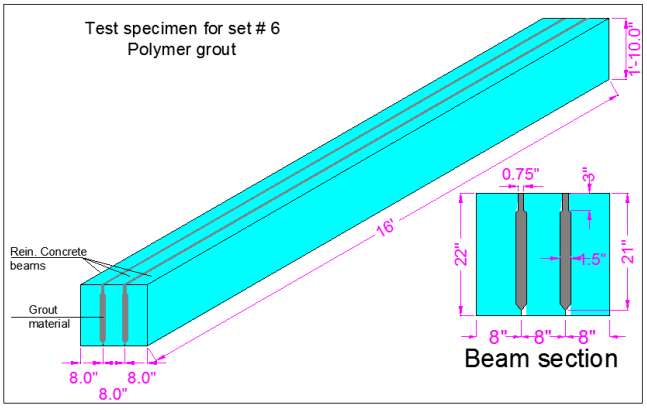

Fig. F.3 Test Specimen Details for Set # 6

F.4 Specimen Design

Each of the seven sets comprised three beam units tied together using 1" tie rod at the ends of the beams through 2" holes. A torque of 250 ft-lb was applied to the tie rods to provide 15

kips of clamping force at each end of the beam to match the applied force that is specified in ODOT current practice. Lengths of 1 foot at each end of each unit were formed without key way, and the rest of the joints had different key way geometry. Supports were provided to the external beam units only at both ends of each beam. LVDT's (Linear Variable Differential Transducers) and dial gages were provided to measure the vertical deflection, lateral movements, and the vertical movements for the middle "unsupported" beam unit at the ends (near the tie rods). Strains in the internal reinforcing bars and concrete top surface at the midspan were recorded using strain gages and a data acquisition system.

F.5 Section Design

The three concrete units were designed to fail in a tension control mode using a strain-compatibility design method. Actual stress–strain curve for the reinforcing steel bar was used to determine the load-carrying capacity of the beams. Each beam was designed to support a point load of 74 kips at the midspan. The analytical moment capacity of the beam at failure was determined to be 278 ft-kips. The overall length of the beam was 16 feet and the simply supported span was 15 feet. The 28-day average target compressive strength of concrete units was 10,000 psi. The design mix of the concrete units and reinforcement details for a typical cross section are shown in Table F.1 and Fig. F.4.

Table F.1: Mix Design of Concrete Units

#8 Limestone	1500 lb/yd^3
Sand	1320 lb/yd^3
Type I Cement	750 lb/yd^3
Micro Silica Fume	50 lb/yd^3
Air Entrainment	0.20 oz/cwt
Viscocrete 2100	5.0 (±) oz/cwt
Potable Water	280 lb/yd^3

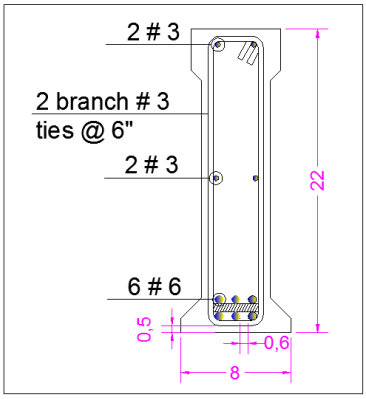

Fig. F.4 Mix Design of Concrete Units

F.6 Curing and Shrinkage Cracks

Sets # 1 and #2 were cast and tested in the Civil Engineering laboratory at room temperature of about 70° F. The beams were wetted periodically throughout the day for 7 days. However, shrinkage cracks parallel to the beam longitudinal axis appeared on the top surface throughout the length of the joint shortly after grouting. The width of the shrinkage cracks were 0.006 and 0.02 for Set # 1, and Set # 2 respectively, as shown in Fig. F.5.

Fig. F.5 Shrinkage Cracks for Set # 1 (Left) – for Set # 2 (Right)

Set # 3 through Set # 6 were wet cured for seven days and covered with wet burlap and plastic sheets. No shrinkage cracks appeared during the curing period, but very narrow cracks appeared after wet curing was completed. The longitudinal joints of Set # 7 were cured once by coating a curing compound immediately after grouting and covered with plastic sheet. Shrinkage cracks did not appear at all as seen in Fig. F.6.

Fig. F.6 Curing Compound Eliminates Shrinkage Cracks

F.7 Loading

A static load was applied at the midspan of the middle unsupported concrete unit using a closed-loop hydraulic actuator. The test setup with the maximum capacity of 55 kips as shown in Fig. F.7 was used for Sets # 1 and #2. For Sets # 3 through #6, load was applied using a 300-kip hydraulic jack with a 200-kip capacity load cell attached to record the loading. The load was applied at a rate of 70 lb/sec until the joint failed. Set# 7 was loaded once to 100 kips, and then unloaded and loaded a second time up to 200 kips (i.e., loaded up to 100 kips and unloaded before loading again up to 200 kips), but it did not fail at 200 kip

load. The beam was then unloaded and the tie rod removed from the beam assembly ends. The assembly without tie rods was loaded again up to 200 kips but the beam did not fail at that loading either. In order to fail the beam, an increased loading capacity was needed. Therefore the beam was unloaded and a 300 kips load cell was used to fail it using the same test set-up as shown in Fig. F.7.

Fig. F.7 Test Setup for Beam Assemblies

F.8 Test Setup, Instrumentation, and Measurements

F.8.1 Strain Gages

Two steel reinforcing bar strain gages were attached to the bottom reinforcement in the tension zone of each unit of the three-beam assembly to measure the strains in the tensile reinforcing bars. A strain gage was attached on the top surface at the top compression fiber to measure the compressive strain on the surface of the concrete. The strain gage data were acquired through a data acquisition system during testing.

F.8.2 Dial Gages and LVDTs

LVDTs were attached to the concrete surface at the locations shown in Fig. F.8 to measure the vertical deflection and the lateral spread of the concrete units during testing. The total lateral spread at the quarter span at the bottom of the two external beams was measured by adding the lateral movements of the two external beams acquired from LVDT 1 and LVDT 2.

Dial gages and LVDTs were employed as follows:

- Gages G2 and G3 measured the total lateral spread at the top at the quarter span
- LVDT#3 and LVDT#4 measured the lateral spread at midspan at the bottom of the concrete beams
- LVDT#5 and LVDT#9 measured the lateral spread at midspan at the top of the concrete beams

- LVDT#10 and LVDT#11 measured the lateral spread at the ¾ span at the bottom of the concrete beams
- Gages G6 and G7 measured the total lateral spread at the top at the ¾ span
- Gage G4 measured the vertical differential deflection between the middle loaded concrete unit and one of the external concrete units at the quarter span
- Gage G5 measured the vertical differential deflection between the middle loaded concrete unit and the other external concrete unit
- Gage G8 measured the vertical differential deflection between the middle loaded concrete unit and one of the external concrete units at the ¾ spans
- G9 measured the vertical differential deflection between the middle loaded concrete unit and the other external concrete unit
- The vertical differential deflection between the middle loaded concrete unit and the external units was measured by subtracting the deflections at LVDT#6 from LVDT#7 on one side and LVDT#8 from LVDT#7 on the other side
- The vertical differential deflections at supports were measured from LVDT #12 and G1 directly as the external units were prevented from vertical movements with roller supports, as shown in Fig. F.9.

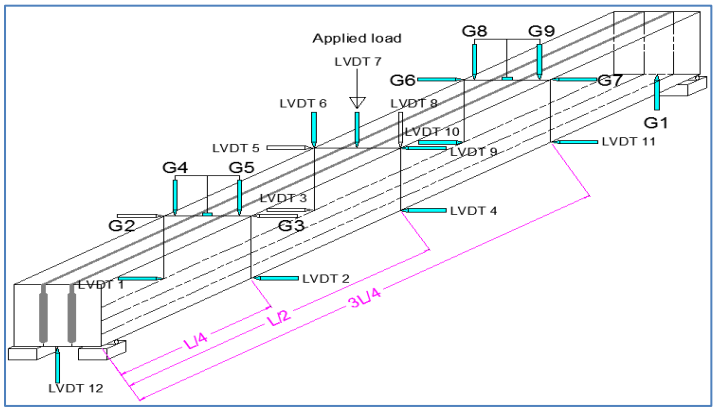

Fig. F.8 Instrument Layout for Beam Assemblies

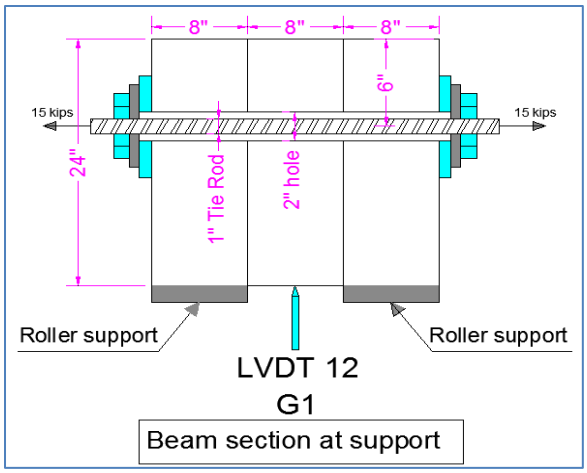

Fig. F.9 Typical Cross-Section of Beam Assembly at Supports

The base holders for G4, G5, G8, and G9 were rigidly attached to the middle concrete unit so that the gages could obtain the vertical differential deflection readings directly, as shown in Fig. F.10.

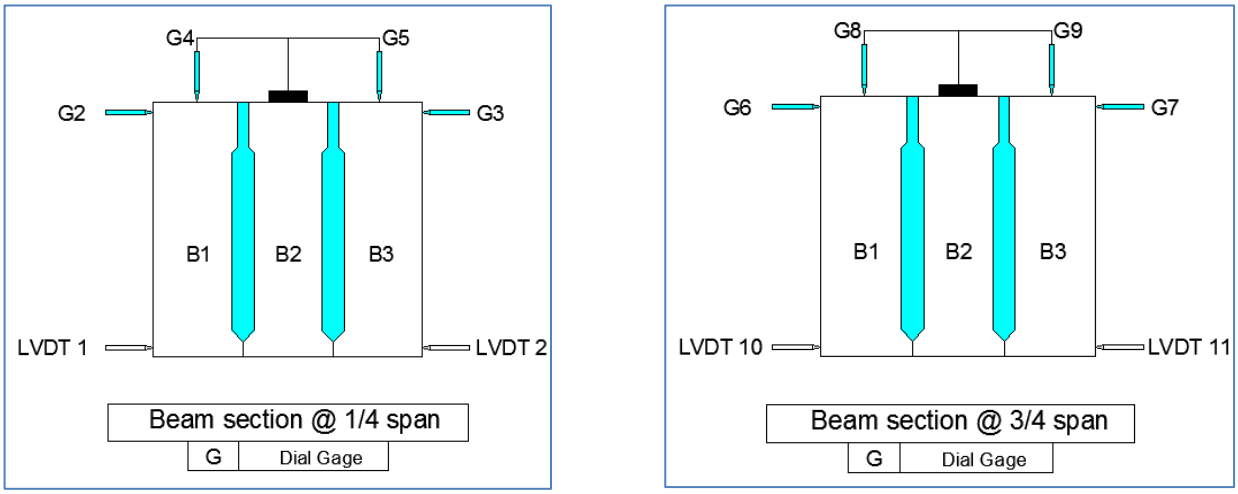

Fig. F.10 Typical Cross-Section of Beam Assembly at Quarter Spans

The LVDTs were installed in each beam unit as shown in Fig. F.11. Concrete strain gages were attached to the concrete surface of the beam units.

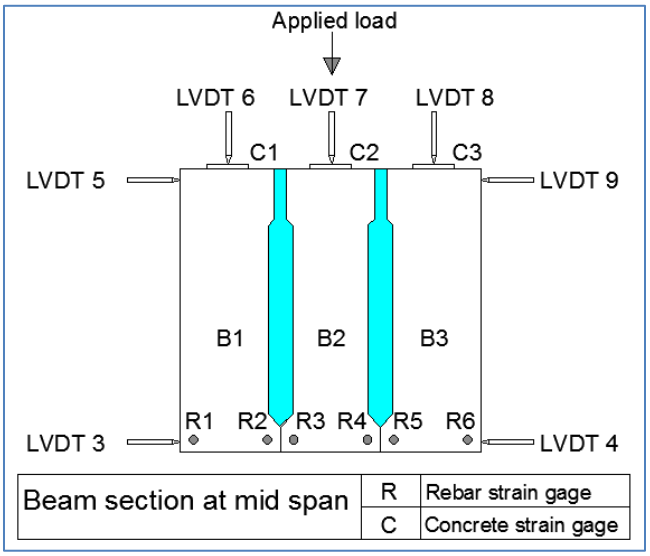

Fig. F.11 Typical Cross-Section of Beam Assembly at the Midspan

F.9 Test Results

F.9.1 Load Carrying Capacity

Table F.2 and Figs. F.12 and F.13 present the results of the symmetric loading tests of the beam assembly specimens. The following observations were made from these tests:

- For Set # 1 and Set # 2 with ODOT-approved grout and standard geometry, which are considered as control test specimens, the first cracking load was 37,500 lb and 38,000 lb for these two specimens, respectively.
- The load carrying capacity was increased by 95% when a deeper keyway of 21 inches was used with a top opening of 1" and a 2" wide keyway using the same grout material as Set # 4 when compared to the average cracking load of Set # 1 and Set # 2.
- Comparing the results of Set # 1 with those of Set # 3, a 223% increase in the first cracking load was obtained for the same keyway geometry when polymer grout was used, with an increase in the load from 37,500 lb to 121,140 lb. This suggests that polymer grout could be considered for rehabilitation of existing bridges.
- For full depth keyway (21 inch), the HSC grout was stronger than the currently used grout with a load capacity of 107,027 lb compared to 72,994 lb. This reflects a 46% increase from Set # 4 to Set # 5.
- The full depth keyway (21 inch) with polymer grout in Set # 6 had a superior load carrying capacity compared to all grouts with as-cast concrete surface, with a strength of 131,191 lb. and 250% increase in first crack load when compared to a strength of 37,500 lb obtained for Set # 1.
- The full depth keyway (21 inch) with HSC grout in Set # 7 had the largest load carrying capacity, when compared to all the grout materials tested in this project, with a strength of 275,000 lb. even after removing the tie rods from the beam assembly. This is a 633% increase in first crack load when compared to a strength of 37,500 lb obtained for Set # 1.

Table F.2: First Crack Load of Tested Assemblies

Set#	Grout Material	Cracking Load (lb)
1	ODOT-Approved Grout As-Cast Concrete Surface	37,500
2	ODOT-Approved Grout As-Cast Concrete Surface	38,000
3	Polymer Grout As-Cast Concrete Surface	121,140
4	ODOT-Approved Grout As-Cast Concrete Surface	72,994
5	High Strength Concrete As-Cast Concrete Surface	107,026
6	Polymer Grout As-Cast Concrete Surface	131,191
7	HSC Grout sandblasted concrete surface	275,000

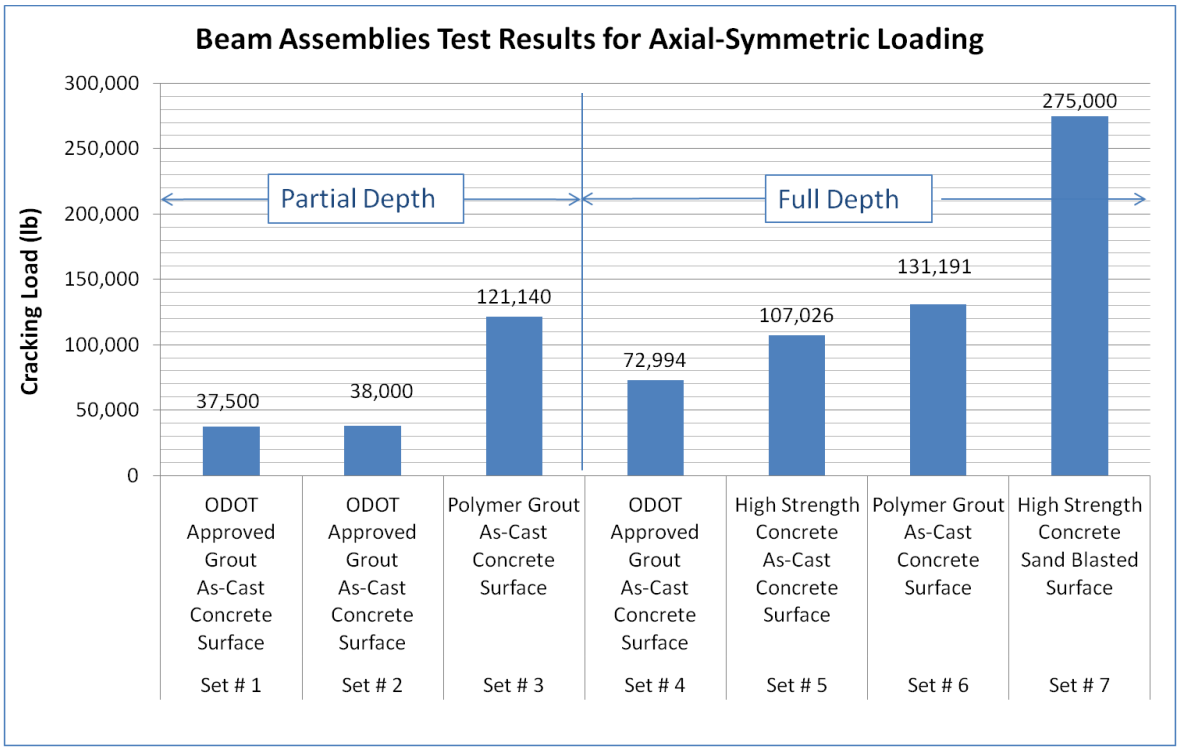

Fig. F.12 First Crack Load of Tested Assemblies

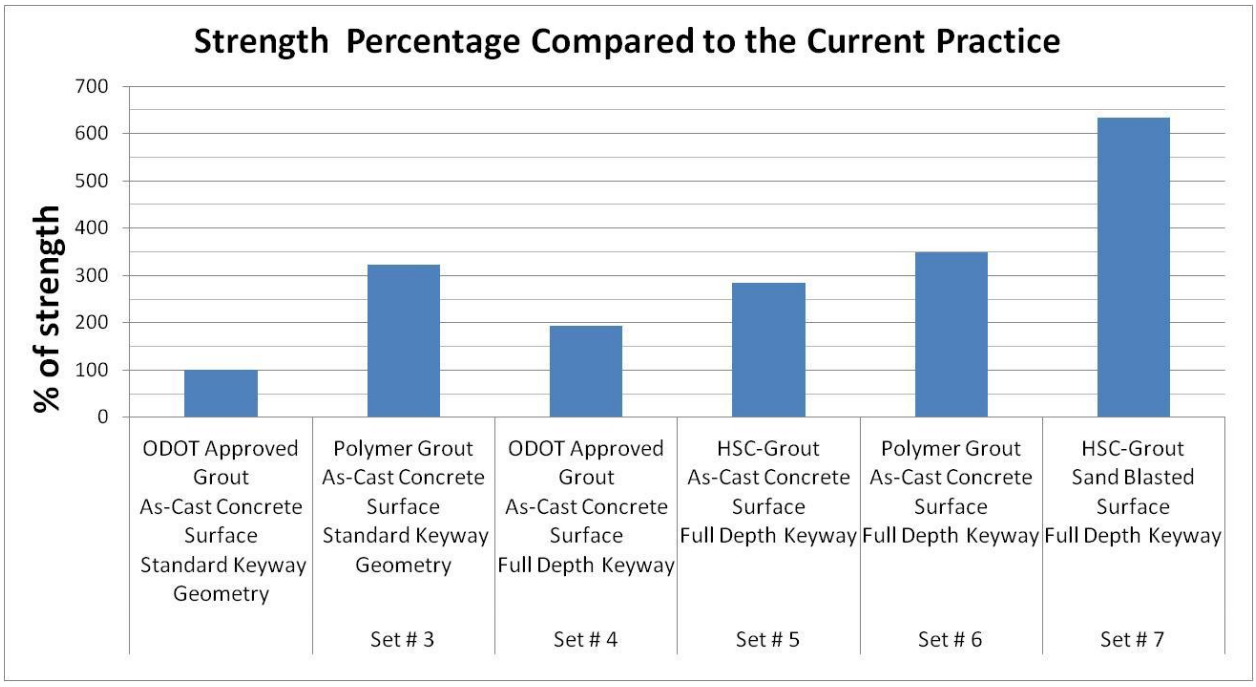

Fig. F.13 Percentage Change in the Strength of the Tested Assemblies

F.9.2 Lateral Separation of Set # 1

For Set # 1, the assembly was loaded until failure, and the first cracking load was 37.5 kips. Large horizontal movement was recorded at the top of the assembly at mid-span. A change from 0.002 inch to 0.016 inch was recorded before and after the failure load as shown in Fig. F.14. When the assembly was unloaded, the lateral spread had a 0.006-inch permanent spread. The assembly was reloaded again to capture the behavior of the assembly with the failed joint. The lateral spread at 37.5 kips was 0.0185 inch during reloading. This lateral spread was significantly higher than the spread for the beam at the first crack. Therefore, the first crack was considered as the basis to define the failure of the joint.

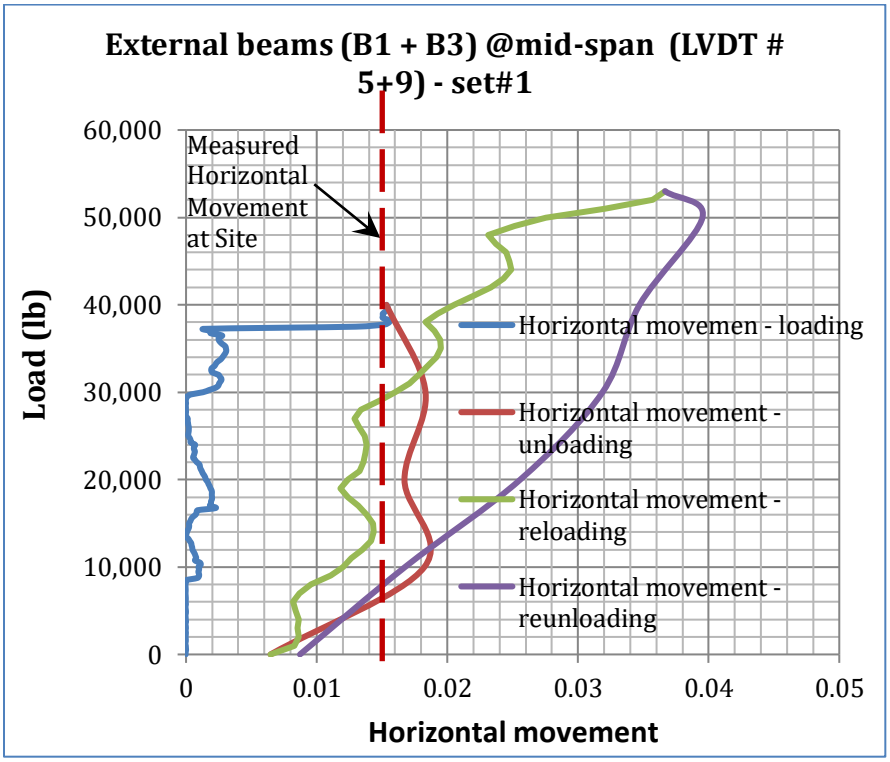

Fig. F.14 Set#1 - Lateral Spread vs. Load at Midspan

F.9.3 Vertical Differential Deflection of Set#1

For Set # 1, the first cracking load was 37.5 kips. The differential deflection at midspan at first crack load was 0.12 inch as shown in Fig. F.15, which is larger than the vertical differential deflection measured at site on a typical bridge. With a truck weighing 67.4 kips and driving at 70 mph, the maximum vertical differential deflection was measured for bridge ASD-42-12.49 to be 0.0045 inch and is reported in Appendix C.

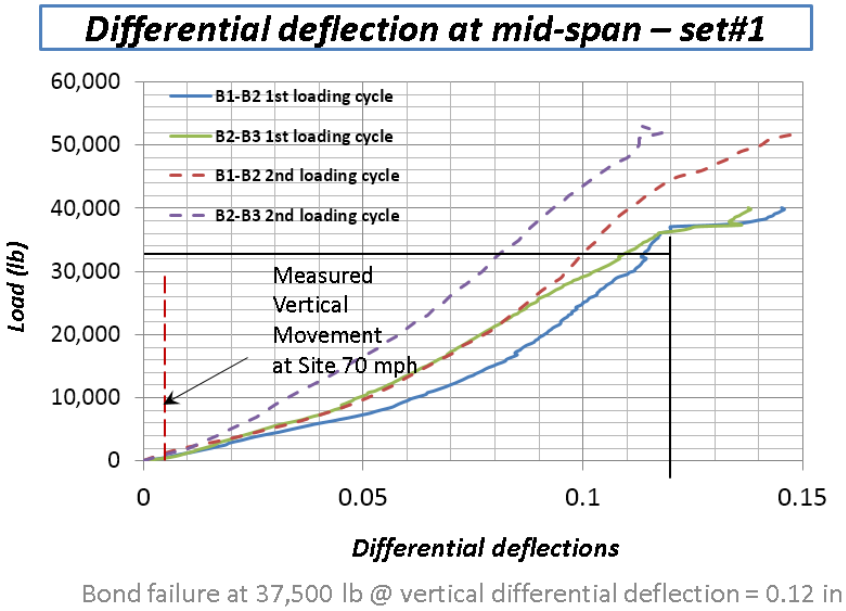

Fig. F.15 Set# 1 - Differential Deflection at Midspan for Set # 1

F.9.4 Failure Modes

Typical failure occurred in the tested assemblies by cracking along the joint at the middle of the beam length under the applied loads. These cracks did not extend to the supports at the end of the beams. This may be due to the local failure from stress concentration under the applied load and/or the clamping force of the tie rods at the ends that may have prevented the lateral spread and reduced the vertical differential deflection. It was previously stated in this report that the tie rods increase the shear strength and reduce the vertical slip locally at its location due to (i) the clamping force and (ii) the shear resistance provided by the cross sectional area of the tie rod itself.

The three beam units forming a beam assembly specimen were completely disassembled after testing Set #1 in order to fully break the bond between the grout and the concrete units at locations away from the cracked regions. The disassembly of the beams was very hard and required a great deal of effort demonstrating that the three beam units adhered well. The assemblies were taken apart without damaging the concrete units for Set # 1 as shown in Fig. F.16. These units were re-grouted to form Set # 3 to test the polymer grout to simulate rehabilitation/repair processes.

Fig. F.16 Set# 1 - Failed Joint After Testing

In Set # 2, the grout was firmly attached to the concrete units. It was not possible to separate the grout from the concrete units without damaging them, as shown in Fig. F.17. Therefore, it was not possible to reuse the concrete units from Set # 2 for further rehabilitation or testing.

Fig. F.17 Set # 2 Failed Joint After Testing

During the testing of the beam assembly with polymer grout (Set # 6), the first cracking was detected at a load of 131,191 lb. The joints between the concrete beam units had longitudinal cracks at the middle of the joint length under the applied loads. The grout detached from the middle beam as shown in Fig. F.18.

Fig. F.18 Set # 6 Middle Concrete Unit After Failure

However, the polymer grout in Set # 6 was still intact and well bonded with one of the external concrete units at the same location as shown in Fig. F.19, which indicates that a local failure of the joint may have occurred at one side only, near the middle cracked portion of the joint.

Fig. F.19 Set # 6 External Concrete Unit After Failure

Grout was removed from the tested beam assemblies using a jackhammer without damaging the concrete beam units or the joint surfaces for Set # 4. The restored concrete units were used to assemble Set # 7 to test and determine the effects of sand blasting with full depth key way and with HSC grout as shown in Fig. F.20.

Fig. F.20 Set#4 Removed Grout After Testing for Re-Grouting

The beam assembly that was originally grouted with ODOT-approved grout failed at 73 kips (Set #4) without damage to the concrete units. It was possible to remove the grout, sandblast the surface, and re-grout this beam assembly with HSC containing #8 aggregate.

The beam assembly that was originally grouted with HSC with #8 maximum aggregate size (Set #5) failed at 107 kips with damage to the bottom flange. This beam assembly could not be reused after its failure.

The assembly that was originally grouted with polymer grout (Set #6) failed at 131 kips resulting in the top compression zone being crushed and wide cracks in the bottom flange. It was not possible to reuse this beam assembly.

For Set # 7, a flexure failure in the middle concrete unit occurred with minor cracking at the joint. An excessive force applied using jackhammer was needed to separate the three units after the test was completed. The beams developed excellent bond with the HSC-grout at the joint interface. The concrete cover was detached from the beam and the reinforcement was exposed as shown in Fig. 7.21 demonstrating that the grout bonded with the keyway surface better than the monolithic concrete in the beam units.

F.9.5 Load Sharing Between the Concrete Units Before and After Cracking

Concrete compressive strains and the tensile strains in the bottom reinforcing bars indicated equal load distribution between the un-supported middle concrete unit (which is actually loaded from the top) and the two external concrete units that are supported at the bottom at the two ends.

For Set # 6 with first cracking load of 131 kips, the beam assembly failed by bond failure between beam units B3 and B2. This is indicated from the drop in concrete strain at gage C3 which is attached to beam unit B3 (Fig. F.22).There was no drop in concrete strain in gage C1 which is attached to beam unit B1 meaning that the load shared by this beam unit did not

change at failure. However, an increase in strain in gage C2 at failure as seen in Fig. F.22 indicates that the load released by B3 at failure was redistributed and transferred to B2.

Fig. F.21 Set#7 Separation of Concrete Cover After Testing

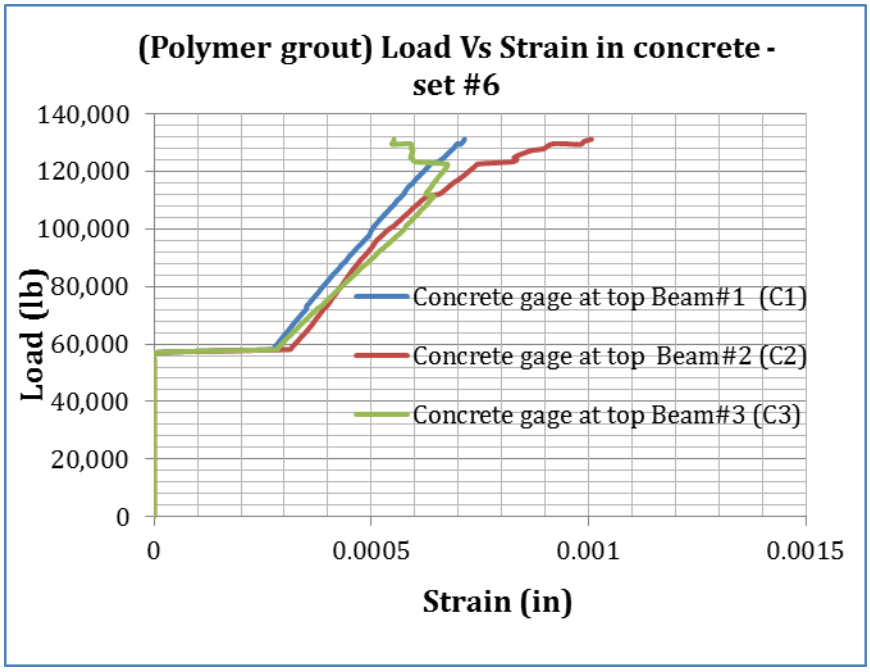

Fig. F.22 Set # 6 Concrete Strain Gages

For Set # 5, the compressive strains in the concrete at the top fibers of the three beam units were identical up to a failure load of 107 kips. The subsequent drop in concrete strain in gage C1 and increase in stains at C2 and C3, indicated bond failure in one joint only (i.e., the joint between units B1 and B2). The drop in C1 indicates that the load was released from the detached unit B1. The increased strain in C2 and C3 indicates that beam units B2 and B3

compensated for the load drop in beam unit B1 by picking up additional load after the joint failure (Fig. F.23).

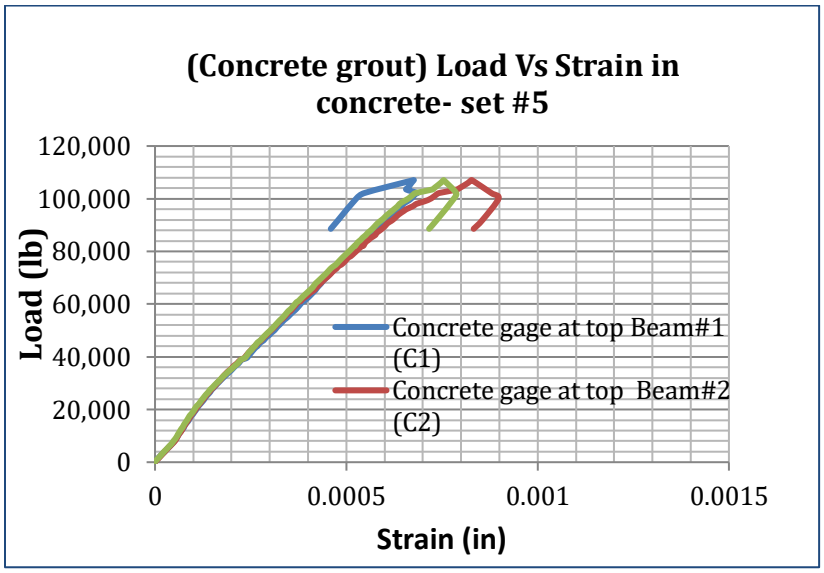

Fig. F.23 Set# 5 Concrete Strain Gages

For Set #4 with a cracking load of 73 kips, the load sharing between the beam units was significantly reduced and the strain in the bottom tensile reinforcement increased for R2 and R3. However, R1 had reduced strain, indicating de-bonding between beam units B1 and B2, and not failure between B2 and B3 as shown in Fig. F.24.

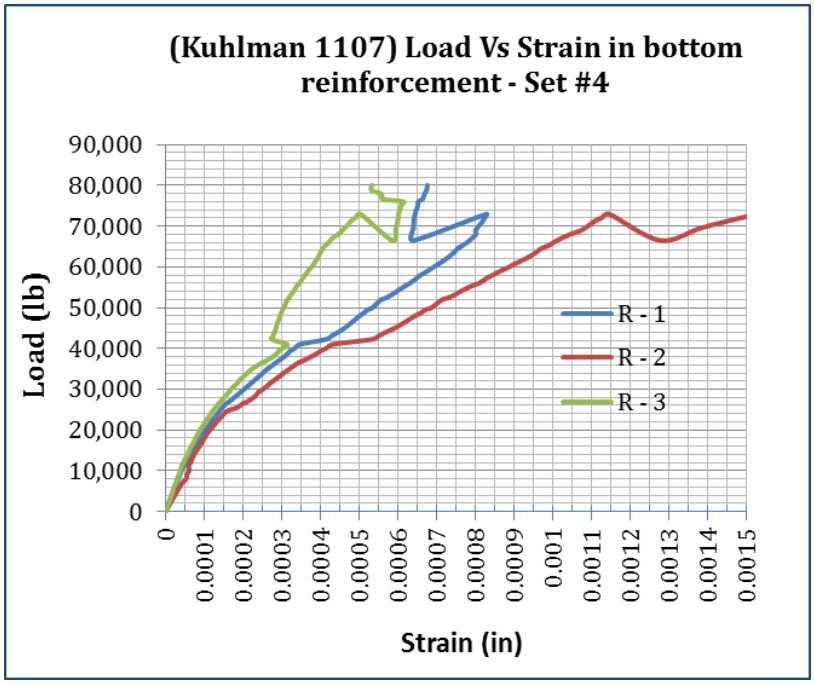

Fig. F.24 Rebar Strains for Set # 4

F.9.6 Differential Deflection and Lateral Spread of Beam Assemblies

The conclusion of local failure from the previously discussed failure modes can be supported by investigating the differential deflection behavior of the tested assemblies. In Set # 3 with polymer grout and standard key way geometry, the vertical differential deflection at the quarter span measured by gages G4 and G5 indicated no vertical differential deflection occurred up to 100 kips of load. However, at that load, a sudden increase in strain occurred in gage G4 before reaching the failure load. Likewise, a sudden increase in strain from 0.00 to 0.001 occurred in gage G5 at the failure load of 121 kips as shown in Fig. F.25.

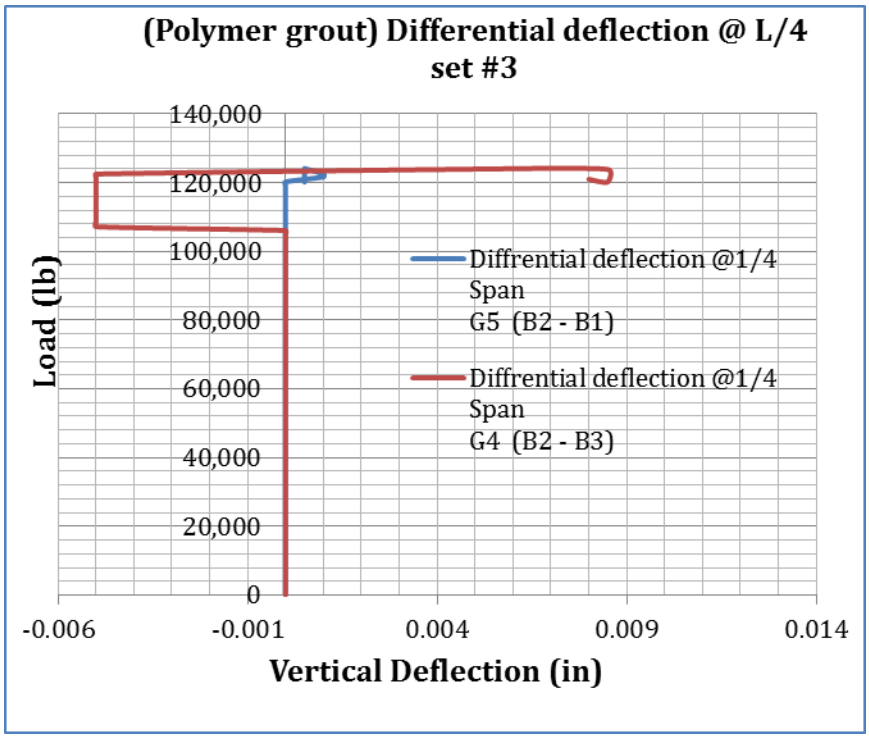

Fig. F.25 Set# 3 Differential Deflection at Quarter Span

Set # 6 with polymer grout and full depth key way reached a cracking load of 131 kips. However, the vertical slip at midspan started at 60 kips of load, which is less than half the cracking load of 131 kips. Polymer grout however was able to accommodate up to ±0.04 inch of differential deflection before the joint failure, as seen in Fig. F.26. Therefore, the ability of polymer grout to accommodate the differential deflection is better than that of HSC grout. By comparison, Set # 5 with HSC grout with the same key way depth as Set #6 had a smaller vertical differential deflection of 0.02 inch at a failure load of 107 kips.

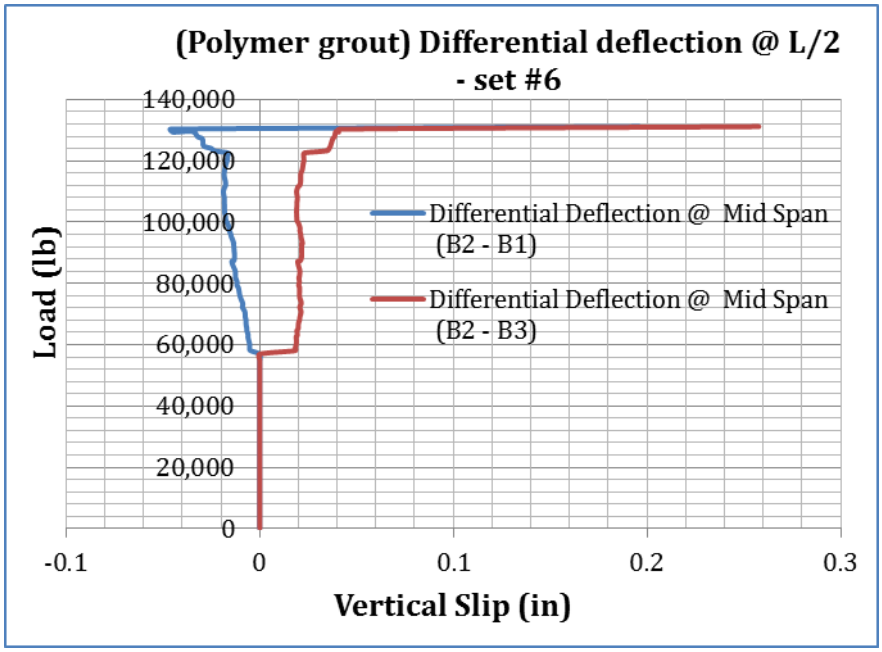

Fig. F.26 Set# 6 Differential Deflection at Midspan

In Set # 5, where HSC was used as a grout material with failure load of 107 kips, no lateral spread occurred at the quarter span before the failure at both joints. The increase in readings in G5 indicates that there is separation and joint failure between B1 and the middle beam unit B2, while the joint between B2 and B3 is still intact. The separation and the vertical differential deflections took place before the actual crack at a load of 92 kips, which is slightly lower than the first cracking load of 107 kips as seen in Fig. F.27. Similar behavior was observed before and after failure at the three-quarter span as shown in Fig. F.28.

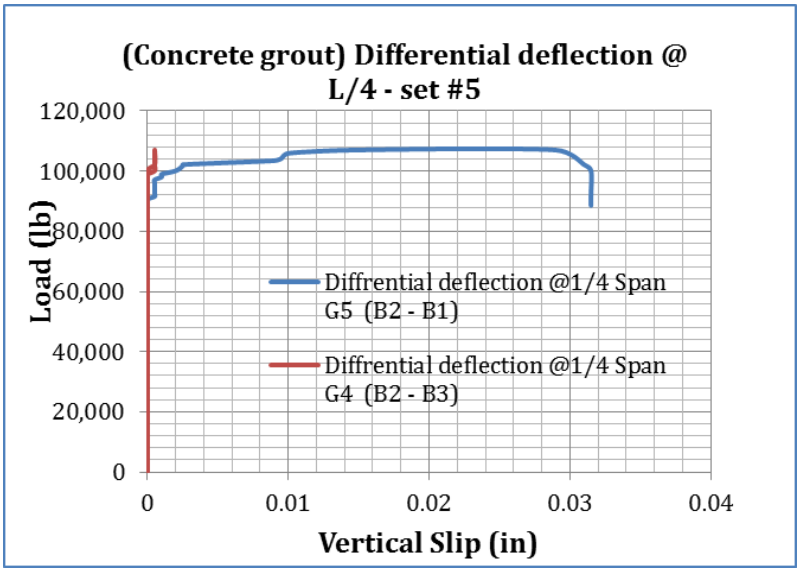

Fig. F.27 Differential Deflection at Quarter Span

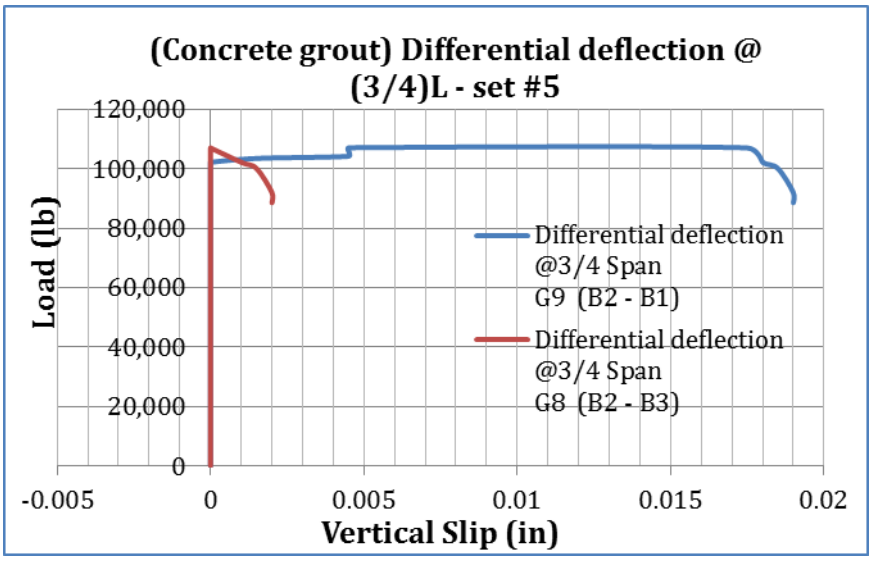

Fig. F.28 Set # 5 Differential Deflection at Three Quarter Span

For Set # 3, at the quarter span, no lateral spread was recorded up to a load of 100 kips, and at the three-quarter span. The negative lateral spread at the midspan indicated compressive stresses at the top fibers before failure while the joint was still intact. At higher loads and at failure, that compression was released when the joint failed (i.e., debonded) and allowed the units to move separately as shown in Fig. F.29.

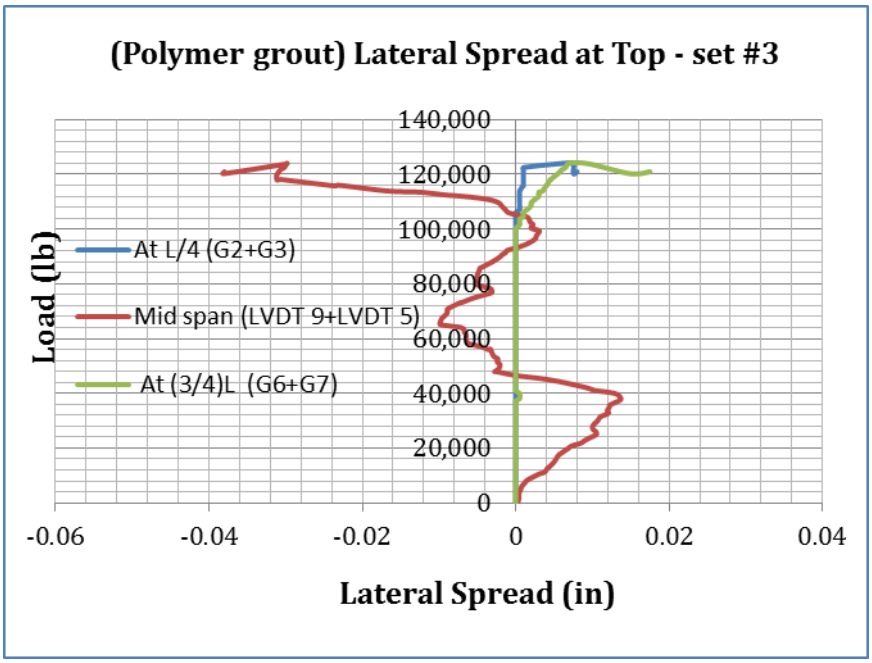

Fig. F.29 Set # 3 Lateral Spread at Top

F.10 Summary

The following observations were made based on the laboratory tests of box-beam assemblies:

1. Polymer grout shows superior performance with flowable, self-consolidating properties that do not require vibration or widening of the keyway opening to be effective. Polymer grout has three hours' working time after mixing over a wide range of temperatures. This can provide flexibility in terms of temperature conditions at the time of grouting. Polymer grout had 3.2 times the strength of the current ODOT-approved cementitious grout using ODOT standard keyway geometry. Therefore, polymer grout is a potentially implementable grout for box beam assemblies.
2. HSC concrete with a maximum #8 aggregate size is an attractive option to develop higher shear strength obtained with full depth keyway. The shear strength with HSC concrete was 107 kips compared to the current ODOT-specified grout that had 73 kips of shear strength.
3. Deeper keyways can increase the shear strength by 95% when using the same grout material.
4. Sandblasting the keyway surface can effectively increase the shear strength by 157% for the same grout material compacted to the keyway without sandblasting.
5. Shear failure is local under the applied loads. The effects of joint cracks and tie rods are also local.
6. The failed joints may undergo higher deflections after failure when subjected to further loading beyond the time at which the first crack appears. Therefore the load corresponding to the first crack is considered failure load from a waterproofing point of view.

Waterproofing Details of Connections for Adjacent Precast Concrete Box-Beam Bridges

Appendix G: Analysis for Eccentric Loading

Prepared by:

Mohamed Habouh, PhD (Former Graduate Student)
Anil Patnaik, PhD (Principal Investigator)

Prepared for:

The Ohio Department of Transportation
Office of Statewide Planning & Research

State Job Number 134847
07/25/2018

Waterproofing Details of Connections for Adjacent Precast Concrete Box-Beam Bridges

Appendix G: Analysis for Eccentric Loading

Prepared by:

Mohamed Habouh, PhD
Former Graduate Student, Department of Civil Engineering
The University of Akron, Akron, OH 44325-3905

Dr. Anil Patnaik (PI)
Professor, Department of Civil Engineering
The University of Akron, Akron, OH 44325-3905
Phone: 330-972-5226 Email: Patnaik@uakron.edu

July 2018

Prepared in cooperation with the Ohio Department of Transportation, Ohio's Research Initiative for Locals, and the U.S. Department of Transportation, Federal Highway Administration

TABLE OF CONTENTS

LIST OF FIGURES

LIST OF TABLES

APPENDIX G: ANALYSIS FOR ECCENTRIC LOADING

G.1 Introduction

The joint tests and the beam assembly tests presented in Appendix E and Appendix F were designed to determine the shear transfer strengths at the joints with standard and modified geometries and to determine the suitability of the grouts under symmetric loading conditions. In reality, the load application under traffic loading condition on the box beams may not be symmetric. Multiple adjacent box beams need to act together in sharing the loads from axle loads so that the load is transferred over more than one beam. For this interaction to happen between box beams, the longitudinal joints between adjacent box beams need to transfer the load resulting from the beams located within the effective width of the loading (see Fig. 8.1).

The interacting forces at the joints depend on the joint details, the bond that is mobilized between the grout and the box beam keyway recess, and the joint response to the internal forces developed at the interface. It is generally well accepted that the interacting forces can cause shear loading at the longitudinal joints. However, the positioning of wheel loads relative to the joints is expected to cause out-of-plane moments at the joint concurrent with the shear loading.

The out-of-plane moments are developed due to the eccentricity of the loading relative to the centerline of individual box beams. This aspect of longitudinal joint behavior was studied using finite element analyses for three spans and the corresponding beam cross sections.

G.2 Objective

The primary objective of the eccentric loading analysis is to develop an understanding and to determine the interacting forces for various combinations of in-plane shear loading and out-of-plane moments through structural or finite element analysis of adjacent box beams under design truck wheel loading.

Suitable structural analyses were also needed to design the test specimens to represent the stress conditions caused by the combinations of out-of-plane moments and the joint shears acting concurrently at the keyway joints in bridges that use box beams conforming to ODOT standard dimensions and typical spans.

In this task, three sets of analyses for 90 ft., 65 ft. and 40 ft. simple span bridges were included. The analyses for 90 ft. simple span bridge with B42-48 beam cross section was considered because it is the largest cross section used by ODOT (see Fig. G.2). A second set of analyses for 65 ft. simple span was performed to determine the factors of safety provided by the grouted joint. Factors of safety were determined by comparing the strength determined from the structural tests with stresses predicted from the analyses for the corresponding loading conditions. The corresponding test results are presented in Appendix G. The results of the analyses for a 40 ft. simple span bridge with B17-48 beam cross section are presented in Appendix I.

G.3 Assumptions for Analyses

Box beam bridge models were developed with SAP2000, a structural analysis program that also has finite element analysis features. The models presented in this report used the finite element modules of the program. The following assumptions were made in the analyses:

- The keyway grout and the box beam concrete have linearly elastic material properties
- The torsional rigidity of the box beams are automatically included in the analysis because finite elements using plates or solid elements are able to include the rigidity of box section due to geometry alone.
- Elastomeric bearings provide stiffness in compression and shear, but not in tension. Other aspects of modeling elastomeric bearings are given in a later section.
- Two anchor dowel bars of 1-inch diameter are provided at the two ends of each box beam, i.e., one anchor dowel bar at each end. The nominal shear strength of about 28 kips for each dowel bar of 1-inch diameter ($\approx 0.6 \times f_y \times A_b = 0.6 \times 60 \times 0.79 = 28$ kips) is not adequate to prevent longitudinal and transverse sliding of the beam ends. Therefore a roller support condition is more realistic at the ends for modeling the current practice, and various other support conditions were also considered in this study.
- A small-deflection linearly elastic structural or finite element analysis is suitable because of the small strains resulting from the loading considered in these analyses.
- The longitudinal joints were assumed to be uncracked.
- The use of fine mesh captures joint behavior adequately to predict the state-of-stresses at the joints. Validation of this assumption is presented in other sections.
- Two adjacent box beams were modeled for the load case causing maximum out-of-plane moment, but no shear (Load Case I) in Figure G.3. Three box beams were modeled together for the load case that causes simultaneous shear and moment (Load Case II) in Figure G.4. It is assumed that the box beams are able to accommodate torsional movements.
- A width of box beams of 36" or 48" is specified in the standard ODOT drawings for spans ranging from 20 ft. to 90 ft. Finite element analyses were performed using beam sections with 48 in. width for all the analyzed spans to maximize the effect of the out-of–plane moment compared to the beam sections with 36-in. width.
- Pre-tensioning the tie rods prior to grouting the keyway will not influence the stress condition in the hardened grout of the longitudinal joints.
- The interaction and the effects of the beams next to the two beams included in the analyses for Load Case I or the three-beam arrangement for Load Case II are minimal on the box beams included in the analysis.
- Stresses are transferred at the longitudinal joints through the grout only, which indicate that the adjacent box beams are not in contact with each other below the grouted joint.

G.3.1 Design Truck

The AASHTO HL-93 highway design truck loading configuration was employed to determine the stress conditions at the longitudinal joints of typical bridges according to AASHTO LRFD 2012 Bridge Design Specifications (6th edition). Load configurations (Figure G.1) were selected to maximize the number of axle loads on the box beam models. Only standard design truck wheel load configurations from HL-93 were considered because the lane load is expected to provide a symmetric and uniform loading condition on adjacent box beams and therefore may not cause any differential vertical movements or torsional effect.

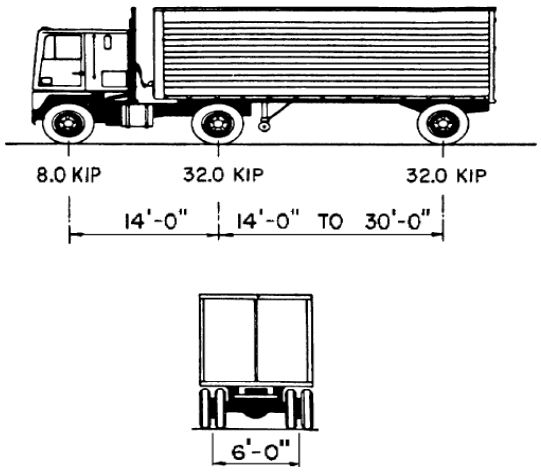

Figure 3.6.1.2.2-1—Characteristics of the Design Truck

Fig. G.1 AASHTO HL-93 Design Truck Loads

For HL-93 loading (Figure G.1), the front axle is 8 kips and two following axles are 32 kips each spaced at a minimum spacing of 14 ft. The width of the standard ODOT box beams will allow the placement of only one set of wheel loads because the width between wheels to be considered in the axle loads is 6 ft. (72 inch) and the standard widths of the box beams can be either 36 inch or 48 inch. Both these standard widths are less than 72 inch and therefore it is unlikely that both wheel loads from an axle can occur over the width on a single box beam. One set of wheels with unfactored loading condition can therefore be 4 kips followed by two 16 kip loads (for example, see Figure G.2).

In this report, the worst case scenario for the joints in box beams with a maximum simple span of 90 ft. was considered. The positions of the set of wheel loads used to maximize the effects on the joint are shown in Figure G.2.

G.3.2 Position of Loads in Transverse Direction Relative to the Longitudinal Joint

Wheel loads can be eccentric with respect to the centerline of an individual box beam. Initially, two critical load cases were considered to maximize the eccentric load effects.

Load Case I simulates two adjacent trucks moving next to each other at the edges of the adjacent girders remote from the joint, where the joint under study is subjected to stresses

from the out-of-plane moments caused by the wheel loads. The keyway needs to have adequate strength to transfer the stresses resulting from the out-of-plane moment at the joint between two adjacent beams. It is assumed that the two box beams are able to accommodate torsional displacements because these displacements are very small compared to the dimensions of the box beams.

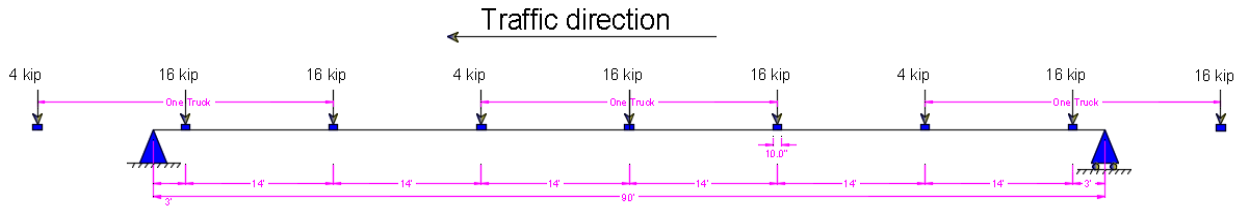

Fig. G.2 Loads in Longitudinal Direction

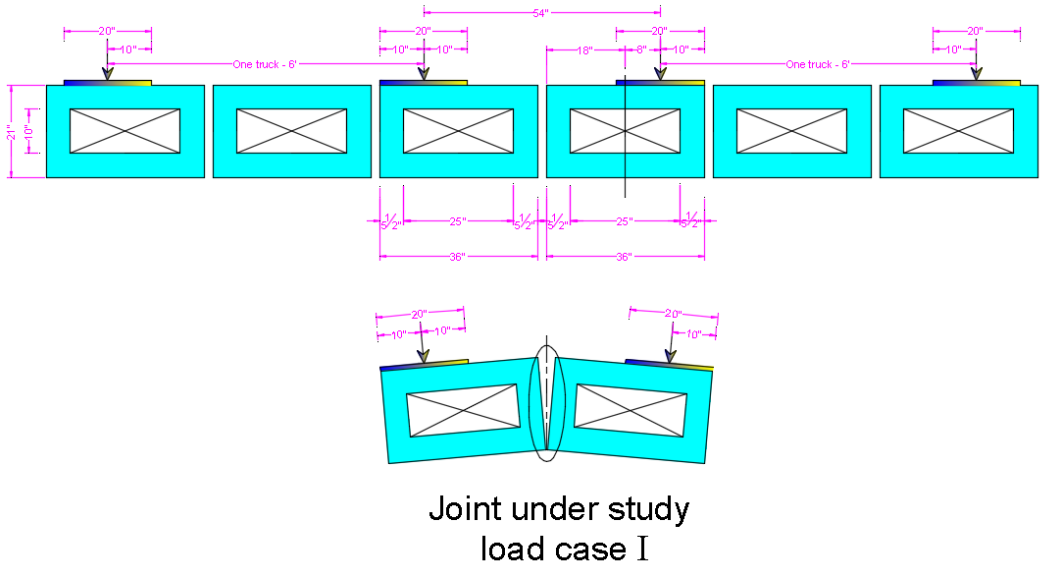

Fig. G.3 Load Position in Transverse Direction for Load Case I

Load Case I is expected to result in tension at the top and compression at the bottom over the keyway depth. The maximum tension will occur when two trucks are moving in the same direction in line with and next to each other. The shear force at the joint is zero due to the symmetric geometry of the two adjacent box beams and the symmetric loading condition, as shown in Figure G.3.

Load Case II applies when one set of the wheels of the trucks are placed at the edge of the girder next to the joint. In this load configuration, the wheel loads cause out-of-plane moment at the longitudinal joints, causing tensile stresses at the bottom of the joint and compressive stresses at the top of the joint (Figure G.4) simultaneous with shear. Once again, it is assumed to be able to accommodate torsional displacements.

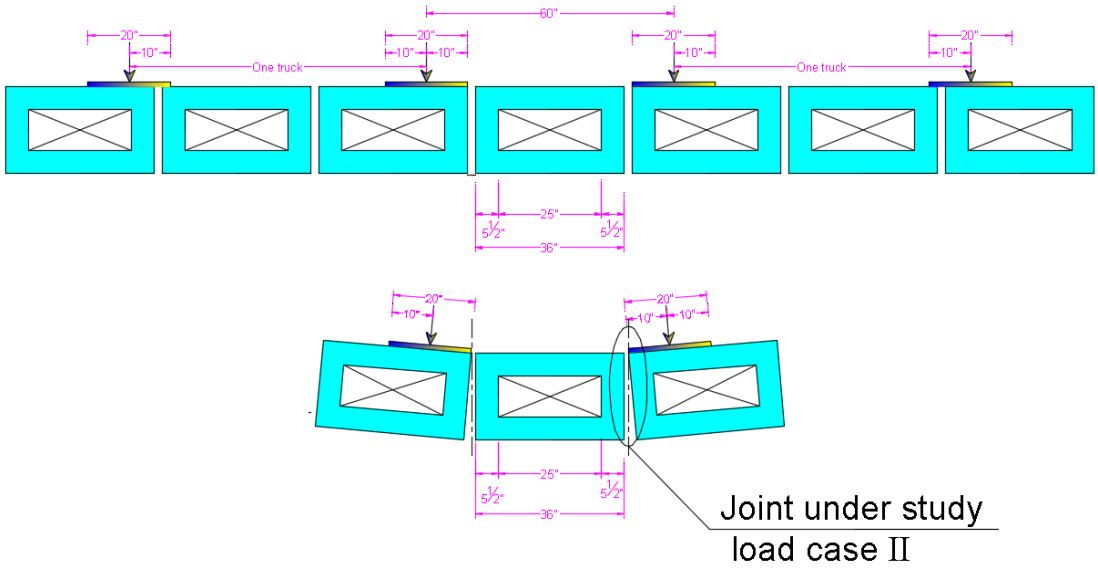

Fig. G.4 Load Case II - Load Position in Transverse Direction

This load case simulates the situation when two trucks are driving next to each other at the edges of two adjacent box beams separated by a middle box beam.

G.3.3 Tie Rods

G.3.3.1 ODOT Design Specification for Tie Rods

Tie rods are needed to provide lateral stability to the adjacent box beams for structural integrity. Spacing between tie rods is currently specified by ODOT to be no more than 25 feet. Tie rods are installed at the locations of the diaphragms that are provided within the box beams. Each tie rod is required to be tensioned to 15 kips of transverse clamping force, which will translate to 250 ft-lb torque.

G.3.3.2 Tie Rod Effects

In previous studies, tie rod effects were found to be local at the diaphragm location (Henry, 2011). In ODOT current practice, tie rod forces are applied to the girders before grouting, and therefore no stresses are imposed on the hardened grout material by the tie rod. The tie rod effects were not considered to be significant in this analysis.

G.3.4 Support Conditions

The following three aspects of support conditions were considered and are being reported:

(i) The uncertainty related to the stiffness of the elastomeric bearing pads,
(ii) The role of the bearing pads in allowing or restraining rotation of the beam ends, and
(iii) The effects of any reaction provided by the anchor dowel bars at the ends of the box beams

These effects were determined using two models with 36-inch-deep keyway for Load Case I. The box beams had intermediate diaphragms.

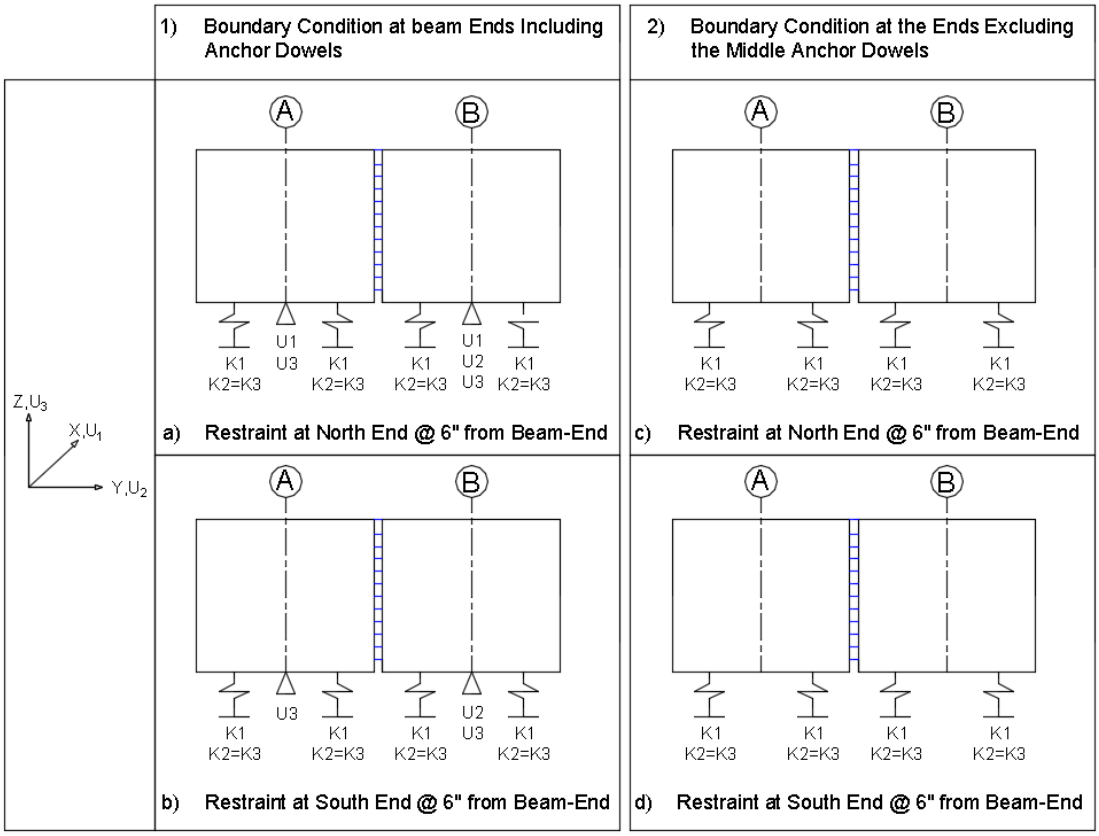

Note: X-direction and U-displacement are along the longitudinal axis of the box beams.

Fig. G.5 Boundary Conditions at the Beam Ends with Anchor Dowel Bar (a & b) and without Anchor Dowel Bars (c & d).

G.4 ODOT Design Specifications for Box Beam Ends

Prestressed box beams are supported on two elastomeric bearings at each support (BDM ODOT, 2010 section 302.5.1) as shown in Figure G.6 (PSBD-02-07), according to section 711.23 of the ODOT Construction and Material Specification manual.

A one-inch-diameter dowel bar is inserted on the centerline of the box beam at each end through a 2-inch hole at 6" from the edge of the beam (Figure G.7) by drilling a 12-inch-deep hole in the abutment.

Preformed expansion joint filler (Section 705.03 ODOT BDM), to be installed with the same thickness as the elastomeric bearing, is installed under the box beam around each anchor dowel bar to prevent the grout or sealer from leaking through to the beam seat. Because the

beam ends are seated on the bearing pads, no vertical load is transferred from the beam ends into the abutments outside the elastomeric bearing locations. The anchor dowel bars are not expected to provide any vertical reaction after the grouting or filling the annular space around the anchor bars with a sealer. The preceding explanation leads to an important aspect of modeling the beam ends in the structural and finite element analyses.

The box beam ends are set on four elastomeric bearing pads (two at each end). The entire beam self-weight is transferred through the four bearing pads soon after the beams are set in position. We believe that four bearing pads for each beam (two at each end) must be modeled as vertical springs. These pads also provide some lateral shear stiffness as claimed by their manufacturers. We do not believe that anchor dowel bars will provide any vertical support at the beam ends. The shear strength of 1-inch-diameter Grade 60 bars is about 28 kips.

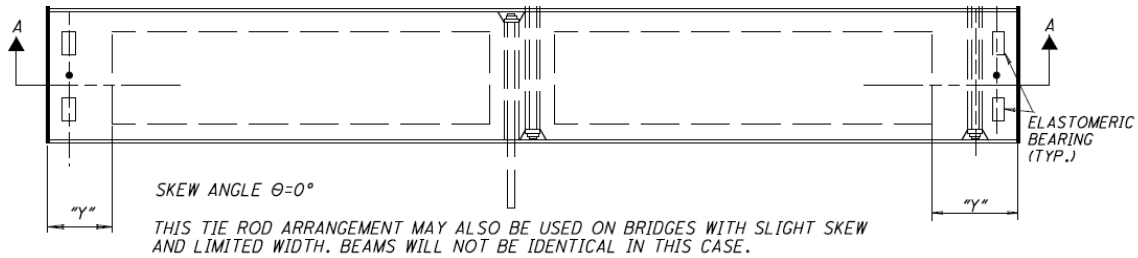

Fig. G.6 Elastomeric Bearing (ODOT, 2011)

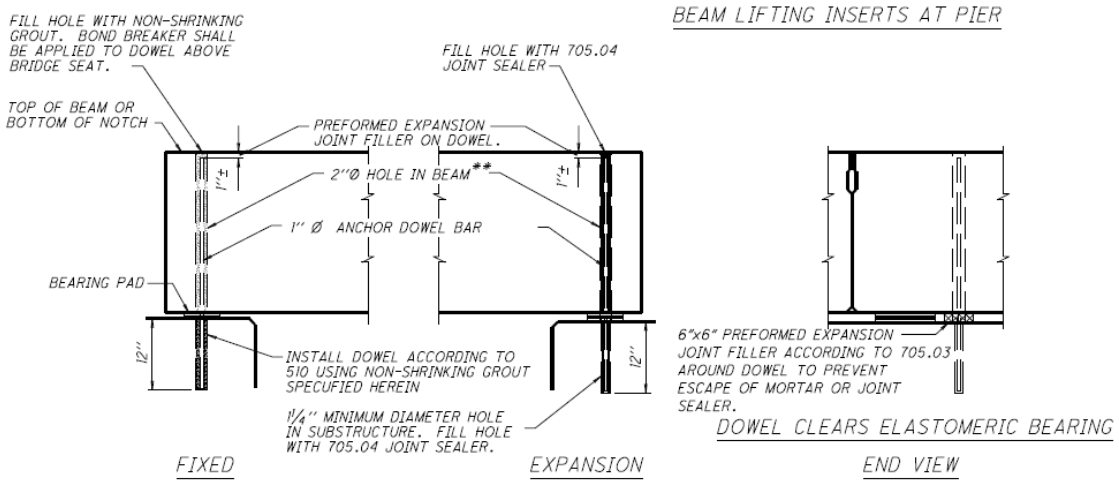

Fig. G.7 Dowel Bars (ODOT, 2011)

Bearing pads must satisfy the requirements of slip, shear, compressive stress, deflection, and rotation requirements of AASHTO LRFD Bridge Design Specifications, (2012). Typical stress-strain curves of elastomers (Figure 7.8) show that these pads need to deform significantly to provide the adequate reaction at the beam ends.

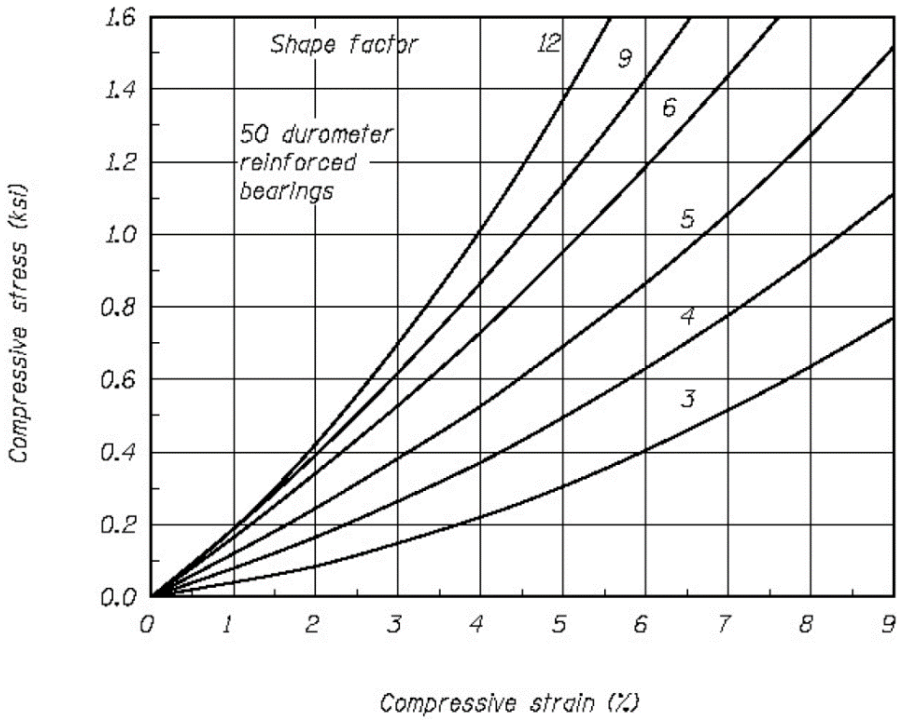

Fig. G.8 Typical Stress-strain Behavior of Elastomers (AASHTO, 2012)

G.5 Modeling Approaches used for the Analyses

The following two computer analysis software programs were used to determine the state of stresses: (i) SAP2000 and (ii) SpaceGass. Only service loads were applied in these models. The required joint strengths under the eccentric load effects due to the out-of-plane moments were determined for the two load cases for the load arrangements described previously using three independent analysis approaches with i) Shell elements for the box beam and the diaphragms and beam elements for grout, ii) Shell elements for the box beam and the diaphragms and springs for the grout for symmetric loading when no shear forces are transferred across the longitudinal joint, and iii) Eight-node solid elements.

G.5.1 Spring Factors in Compression

For the purpose of structural analysis and finite element (FE) analysis, the live load deformation of the elastomer was assumed to be 0.125-in, at the upper limit, for 2.5-in thick elastomer with strain = 0.125/2.5 = 5% and corresponding stress of 1.4 ksi (Fig. 7.8) for a 90 in^2 bearing pad.

$$K = (\sigma \times A) \div (\varepsilon \times L) = (1.4 \text{ ksi} \times 90 \text{ in}^2) \div (0.05 \text{ in/in} \times 2.5 \text{ in}) \approx 1{,}000 \text{ ksi}$$

G.5.2 Spring Factors in Shear

Shear modulus G_{73} at 73°F is less than G_0 at 0°F, therefore, a value of G_{73} = 95 psi was used. A shape factor of an elastomer area of 12 (see Fig. G.8), and a bearing pad area of 90 in^2 were applied:

$$K2 = G \times A/h_{rt} = 0.095 \times 90/2.5 = 4 \text{ ksi.}$$

G.5.3 Modeling with Shell and Beam Elements

Beam elements known as "Frame" elements in SAP2000 with six degrees of freedom were used for modeling the hardened grout within the keyway recess of box beams with a very fine mesh. "Shell" elements were used for modeling the walls of the box beams and for modeling the diaphragms in SAP2000. A width of box beams of 36" or 48" is specified in the standard ODOT drawings for spans ranging from 20 ft to 90 ft. Typical sections specified in ODOT standard drawings (PSBD-2-07) are shown in Figure G.9 for 48-inch-wide sections.

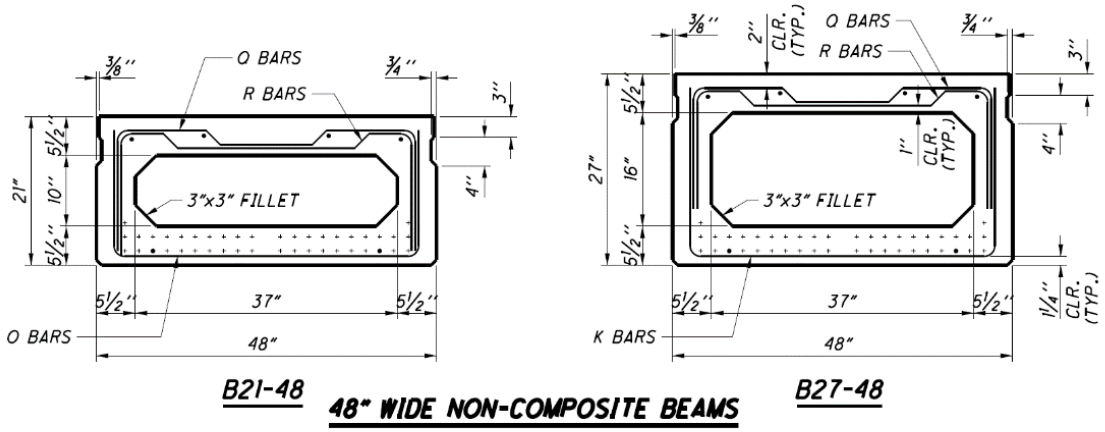

Fig. G.9 Standard Sections and Details of the Keyway Geometry

G.5.3.1 Modeling of Box Beam with Shell Elements

The "Shell" element is a type of area object that is used to model membrane, plate, and shell behavior in planar and three-dimensional structures. A non-layered, homogeneous material with constant thickness was used to define the "Shell" element. A homogeneous quadrilateral element with four-node formulation that combines membrane and plate-bending behavior was used to form the box beam plates and walls (CSi, 2015).

Plate-bending behavior includes two-way, out-of-plane, plate rotational stiffness components and a translational stiffness component in the direction normal to the plane of the element. A thin-plate (Kirchhoff) formulation that neglects transverse shear deformation may be selected or a thick-plate (Minlin/Reissner) formulation which includes the effects of transverse shear deformation may be selected. Out-of-plane displacements are cubic. The use of the full shell behavior (membrane plus plate) is recommended for all three-

dimensional structures. "The surface pressure load feature" is used to apply external pressure loads on any of the six faces of the "Shell" element (CSi, 2015).

Box beams were modeled as "Shells" with a thickness of 5.5 inch. The girder centerline dimensions used in The SAP analysis with plates were 42.5" width and 36.5" height to account for the thickness of the "Shell" elements forming the girder. Wheel loads were divided by equivalent tire contact area to retain an eccentricity of 14 inch between the center of the load area and the centroid of the girder while accounting for the reduced girder width due to the 5.5" thickness of the "Shell" elements. Typical cross sections used in the analysis for 48-inch-wide box beam sections are shown in Figure G.10.

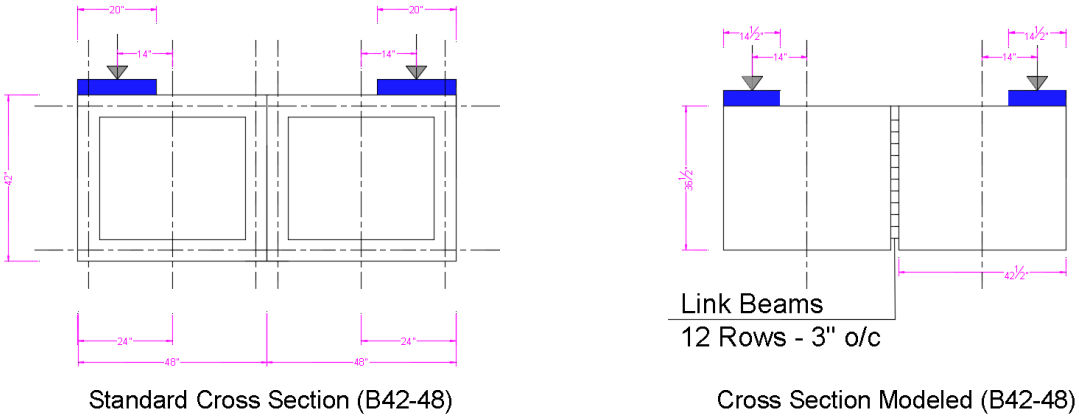

Fig. G.10 Cross Sections of Typical Models

G.5.3.2 Modeling of Diaphragms with Shell Elements

ODOT requires two diaphragms at the box beam ends and requires intermediate diaphragms at the tie rod locations in the transverse direction. At least one intermediate diaphragm should be provided for spans less than 50 ft, two intermediate diaphragms should be provided for spans larger than 50 ft and less than 75-ft, and three intermediate diaphragms should be provided for spans larger than 75 ft (Standard drawing PSBD 02-07). The diaphragm was modeled as a series of two-dimensional plate "Shell" elements spaced at 3 in. in the longitudinal direction with thickness of each plate equal to 1.5 in for the two exterior plates and a thickness of 3 in. for the interior plates. Figure G.11 shows typical modeling of the end diaphragm and interior diaphragms.

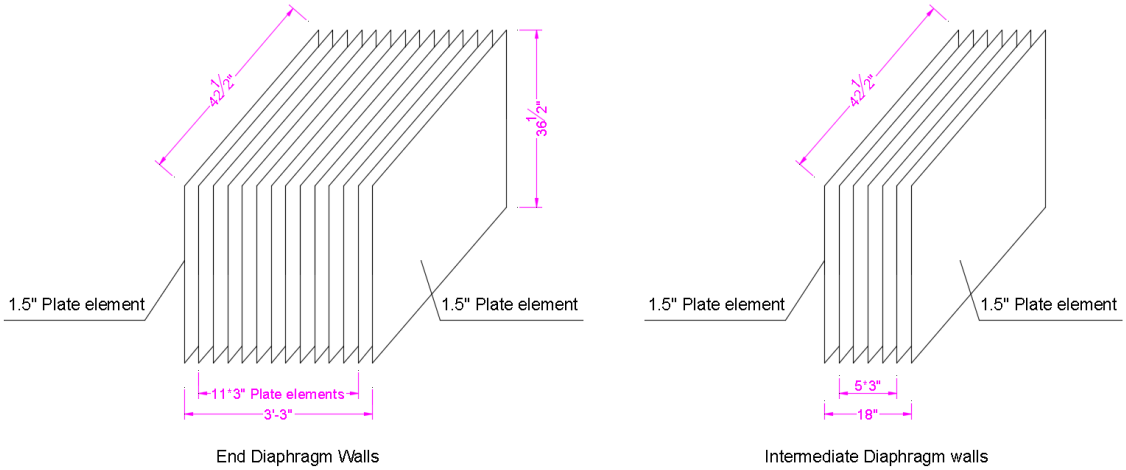

Fig. G.11 Modeling of Diaphragms for B42-48

G.5.3.3 Modeling of Grout with Frame Elements

The grout material was modeled with "Frame" elements that can be used to model beams, columns, braces, and trusses in planar and three-dimensional structures according to the CSI manual. Linear material properties were used to define the cementitious grout. The "Frame" element uses a general, three-dimensional, beam-column formulation, which includes the effects of biaxial bending, torsion, axial deformation, and biaxial shear deformations. A prismatic section of the element was used to have linear variation of the axial, shear, torsional, mass, and weight properties over each segment. The "Frame" element has six degrees of freedom at each of its ends. The "Frame" element uses only isotropic material properties (CSI, 2015).

The longitudinal joints between the box beams were modeled using link beams with 10,000 psi compressive strength and using the corresponding concrete material properties such as the elastic modulus. These link beams were spaced at 3 inches in both longitudinal and vertical directions (i.e., along the length and the depth of the box beams). The length of the link beams was one inch within the top opening region and two inches below the top opening in order to match the recommended keyway widths for the test specimens. The stiffness of the link beams was determined based on the length, the loading area, and the type of stresses.

The modulus of elasticity for concrete in compression (E_C) was used in considering the stiffness calculations for link beams in the expected compressive stress regions, and the modulus of elasticity for concrete in tension (E_T) was considered for the link beams in the expected tensile regions. The tensile modulus of elasticity was approximately half of the compressive modulus of elasticity.

Figure G.12 shows the link beam distribution along the height of the keyway for beams with 42 inches of actual height. However, to match the centerline dimensions for models with

plate elements for box beams, the dimensions of 42.5 inch by 36.5 inch were used as shown in the figure.

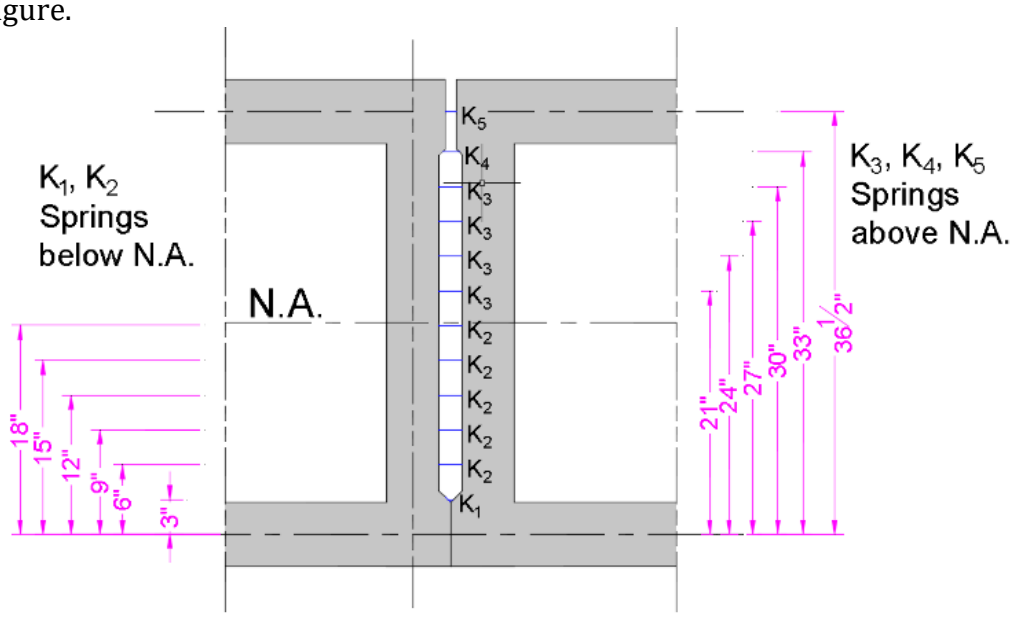

Fig. G.12 Link Beam Distribution in a B42-48 Cross Section

In Load Case I with tension expected above the neutral axis and compression expected below the neutral axis of the vertical joint section with a depth of 33.5 inch, the stiffness of the link beams was calculated as follows:

At height = 3”

$K_1 = E_C \times A \div L$ = 5,700 ksi × (1.5 in × 3.0 in) ÷ 2 in = 12,825 kip/in

With $E_c = 57\sqrt{f_c'} = 57\sqrt{10{,}000}$ 5,700 ksi

E_T = 2,500ksi (assumed as a minimum)

At height = 6” to 18”

$K_2 = E_C \times A \div L$ = 5,700 ksi × (3.0 in × 3.0 in) ÷ 2 in = 25,650 kip/in

At height = 21” to 30”

$K_3 = E_T \times A \div L$ = 2,500 ksi × (3.0 in × 3.0 in) ÷ 2 in = 11,250 kip/in

At height = 33”

$K_4 = E_T \times A \div L$ = 2,500 ksi × ((3.0 in × 1.5 in) ÷ 2 in + (3.00 in × 1.5 in) ÷1) = 16875 kip/in

At height = 36.5”

$K_5 = E_T \times A \div L$ = 2,500 ksi × (4.25 in × 3.0 in) ÷ 1 in = 31,875 kip/in

Adjusted cross-sectional areas were calculated accordingly to match the calculated stiffness value.

For example, the cross-sectional area of elements with heights of 21 inch to 30 inch was calculated to provide 11,250 kip/in stiffness:

$$A=K\times L\div E = 11{,}250 \text{ kip/in} \times 2 \text{ in} \div 5700 \text{ ksi} = 3.947 \text{ in}^2$$

G.5.4 Solid Modeling with Three-dimensional Eight-node Elements for the Grout and the Box Beams (CSI manual)

Eight-node solid elements were used for modeling the box beams and the grout material. According to the CSI manual, the "Solid Elements" are suitable for modeling three-dimensional structures and solids and are based on an iso-parametric formulation that includes nine optional incompatible bending modes. The "Solid" element activates the three translational degrees of freedom at each of its connected joints. Rotational degrees of freedom are not activated. This element contributes stiffness to all of these translational degrees of freedom. The "Solid Element" models a general state of stress and strain in a three-dimensional solid. All six stress and strain components are active for this element. Figure G.13 shows a cross section of the modeled beam in the longitudinal direction.

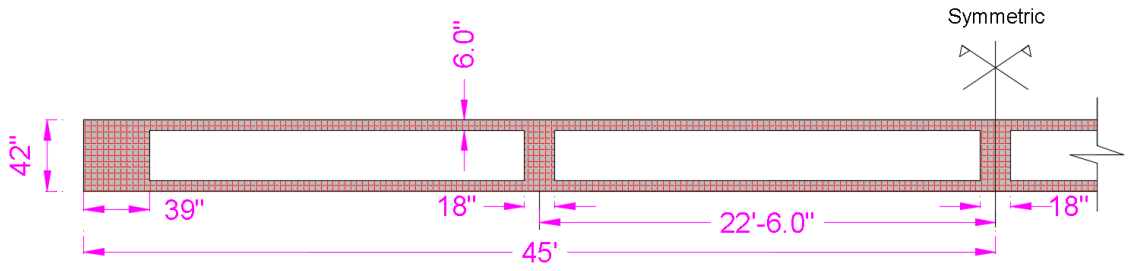

Fig. G.13 Cross Section at the Middle of the Modeled Box Beam

Three dimensional finite element models were developed with 3D-solid elements. All the models were developed for 90-ft. span simply supported box beam bridges with B42-48 ODOT standard section dimensions.

The following results were extracted from these models for Load Case I and Load Case II:

(i) Normal stresses perpendicular to the longitudinal joint surface and shear stresses in the plane of the longitudinal joints
(ii) Deflections at key points
(iii) Reactions in the elastomeric bearing pads
(iv) Shear force transferred at the joints along the length of the beams
(v) Graphs and contours of normal stresses and shear stresses

Nine models were developed to study the beam behavior considering the following factors: (i) models with and without intermediate diaphragms, (ii) models using full depth keyways and partial depth keyways, (iii) models using cracked and un-cracked grout. Figure G.14 shows a summary of the different models used in this study. All the analyses were performed

for service load conditions without any load factors. However, because of the assumption regarding linear elastic material properties and linear elastic analysis with uncracked condition, the stresses for factored load conditions can be obtained by multiplying suitable load factors by the results obtained in this report, particularly, in cases when strength limit state checks are needed.

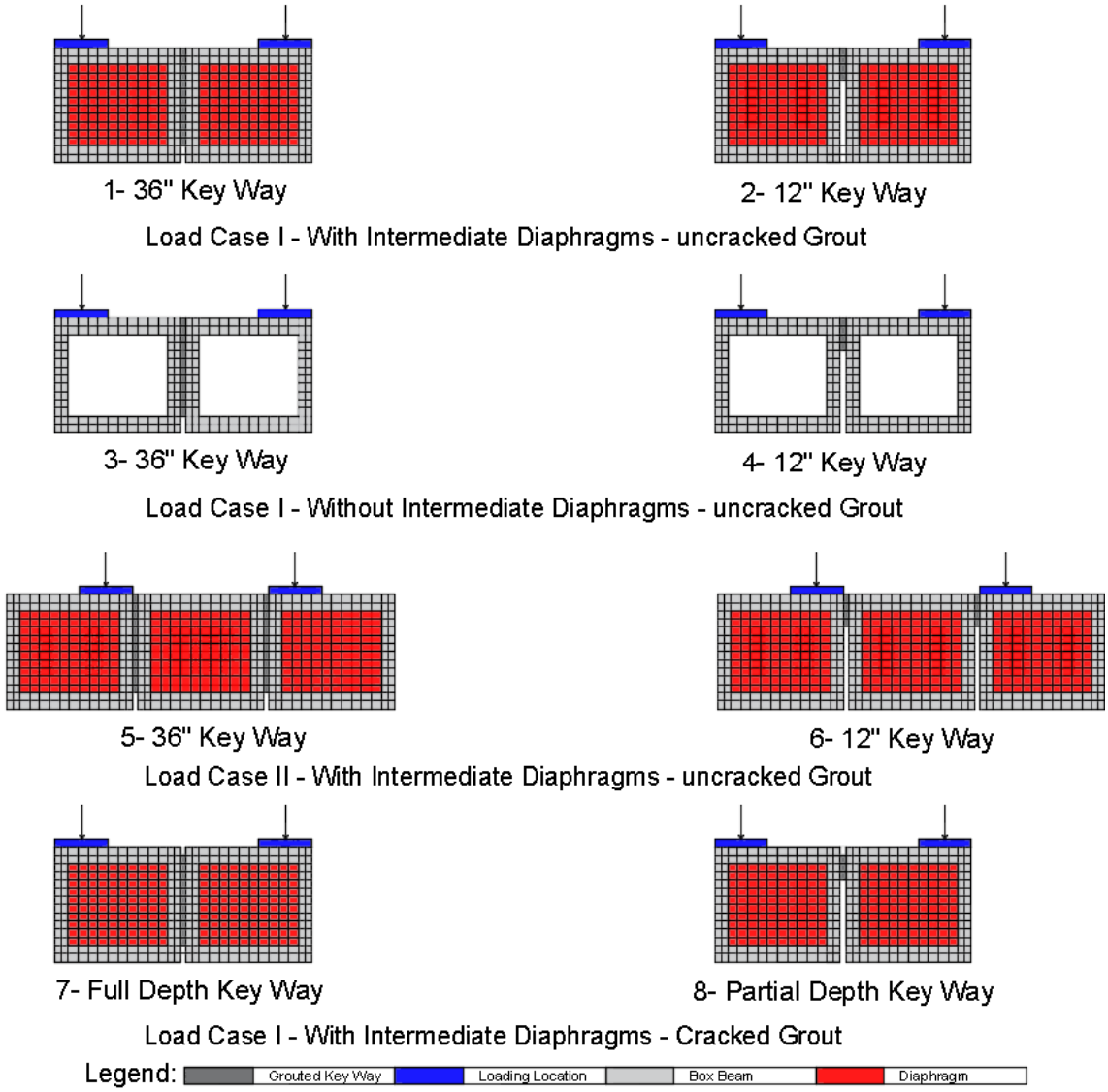

Fig. G.14 Summary of Models Developed with 3D-Solid Elements in SAP2000

G.6 Analysis Results

The results for the analysis to determine the effects of the support conditions are presented in this section. In general normal stress concentration was observed at diaphragm locations and local peak shear stresses at wheel load locations. In addition, stresses were found to be nonlinear along the depth of the grouted joint. The following subsections provide additional details.

G.6.1 Effects of Modeling Support Reactions Considering Bearing Pads and Anchor Dowel Bars

The support reactions including the spring forces representing the reactions provided by elastomeric bearing pads at the beam ends for different load cases and different models are shown in Tables G.1 through Table G.4. The following conclusions were drawn from the results of the analyses.

(i) At any end, the two springs representing the two bearing pads along with one anchor dowel bar resist all the end reaction force transferred from the corresponding beam end. Removing the dowel bar from the analysis models allows the redistribution of the reaction forces into the springs, thereby increasing the axial force resisted by the two springs at each end. However, any redistribution of the end reactions between the springs and the dowel bar did not have any effect on the normal stresses or shear stresses at the longitudinal joint. This is possibly because there seem to be no significant rotational displacements at the beam ends and therefore the bearing pads were attracting nearly equal amounts of vertical compressive reactions. The two pairs of bearing pads at either end of each box beam were seen to be settling by approximately the same amount, similar to what was observed from the analyses with pinned or roller supports simulating the end anchor dowel bars. Therefore, there is no change in the state of stresses at the longitudinal joints.

(ii) The axial spring stiffness representing the bearing pads used in the analyses had no effects on the state of stresses at the longitudinal joint. A larger spring stiffness results in a reduced amount of settlement at the pads, and a smaller spring stiffness increases the amount of settlement at the pads. As long as there is no differential settlement, there are no changes observed in the state of stresses at the joint. A typical comparison of normal stresses at the top support for Load Case I of a 36-inch keyway with intermediate diaphragms is shown in Figure G.15 for two conditions: (i) with vertical displacement prevented at the anchor dowel bar location and (ii) with vertical displacement not prevented at the anchor dowel bar location. The two curves for the two conditions are identical and are overlapping except over a small length of about 3 ft. at the beam ends. This observation is particularly significant because it proved that any inaccuracies in assuming stiffness constants in the analysis to represent the bearing pads have no effect on the normal and shear stresses developed at the longitudinal joints.

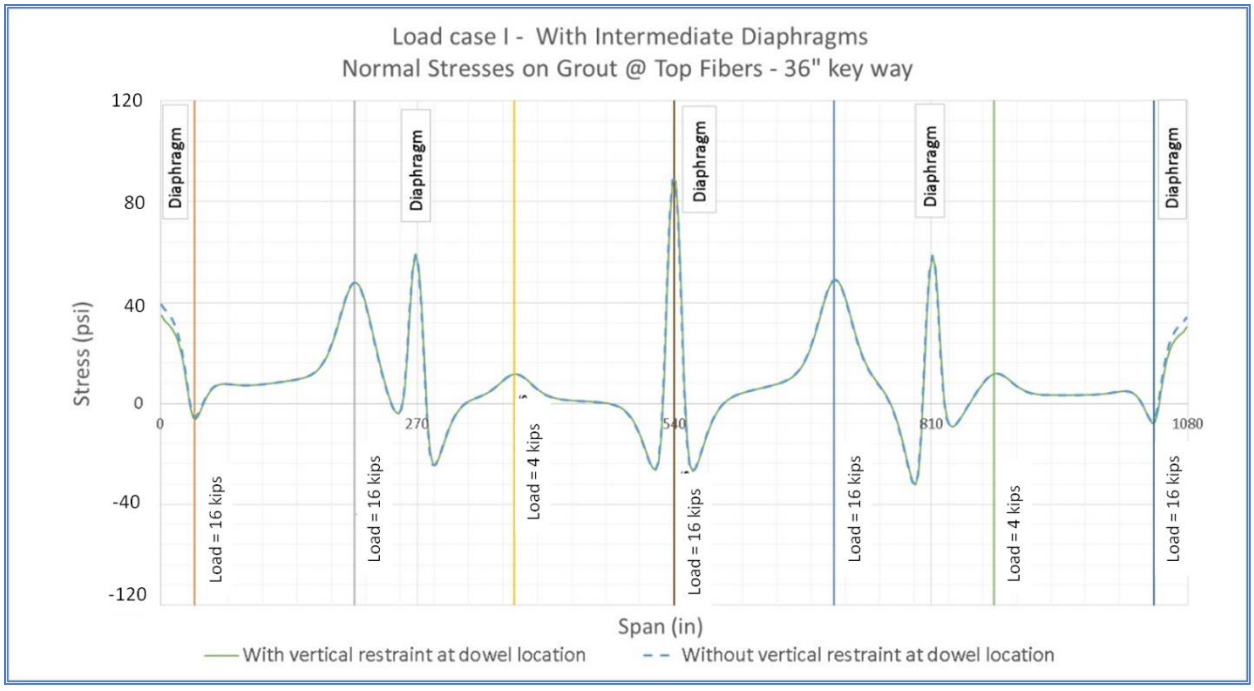

Fig. G.15 Effect of Support Conditions

Support reactions at key points for different models with different load cases are shown in Tables G.1 to G.4.

Table G.1: Support Reaction with Constraint at the Dowel Locations for Load Case I – Without Intermediate Diaphragm

			Load Case I 1- 36" deep with intermediate diaphragm			Load Case I 2- 12" deep with intermediate diaphragm		
		Support	**F1** (kip)	**F2** (kip)	**F3** (kip)	**F1** (kip)	**F2** (kip)	**F3** (kip)
Beam 1	North	S1	0.64*	0.00	4.66	0.65*	-0.016	4.97
	South	S2	0.00	0.00	4.24	0.00	-0.02	4.52
	North	H1	NR*	NR	41.06	NR	NR	40.75
	South	H2	-1.28	NR	37.86	-1.28	NR	37.58
	North	S3	0.64*	0.00	NR	0.65*	-0.02	NR
	South	S4	0.00	0.00	NR	0.00	-0.01	NR
Beam 2	North	S5	0.64*	0.00	NR	0.65*	0.00	NR
	South	S6	0.00	0.00	NR	0.00	0.00	NR
	North	H3	NR	0.00	41.05	NR	0.03	40.75
	South	H4	-1.28	0.00	37.86	-1.32	0.02	37.59
	North	S7	0.64*	0.00	4.66	0.65*	0.00	4.97
	South	S8	0.00	0.00	4.24	0.00	0.00	4.52
∑ F			0.00	0.00	0.00	175.6	0.00	0.00

* Movement in the longitudinal direction = 0.2 in NR = Not restrained.

Table G.2: Support Reaction with Constraint at the Dowel Locations for Load Case II – With Intermediate Diaphragm

			Load Case II 3- 36" depth with intermediate diaphragm			Load Case II 4- 12" deep with intermediate diaphragm		
		Support	**F1** (kip)	**F2** (kip)	**F3** (kip)	**F1** (kip)	**F2** (kip)	**F3** (kip)
Beam 1	North	H1	0.18	1.10	3.86	-0.14	0.70	2.90
	South	H2	NR**	0.85	3.18	NR**	0.55	2.27
	North	S1	0.00	0.00	15.75	0.00	0.00	15.46
	South	S2	-0.44**	0.00	15.18	-0.44**	0.00	14.86
Beam 2	North	S3	0.00	0.00	16.06	0.00	0.01	16.24
	South	S4	-0.44**	0.00	15.46	-0.44**	0.01	15.64
	North	H3	0.70	NR	10.06	1.03	NR	11.14
	South	H4	0.00**	NR	8.33	0.00**	NR	9.40
∑ F			0.00	1.94	87.92	0.00	1.26	87.92

** Movement in the longitudinal direction = 0.14 in NR = Not restrained.

Table G.3: Support Reaction with Constraint at the Dowel Locations for Load Case I – Without Intermediate Diaphragm

			Load Case I 5- 36" depth without intermediate diaphragm			Load Case I 6- 12" deep without intermediate diaphragm		
		Support	**F1** (kip)	**F2** (kip)	**F3** (kip)	**F1** (kip)	**F2** (kip)	**F3** (kip)
Beam 1	North	S1	0.65*	0.00	4.66	0.66*	-0.02	4.99
	South	S2	0.00	0.00	4.24	0.00	-0.02	4.54
	North	H1	NR*	NR	41.06	NR*	NR	40.73
	South	H2	-1.29	NR	37.86	-1.61	NR	37.56
	North	S3	0.65*	0.00	NR	0.66*	-0.02	NR
	South	S4	0.00	0.00	NR	0.00	-0.02	NR
Beam 2	North	S5	0.65*	0.00	NR	0.66*	0.00	NR
	South	S6	0.00	0.00	NR	0.00	0.00	NR
	North	H3	NR*	0.00	41.06	NR*	0.03	40.72
	South	H4	-1.30	0.00	37.86	-1.33	0.02	37.57
	North	S7	0.65*	0.00	4.66	0.66*	0.00	4.99
	South	S8	0.00	0.00	4.24	0.00	0.00	4.99
∑ F			0.00	0.00	0.00	175.60	0.00	0.00

* Movement in the longitudinal direction = 0.2 in NR = Not restrained.

Table G.4: Support Reaction without Vertical Constraint at the Dowel Locations
For Load Case I – With Intermediate Diaphragm

			Load Case I		
			7- Full depth with intermediate diaphragm		
		Support	**F1** (kip)	**F2** (kip)	**F3** (kip)
Beam 1	North	S1	0.64	0.00	22.94
	South	S2	0.00	0.00	21.12
	North	H1	NR*	NR	NR
	South	H2	-1.28	NR	NR
	North	S3	0.64	0.00	22.78
	South	S4	0.00	0.00	20.98
Beam 2	North	S5	0.64	0.00	22.78
	South	S6	0.00	0.00	20.98
	North	H3	NR*	0.00	NR
	South	H4	-1.28	0.00	NR
	North	S7	0.64	0.00	22.94
	South	S8	0.00	0.00	21.12
∑ F			0.00	0.00	0.00

* Movement in the longitudinal direction = 0.2 in NR – Not restrained.

G.6.2 Normal Stresses along the Length of the Box Beams

Tensile and compressive stresses in the keyway joint were extracted from the model by averaging the stresses at the eight nodes of each element and plotted at the centroid of the element.

G.6.2.1 Comparison of Results Obtained from Eight-Node Solid Element Models with Those Obtained from Models using Shell and Beam Elements.

The peak normal stresses at the top edge of the longitudinal joint that were obtained from eight-node solid elements are much lower at the diaphragm location but are slightly higher at other locations (Figure G.16). From here on, only the results obtained from the finite element models with eight-node solid elements are presented.

G.6.2.2 Load Case I

The normal stresses along the length of the longitudinal joints of adjacent box beams at the top of the keyway are plotted in Figure G.17. This figure shows the tensile stresses for Load Case I for models with 12-in, and 36-in deep keyways, both with and without diaphragms.

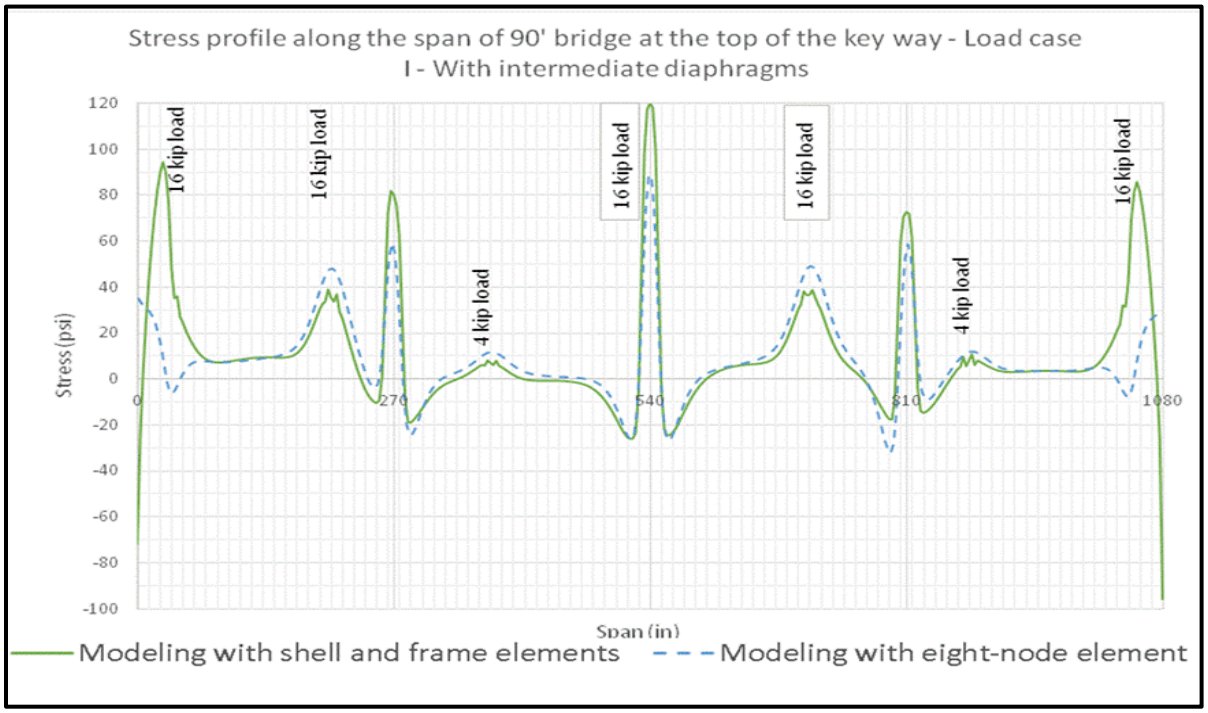

Fig. G.16 Shell and Frame Model vs. Eight-node Model

G.6.2.2.1 Top Stresses

The following observations were made based on the normal stresses within the longitudinal joints at the top surface of the box beams using six models for the two load cases:

G.6.2.2.1.1 Box Beams with Intermediate Diaphragms (Load Case I)

The load configuration in Load Case I, as seen in Figure G.3, is expected to cause tension at the top edge of the grouted longitudinal joint and compression at the bottom edge of the joint. Because of the symmetric nature of the geometry, stiffness, and loading, the shear stresses at the joint are expected to be zero. Therefore, the peak normal stresses within the longitudinal joints are expected to occur when there are no shear stresses at the joint. The following observations were made:

(i) The normal stresses on the joints within the diaphragm width were much larger than the normal stresses obtained at locations away from the diaphragms, suggesting that much of the out-of-plane moment is transferred between the box beams primarily through the diaphragms.

(ii) The peak normal stresses occur at the diaphragm locations. Large normal stresses also occur at the wheel load locations.

(iii) Increase in the depth of the joint from 12 inches to 36 inches decreases the normal stresses at the diaphragm location at the quarter and three quarters spans by a factor of 2.0, and by a factor of 1.85 at the mid-span diaphragm.

(iv) Remote from the diaphragms, there are larger normal stresses at the locations of the wheel loads. These normal stresses are slightly smaller than those at the diaphragm locations, but larger than everywhere else. Decrease in normal stresses at the wheel loads is also observed with an increase in the joint depth, but the decrease occurs to a smaller extent.

(v) The occurrence of large normal stresses at the location of the wheel loads other than at the diaphragms suggests that these peaks can occur at any point along the length of the joint because the moving wheel loads can occur at any point. Therefore, there is an equal chance that the peak normal stresses at the wheel loads will occur all along the joint length because of the moving nature of truck axle loads. However, the normal stresses at the diaphragms are found to be the largest, particularly when the wheel loads are at the locations of the diaphragm.

(vi) Increase in joint depth from 12 inches to 36 inches reduced the normal stresses close to the beams ends by a factor 3 to 4 where the sections are solid (for the 39-inch-length at each end). A similar trend was observed for normal stresses at the bottom of the joint. However, the normal stresses at the bottom are compressive and therefore of less concern when high strength grout is used.

(vii) As expected, the shear stresses at the joint were close to zero.

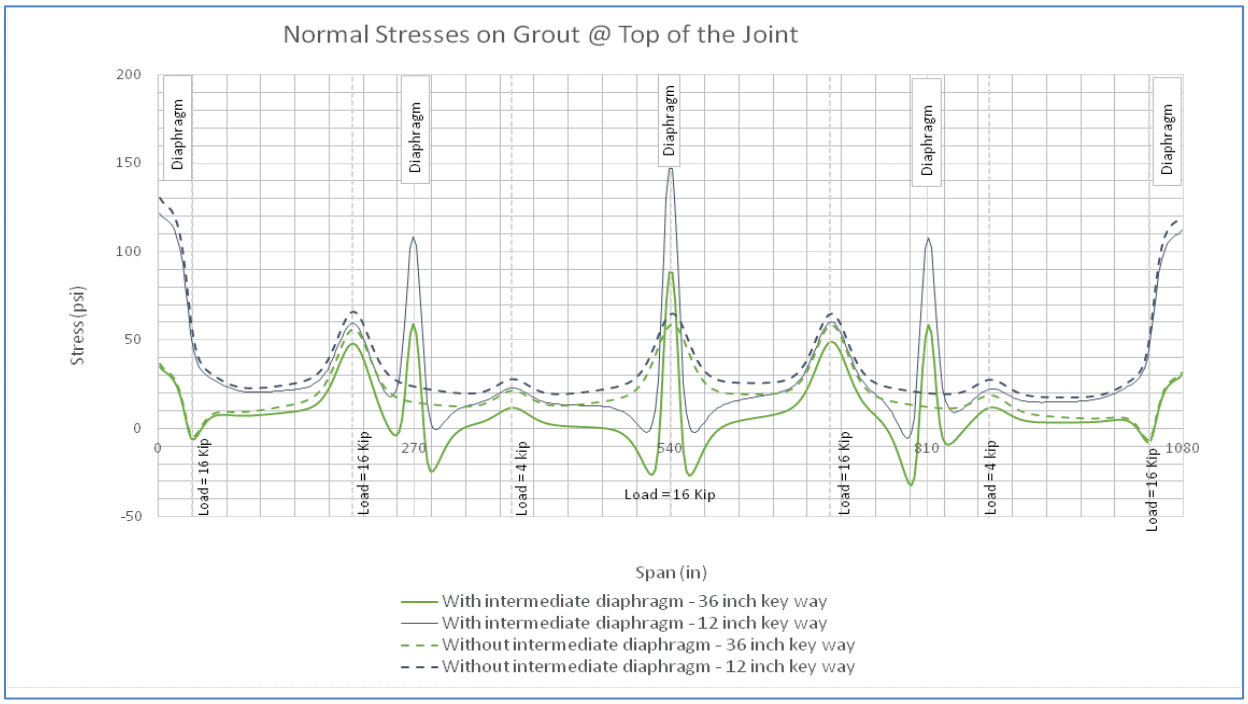

Fig. G.17 Normal Stresses at the Top Surface along the Length of the Longitudinal Joint for Load Case I with Intermediate Diaphragms

G.6.2.2.1.2 Box Beams without Intermediate Diaphragms

For Load Case I without intermediate diaphragms, the normal tensile stresses in the joints at the top surface occur at the location of the wheel loads. The magnitudes of stresses are less than about 75 psi for 12-inch-deep joint and less than 60 psi for the 36-inch-deep joint, suggesting a reduction of stresses up to about 25% when diaphragms are not provided.

(i) The normal stresses in box beams without intermediate diaphragms have peaks only at the locations of the wheel loads. In the absence of the intermediate diaphragms, these peaks follow the wheel loads along the length of the joint. Therefore, these peak normal stresses occur over the entire length of the beams due to the moving nature of the wheel loads.

(ii) Reduction in normal stresses due the increase in joint depth from 12 inches to 36 inches is only about 15% under the different wheel loads applied along the length of the joint.

(iii) While the peak normal tensile stresses occur at the locations of wheel loads when there are no intermediate diaphragms, the magnitudes of the peaks are smaller than those obtained for the corresponding load conditions for both 36-inch and 12-inch joint depths for box beams with intermediate diaphragms. From Figures G.18 and G.19, the difference between the normal stresses at the bottom of the joint for beams without diaphragms for 36-inch-deep keyway and those for 12-inch-deep keyway is not as large as it is for box beams with diaphragms. However, compared to the normal tensile stresses at the diaphragm locations, the corresponding stresses at the wheel loads are smaller by a factor of at least 2.0 for a 36-inch-deep keyway joint.

(iv) Removing the intermediate diaphragms from the current practice and using a full depth keyway may result in more uniform peak normal stresses along the entire length of the longitudinal joint and will eliminate the stress concentration at the intermediate diaphragm location. For the 12-inch keyway, removing the intermediate diaphragms reduces the stresses significantly along the span except for the end diaphragm locations. End diaphragms cannot be removed in prestressed box beams because they are needed to transfer the prestressing forces from the strands to the concrete section and to satisfy the diagonal shear strength requirements.

G.6.2.2.2 Bottom Stresses

The normal stresses at the bottom of the joint are generally low for both depths (12 inches and 36 inches) when diaphragms are not provided. The peak stresses still occur at the location of the wheel loads as shown in Figures G.18 and G.19.

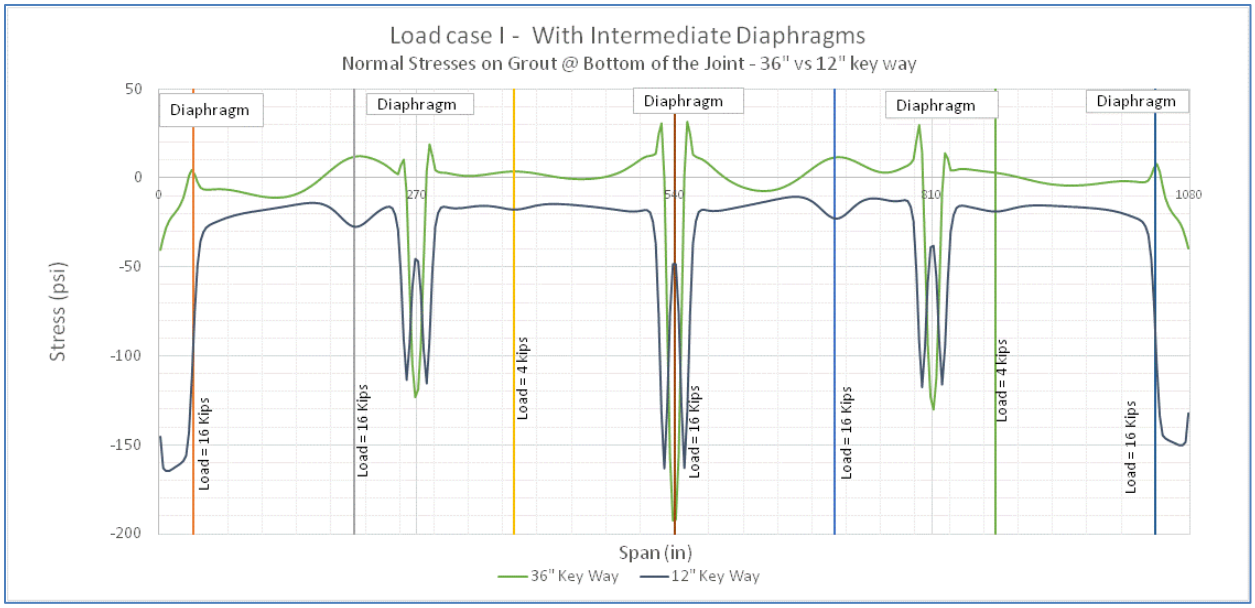

Fig. G.18 Normal Stresses at the Bottom Surface along the Length of the Longitudinal Joint for Load Case I with Intermediate Diaphragms - 36" vs. 12" Keyway

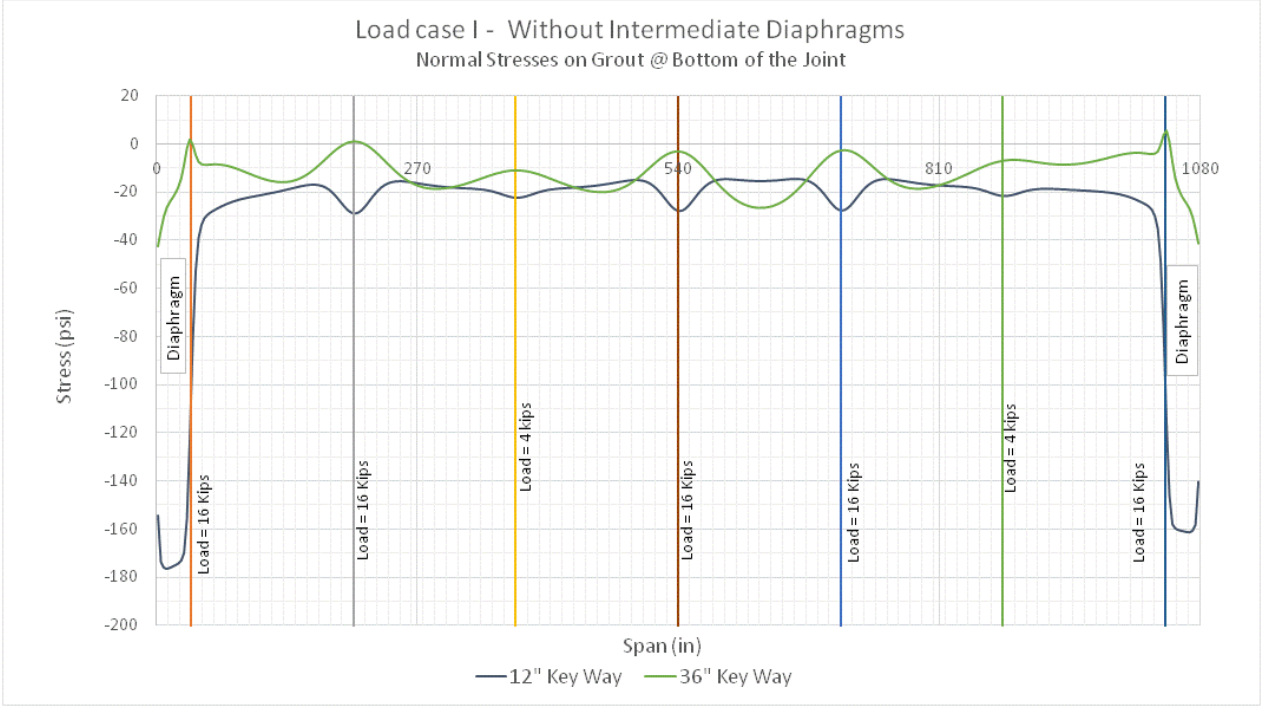

Fig. G.19 Normal Stresses at the Bottom Surface along the Length of the Longitudinal Joint for Load Case I without Intermediate Diaphragms - 36" vs. 12" Keyway

G.6.2.3 Load Case II

The load configuration in Load Case II, as seen in Figure G.4 is expected to cause compression at the top edge of the grouted longitudinal joint and tension at the bottom of the joint. In this load case, the joint is not at the axis of symmetry. Therefore, the joint will be subjected to both normal stresses and shear stresses. The normal stresses are expected to be smaller in this load case than those in Load Case I. The shear stresses at the joint for Load Case I were zero.

(i) As shown in Figure G.20, the normal tensile stresses on the joints at the bottom edge within the diaphragm width were much larger than the normal stresses obtained at locations remote from the diaphragms suggesting that much of the out-of-plane moment is transferred between the box beams primarily through the diaphragms.

(ii) For joints with 12 inch depth, shown in Figure G.21, there is a reversal of stresses at the diaphragms. While it is difficult to explain this reversal at the locations of the diaphragms, the stresses are reduced throughout the length of the beam when 36 inch keyway is used. Therefore 12-inch deep joint is less efficient than a 36-inch deep joint for this load case.

(iii) Similar trends can be observed for normal compressive stresses at the top of the joint as seen in Figure G.20. However, the normal stresses at the top are mostly compressive and therefore of less concern.

(iv) Providing a deeper joint reduces the normal (tensile) stresses by a factor of about 3.0 for this case. Figure G.20 shows that for Load Case II with intermediate diaphragms, the normal stresses at the top surface are mostly not influenced by the depth of the joint. The peak stresses still occur at the location of the wheel loads or at the diaphragm locations, but the stresses at the wheel load locations are larger.

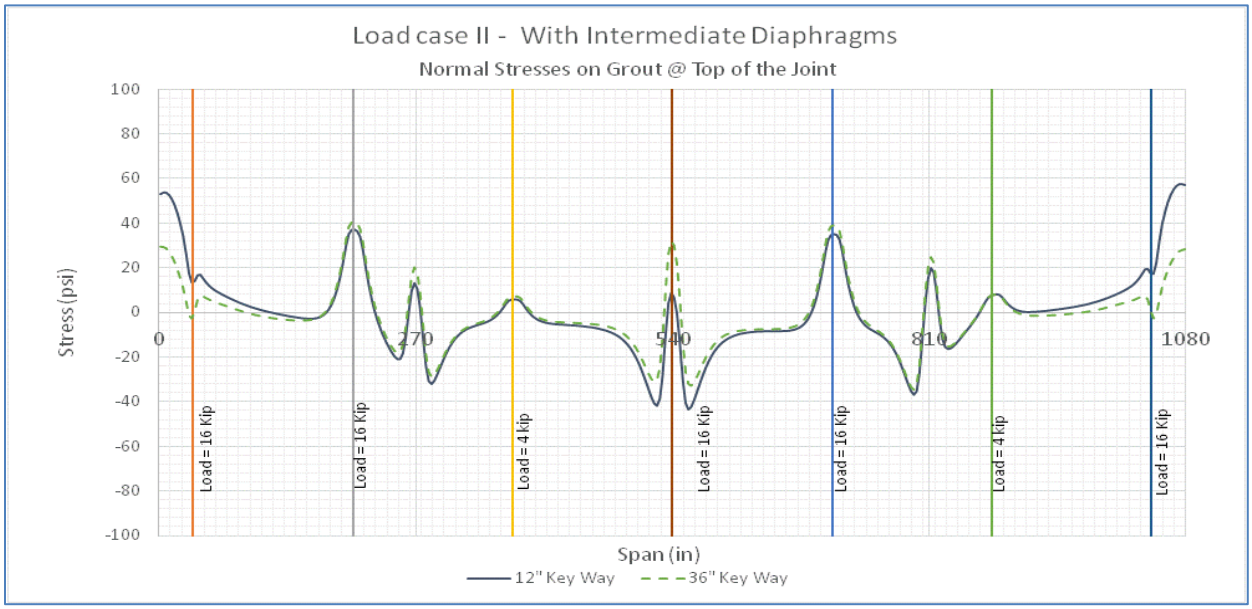

Fig. G.20 Normal Stresses at the Top Surface along the Length of the Longitudinal Joint for Load Case II with Intermediate Diaphragms

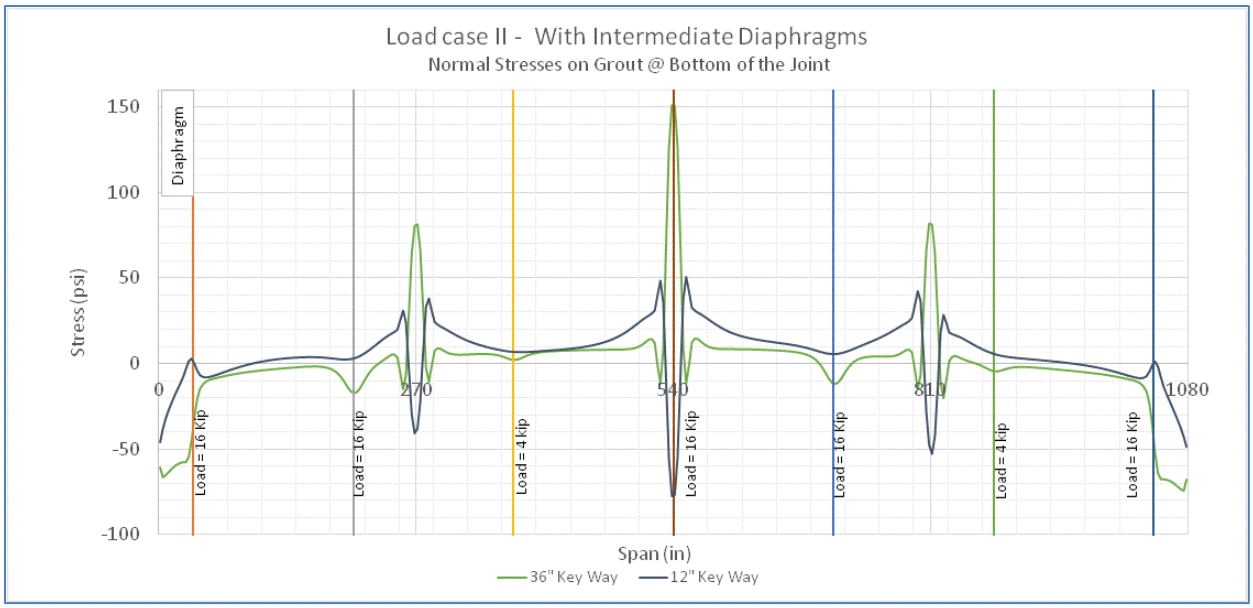

Fig. G.21 Normal Stresses at the Bottom Surface along the Length of the Longitudinal Joint for Load Case II with Intermediate Diaphragms

G.6.3 Shear Force Transferred Through the Joints

The shear stresses developed at the joint for box beams with intermediate diaphragms are shown in Figures G.22 and G.23 for Load Case II with a 36-inch-deep joint and 12-inch-deep joint, respectively. The figures show shear stress along the length of the joint, which is calculated by integrating the shear stresses over the depth at each location (36 inches or 12 inches). For beams with a 36-inch-deep joint, most of the shear is transferred at the wheel load locations only, regardless of the location of the diaphragm. With a smaller joint depth of 12 inches (Figure G.23), the maximum shear was found to occur when the wheel loads were at the diaphragm locations. The peak stresses for a 36-inch-deep joint (11 psi) are about two thirds smaller than those for 12-inch-deep joint (30 psi).

Fig. G.22 shows the shear stress at the joint over the length of the box beams with intermediate diaphragms. The shear force is mostly transferred between adjacent box beams at the wheel load locations only. The peak shear stress at the diaphragm location and remote from the diaphragms is about 11 psi in the vicinity of the 16-kip wheel load and a depth of 36 inches. This suggests that the shear force at the wheel loads will govern the required strength throughout the length of the box beams because the wheel loads can occur anywhere along the length of the beams.

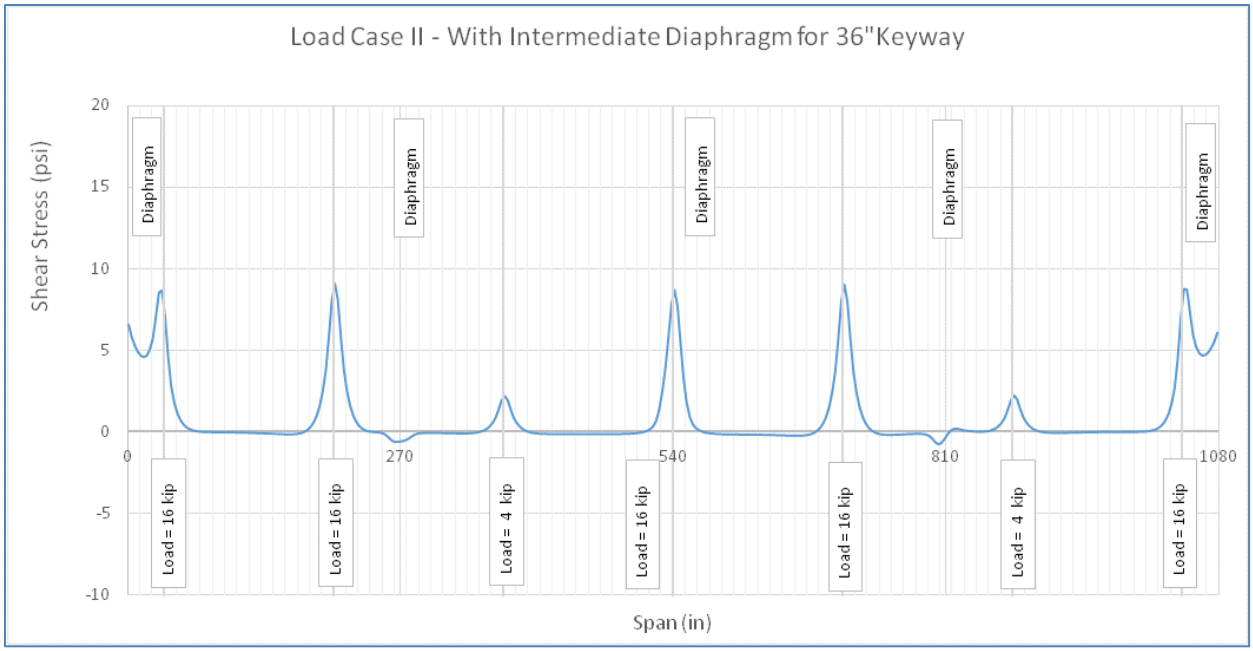

Fig. G.22 Shear Stress – 36" Keyway

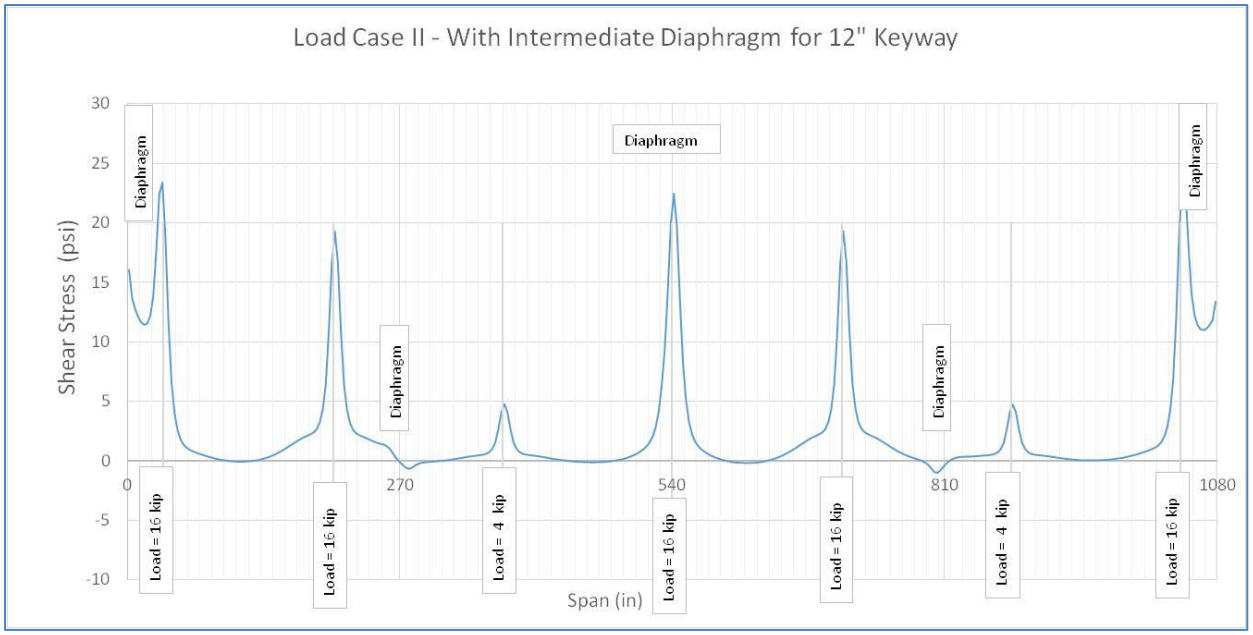

Fig. G.23 Shear Stress – 12" Keyway

G.6.4 Effects of Tie Rods

The finite element models presented in this report did not include beam elements corresponding to the tie rods. However, the relative transverse displacements at the far ends of the adjacent beams at the level of the tie rods (14 inches from the top) provide an

indication of how much load would be attracted by the tie rods and their effectiveness, if they were included in the models. From Figure G.24, it is clear that in all cases with 12-inch keyways, and one case with 36-inch keyway (Load Case II), the relative normal movements are compressive. Therefore, the tie rods will not participate in preventing the box beams from spreading outward because the beams are not even spreading (i.e. no separation). For the remaining two cases with 36-inch-deep keyways, the maximum tensile elongation at the level of the tie rod is 0.0024 inch (2 × 0.0012 inch) over a length of 96 inches. Considering E_s = 29,000 ksi, which is the modulus of steel, and area of tie rod of 0.79 inch^2 for a 1-inch-diameter tie rod, the tensile force caused by the elongation over 96-inch length of the tie rods is 0.725 kip. This tie force is mostly insignificant. In this calculation of increased tie force due to the spreading of the beams, it is assumed that the tie rods are tensioned first, and the grout is placed after the tensioning of the tie rods. Therefore, there is no pre-compression developed in the hardened grout due to the tie rod tension.

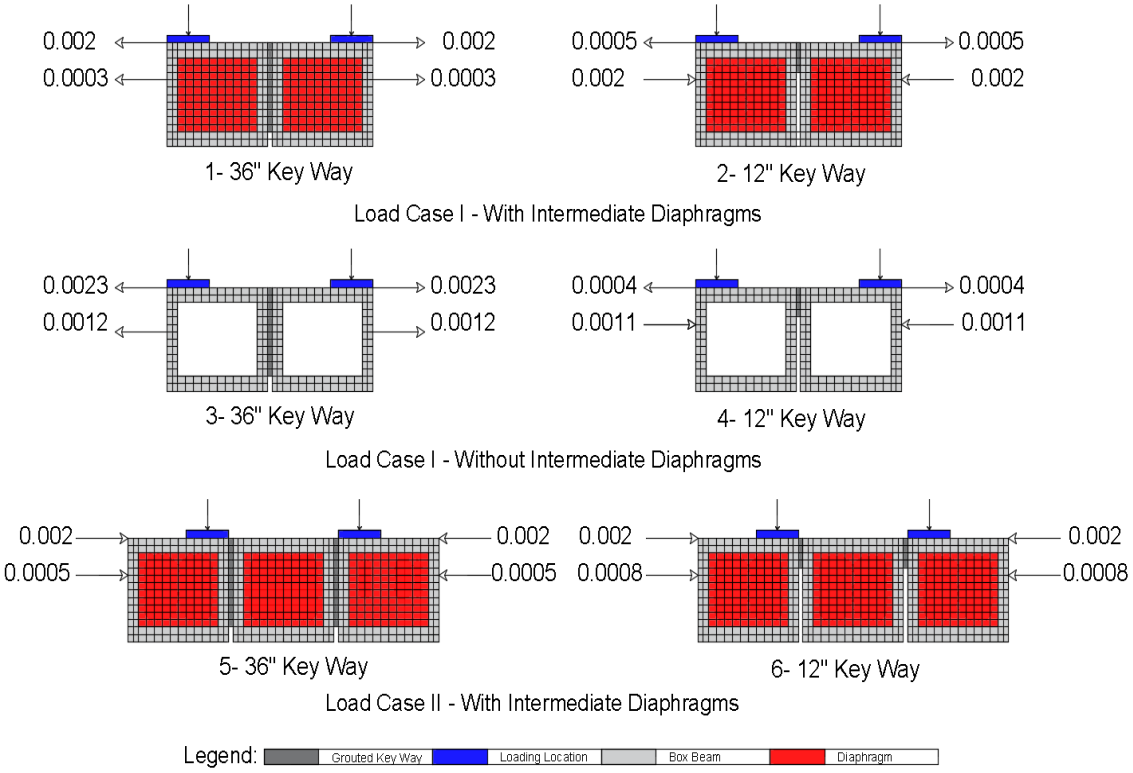

Fig. G.24 Transverse Movement at Mid-Span of the Box Beams

G.6.5 Effects of Cracking at the Top Edge of Keyways

The effects of cracking at the top surface of the joints were determined using an approximate approach. Solid elements were removed from the top three inches of the finite element mesh (i.e., from 39 inches to 42 inches from the bottom) only at the locations of the maximum tensile stresses (at the diaphragms and the wheel loads). When the elements are removed, the physical condition is similar to when a crack occurs at that point.

Figure G.25 shows the resulting normal tensile stresses at the top surface before and after the removal of the elements at the highly stressed locations (i.e., uncracked and cracked conditions). Figure 7.26 shows that the normal tensile stresses are redistributed to the elements surrounding those elements that have been removed from the mesh, particularly to those elements located three inches below the top surface. The figure shows that substantial increase in tensile stresses will occur three inches below the top surface, and the cracks will propagate progressively deeper and deeper as the cracks extend downward.

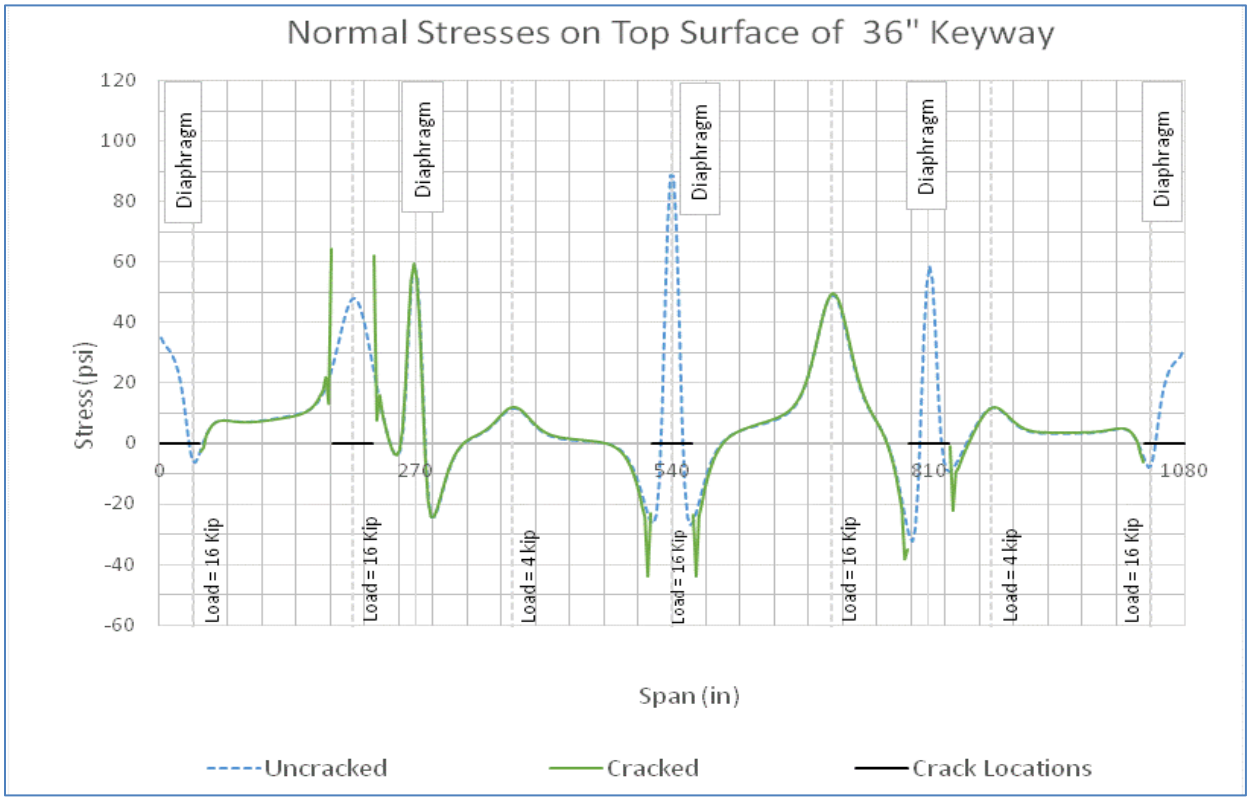

Fig. G.25 Crack Effect on Normal Stresses at Top Surface for 36" Keyway

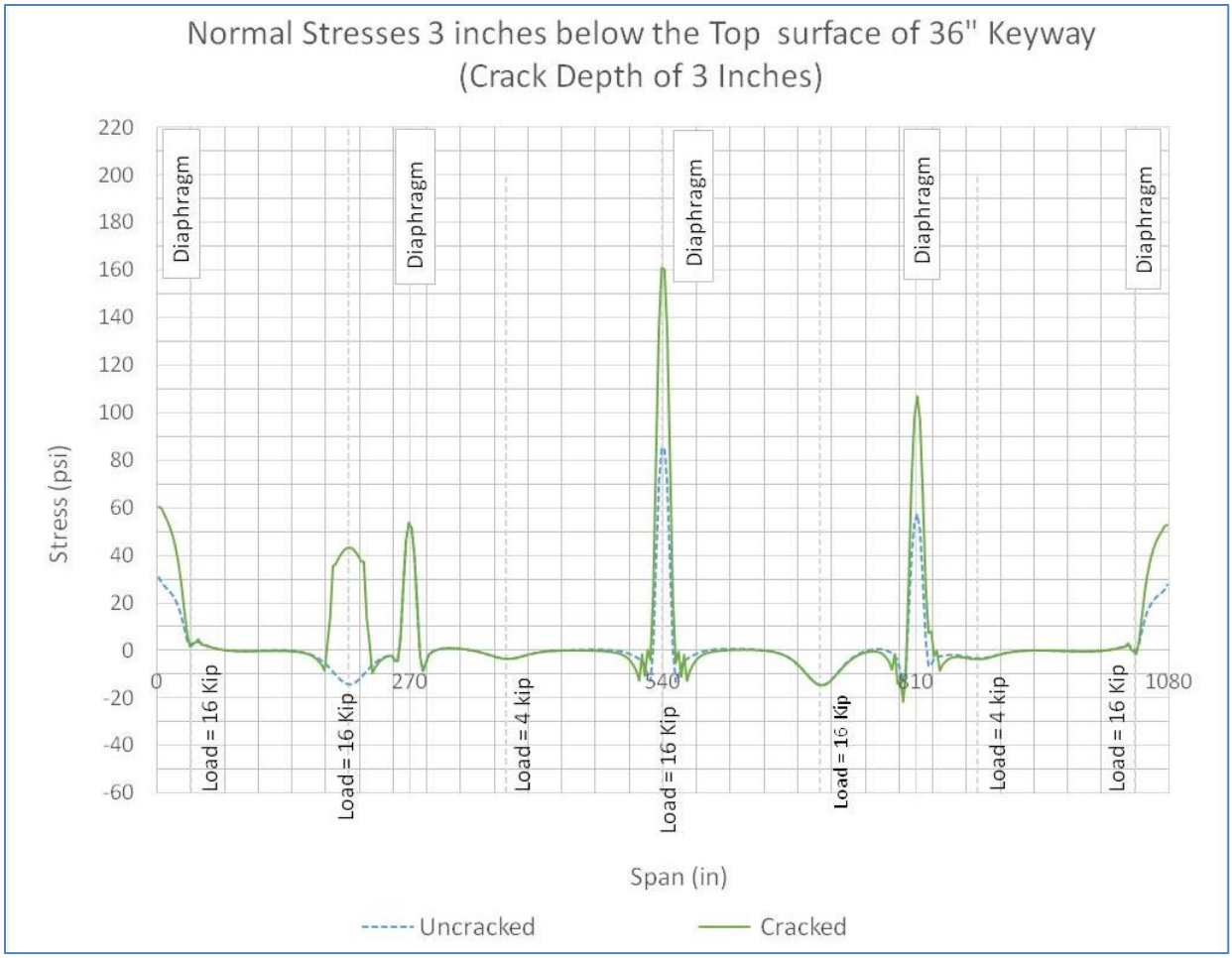

Fig. G.26 Crack Effect on Normal Stresses 3 inches Below Top Surface 36" Keyway

Similar change in tensile stresses will occur in the box beams with 12-inch-deep joints as shown in Figures G.27 and G.28. However, the increases in tensile stresses in the elements 3 inches below the induced cracking are much more severe than what was observed for 36-inch-deep joints.

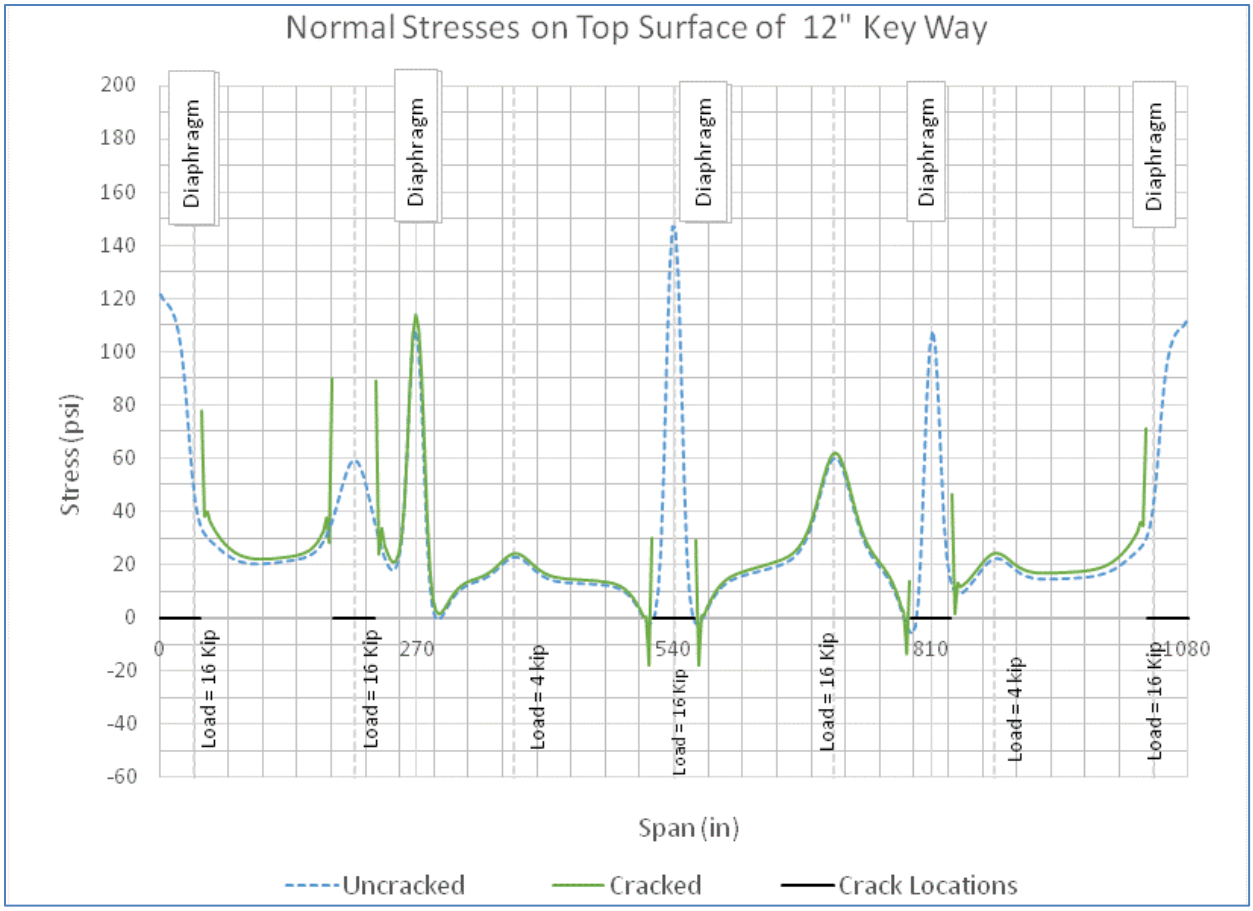

Fig. G.27 Crack Effect on Normal Stresses at top Surface for 12" Keyway

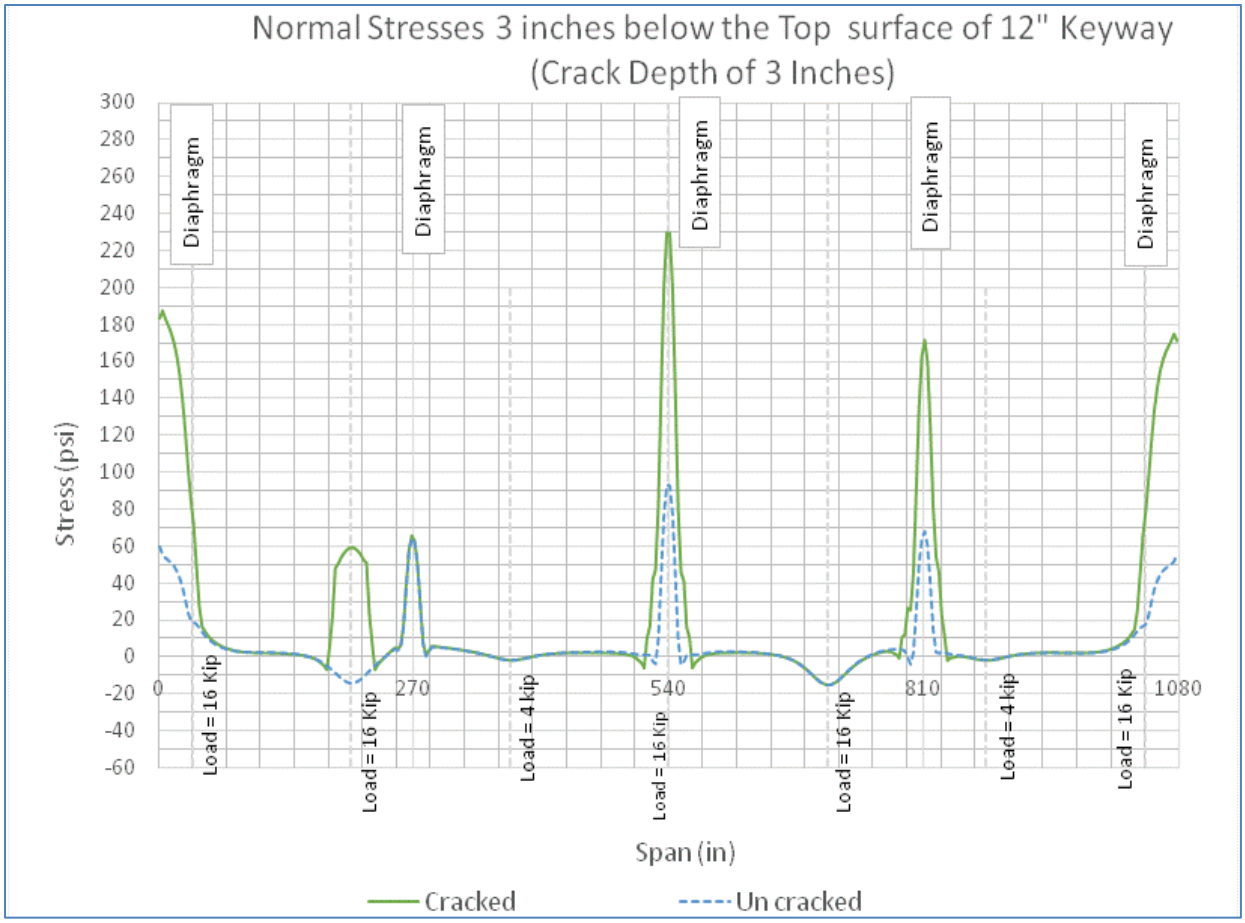

Fig. G.28 Crack Effect on Normal Stresses 3 inches below Top Surface for 12" Keyway

G.6.4 Normal Stress and Shear Stress Contours

Many of the relevant normal stress and shear stress contours for six models showing stress distribution were developed. These contours provided the required information to support some of the conclusions drawn in this report.

G.7 Summary and Conclusions

The following conclusions may be drawn from the results of the analyses presented in this chapter:

1. Any redistribution of the end reactions between the springs and the dowel bar did not have any effects on the normal stresses or shear stresses on the longitudinal joint as long as all bearing pads have the same stiffness properties. There is no change in the state of stresses in terms of normal stresses and shear stresses at the longitudinal joints due to the inclusion or exclusion of the end anchor dowel bars in modeling the end supports.
2. The axial spring stiffness representing the bearing pads used in the analyses has no effect on the state of stresses at the longitudinal joint. As long as there was no differential settlement, no changes were observed in the state of stresses at the joint. Any inaccuracies in assuming the stiffness constants in finite element analyses to represent the bearing pads have no effect on the normal and shear stresses at the longitudinal joints.
3. For box beams with intermediate diaphragms, most of the out-of-plane moment at the joint is mainly transferred to the adjacent box beam at the locations of the diaphragms. The peak normal stresses occur at the diaphragm locations. However, most of the shear forces are transferred at the locations of the wheel loads.
4. Box beams with intermediate diaphragms and deeper keyways (depth of 36 inches) have smaller normal tensile stresses than those with 12-inch-deep keyways by a factor of about 2.0 in normal tensile stresses and a factor of 3 in shear stresses, suggesting that the joints with deeper keyways will have a smaller tendency to crack at the joint surface.
5. Box beams without intermediate diaphragms and deeper keyways (depth of 36 inches) also have smaller normal tensile stresses than those with 12-inch-deep keyways, but the reduction of normal stresses is not as much as it is for box beams with diaphragms.
6. The effectiveness of tie rod clamping force is negligible when the tie rods are tensioned prior to grouting. Therefore, there is no significant contribution of tie rods in controlling the spreading of adjacent box beams or in the tendency to crack at the joint.
7. Any cracking in the top 3 inches of a joint with a 12-inch-deep keyway has a significant effect on the normal stresses in the vicinity of the cracks, suggesting that the crack propagation will be more severe in such joints compared to that of joints with deeper keyway joints.
8. Overall, the cracking potential is significantly reduced by increasing the depth of the keyway joint from 12 inches to 36 inches.

STRESS CONTOURS

Load Case I – With Intermediate Diaphragm
36-in Key Way
Normal Stresses (S22) at Key Way Joint

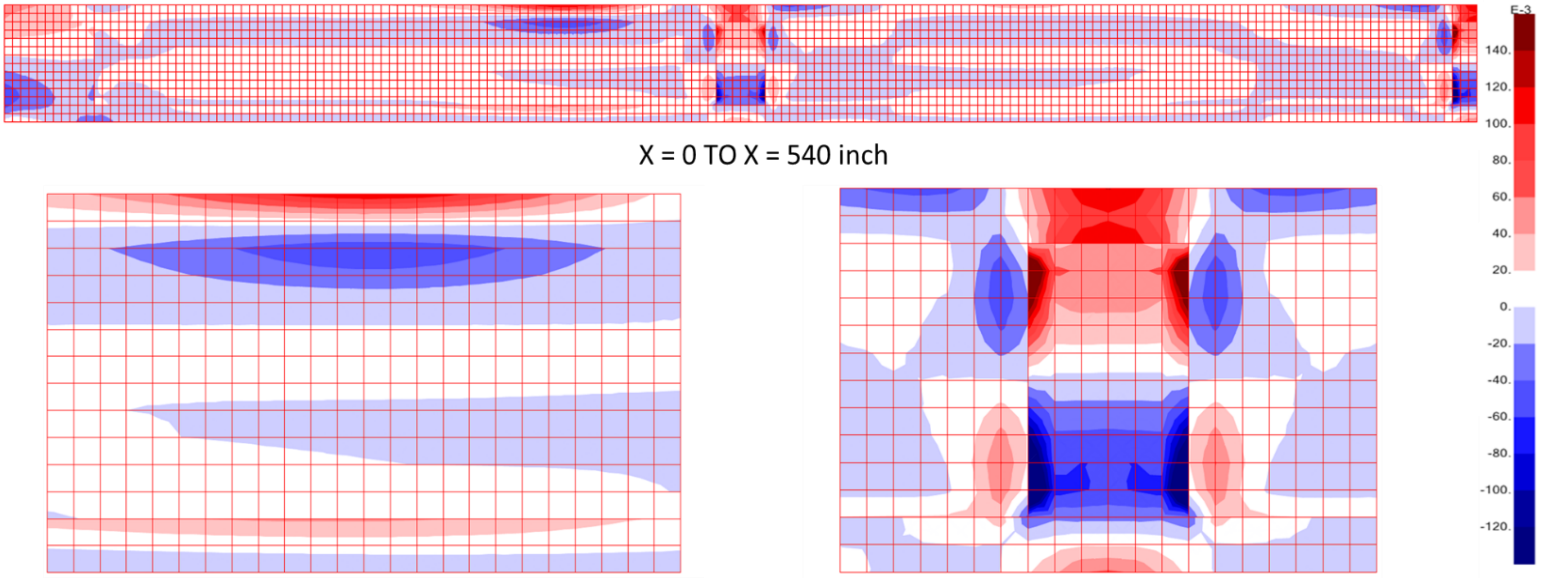

X = 0 TO X = 540 inch

X=204 in. Under 20 kip Wheel Load
Far from the Diaphragm

X=540 in. Under 20 kip Wheel Load
At Diaphragm Location

Load Case II - With Intermediate Diaphragm
36-in Key Way
Normal Stresses (S22) at Key Way Joint

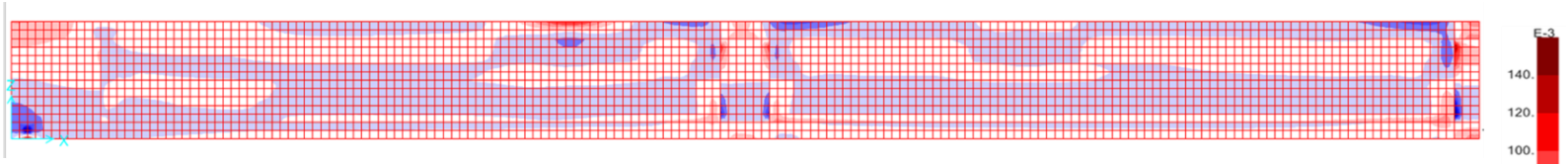

X = 0 TO X = 540 inch

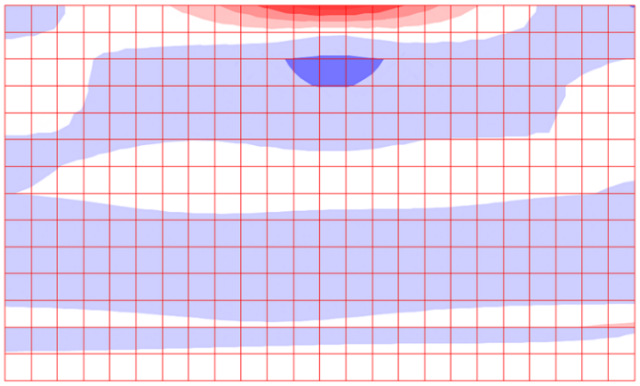

X=204 in. Under 20 kip Wheel Load
Far from the Diaphragm

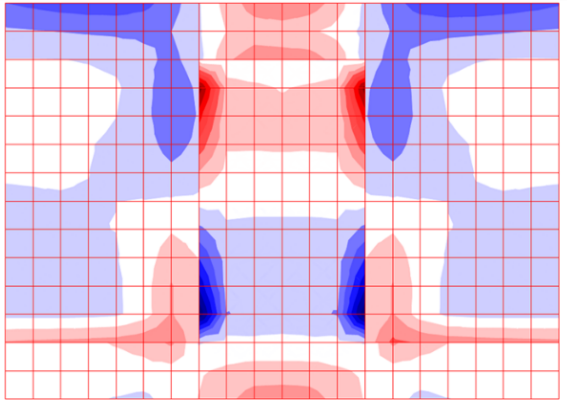

X=540 in. Under 20 kip Wheel Load
At Diaphragm Location

Load Case II - With Intermediate Diaphragm
12-in Key Way
Normal Stresses (S22) at Key Way Joint

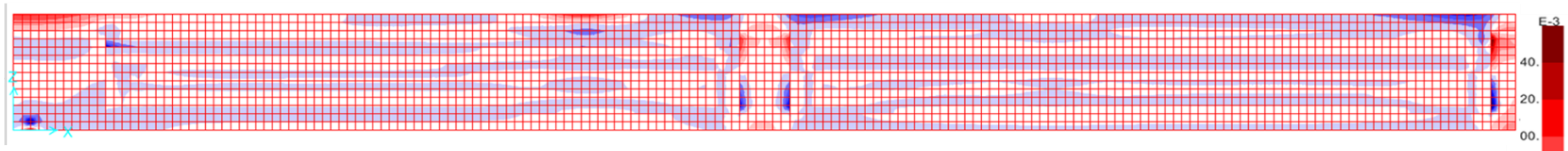

X = 0 TO X = 540 inch

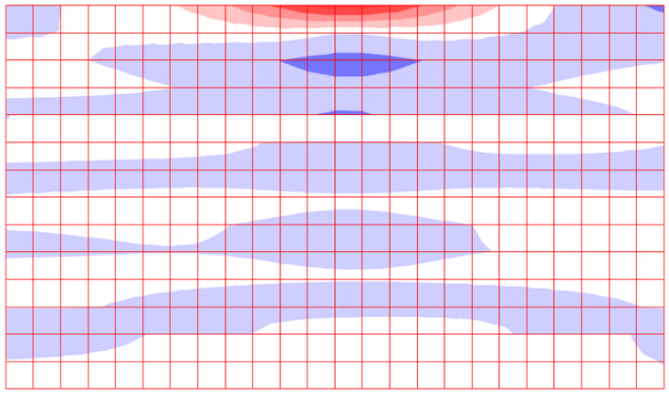

X=204-in. Under 20 kip Wheel Load
Far from the Diaphragm

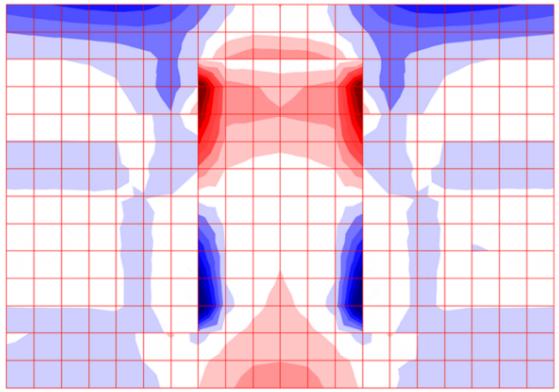

X=540-in. Under 20 kip Wheel Load
At Diaphragm Location

Load Case I - With Intermediate Diaphragm
12-in Key Way
Normal Stresses (S22) at Key Way Joint

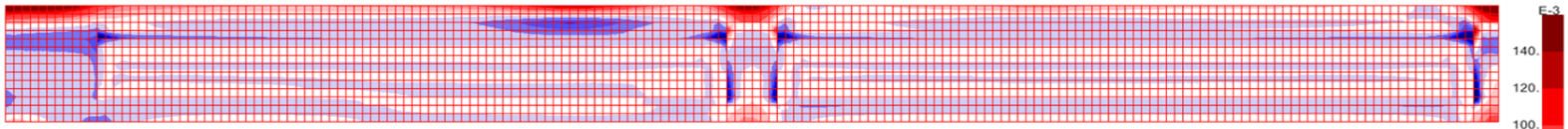

X = 0.00 TO X = 45-ft

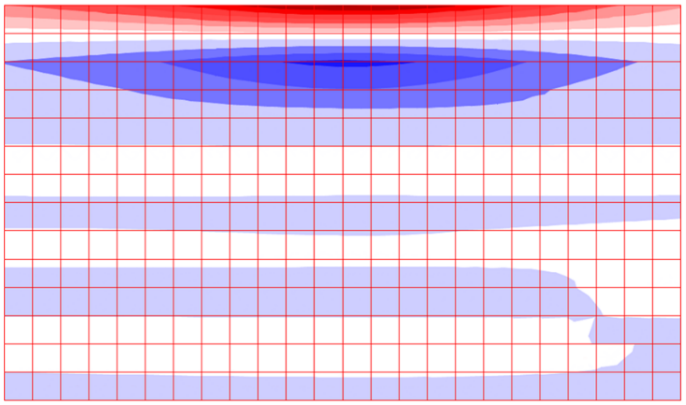

X=204-in. Under 20 kip Wheel Load
Far from the Diaphragm

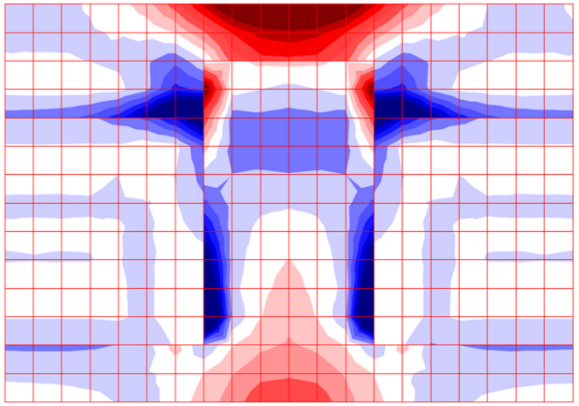

X=540-in. Under 20 kip Wheel Load
At Diaphragm Location

Load Case I - Without Intermediate Diaphragm
36-in Key Way
Normal Stresses (S22) at Key Way Joint

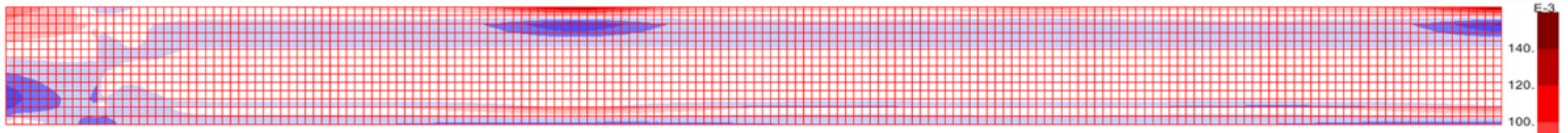

X = 0 TO X = 540 inch

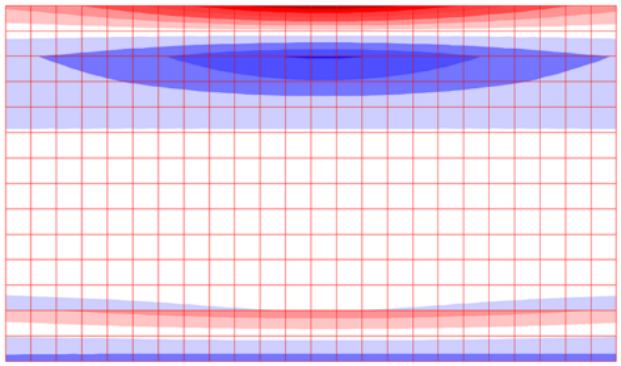

X=204-in. Under 20 kip Wheel Load
Far from the Diaphragm

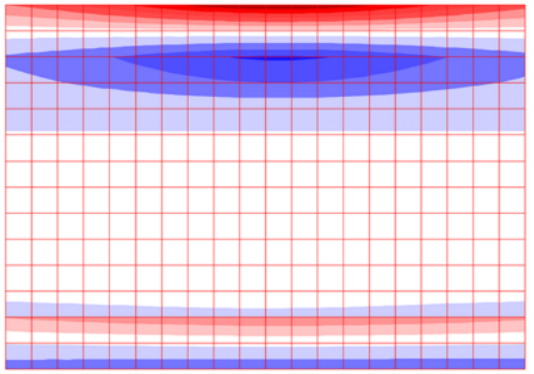

X=540-in. Under 20 kip Wheel Load
At Diaphragm Location

Load Case I - Without Intermediate Diaphragm
12-in Key Way
Normal Stresses (S22) at Key Way Joint

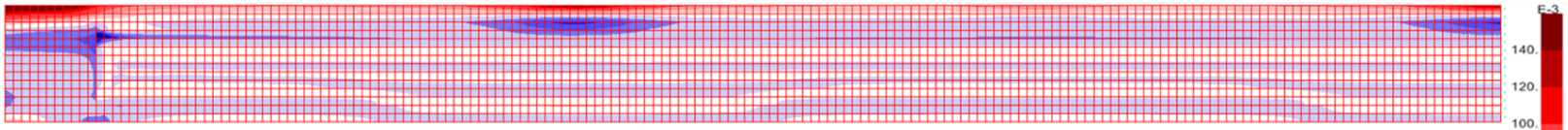

X = 0 TO X = 540 inch

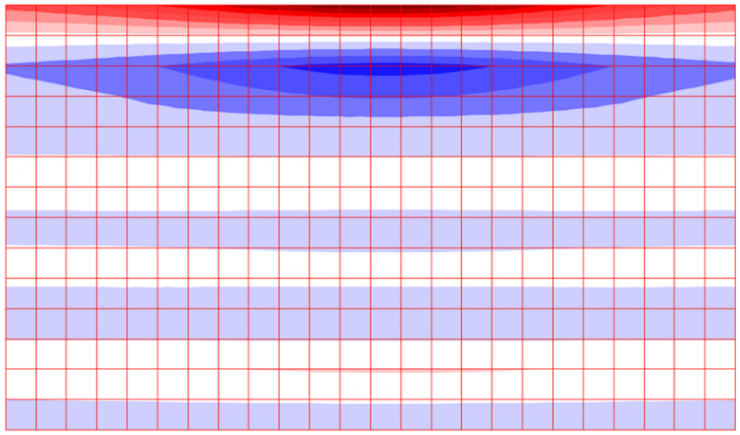

X=204-in. Under 20 kip Wheel Load
Far from the Diaphragm

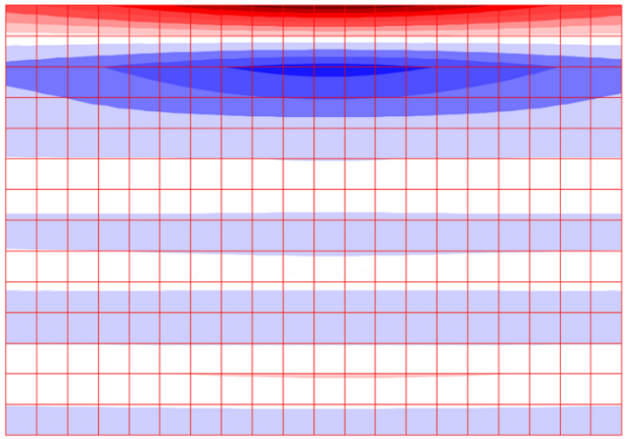

X=540-in. Under 20 kip Wheel Load
At Diaphragm Location

Load Case I – With Intermediate Diaphragm
36-in Key Way
Shear Stresses (S23) at Key Way Joint

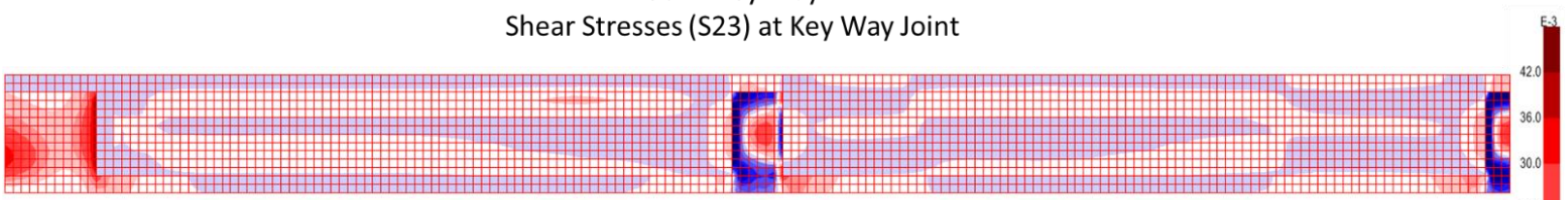

X = 0 TO X = 540 inch

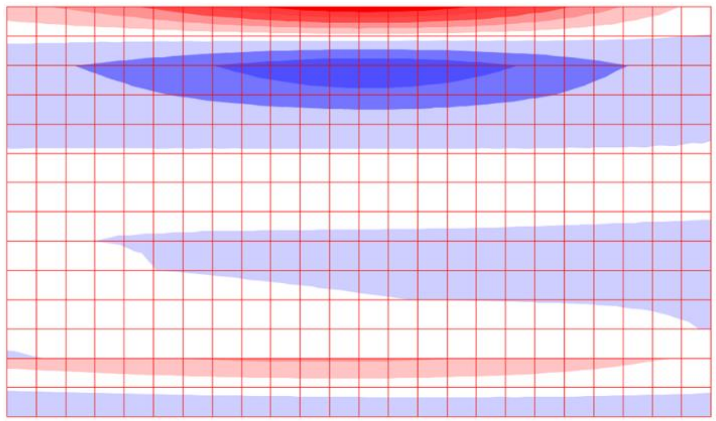

X=204 in. Under 20 kip Wheel Load
Remote from the Diaphragm

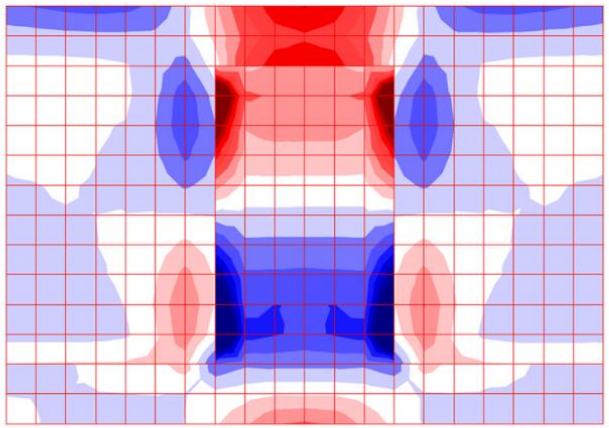

X=540 in. Under 20 kip Wheel Load
At Diaphragm Location

Load Case I – With Intermediate Diaphragm
36-in Key Way
Shear Stresses (S23) – Cross Section

X=204in.

X=540in.

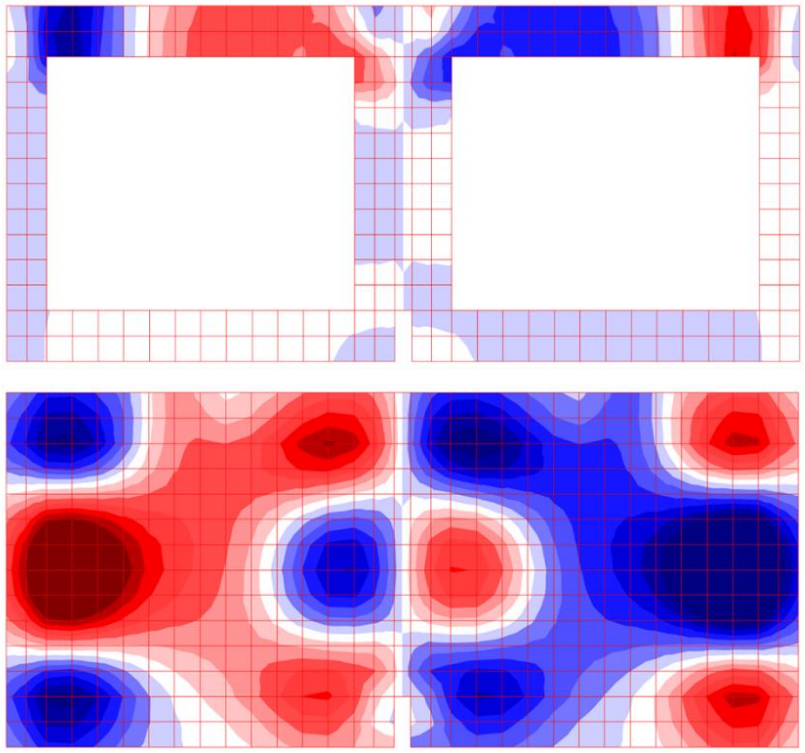

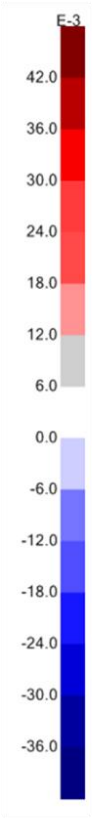

Load Case I - With Intermediate Diaphragm
12-in Key Way
Shear Stresses (S23) at Key Way Joint

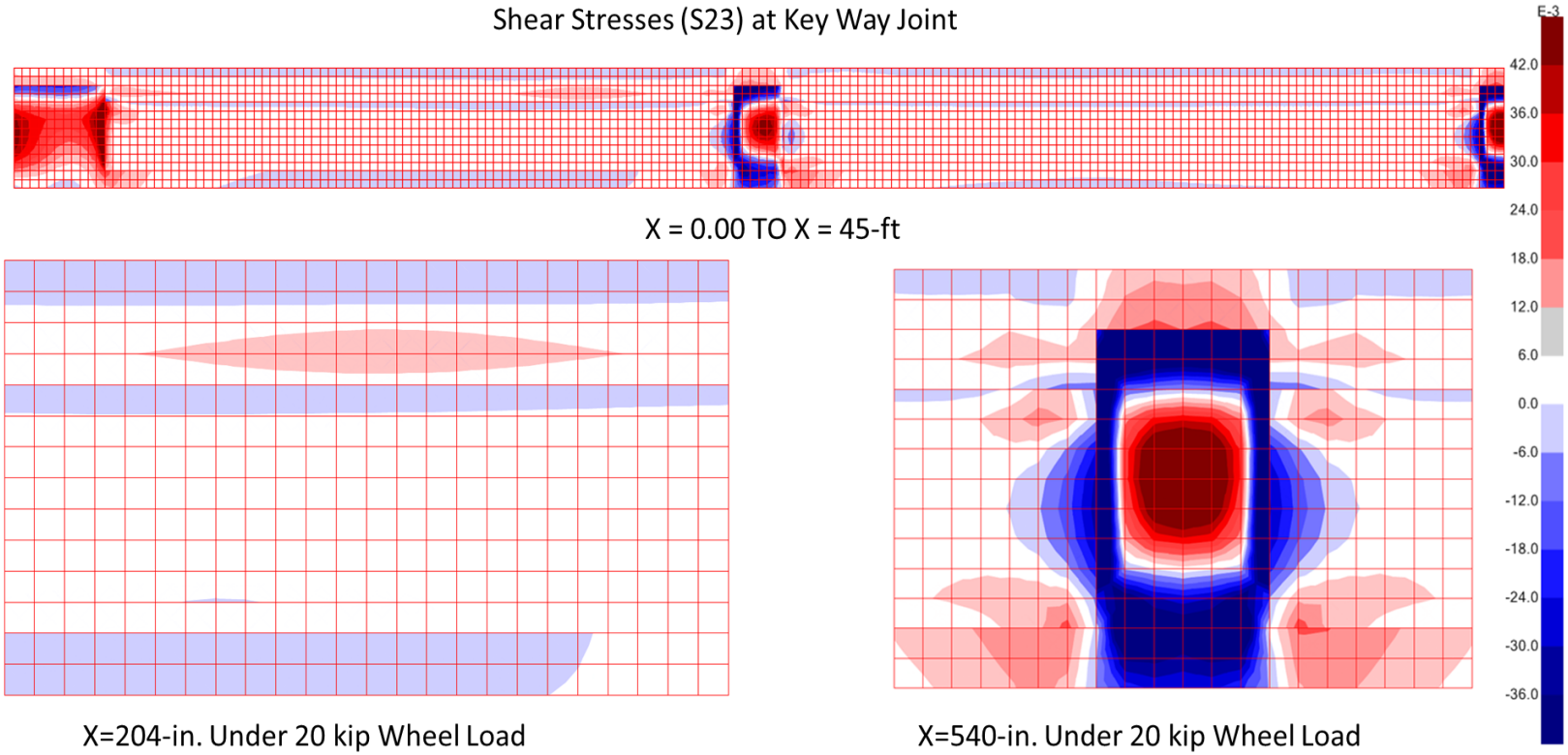

X = 0.00 TO X = 45-ft

X=204-in. Under 20 kip Wheel Load
Remote from the Diaphragm

X=540-in. Under 20 kip Wheel Load
At Diaphragm Location

Load Case I – With Intermediate Diaphragm
12-in Key Way
Shear Stresses (S23) – Cross Section

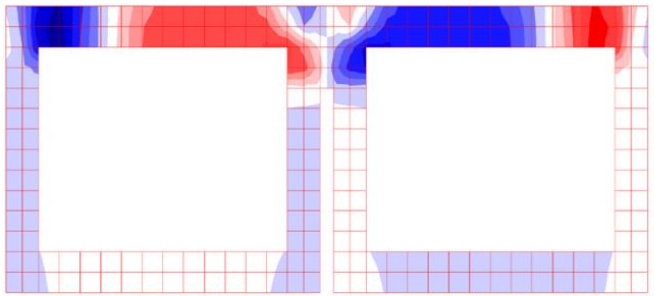

X=204in.

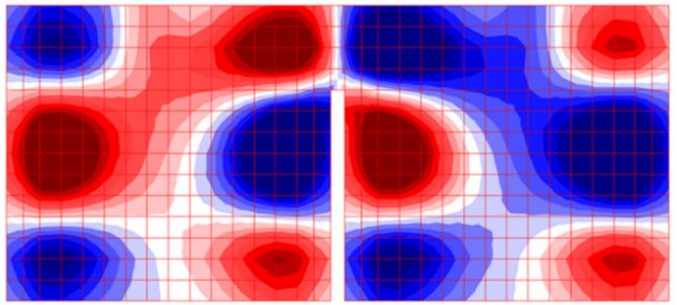

X=504in.

Load Case I - Without Intermediate Diaphragm
12-in Key Way
Shear Stresses (S23) at Key Way Joint

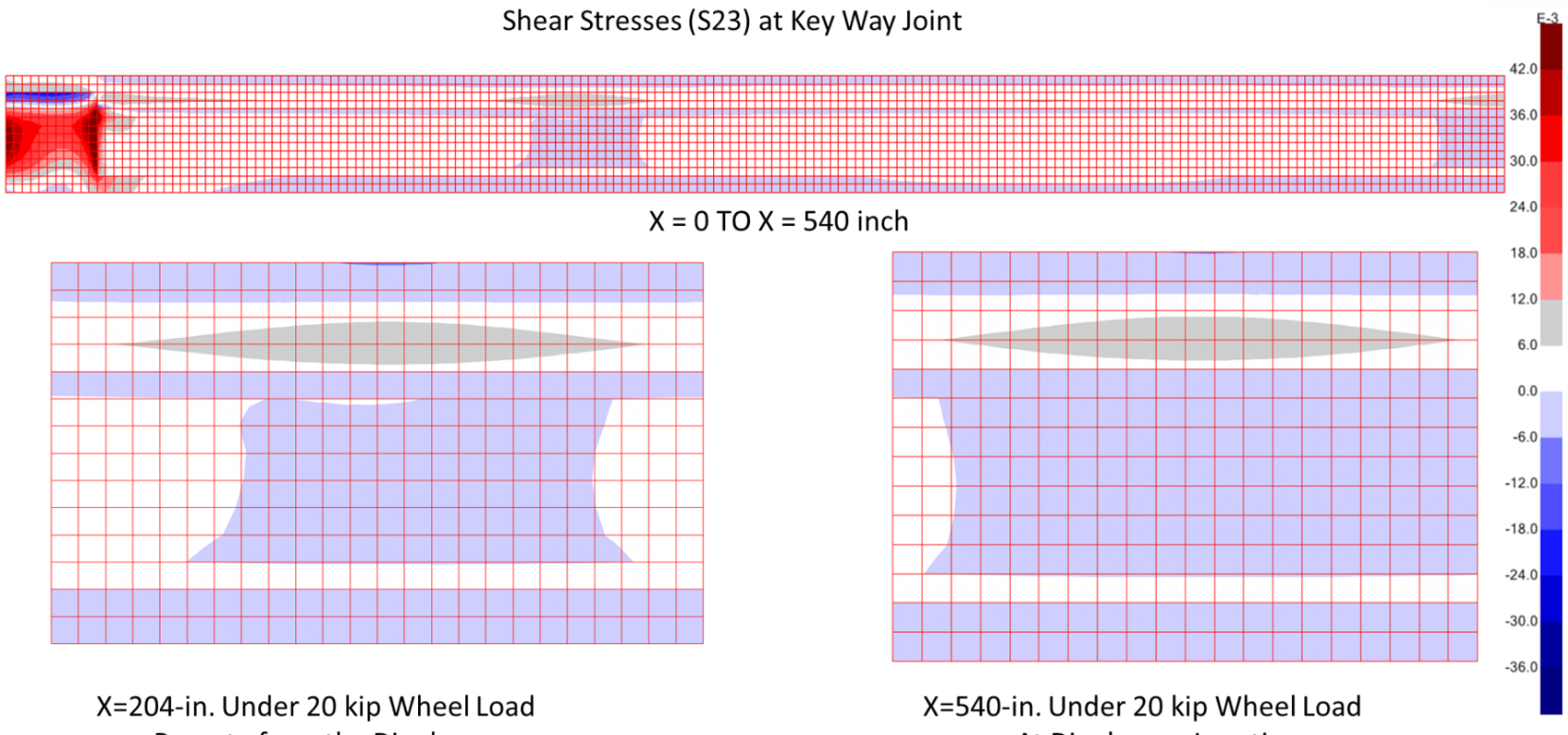

X = 0 TO X = 540 inch

X=204-in. Under 20 kip Wheel Load
Remote from the Diaphragm

X=540-in. Under 20 kip Wheel Load
At Diaphragm Location

Load Case II - With Intermediate Diaphragm
36-in Key Way
Shear Stresses (S23) at Key Way Joint

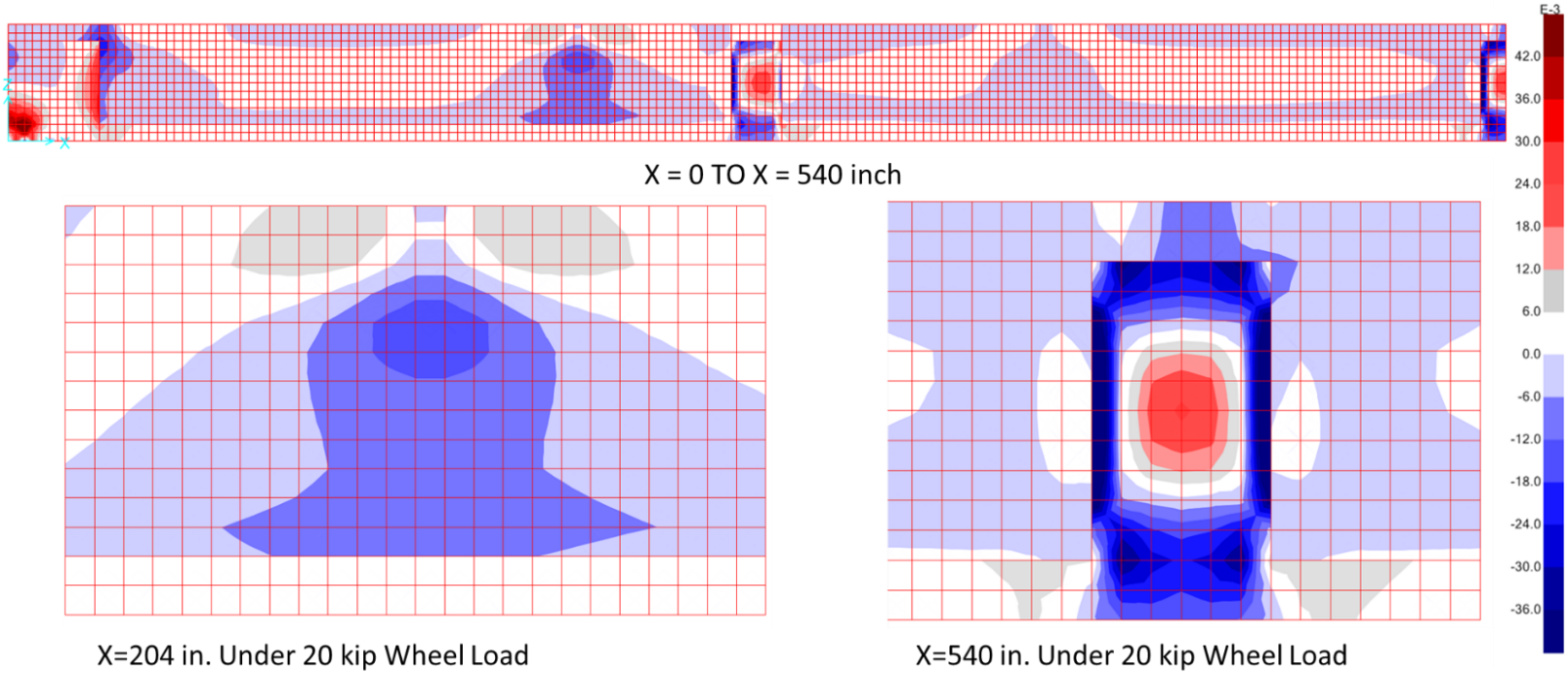

X = 0 TO X = 540 inch

X=204 in. Under 20 kip Wheel Load
Remote from the Diaphragm

X=540 in. Under 20 kip Wheel Load
At Diaphragm Location

Load Case II – With Intermediate Diaphragm
36-in Key Way
Shear Stresses (S23) – Cross Section

X=204in.

X=540in.

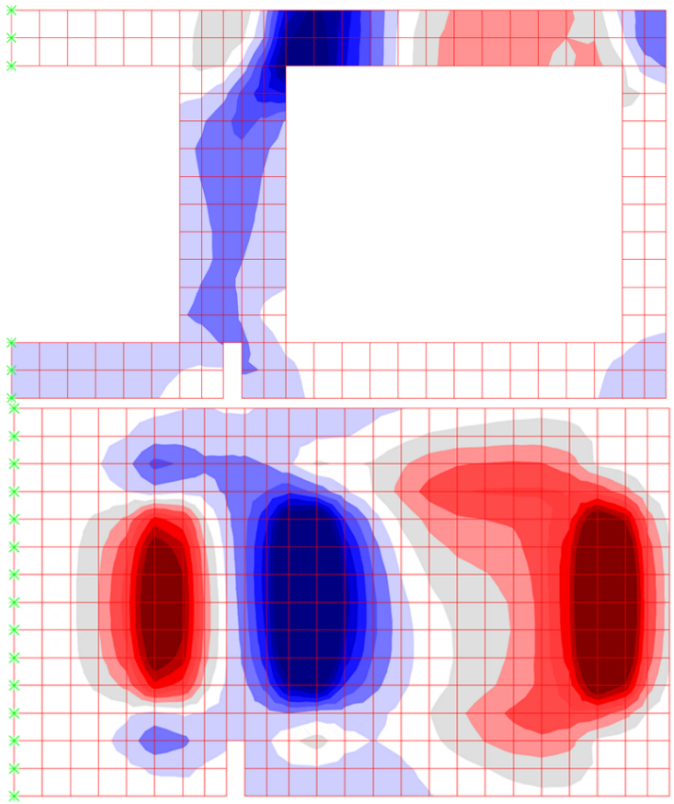

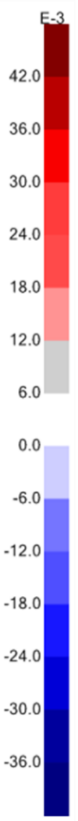

Load Case II - With Intermediate Diaphragm
12-in Key Way
Shear Stresses (S23) at Key Way Joint

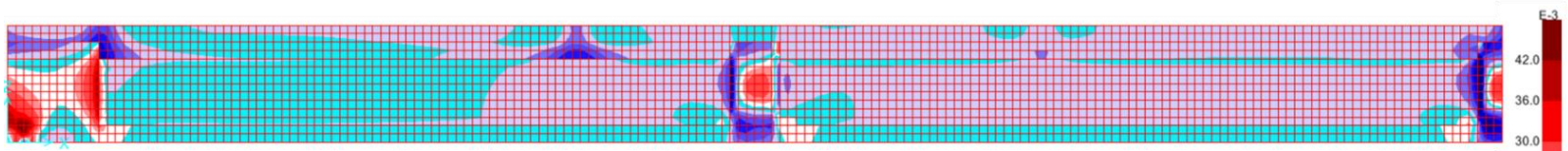

X = 0 TO X = 540 inch

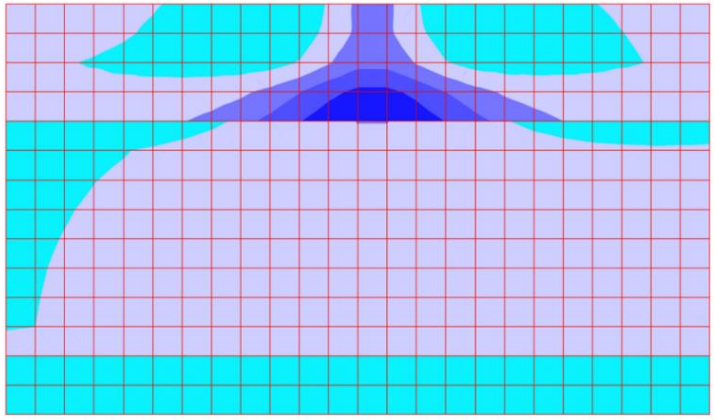

X=204-in. Under 20 kip Wheel Load
Remote from the Diaphragm

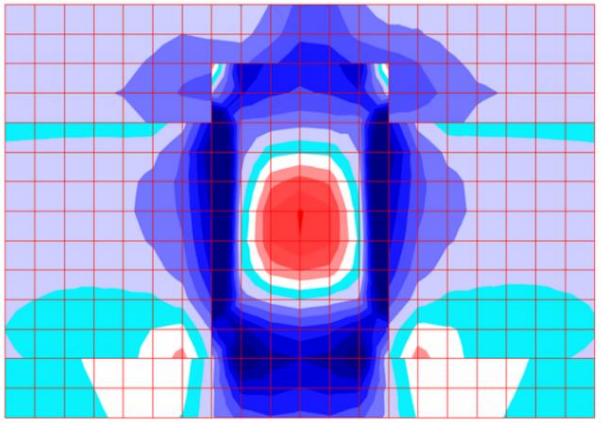

X=540-in. Under 20 kip Wheel Load
At Diaphragm Location

Load Case II – With Intermediate Diaphragm
12-in Key Way
Shear Stresses (S23) – Cross Section

X=204in.

X=540in.

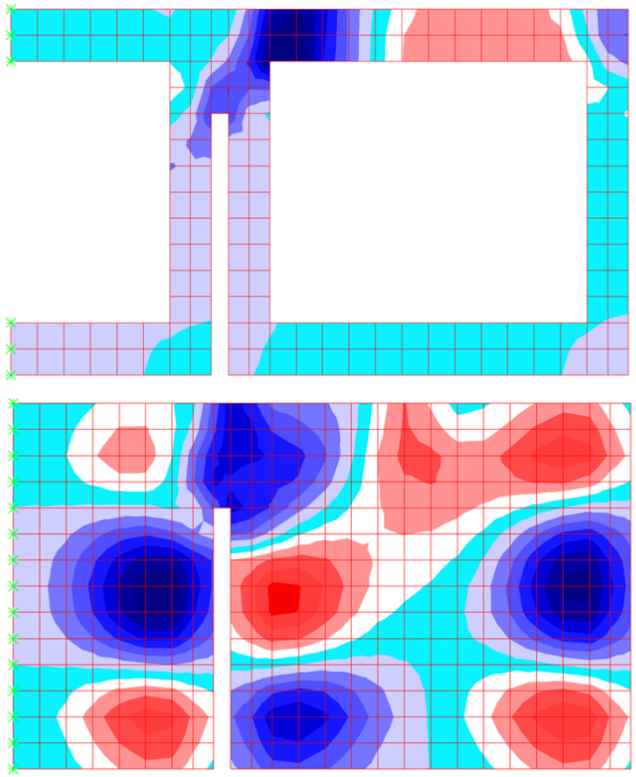

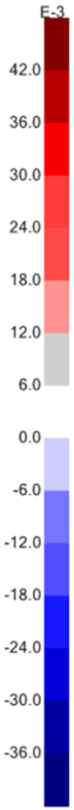

Load Case I - Without Intermediate Diaphragm
36-in Key Way
Shear Stresses (S23) at Key Way Joint

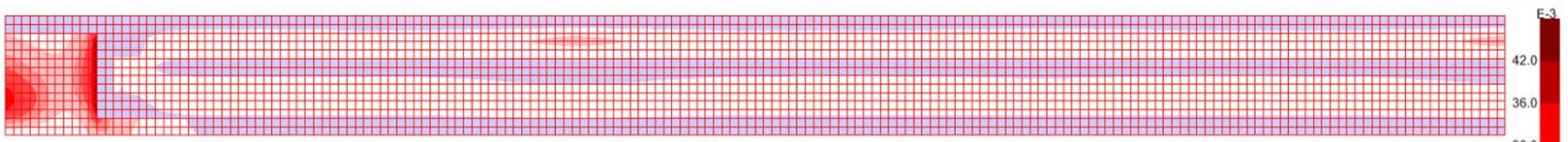

X = 0 TO X = 540 inch

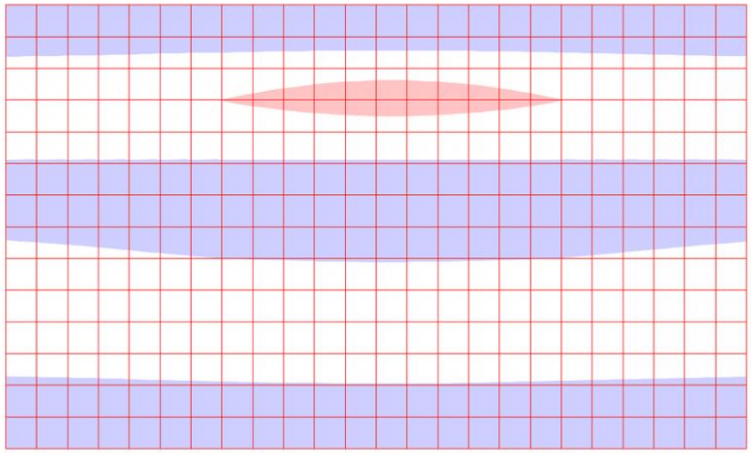

X=204-in. Under 20 kip Wheel Load
Remote from the Diaphragm

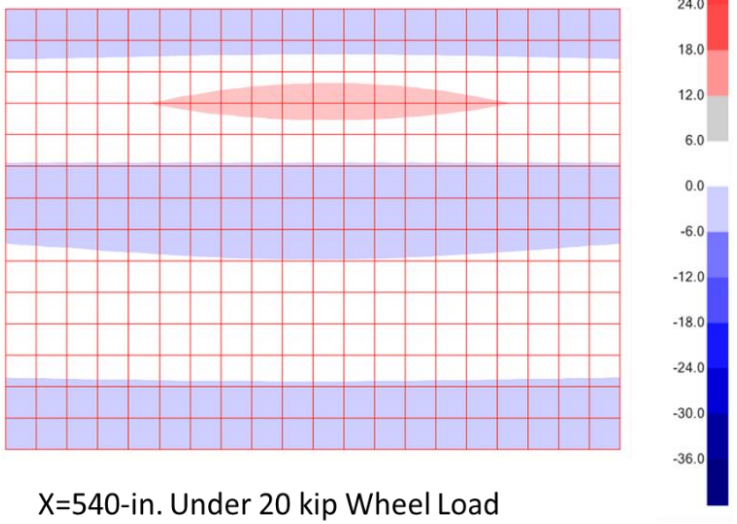

X=540-in. Under 20 kip Wheel Load
At Diaphragm Location

Load Case I – Without Intermediate Diaphragm
36-in Key Way
Shear Stresses (S23) – Cross Section

X=204in.

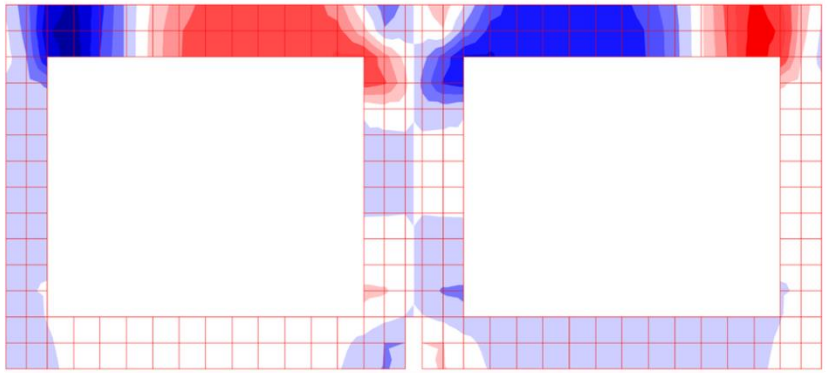

X=540in.

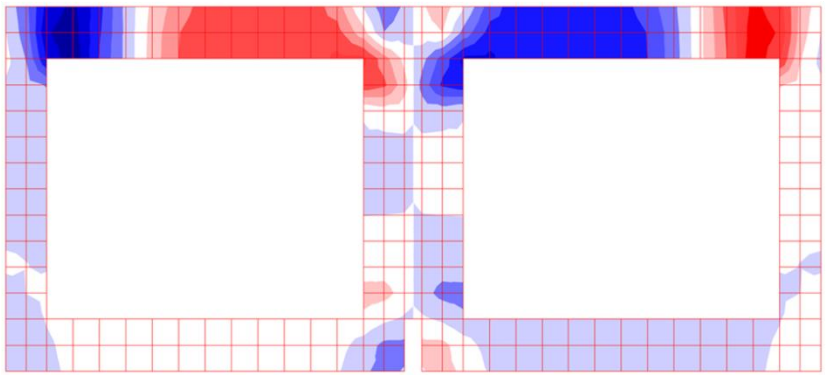

Waterproofing Details of Connections for Adjacent Precast Concrete Box-Beam Bridges

Appendix H: Structural Tests for Eccentric Loads

Prepared by:

Mohamed Habouh, PhD (Former Graduate Student)
Anil Patnaik, PhD (Principal Investigator)

Prepared for:

The Ohio Department of Transportation
Office of Statewide Planning & Research

State Job Number 134847
07/25/2018

Waterproofing Details of Connections for Adjacent Precast Concrete Box-Beam Bridges

Appendix H: Structural Tests for Eccentric Loads

Prepared by:

Mohamed Habouh, PhD
Former Graduate Student, Department of Civil Engineering
The University of Akron, Akron, OH 44325-3905

Dr. Anil Patnaik (PI)
Professor, Department of Civil Engineering
The University of Akron, Akron, OH 44325-3905
Phone: 330-972-5226 Email: Patnaik@uakron.edu

July 2018

Prepared in cooperation with the Ohio Department of Transportation,
Ohio's Research Initiative for Locals, and the U.S. Department of Transportation, Federal Highway Administration

TABLE OF CONTENTS

LIST OF FIGURES

LIST OF TABLES

APPENDIX H: STRUCTURAL TESTS FOR ECCENTRIC LOADS

H.1 Objective

The objective of the tests described in this appendix is to determine the strength of the joints under the possible concurrent action of shear loading and the corresponding out-of-plane moment using structural load tests. A study of eccentric load effects at a full or large scale requires larger beams than those used for symmetric loading (Appendix F) with comparable cross sections and spans. Such tests are expensive and time consuming. Therefore, simplified smaller test specimens with a length of 42 inches and depth of 21 inches were designed to capture the behavior of full-scale box beams for the select keyway geometries, interface conditions, and loading conditions. Structural tests were conducted in order to determine if the keyway geometries and grouts developed in this study would satisfy the load carrying requirements at the longitudinal joints of box beam bridges with typical spans.

H.2 Methodology

i) According to the findings from Appendices D and F, a deeper keyway can improve the shear capacity of the joint, and sandblasting the keyway surface can increase the shear strength by 157% for the same grout material (Section 7.10).
ii) Beam B27-48 with the maximum allowable span of 65 ft. for this section was modeled with the standard 7-inch-deep keyway and a larger depth keyway to determine the changes in the stresses at the joint.
iii) A full depth keyway was considered to be the beam depth minus the thickness of the bottom flange (27 inches – 6 inches = 21 inches). Six inches at the bottom of the keyway were excluded to avoid reducing the cross-sectional area of the bottom plate of the box beam.
iv) The required strength was determined using finite element analyses models and the available strength was determined using test results from tests with eccentric loads to determine a factor of safety for the current keyway geometries and grouts.

Possible improvements with the recommended alternatives were established.

H.3 Finite Element Analyses

H.3.1 Assumptions and Load Arrangements

Finite element analyses for 3-D models with eight-node solid elements with the same assumptions as described in Appendix F were conducted. The loads were placed in the longitudinal direction to maximize the number of axle loads that can be placed over the span of the beam as shown in Fig. H.1.

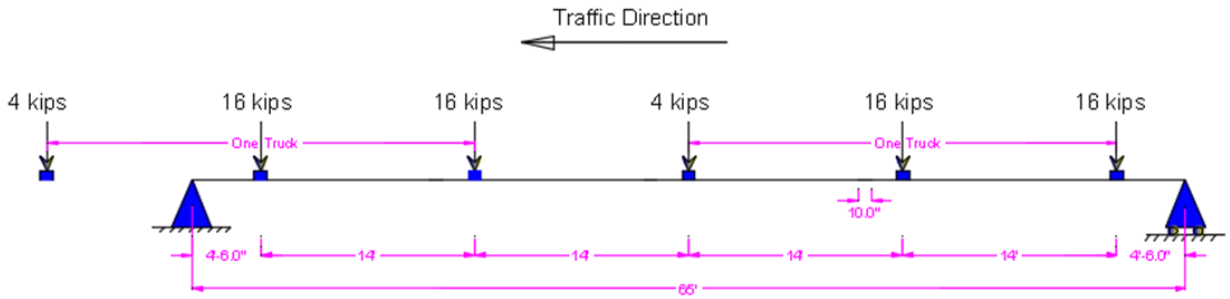

Fig. H.1 Loads in Longitudinal Direction for HL-93 Design Truck

Six models were analyzed to determine the stresses at the joint for partial and full depth keyways under three load cases in the transverse direction, as shown in Fig. H.2.

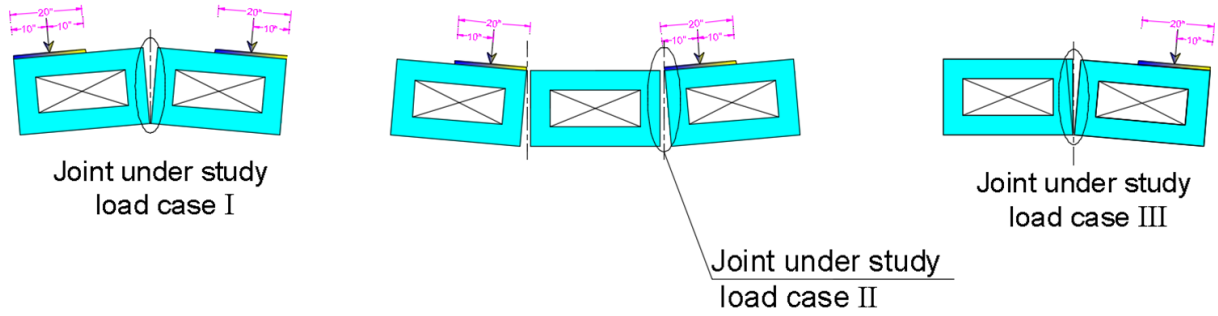

Fig. H.2 Load Arrangement in Transverse Direction

H.3.2 Analysis results

Shear and normal stresses for a 7- inch-deep keyway are shown in Figure H.3. Shear and normal stresses for a 21-inch-deep keyway are shown in Figure H.4.

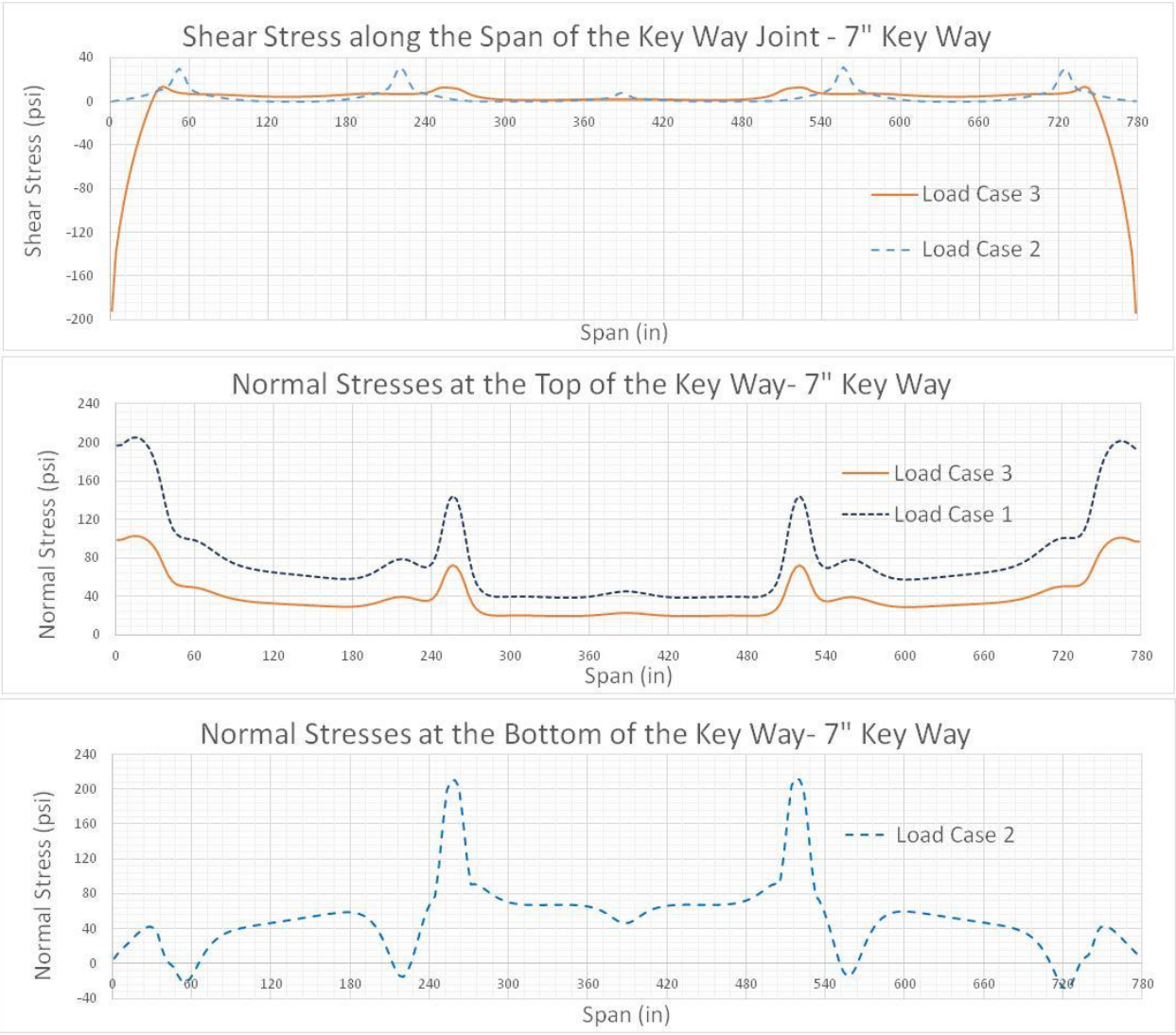

Fig. H.3 Normal and Shear Stresses for a 7- inches-deep Keyway

H.3.3 Discussion

- For Load Case I, the shear stresses are zero due to symmetry.
- Shear and normal stresses are local under wheel loads.
- Tensile stresses are developed at the top of the joint for Load Case I and II, and the tensile stresses are developed at the bottom for Load Case III.
- The 21-inch-keyway reduced the shear and normal stresses significantly compared the 7-inch-deep keyway.

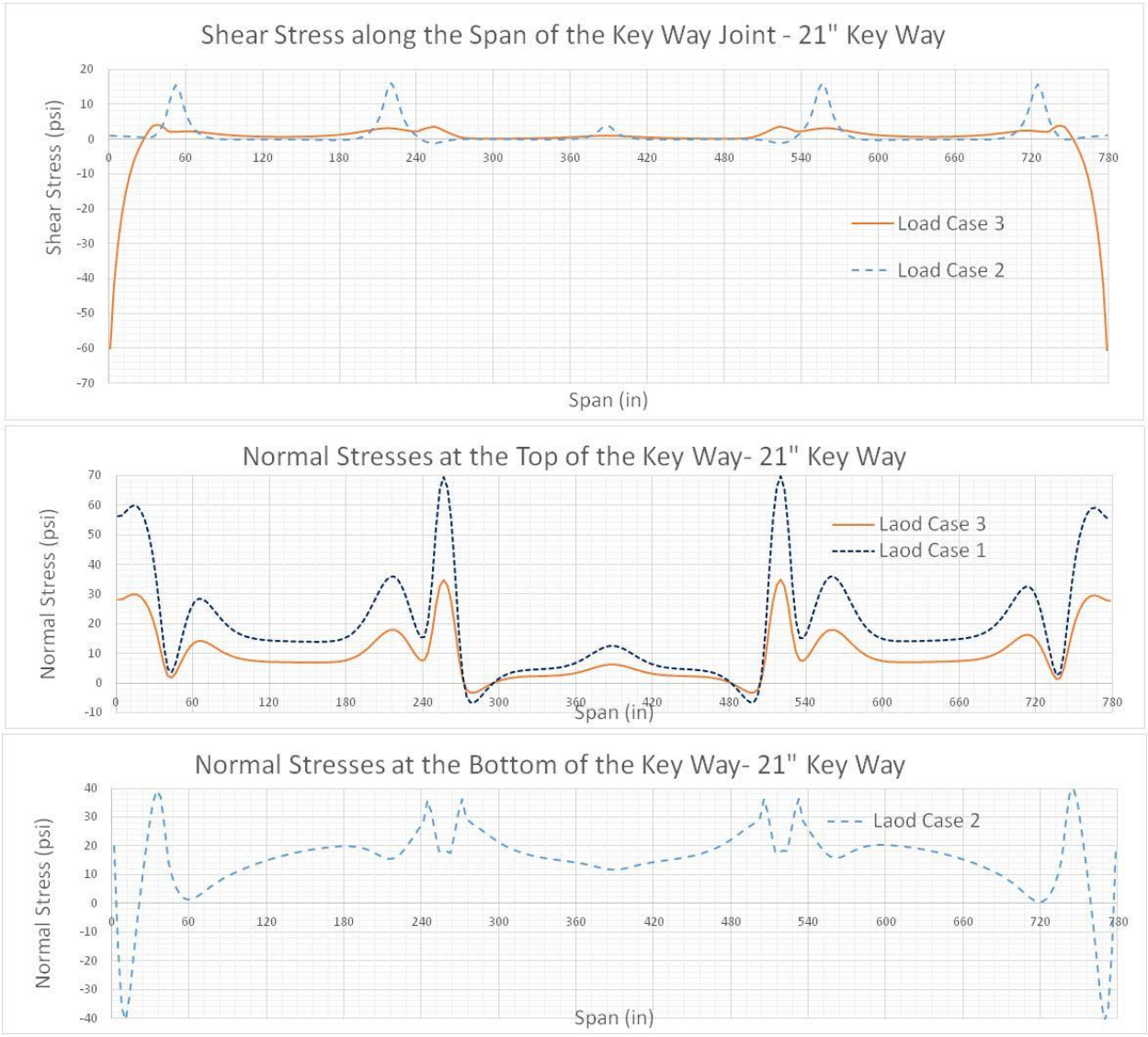

Fig. H.4 Normal and Shear Stresses for a 21- inch-deep Keyway

H.4 Test Specimen Set # 1

Simplified test specimens were designed to simulate the corresponding full-scale tests for different keyway geometries and load combinations. The details of the test specimens and the typical test setup are shown in Figure H.5. Table H.1 shows the details of the specimens for the first set of test specimens.

Table H.1: Details of Specimens for Eccentricities Load Set #1

Grout Material	Keyway Geometry	Surface Roughness
ODOT-Approved Grout	Standard geometry - 7" deep (0.75" - 1.5" wide)	Sandblasted
	Wider keyway - 21" deep (1" - 2" wide)	Sandblasted
	Wider keyway - 21" deep (1" - 2" wide)	As-Cast
Polymer Grout	Standard width keyway - 21" deep (0.75" - 1.5" wide)	Sandblasted
UHPG	Wider keyway - 21" deep (1" - 2" wide)	Sandblasted
HSC with Maximum #8 Aggregates Size	Wider keyway - 21" deep (1" - 2" wide)	Sandblasted
	Wider keyway - 21" deep (1" - 2" wide)	As-Cast

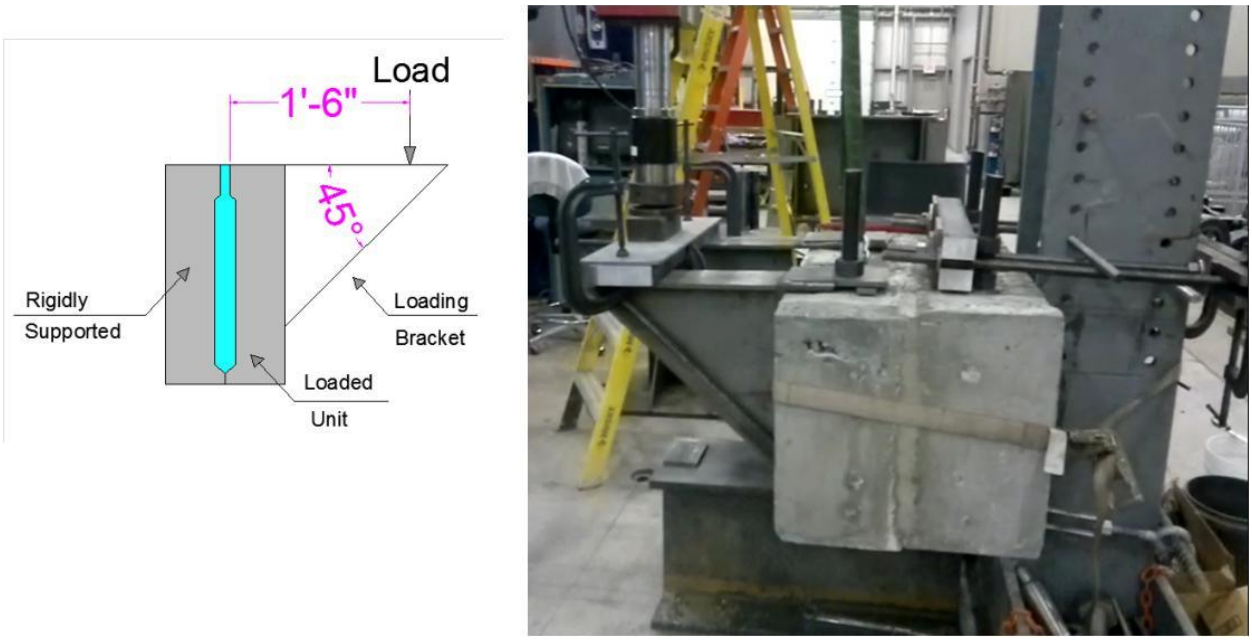

Fig. H.5 Load Configuration for Eccentric Load Tests

In the test setup, one unit was fixed to a rigid support, while the other unit was loaded under eccentric loading to simulate the out-of-plane moment on the joint. The test variables used in this study are summarized in Figure H.6.

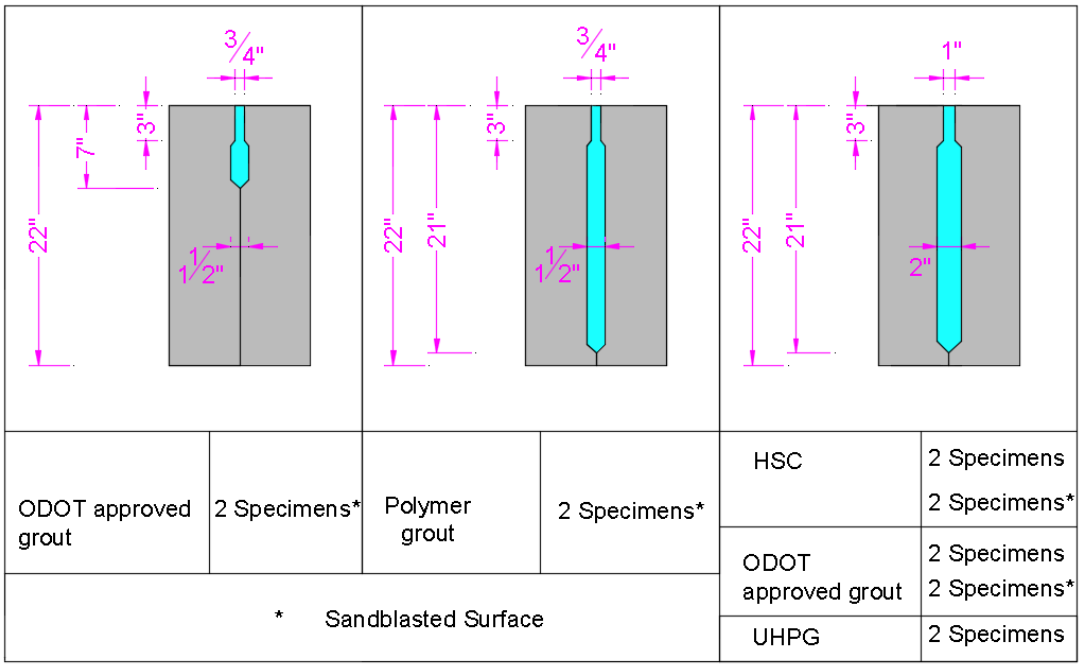

Fig. H.6 Test Combinations and Keyway Geometry for Eccentric Load Tests

H.4 Factors Studied in the Eccentric Load Tests

Grout material, surface roughness, and eccentric loading are the three factors that were studied in this test, and they are discussed in the following section. Bond enhancing chemicals were not considered based on the outcomes from the joint tests from Appendix D. All specimens were cast, grouted, properly cured and stored outdoors in the summer.

H.4.1 Grout Material

Based on the joint tests and the symmetric load tests on beam assemblies, the polymer-based grout, ultra-high performance grout (UHPG), and high-strength concrete (HSC) were selected as the tentative grouts that are likely to be suitable for possible implementation. With high shear strength, polymer-based grout and UHPG were found to be very flowable and self-consolidating, with no vibration needed for compaction. The HSC concrete with maximum # 8 coarse aggregate size required some amount of vibration for proper consolidation. The ODOT-approved grout was considered for comparison purposes, as was the possibility of achieving the desired strength using a rough sandblasted surface with a deeper and wider keyway. The current ODOT-specified keyway geometry was also used in the test plan for the sake of comparison.

H.4.2 Surface Roughness and Interface Sandblasting

Based on the joint tests, roughening of the joint surface by sandblasting improved the shear strength of the joint significantly. For UHPG, the average joint shear strength was found to have increased by a factor of about 3.3. For the HSC with # 8 aggregates, the joint strength was increased by a factor of 1.7. As-cast concrete surfaces and concrete surfaces roughened by sandblasting were considered in this study to determine the joint strength under eccentric loads for both surface conditions. Sandblasting was performed using a 3,500 psi pressure washer and fine sand with a wet blasting kit (Figure H.7). An air pressure of 120 psi may provide similar roughness if air blasting were to be used instead.

Fig. H.7 Sandblasted Surface Preparation for Eccentric Load Tests

H.4.3 Eccentric Loads

The applied loads were designed to result in tension and compression normal to the joint surface and shear forces parallel to the joint surface to match the required stresses obtained from finite element analyses. One of the two units comprising each test specimen assembly was firmly attached to the very rigid testing frame using turnbuckles and/or tie rods to prevent any rotation or translation in the transverse direction. This unit was supported so that there was no vertical movement. The other unit of the specimen was hanging free of the supports and was connected to the supported unit only through the grout in the keyway. The loading brackets were attached to the free concrete unit to apply eccentric load at 18 inches of eccentricity to result in tension, compression, and shear forces (Figure H.8).

Table H.2: Summary of Test Plan for Eccentric Load Tests

Grout Material	Surface Preparation	No. of specimens	Keyway Configuration			Comments
			Width of the opening (in)	Keyway Dimensions		
				Width (in)	Depth (in)	
ODOT-Approved List	Sandblasted	2	0.75	1.5	4	Standard Geometry
Polymer Grout	Sandblasted	2	0.75	1.5	18	Vibration not Needed
ODOT-Approved List	Sandblasted	2	1	2	18	Wider opening to allow vibration
ODOT-Approved List	As Cast	2	1	2	18	
HSC-Grout	Sandblasted	2	1	2	18	
HSC-Grout	As Cast	2	1	2	18	
UHPG	Sandblasted	2	1	2	18	
Total No. of Test Specimens		14				

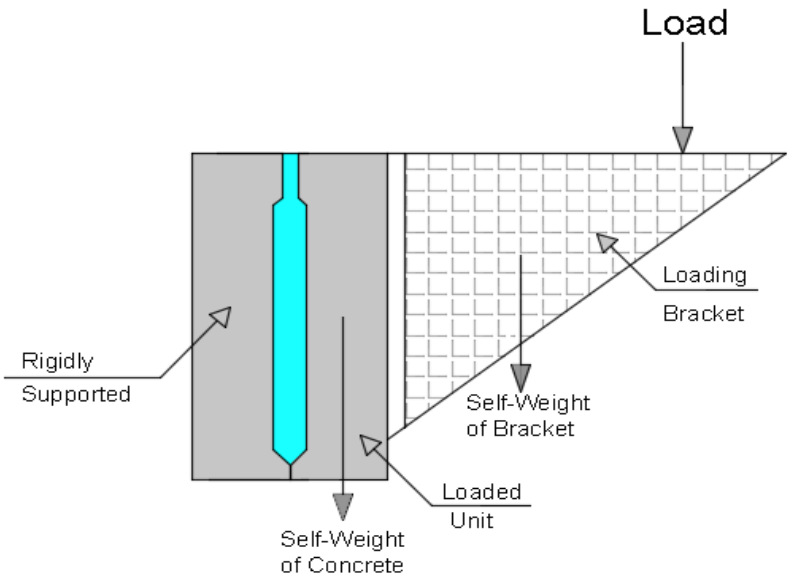

Fig. H.8 Setup for Eccentric Load Tests

H.5 Results of Eccentric Load Test Set # 1

For the specimen with full a depth keyway and as-cast concrete surface using ODOT-approved grout, the joint failed under its own self-weight (500 lb) plus the weight of the loading brackets (300 lb) before any external loads were applied. The joint failed through the entire length and entire depth by de-bonding and separation at the interface without any damage to the concrete units or the grout material, as seen in Figure H.9.

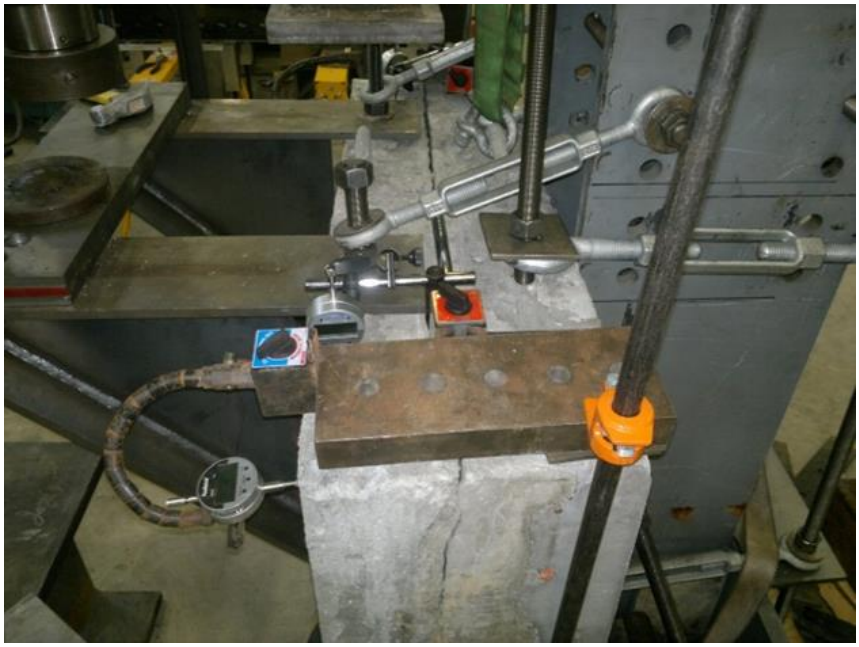

Fig. H.9 Failure of the Test Specimen with Kuhlman Grout under Self-Weight

For the specimen with partial depth keyway and sandblasted surface using ODOT-approved grout, the joint failed after applying 500 lb of eccentric load in addition to its self-weight and the weight of the loading brackets. The joint failed through the entire length and entire depth by de-bonding and separation at the interface with minor damage to the grout as seen in Figure H.10.

Fig. H.10 Failure of the Test Specimen with Kuhlman Grout and Partial Depth Keyway

For specimens with a sandblasted surface and a full-depth keyway, the joint did not fail. For these tests, the concrete unit failed at 10,000 lb of tension by splitting at the tie rod location as shown in Figure H.11 and Figure H.12. The strength of the concrete units was less than the required strength to fail the joint.

Fig. H.11 Typical Failure in Concrete Units

Fig. H.12 Typical Failure in Concrete Units

H.6 Test Specimen Set# 2

It was not possible to determine the failure load and joint strength for different keyway geometries and grout materials with this test specimen design because the concrete test specimens failed locally before joint failure could occur. A second set of test specimens with higher strength was needed to determine the available strength of the specimens with high strength concrete grouts. A new set of eight test specimens with larger width were cast and grouted to determine the available strength of each of the four grouts under study (polymer, high strength concrete, ODOT-approved grout, and UHPG) with a sandblasted surface. The concrete units were designed to avoid tensile splitting under eccentric loads, the reinforcement details for Set # 1 and Set # 2 are shown in Figure H.13. The formwork and rebar for Set # 2 are shown in Figure H.14.

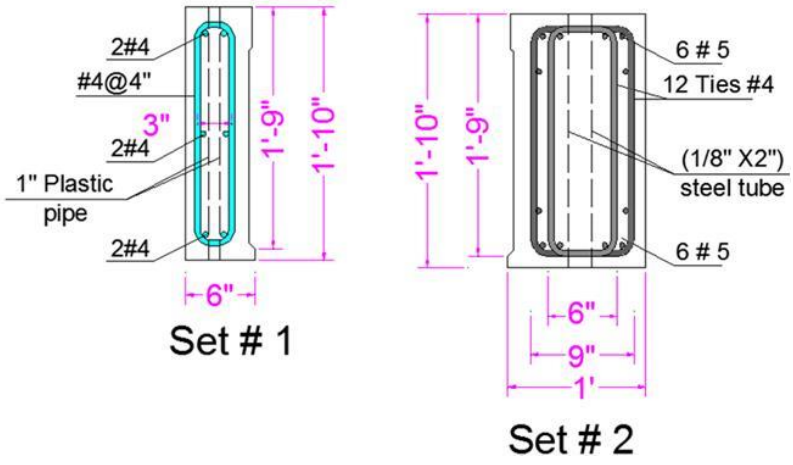

Fig. H.13 Reinforcement Details for Set#1 (Left), and Set#2 (Right)

Fig. H.14 Formwork and Rebar for Set#2

Eight test specimens were cast and tested under eccentric loads. The eccentric load was applied at 27" from the keyway surface.

H.7 Results for Eccentric Load Test Set # 2

The failure loads from the eight tests are shown in Table H.3. The largest bond strength between the grout and the concrete units was obtained when HSC was used as grout material, with average eccentric load of 32 kips.

Table H.3: Test Results for Set # 2

Specimen #	Grout Material	Keyway Surface	Failure Load (lb)	Average Failure Load (lb)
1	High Strength Concrete	Sandblasted	30,000	32,000
2			34,000	
3	ODOT-Approved Grout	Sandblasted	18,000	20,000
4			22,000	
5	Polymer 4316	Sandblasted	12,000	13,000
6			14,000	
7	Ultra High Performance Grout	Sandblasted	8,000	8,500
8			9,000	

An elastic behavior of the grout before failure was assumed to develop the stress diagram for the test specimens to determine the maximum tensile stress at the extreme top fibers at failure. Figures H.15 and H.16 show the load arrangement and the corresponding elastic linear bending stress diagram due to the out-of-plane moment and the resultant compressive and tensile resultant forces on the surface of the keyway joint for the tested specimens.

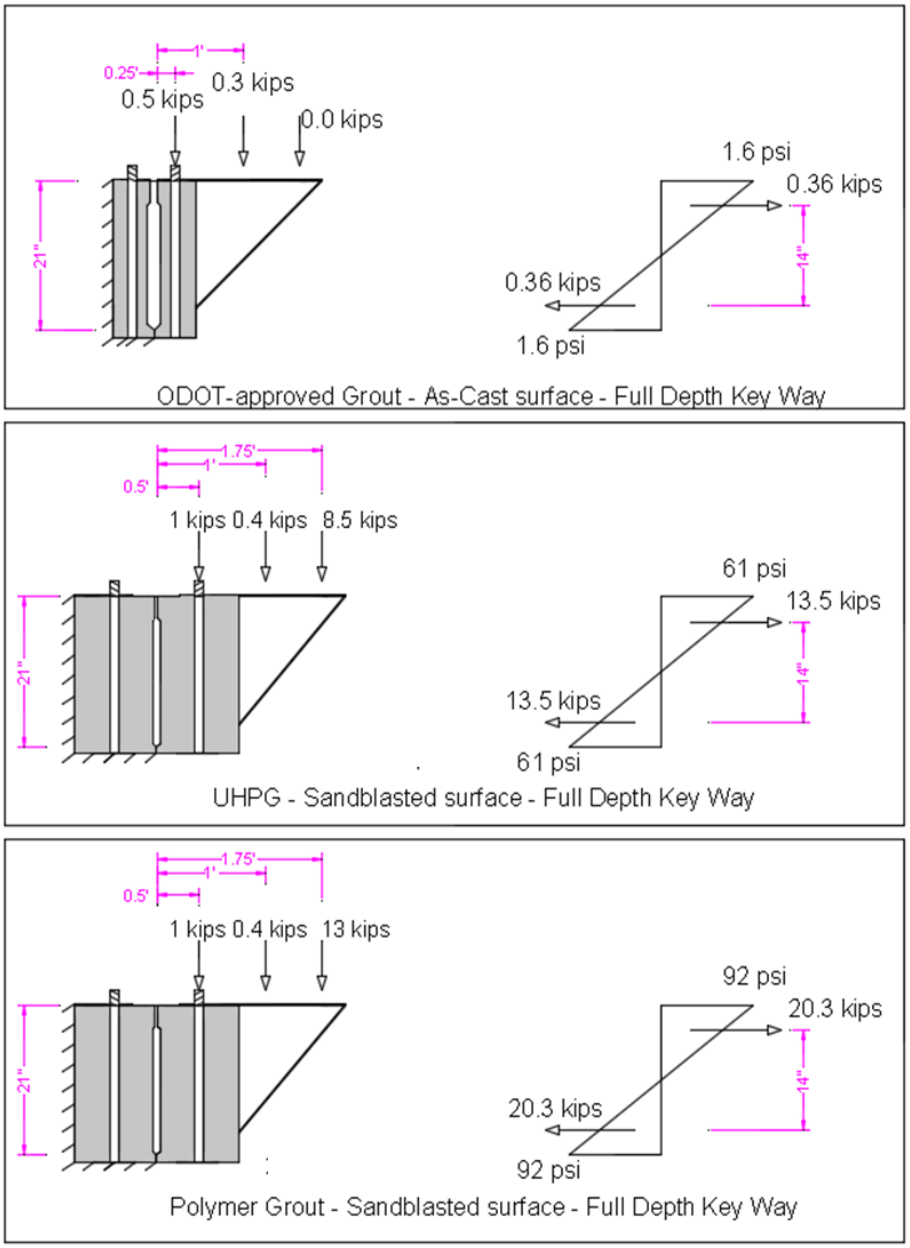

Fig. H.15 Linear Elastic Analysis for the Tested Specimens - I

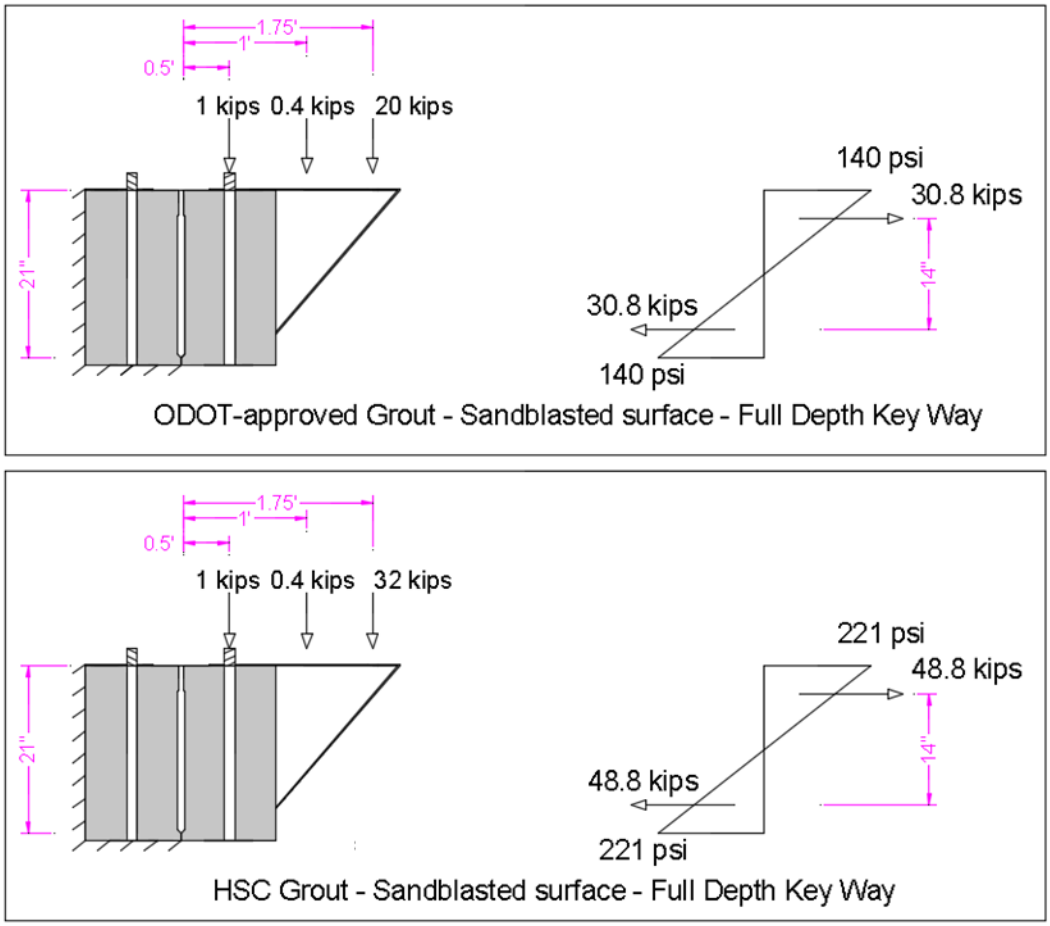

Fig. H.16 Linear Elastic Analysis for the Tested Specimens – II

H.7.1 Failure Modes for Set # 2

A sudden failure was observed in all the test specimens. A monolithic failure pattern was observed only when the HSC was used as grout material, with an average failure load of 32 kips as shown in Figure H.17. Sandblasting the concrete surface improved the strength of the test specimens for all the tested grouts. ODOT-approved grout failed at an average load of 20 kips with superior performance obtained with polymer grout and UHPG with failure loads of 13 kips, and 8.5 kips, respectively. The best performance was recorded when HSC was used as the grout material.

The failure mode of the test specimens for each grout type is shown in Figures H.17 to H.20.

Fig. H.17 Failure of Specimens with HSC Grout

Note: Failure occurred within the concrete specimen and not through the grouted joint.

Fig. H.18 Failure of Specimens with Polymer Grout

Fig. H.19 Failure of Specimens with UHPG

Fig. H.20 Failure of Specimens with ODOT-approved Grout

A summary of the test results for Set # 1 and Set # 2 are presented in Table H.4.

Table H.4: Summary of Test Results for Set # 1 and Set # 2

Keyway Depth	Grout Materail	# of Specimes	Surface Roughness	Set #	Shear Force at the Interface (lb)	Applied Moment at Failure (kip-ft)	Grout Strength (psi)
Partial depth	ODOT-Approved List	2	Sandblasted Surface	1	800	1.175	4.4
Full depth		2	As-Cast	1	300	0.425	1.6
Full depth		2	Sandblasted Surface	1	Failure in Concrete	15.425	
Full depth		2	Sandblasted Surface	2	20,000	35.9	140
Full depth	HSC-Grout	2	As-Cast	1	Failure in Concrete	15.425	
Full depth		2	Sandblasted Surface	1	Failure in Concrete	15.425	
Full depth		2	Sandblasted Surface	2	32,000	56.9	221
Full depth	UHPG	2	Sandblasted Surface	1	Failure in Concrete	15.425	
Full depth		2	Sandblasted Surface	2	8,500	15.78	61
Full depth	Polymer Grout	2	Sandblasted Surface	1	Failure in Concrete	15.425	
Full depth		2	Sandblasted Surface	2	13,000	23.65	92

H.8 Factor of Safety for Standard and Modified Keyway Geometries

From the test specimens, the strength was recorded at failure and was defined as the load at the first crack. The stresses are due to unfactored wheel loads of the HL-93 design truck. The

resultant stresses from the finite element analyses were determined using the square root of the sum of squares. For the 21-inch-keyway at span X = 0 inches the resultant stresses for Load Case III was calculated as follows:

$$\text{Resultant Stress} = \sqrt{Normal\ Stress^2 + Shear\ Stress^2} = \sqrt{28^2 + 60^2} = 66\ psi$$

$$\text{The calculated factor of safety equal to } \frac{Available\ Strength}{Required\ Strength} = \frac{223\ psi}{66\ psi} = 3.38$$

Table H.5 shows the factor of safety provided by 7-in. and 21-in. keyways based on the experimental strength of the HSC-grout with a keyway depth of 21 inches.

Table H.5: Factor of Safety from Analysis and Experimental tests

Key Way Depth	Standard Key Way (7")				Modified Key Way (21")			
	Stresses from FE Analysis			Available Strength	Stresses from FE Analysis			Available Strength
	Load Case I (psi)	Load Case II (psi)	Load Case III (psi)	Test Results (psi)	Load Case I (psi)	Load Case II (psi)	Load Case III (psi)	Test Results (psi)
Location X (in)=	18	255	0		255	12 and 36	0	
Normal Stress	205	210	194	4.4	70	41	28	220
Shear Stress	0	0	102	2.7	0	0.8	60	36
Resultant Stress	205	210	218	5	70	41	66	223
FOS	**0.02**	**0.02**	**0.02**		**3.18**	5.43	3.38	
	Unsafe				**Okay Governs**	**Okay**	**Okay**	

H.9 Discussion and Summary from Eccentric Load Tests

The test specimen with the currently used ODOT keyway geometry with ODOT-approved grout failed under the self-weight of the test specimen unit, proving that the current keyway with currently used grout is totally incapable of carrying any shear load in conjunction with out-of-plane tension or moment. For this reason, changes in keyway geometry details and

grout material specifications are needed. Increasing the keyway depth alone without proper surface preparation did not improve the strength of the joint when using ODOT-approved grout.

The shear transfer strength of specimens with a sandblasted surface and full-depth keyway and with high strength grout or ODOT-approved grout was significantly larger.

The structural tests to determine the joint strength under eccentric loads identified a serious inadequacy of the current keyway geometry and ODOT-approved grout. Increasing the depth of the keyway to full depth but with no sandblasting was not adequate to improve the joint strength under the simultaneous action of out-of-plane moment and shear. However, the changes made to the keyway geometry and the new grout materials were found to improve the joint performance substantially.

The HSC concrete with #8 coarse aggregate had excellent bond with the concrete units, resulting in a high tensile strength across the joint.

The test results for the test specimens with eccentric loads and the beam assembly tests in Appendix F indicate that the compressive strength of the grout material is not the only measure to qualify the grout for all applications; the bond strength is an equally important factor that might disqualify a high compressive strength grout. Stress analysis of a specific bridge may be required to select the grout for a given bridge based on the relevant load combinations and the corresponding joint depth.

The modified geometry of the keyway with HSC-grout provides strength to resist the resulting stresses with a factor of safety of about 3.2 for the load cases considered in this study.

Waterproofing Details of Connections for Adjacent Precast Concrete Box-Beam Bridges

Appendix I: Basis for Implementation

Prepared by:

Mohamed Habouh, PhD (Former Graduate Student)
Anil Patnaik, PhD (Principal Investigator)

Prepared for:

The Ohio Department of Transportation
Office of Statewide Planning & Research

State Job Number 134847
07/25/2018

U.S. Department of Transportation
Federal Highway Administration

Waterproofing Details of Connections for Adjacent Precast Concrete Box-Beam Bridges

Appendix I: Basis for Implementation

Prepared by:

Mohamed Habouh, PhD
Former Graduate Student, Department of Civil Engineering
The University of Akron, Akron, OH 44325-3905

Dr. Anil Patnaik (PI)
Professor, Department of Civil Engineering
The University of Akron, Akron, OH 44325-3905
Phone: 330-972-5226 Email: Patnaik@uakron.edu

July 2018

Prepared in cooperation with the Ohio Department of Transportation,
Ohio's Research Initiative for Locals, and the U.S. Department of Transportation, Federal Highway Administration

TABLE OF CONTENTS

LIST OF FIGURES

LIST OF TABLES

APPENDIX I: BASIS FOR IMPLEMENTATION

I.1 Introduction

Typical finite element models were developed to model a bridge over Cedar Fork (RIC-TR037-0.21), which is a tributary of the Clear Fork river on Shauck Road in Richland County, Ohio. This bridge was selected for potential implementation of the findings from the project. The finite element model was developed with three-dimensional 8-noded solid elements, using the same assumptions and load cases in the transverse direction as described in Appendix G. The bridge is a box beam bridge with a 39-ft of total length (38-ft span which is center-to-center of the end bearings) and a 28-ft width. The box beams in this bridge are designed to have the B17-48 cross-section. The B17- 48 section is allowed to be used for bridges with spans up to 40 ft. (total length of 41 ft.) as summarized in ODOT standard drawings PSBD-2-07 and PSBDD-2-07. The beam was modeled with the maximum permitted span of 40 ft. for this section instead of the actual span of 38-ft (SFN: 7032048) to determine the maximum normal and shear stresses at the longitudinal joints for box beams of spans up to 40 ft.

I.2 Objective

The primary objective for the research presented in this appendix is to provide implementation recommendations for the keyway geometry, grout material, dowel bar arrangement and construction specifications based on the design calculations for the revised box beam cross-section for bridge # RIC-TR037-0.21 with the intent to move forward with implementation.

I.3 Methodology

i) Six models were developed and analyzed to (1) study the keyway performance with the proposed modifications for the joints under two load cases. Analyses were done for both standard keyway geometry and modified geometry under only unfactored wheel loads of HL-93 design truck, and (2) study the effects of using multiple dowel bars at the end diaphragms on the normal stresses at the joint.

ii) Two design approaches were investigated for the beam to abutment connection: (1) under restrained beam-abutment connections at anchor dowel bar locations, and (2) beam-to-abutment connection with horizontal unrestrained condition at the anchor dowel bars.

I.4 Assumptions for the Analyses

I.4.1 Load Arrangement in the Longitudinal Direction

The location of the truck wheel loads that will maximize the moment on the simply supported box beam span was determined to be as shown in Fig. I.1.

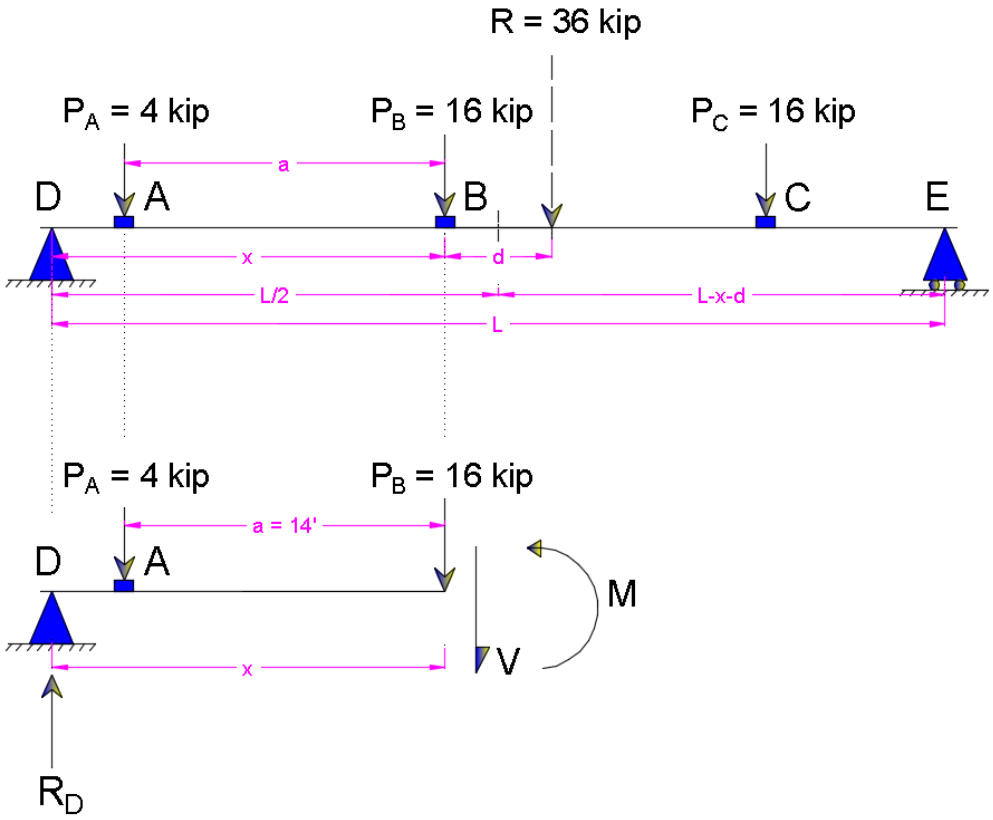

Fig. I.1 Load Location in Longitudinal Direction

Fig. I.2 shows the wheel load location, the bending moment diagram and the support reactions under the selected arrangement of wheel loads.

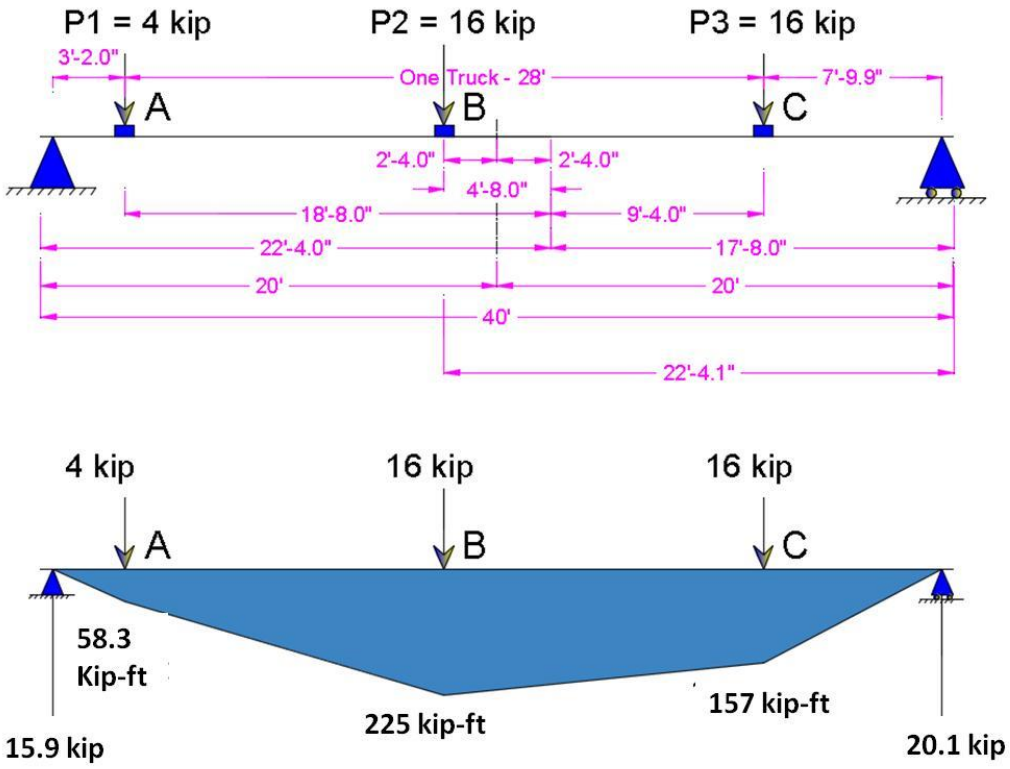

Fig. I.2 Load Arrangement in the Longitudinal Direction and Bending Moment Diagram

The maximum vertical deflection and bending moment of 225 ft-kips occur at the 16-kip load (Point B) as shown in Fig. I.2.

I.4.2 Load Arrangement in the Transverse Direction

Two load cases were considered for this analysis with beam section B17-48, which was adopted from ODOT standard drawings. The arrangement of loads was as shown in Fig. I.3 and Fig. I.4 and discussed earlier in Appendix G.

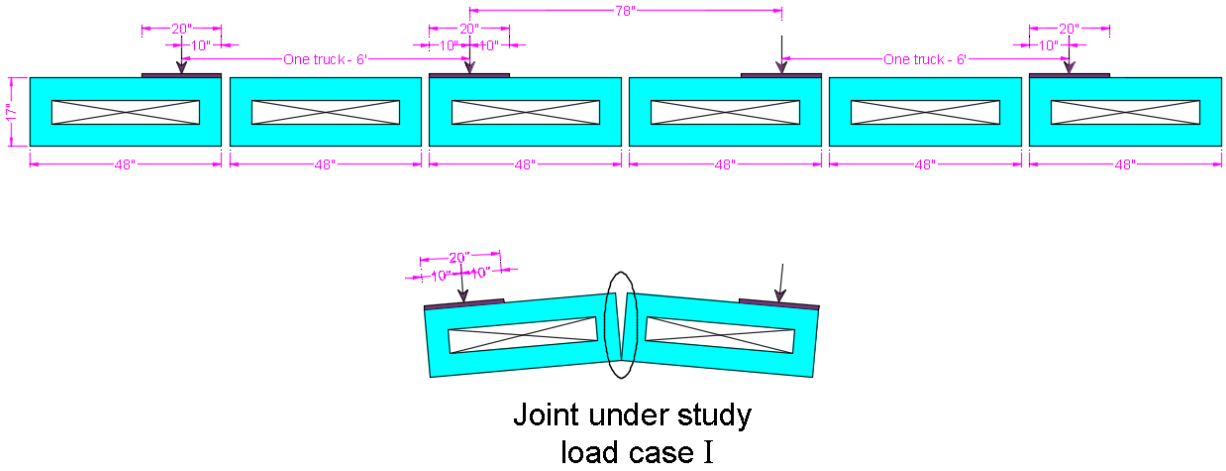

Fig. I.3 Load Case I

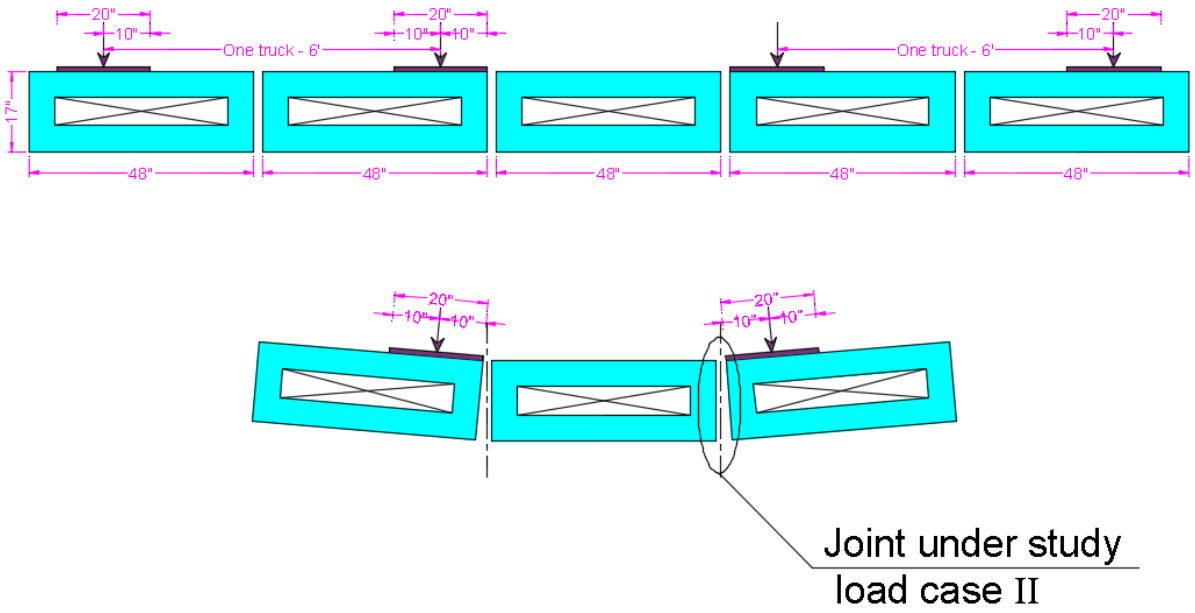

Fig. I.4 Load Case II

I.4.3 Modeling of Elastomeric Bearing

Bearing pads must satisfy the requirements of slip, shear, compressive stress, deflection, and rotation requirements of AASHTO LRFD Bridge Design Specification, 6th Edition (2012). Typical stress-strain curves of elastomers are presented in Fig. I.5, which shows that these pads need to deform significantly to provide noticeable reaction at the beam ends. Figure I.6 shows the spring factors used for the analyses. Further details of modeling elastomeric bearings are given in Appendix G.

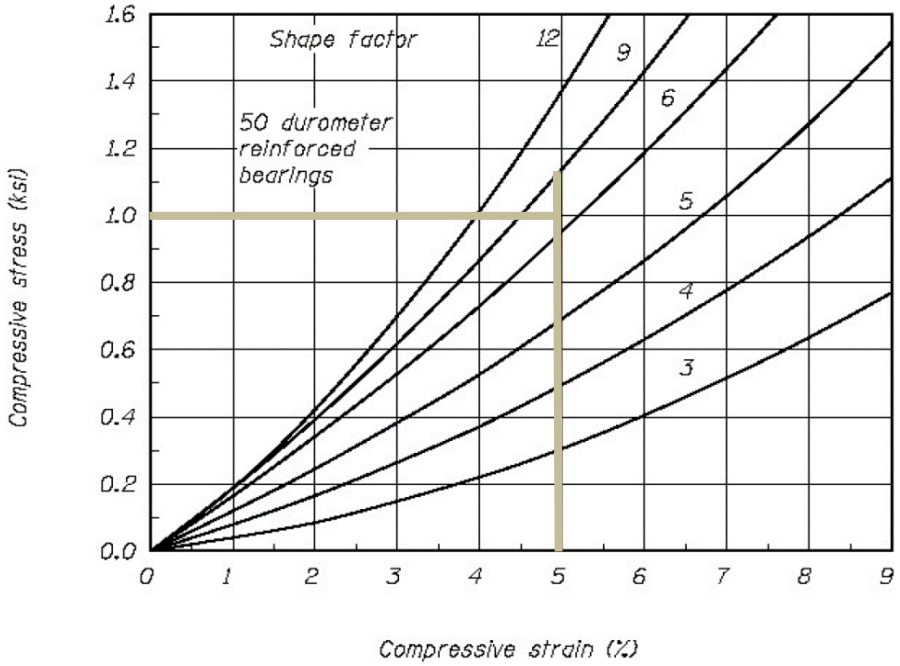

Fig. I.5 Typical Stress-Strain Behavior of Elastomers

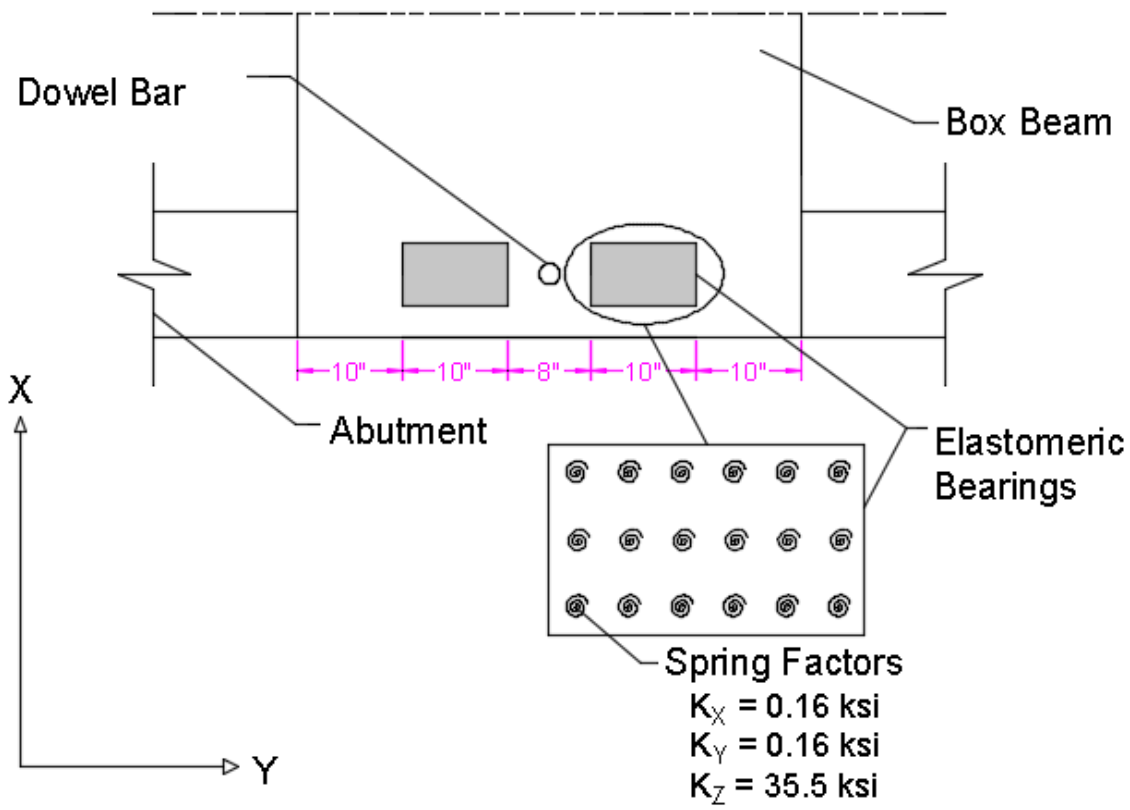

Fig. I.5 Typical Modeling of Elastomers (Plan View)

I.4.3.1 Spring Factors in Compression

For the purpose of structural analysis and finite element analysis (FEA), the live load deformation of the elastomer was assumed to be 0.1 in, at the upper limit for 2.0-in thick elastomer with strain = 0.1÷ 2.0 = 5% and corresponding stress of 1.05 ksi (Fig. I.6). For a 60-in^2 bearing pad, the shape factor =

$$\frac{\text{Horizontal Elastomer Area}}{\text{Vertical Surface Area of each Individual Layer}} = \frac{60}{(2\times(10+6)\times 0.25)} = 7.5$$

$$K = (\sigma \times A) \div (\varepsilon \times L) = (1.05 \text{ ksi} \times 60 \text{ in}^2) \div (0.05 \text{ in/in} \times 2.0 \text{ in}) \approx 630 \text{ksi}$$

Eighteen nodes were used for modeling each 60-in^2 elastomer with vertical compressive spring factor = 630 ÷ 18 = 35 ksi.

I.4.3.2 Spring Factors in Shear

The shear modulus G_{73} at 73°F is less than G_0 at 0°F; therefore, a value of G_{73} = 95 psi was used. For shape factor = 7.5 from Fig. I.5 and a 60-in^2 elastomer bearing pad area,

$$K_2 = G \times A \div h_{rt} = 0.095 \times 60 \div 2 = 2.85 \text{ ksi}$$

Eighteen nodes were used for modeling each 60-in^2 elastomer with shear spring factor = 2.85÷18 = 0.158 ksi, in both lateral directions.

I.5 Results from the Analysis

Stress concentrations in the normal direction were observed at the diaphragm locations and at wheel load locations. Peak shear stresses occurred at wheel load locations. Stresses were nonlinear along the depth of the grout joint at any vertical section.

I.5.1 Normal Stresses – Load Case I

The load configuration in Load Case I (Fig. I.3) is expected to cause tension at the top edge of the grouted longitudinal joint and compression at the bottom edge.

- The peak normal stresses occur under the wheel loads; the intermediate diaphragm attracts the most stress when the wheel load is applied at the diaphragm location.
- Increase in the depth of the joint from 7 inch to 11 inch decreases the peak normal stresses by a factor of 1.5 at the top of the joint at the diaphragm locations, as well as at the load location when the load is not at the diaphragms.
- Remote from the diaphragms, larger normal stresses develop at the location of the wheel loads. These normal stresses are slightly larger than those at the diaphragm locations (Figs. I.7 and I.8).
- The occurrence of large normal stresses at the location of the wheel loads other than at the diaphragms seems to suggest that these peaks can occur at any point along the length of the joint because the moving wheel loads can occur at any point. Therefore, there is an equal chance that the peak normal stresses at the wheel loads will occur all along the joint length.
- A similar trend was observed for normal stresses at the bottom of the joint. However, the normal stresses at the bottom are compressive and therefore of less concern when high strength grout is used.

I.5.2 Normal Stresses – Load Case II

The load configuration in Load Case II as seen in Fig. I.4, is expected to cause compression at the top edge of the grouted longitudinal joint and tension at the bottom of the joint. In this load case, the joint is not at the axis of symmetry. Therefore, the joint will be subjected to both normal stresses and shear stresses.

As seen in Fig. I.7 and Fig. I.8, the normal tensile stresses on the joints at the bottom edge within the diaphragm width were much larger than the normal stresses obtained at locations remote from the diaphragms. This suggests that much of the out-of-plane moment is transferred between the box beams primarily through the diaphragms.

Similar trends can be observed for normal compressive stresses at the top of the joint as seen in Fig. I.8. However, the normal stresses at the top are mostly compressive in this load case and therefore of less concern.

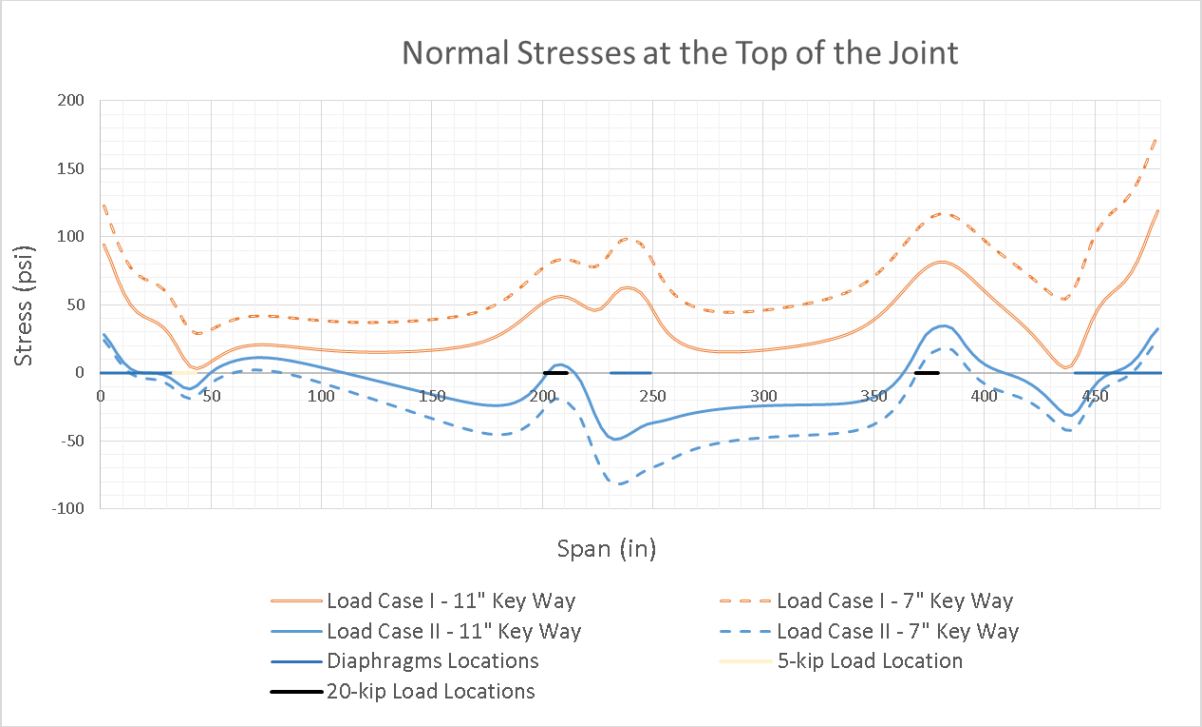

Fig. I.7 Normal Stresses along the Top Edge of the Keyway Joint of the 40-ft Bridge

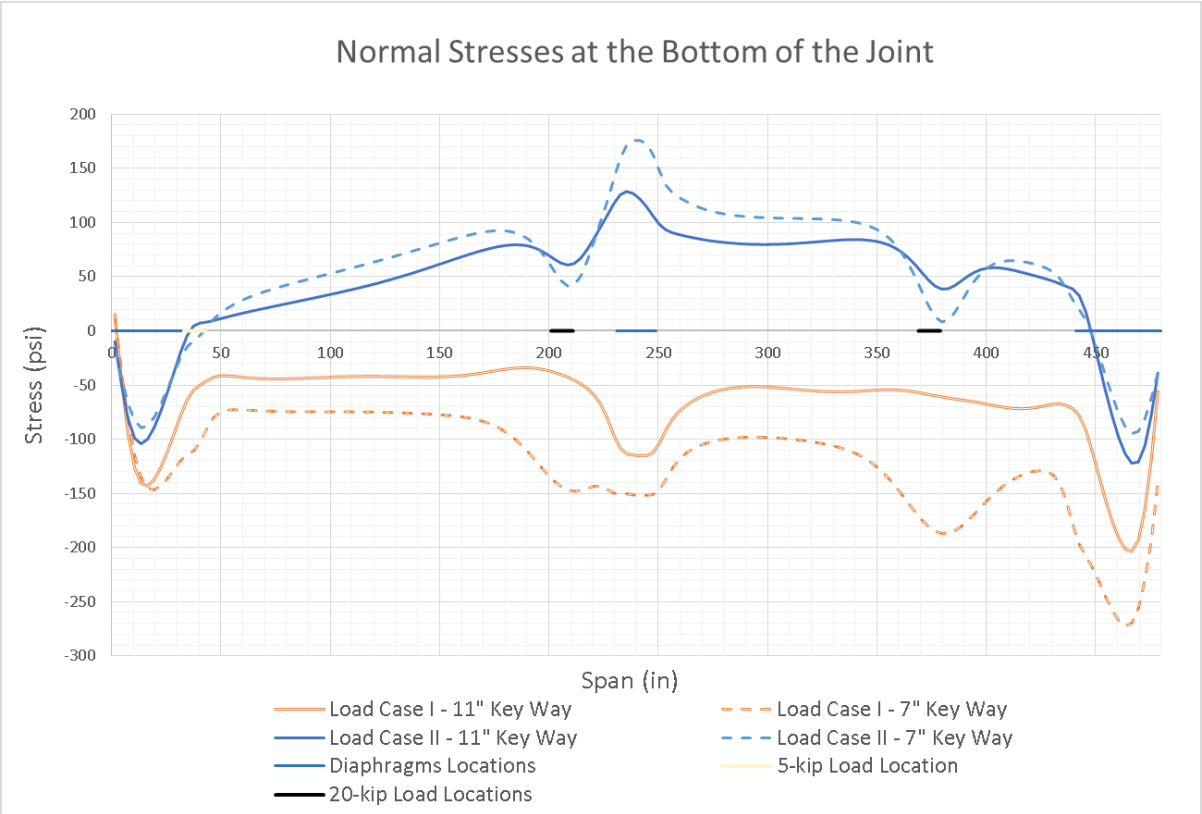

Fig. I.8 Normal Stresses along the Bottom Edge of the Keyway Joint of the 40-ft Bridge

I.5.3 Shear Stresses

Because of the symmetric nature of the geometry, stiffness, and loading for Load Case I, the shear stresses at the joint are expected to be zero. For Load Case II, the shear stresses are transferred to the adjacent box beams mostly at the wheel load locations. The diaphragms attract large shear forces in both Load Cases. Average shear strength for 7-in and 12-in keyway for Load Case I and Load Case II are shown in Fig. I.9.

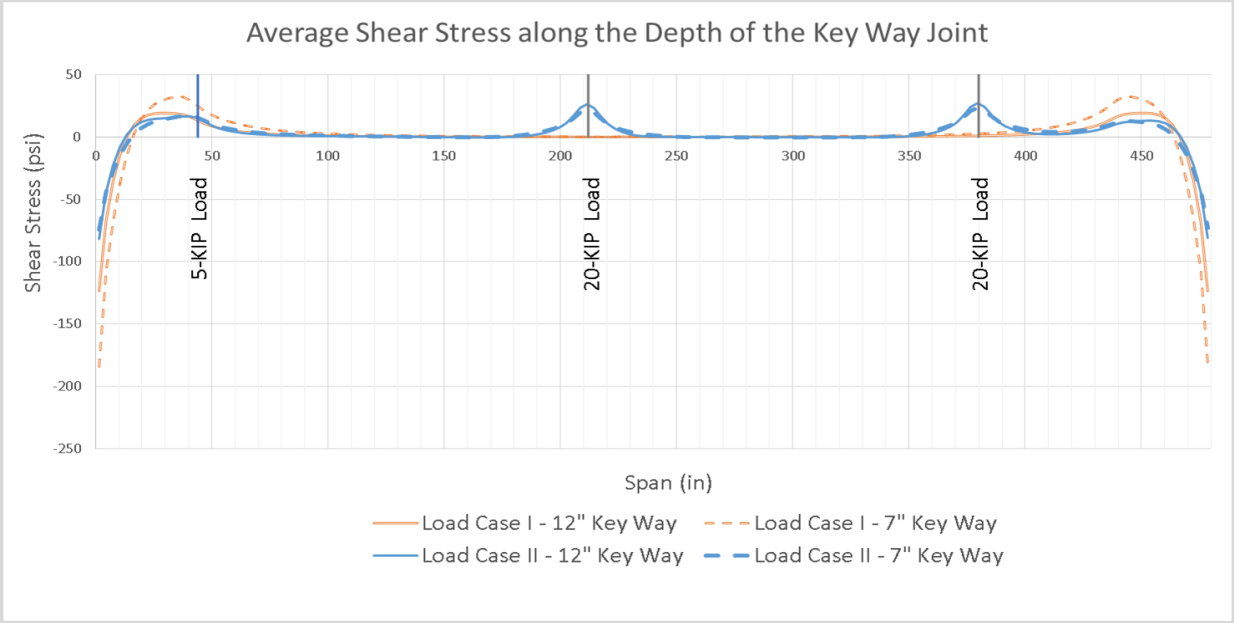

Fig. I.9 Shear Stresses along the Length of the Keyway Joint of the 40-ft Bridge

I.5.4 Keyway Stresses and Effect of Using Multiple Dowel Bars

A 26% reduction in the stresses due to truck loads occurred at the end diaphragms by providing pin supports for the box beams at the abutments, as shown in Fig. I.10.

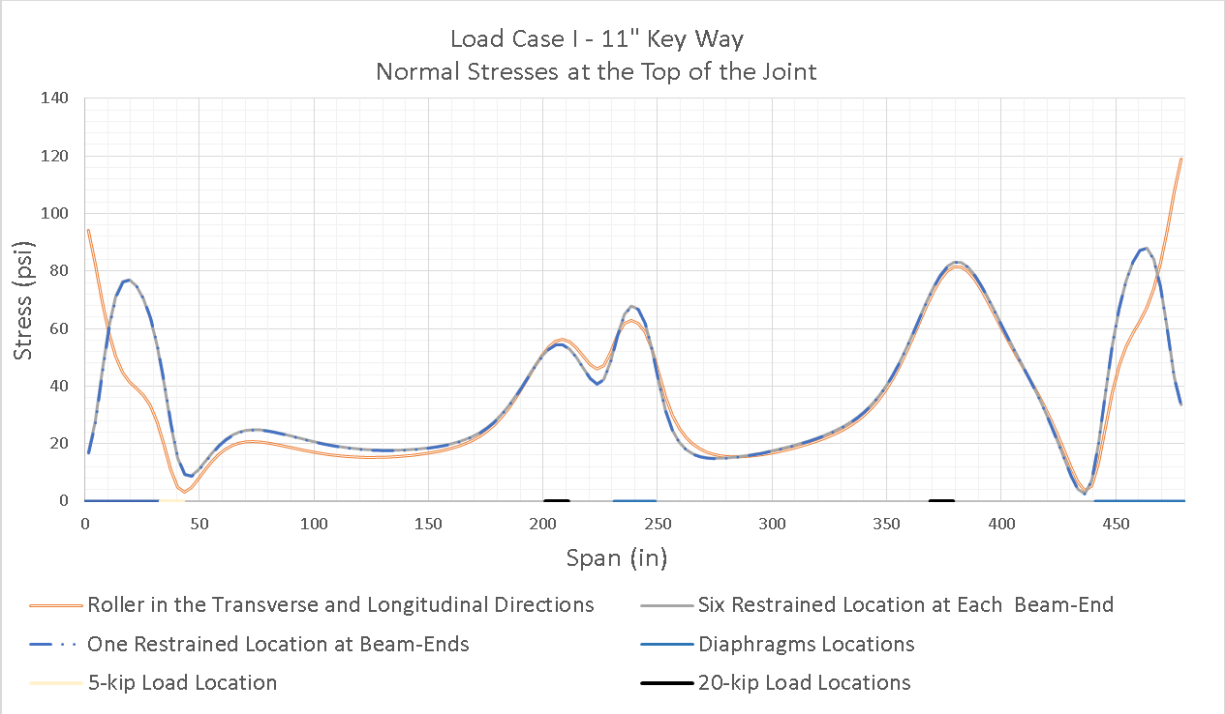

Fig. I.10 Effect of Dowel Bars at Supports

I.6 Design Approaches for Beam–Abutment Connection at Anchor Dowel Bar Locations

I.6.1 Introduction

The normal stresses can be reduced at the end supports by restraining the lateral movements. However, far from the supports along the span of the box beams, the end support conditions do not have any significant effects on the normal stresses for Load Case I with symmetric loading in transverse direction (Fig. I.10).

Figure I.11 demonstrates that when wheel loads are acting on one box beam and not on the beams adjacent to the loaded beam, the tendency of cracking at the longitudinal joints is increased due to any possible (i) differential vertical deflection and (ii) differential horizontal slip at the joint.

To prevent cracking, we need to reduce both vertical and horizontal differential movements. This can be done by restraining the horizontal movements of the end supports of each beam.

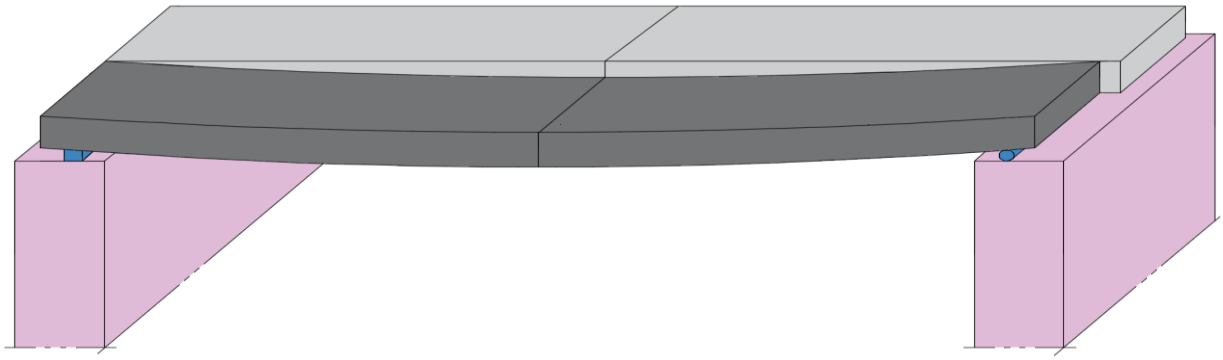

Fig. I.11 Effect of Dowel Bars at Supports

The structural performance of the box beam depends on the end support conditions that govern the load paths in the longitudinal and transverse directions. Two approaches were studied: i) Restrained beam-abutment connection, and ii) Beam-abutment connection with unrestrained condition in the longitudinal direction at anchor dowel bars.

I.6.2 Restrained Beam-Abutment Connection at Anchor Dowel Bars

Restraining the movements at the end supports will result in longitudinal reactions in the dowel bars that will be transferred to the abutments and subsequently to the foundations. Two approaches were used to model the beam-abutment joints to determine the dowel bar reactions: a) modeling only the beam with restrained ends considering very rigid abutment b) modeling the beam and the abutment considering the interaction between the beam and the abutment under the loading.

I.6.2.1 Modeling the Beam (without the abutment) with Restrained Ends Considering Unyielding Supports (Rigid Abutment)

The 3-D finite element analysis shows a large horizontal reaction at the dowel bars in the longitudinal direction. Such forces cannot be mobilized using a 1-in diameter dowel bar at each end. Dowel bars are expected to undergo large deformation to allow the longitudinal movements of the box beams. The box beams are seated on the abutments before the dowel bars are installed. Therefore, the self-weight of the box beams will not develop any stresses in the dowel bars.

To control the stresses near the supports, the joints between the box-beam ends and the end abutments need to be designed to act as a hinge to develop strength and to prevent the relative longitudinal movements between the adjacent box beams. The abutment design should account for the horizontal reaction transferred from the dowel bars. The required dowel bars need to be designed based on the stresses in each specific case depending on the span of the bridge. To reduce the amount of horizontal reaction on the abutments, the dowel bars may be designed to prevent the movements only at service load conditions while allowing the joint to crack under factored load conditions.

I.6.2.1.1 Required Dowel Bar Strength to Fully Restrain the Lateral and Longitudinal Movements for the Ultimate Load Condition

Table I.1 shows the loads used in the analysis. The self-weight of the box beams was excluded in the determination of the dowel bar reactions because these beams are seated before the dowel bars are installed.

Table I.1: Loads Used in the Analysis

HL-93	4 -16 -16	kips		3.5 inch Concrete Asphalt	41	psf
Lane Load	64	plf		Grout Material	17	plf
Future Wearing Coarse	60	psf				

The design horizontal shear force due to the superimposed dead load, lane load, future wearing coarse, and the wheel load of a HL-93 design truck without a dynamic load factor was determined using a 3-D model and were found to be V_u =192 kips. The design shear strength of a 1.5-in diameter dowel bar is

$$\phi V_n = \phi \times 0.6 \times f_y \times A_b = 0.75 \times 0.6 \times 60 \times 1.76 = 47.5 \text{ kip}$$

$$\text{Number of required dowel bars} = 192 \div 47.5 = 4.04 \approx 4 \text{ dowel bars}$$

I.6.2.1.2 Required Dowel Bar Design Strength to Restrain Only the Lateral and Longitudinal Relative Movements under Service Load Conditions

Under service (unfactored) superimposed dead loads, lane load, unfactored future wearing course, and HL-93 truck wheel loads without a dynamic load factor, the dowel bar reaction was determined using 3-D finite element analysis, and it was 118.4 kip. The number of dowel

bars required to prevent longitudinal movement based on the shear strength of a 1.5-in. dowel bar under service load condition is:

$$V_n = (2/3) \times 0.6 \times f_y \times A_b = (2/3) \times 0.6 \times 60 \text{ ksi} \times 1.768 \text{ in}^2 = 42.43 \text{ kips}$$

$$\text{Number of required dowel bars} = 118.4 \div 42.43 = 2.79 \approx 3 \text{ dowel bars}$$

The analysis shows that restraining the end supports in the horizontal direction reduces the vertical deflection at the midspan under service load by 30%. The dowel bar reactions, mid-span deflections, and end-beam movements for both load cases are shown in Table I.2.

Table I.2: Deflections, Beam-End Movements, and Dowel Bar Reactions for Different Load Conditions

Load	Model Description	Dowel Bars Restraint			Dowel Bars Horizontal Reaction		Mid Span Deflection (in)	Slip at the Abutment Location (in)
		Longitudinal X	Transverse Y	Vertical Z	X (kips)	Y (kips)		
Factored	11" Keyway Load Case I	Pin-Pin	Pin-Pin	Free	192.8	2.8	1.14	0.00
Factored		Pin-Roller	Pin-Roller	Free	1.09	0.02	1.64	0.18
Service		Pin-Pin	Pin-Pin	Free	118.4	1.68	0.70	0.00
Service		Pin-Roller	Pin-Roller	Free	0.66	0.01	1.00	0.11

The number of anchor dowel bars will depend on the forces determined for different bridge spans. The anchor dowel bars may be provided if cracking at the longitudinal joints is to be minimized without counting on the grout material to transfer shear stresses.

The above analysis demonstrates that the abutment design and details need to be modified significantly to resist the horizontal reactions transferred from the anchor dowel bars.

Thermal stresses should also be considered for dowel bar reactions, if the ends are considered to be restrained in the longitudinal direction.

I.6.2.2 Modeling the Beam and the Abutment

In this design method, the dowel bars are considered to be restrained longitudinally. Therefore the design needs to accommodate the transfer of the beam reactions that will be transferred to the abutments. The abutments need to then support the horizontal reactions developed at the beam ends due to these longitudinal reactions.

Fourteen piles will be needed in two rows below each abutment to support the reversible vertical and lateral loads as shown in Fig. I.12. In this analysis, the box-beams were modeled using frame elements, and abutments were modeled with 3D solid elements.

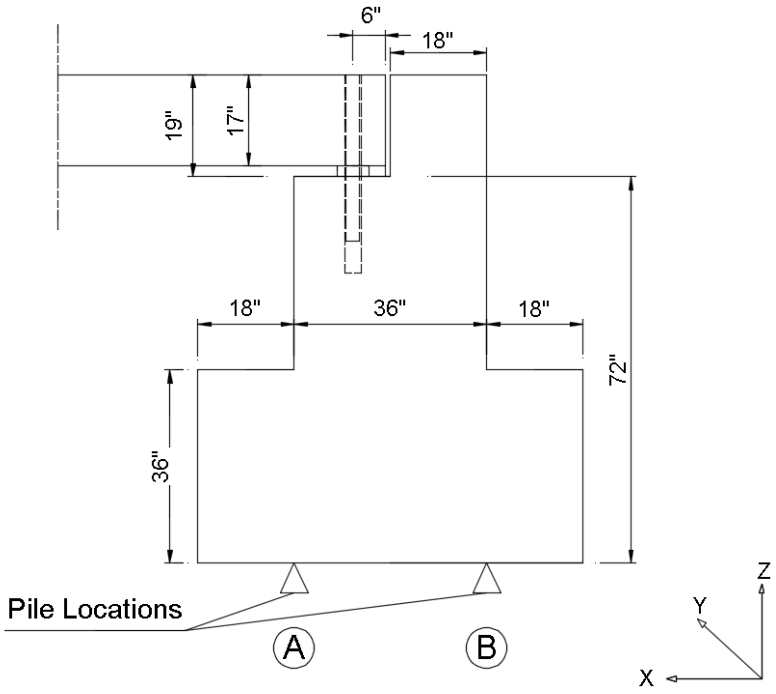

Fig. I.12 Pile locations and Beam-Abutment Connection

Table I.3 shows the loads used in the analysis. The self-weight was included in the determination of the pile reactions.

Table I.3: Loads Used in the Analyses

HL-93	4 -16 -16	kips
Lane Load	64	plf/ft-width
3.5 inch Concrete Asphalt	41	psf
Grout Material	17	plf
Self Weight of Bridge Deck and Abutment	150	lb/ft^3
Thermal stresses – Contraction	-54	°F
Thermal stresses – Expansion	+54	°F

I.6.2.2.1 Thermal Stresses Requirements Based on ODOT BDM 2007

The expansion length at the abutment is considered to be two-thirds (2/3) of the total change in length of the structure due to the total change in temperature.

Figure I.13 shows ODOT BDM 2007 requirement for the determination of the thermal effects for bridges.

S3.12.2 UNIFORM TEMPERATURE

To determine the thermal effects for all bridges, use the following ranges of temperatures:

A. Steel or Aluminum ..... -30° to 120°F
B. Concrete ..... 15° to 95°F
C. Wood ..... 0° to 75°F

Fig. I.13 Thermal Stresses Requirements Based on ODOT BDM 2007

Δ_t = 95°F - 15 °F = 80 °F

Design values Expansion $= \frac{2}{3} \times 80$ °F = 53.3 °F

Contraction $= \frac{2}{3} \times (-80$ °F) = -53.3 °F

Table I.4: Longitudinal Reactions at Anchor Dowel Bars under Restrained Conditions

	Pile A (kips)	Pile B (kips)
Contraction	25	25
Expansion	-51	-51

Table I.5: Pile Reactions

	Pile Group Along A (see Fig. I-12)		Pile Group Along B (see Fig. I-12)	
	Axial Load (kips)	Lateral Load (kips)	Axial Load (kips)	Lateral Load (kips)
All loads and thermal contraction	138	12	-38	12
All loads and thermal expansion	-42	-25	142	-26

I.6.3 Beam-Abutment Connection with Horizontal Unrestrained Condition at Anchor Dowel Bars

In this design method, beam-abutment connections were modeled to allow free horizontal relative movements at the beam ends above the abutment to eliminate the horizontal reactions. Dowel bars were assumed to be provided for overall stability of the box beams and not for providing structural strength.

Table I.6: Loads Used in the Analysis

HL-93	4 -16 -16	kips
Lane Load	64	plf/ft-width
3.5 inch Concrete Asphalt	41	psf
Grout Material	17	plf

The self-weight was excluded in the determination of the longitudinal joint stresses because the beam is seated before the joint is grouted.

The maximum tensile normal stress at the top of the joint is 120 psi (from Fig. I.10), and the maximum shear stress occurs at the location with 180 psi (from Fig. I.9). The resultant stresses can be calculated as follows:

$$\text{Resultant Stress} = \sqrt{Normal\ Stress^2 + Shear\ Stress^2} = \sqrt{120^2 + 180^2} = 216\ psi.$$

I.7 Summary and Conclusion

Substantial changes to the end abutment details are needed if the anchor dowel bar details at the beam ends are to be changed to prevent longitudinal relative movement between the ends of the box beams and the end abutments. These changes will require substantial changes to the abutment details and pile details (i.e, the number of piles and the layout of piles).

All factors considered, it is preferred to retain the original end anchor dowel details so that substantial (and possibly, costly) changes are not included in the abutment and pile details. It is recommended that only the keyway geometry and the grout material type be changed, without any changes to the end anchor dowel bar details or the abutment and pile details.

I.8 Recommendation for Implementation

From the work completed in this research, three items have potential for implementation: (i) revised keyway geometry, (ii) type of grout material, and (iii) construction specifications.

I.8.1 Keyway Geometry

A new keyway geometry as shown in Fig. I.14 that was successfully demonstrated by structural load tests (presented in earlier appendices) to increase the shear transfer strength of grouted joints is recommended with wide-full-depth keyway joint.

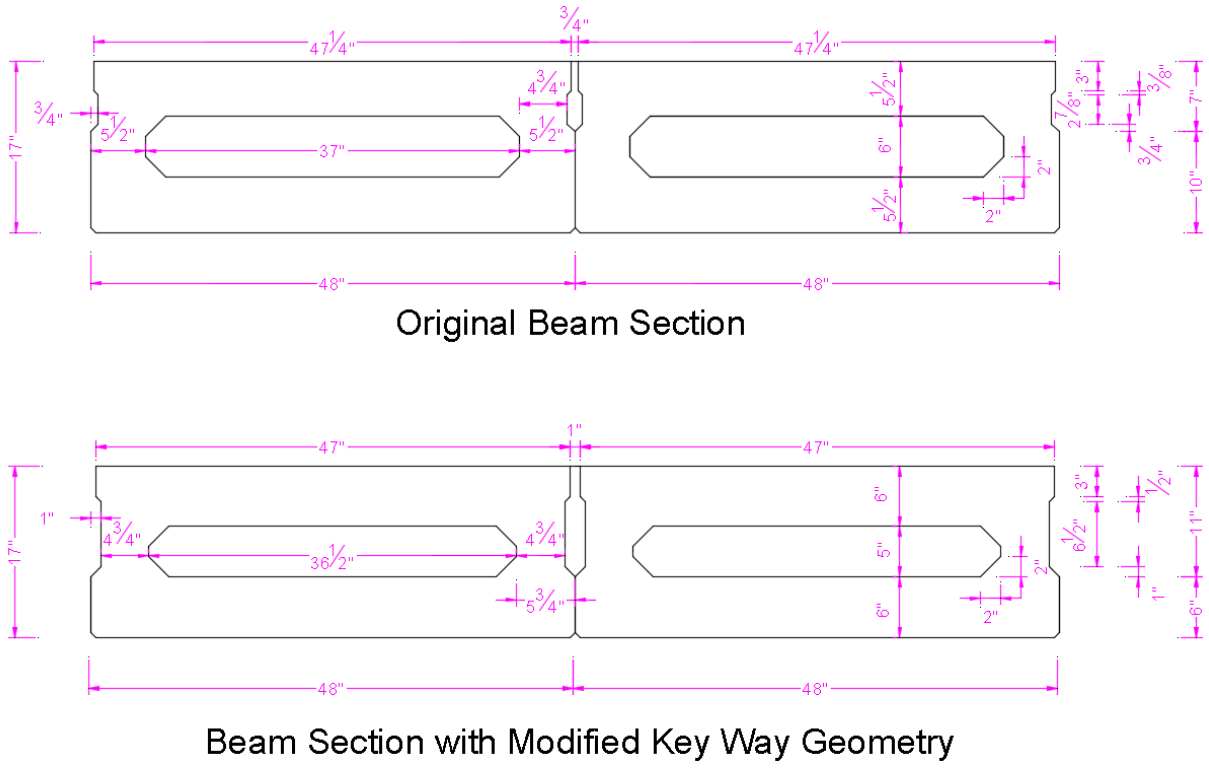

Fig. I.14 Original Keyway Geometry (Top) Modified Geometry (Bottom) for B17-48

I.8.2 Grout Material

The cement-based high-strength concrete grout (9,800 psi) was developed and tested in this study. The test results demonstrated that the grout developed in this study was adequate; therefore, the high-strength concrete grout is recommended for implementation. The recommended grout is made using traditional concrete with maximum #8 coarse aggregate and Type I Portland cement. Compaction of the grout is achieved with a vibrator. The opening at the top of the keyway needs to be at least one inch to allow for vibration. The keyway geometry shown in Fig. I.14 is recommended with high-strength concrete grout.

High-strength concrete grout needs to be flowable with a compressive strength of over 10,000 psi. The mix proportions given in Table I.7 were found to be satisfactory for the high-strength grouts in a laboratory environment. However, other mixes with better optimized aggregate gradation and supplementary cementitous materials may also be used to improve the mix performance and reduce the cement content while maintaining similar minimum strength and performance. Typical mix proportions for high-strength concrete grout are shown in Table I.7.

Table I.7: Mix Proportions for High-Strength Concrete Grout with #8 Aggregate

HSC Grout	Cement	Sand	Aggregates	Water W/C = 0.35	S.P.
Mix proportion by weight	1	1.32	1.45	0.35	0.03
lb/ft^3	41	54	59	14.5	1.7
lb/yd^3	1100	1450	1596	385	46

S.P. = super-plasticizer (a high-range water reducer)

I.8.3 Construction Specifications

The following construction specifications are recommended:

1. Keyways should be grouted after the erection of box beams. Generally, plastic rope or jute is installed at the bottom of the keyway to block the grout from flowing out. Utmost care shall be taken to seal the bottom edge of the keyway to prevent leakage of wet grout during and after the grouting process.
2. Ensure that the installation is done properly. Box beam keys have failed because of improper jute installation. However, suitable foam sealant may be used to seal the keyway and make it watertight before the grouting operation begins.
3. The fabricator shall sandblast the keyway surface within four days of shipment to the project site as specified in ODOT standard drawings PSBD-2-07. The sandblasting shall yield a visual appearance and texture equivalent to or rougher than 100 grit sandpaper over the entire keyway surface. When stains are visible prior to sandblasting the concrete, use a degreaser to ensure removal of grease, oils and other similar contaminants. The degreaser shall be water soluble so it can be removed before the blasting begins. Before mortaring, remove all dirt, dust, grease, oil and other foreign materials from surfaces using a high pressure wash of at least 1,000 psi at a delivery rate of 4 gal/min.
4. Grout needs to meet the material requirements of the Office of Structural Engineering's standard box beam drawings. Additional requirements for high-performance grout with a high-strength concrete using #8 maximum size aggregate needs to be used with the following specifications:
    - Minimum compressive strength of 10,000 psi needs to be achieved before allowing any construction equipment on the deck.
    - The grout shall be designed to include well graded #8 coarse aggregate suitable for high-strength concrete applications.
    - The top surface of the grouted joints shall be cured with approved curing compound that is to be applied on the surface after one hour of grouting.
    - The grout shall have workability that is adequate to fill the keyway.
    - A suitable needle vibrator shall be used to consolidate the grout.

5. The manufacturer's mixing instructions should be followed to ensure that the grout is properly mixed, vibrated into the joints, cured, and sampled for testing.
6. Grouting shall not be performed if construction activities are ongoing. The grout can be cracked by the vibration and deflection movements and make the keyways worthless.
7. Traffic including construction traffic on the deck shall not be permitted before the grout has obtained the required strength of 10,000 psi. This specification must be strictly followed.

I.9 Design Calculations for B17-48 Box Beams

Bridge HUR-CR0048-0055 (SFN 3930001) over the East branch of the Huron River in Huron County, OH was expected in Oct. 2015 to be available for implementation. However, the bidding and construction schedules did not work for the implementation. Therefore, a bridge over Cedar Fork (RIC-TR037-0.21), which is a tributary of the Clear Fork river on Shauck Road in Richland County, Ohio, was selected in Nov. 2015 for potential implementation. The revised details for implementation for this bridge were developed and are presented in Table I.8 and Fig. I.14. The span for this RIC-TR037-0.21 bridge was 40-ft of span and a 28-ft width. The recommended modifications for the keyway geometry will maintain the needed structural strength of the bridge for shear and moment strengths under ultimate load conditions. The suggested design will limit the prestressing stresses under service load conditions to within the allowable stress limits specified in the relevant design codes.

I.10 Design Calculation for B42-48 Box Beams

While bridge HUR-CR0048-0055 (SFN 3930001) in Huron County was not implemented, revised details were developed before it was decided not to proceed with the implementation for this bridge. The span of the bridge was 103 ft and the width was 24 ft. The modifications for the keyway geometry are shown in Fig. I.15, and the revised geometry will maintain the required strength under the design loads for the bridge in shear and moment at ultimate load condition. They will also limit stresses to within the allowable stress limits specified in the relevant design codes under service load conditions. However further specific analyses are needed before implementing these details for bridges with spans as large as 103 ft.

I.11 Revised Details for the Implementation Bridge

The bridge where the research results were actually implemented was a bridge (RIC-CR184-2.17, SFN 7030013) over Kuhn Road in Shelby, OH. The details of the recommendations and revised design are presented in Appendix J.

Table I.8: Design Summary for Original and Modified Geometries for B17-48

Properties for box beam sections	Original Beam	Modified Beam
Area (in^2)	594.20	624
Distance from the centriod to bottom fiber Y_b (in)	8.40	8.43
Moment of inertia (in^4)	18,825	19,022
Distance from the centriod to top fiber C_t (in)	8.56	8.57
Total weight of one box beam including diaphragms (kips)	26.5	27.4
Total length (ft)	40	40
Span between dowel bars(ft)	39	39
Initial prestressing force per strand (lb)	33,818	33,818
Final prestressing force per strand (lb)	26,378	26,378
Loads considered: ▪ Self-weight of the beam ▪ 3.5" Asphalt concrete overlay ▪ Weight of the keyway grout ▪ Moving load from HL-93 including lane load		
Service loads stresses		
Initial stresses at the top fiber at mid-span (psi)	115 (tensile)	131 (tensile)
Initial stresses at the bottom fiber at mid-span (psi)	-2,149 (compressive)	-2,065 (compressive)
Final stresses at the top fiber at mid-span (psi)	-2,216 (compressive)	-2,198 (compressive)
Final stresses at the bottom fiber at mid-span (psi)	599 (tensile)	615 (tensile)
Design flexure strength		
$ØM_n$=	809.6 ft-kips	809.0 ft-kips
Design shear strength including the contribution of the shear reinforcement (was found to be adequate)		
$ØV_n$=	94.8 kips	92.4 kips
Deflection and camber		
Initial camber (in)	0.99	0.96
Maximum deflection under service loads (in)	0.48	0.64

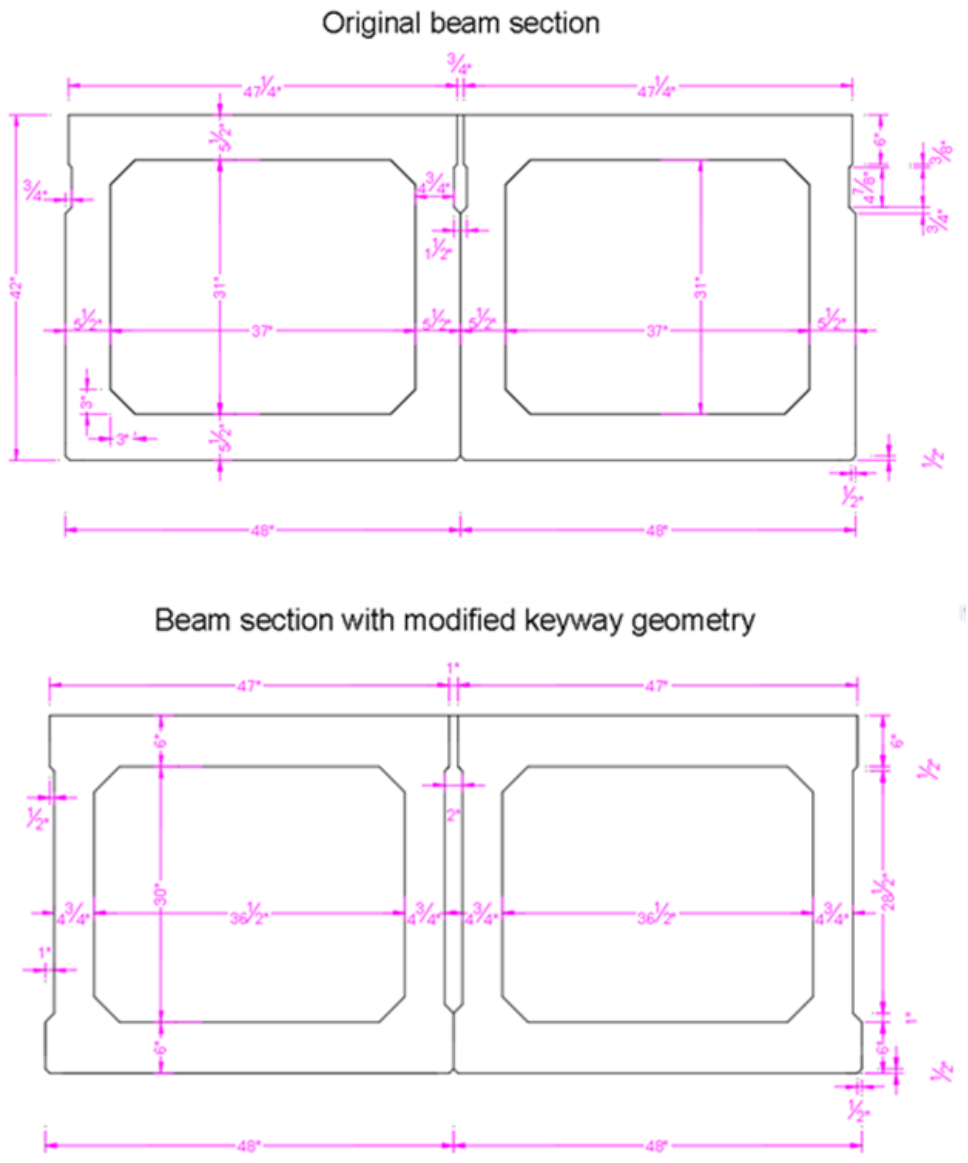

Fig. I.15 Original Geometry (Top) and Modified Geometry (Bottom) for B42-48 Beam Section

Table I.9: Design Summary for Original and Modified Geometries for B42-48

Properties for box beam sections	Original Beam	Modified Beam
Area (in^2)	873.95	874
Distance from the centriod to bottom fiber Y_b (in)	20.8	20.87
Moment of inertia (in^4)	205,435	211,453
Distance from the centriod to top fiber C_t (in)	21.20	21.13
Total weight of one box beam including diaphragms (kips)	106.7	106.1
Total length (ft)	103	103
Span between dowel bars(ft)	102	102
Initial prestressing force per strand (lb)	33,818	33,818
Final prestressing force per strand (lb)	26,378	26,378
Loads considered: ▪ Self-weight of the beam ▪ 3.5" Asphalt concrete overlay ▪ Weight of the keyway grout ▪ Moving load from HL-93 including lane load		
Service loads stresses		
Initial stresses at the top fiber at mid-span (psi)	-686 (compressive)	-710 (compressive)
Initial stresses at the bottom fiber at mid-span (psi)	-2,240 (compressive)	-2,221 (compressive)
Final stresses at the top fiber at mid-span (psi)	-3,029 (compressive)	-3,043 (compressive)
Final stresses at the bottom fiber at mid-span (psi)	699 (tensile)	726 (tensile)
Design flexure strength		
$ØM_n$=	4,525 ft-kips	4,545 ft-kips
Design shear strength including the contribution of the shear reinforcement (was found to be adequate)		
$ØV_n$=	280 kips	265 kips
Deflection and camber		
Initial camber (in)	2.3	2.2
Maximum deflection under service loads (in)	2.7	2.9

Waterproofing Details of Connections for Adjacent Precast Concrete Box-Beam Bridges

Appendix J: Implementation of Research Results

Prepared by:

Anil Patnaik, PhD

Prepared for:

The Ohio Department of Transportation
Office of Statewide Planning & Research

State Job Number 134847
07/25/2018

U.S. Department of Transportation
Federal Highway Administration

Waterproofing Details of Connections for Adjacent Precast Concrete Box-Beam Bridges

Appendix J: Implementation of Research Results

Prepared by:

Dr. Anil Patnaik (PI)
Professor, Department of Civil Engineering
The University of Akron, Akron, OH 44325-3905
Phone: 330-972-5226 Email: Patnaik@uakron.edu

July 2018

Prepared in cooperation with the Ohio Department of Transportation,
Ohio's Research Initiative for Locals, and the U.S. Department of Transportation, Federal Highway Administration

TABLE OF CONTENTS

LIST OF FIGURES

LIST OF TABLES

APPENDIX J: IMPLEMENTATION OF RESEARCH RESULTS

In this appendix, details of the successful implementation of the research results of the project are presented. A bridge (RIC-CR184-2.17, SFN 7030013) over Kuhn Road in Shelby, Ohio, was selected for the implementation. This bridge is 55 ft. long with seven B21-48 box beams. The suggested recommendations and the revised key way details including the slightly modified grout specifications used in the project are presented in this appendix.

J.1 Basis for the Implementation Recommendations and Design Details

The basis for the implementation recommendations and the design implemented in this project were given in Appendix I. Many relevant factors were studied in this project to evaluate their influence on the effectiveness of waterproofing for adjacent box beam bridges. The details of this evaluation have been documented in other appendices of the report. It was decided that the recommended implementation be limited to simple changes to the key way geometry and the use of high strength grout materials in place of the currently used ODOT-approved grout. Therefore, the ODOT specifications relevant to the grouting and waterproofing membrane were marginally modified in order to be consistent with the suggested changes.

J.2 Recommended Modified Design and Construction Specifications

The recommended modified design and construction specifications for RIC-CR184-2.17 are attached in full at the end of this appendix. Engineers from Poggemeyer Design Group developed the structural design and drawings of the precast box beams based on the researchers' recommendations, and they submitted the revised drawings for ODOT approval. A copy of the approved drawing is attached at the end of this appendix. The primary structural changes to the ODOT standard B21-48 box beam section are (i) changes to the key way geometry as shown in Fig. J.1 and (ii) an increase in the number of prestressing strands from 24 to 28. Of the two options suggested for the revised box beam section, the consultant selected the second option, which has a side wall thickness of 5½ inch (Fig. J.1).

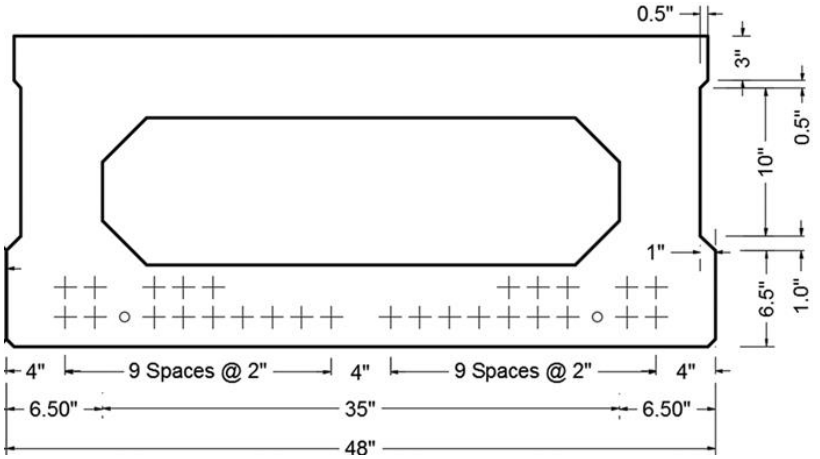

Fig. J.1 Revised Cross Section of B21-48 Box Beam that was Used in the Project

J.3 Casting of the Box Beams

The box beams for the bridge were cast by Prestress Service Industries Inc. in Mt. Vernon, Ohio on Dec. 20, 2017. ODOT engineers and the PI were at the precasting plant to verify that the specified key way geometry is provided, as recommended in the implementation report. While ODOT requires steel forms for box beams, as an exception, the revised profile for the key ways was allowed to be achieved for this project using plywood. Some photos depicting the casting and the key way geometry are shown in Fig. J.2.

Fig. J.2 Key Way Profile Using Plywood (Left); Styrofoam Block for Creating a Void (Right)

J.4 Trial Mix and Placement of Grout

The contractor for the bridge had some concerns regarding the flowability of concrete grout made with the mix proportions suggested in the implementation recommendations. Therefore, they made trial mixes with the suggested proportions on April 24, 2018, i.e., a day before the grouting of the actual bridge. The trial concrete was placed in the annular space between two precast concrete blocks arranged side by side with an opening of approximately 1 inch (Fig. J.3). The consistency of the concrete grout for the trial mix seemed adequate for placing through the narrow opening at the top that was created by the two precast concrete blocks. Figure J.3 shows that the grout flowed freely within the 1-inch wide joint before rapidly reaching the bottom of the joint and spreading over a wide area surrounding the opening. If the joint was contained by formwork, the grout would have self-consolidated as intended. One important detail in the process is to wet the joint surfaces with water before placing the grout.

Fig. J.3 Trial Grout – Note the Spread of the Grout (Left); the Grout Consistency (Right)

J.5 Grouting of the Longitudinal Joints

Box beams were installed and tied together at the bridge site during the week of April 23, 2018. The bridge top surface after the installation of the beam is shown in Fig J.4. Some of the beams adjacent to each other had their top edge at different levels, varying by about 1 inch. Sandblasting of the key way surfaces of beams seemed to be adequate.

Fig. J.4 Joint Opening on Top Surface (Left); Key way Surface and Level Difference (Right)

Because of wider openings, the bottoms of the key ways were well sealed with jute rope (Fig. J.5). A trough was used to place the concrete through the key way opening, and this seemed to work well (Fig. J.6). It was verified that there was no leaking of the grout from the bottom of the joints between the beams. The contractor intended to spray a curing compound on the exposed surface of the key way grout later in the afternoon on the day of grouting.

Fig. J.5 Jute Rope Used to Seal the Bottom of the Key Way

Fig. J.6 Grout Placement Through the Opening of the Key Way

The grout flowed freely (Fig. J.7) through the recess around the tie bars and filled the key way joints adjacent to the one being grouted when grouting any given key way. This is because the key way is deeper than the one currently used in ODOT practice. The tie rods and the openings (recesses) for the tie rods were located within the depth of the key way. The openings for the tie rods provided good access from the key way to the inside of the openings except where plate washers were provided at the ends of tie rods. The interconnection of the key ways and the tie rod recesses must have resulted in completely surrounding the tie rods with grout, which a preferable outcome. As a result, relative vertical movement between the adjacent box beams at the tie rod locations is prevented after the setting of the grout around the tie rods.

Fig. J.7 Free Flow of Grout within a Key Way Joint

J.6 Compressive Strength of the Grout Used in the Key Ways

Many 4”×8” and 3”×6” cylinders were made, and the strengths obtained from testing of these cylinders are provided in Table J.1. The 28-day compressive strength determined from the testing of 3”×6” cylinders was about 10,500 psi, and the strength obtained from 4”×8” cylinders was about 9,300 psi.

J.7 Installation of the Waterproofing Membrane

The waterproofing membrane was installed on the bridge deck a week after the grouting. An inspection of the membrane on May 8, 2018, prior to the placement of the asphalt concrete, revealed that the underside of the membrane adhered well to the top surface of the deck. Any difference between the levels of adjacent beams was made up by filling the underside of the membrane at locations along the longitudinal joints (Figs. J.8 and J.9).

Table J.1: Compressive Strengths of the Grout Material (Provided by ODOT)

10, 000 psi grout
Date made: April 25, 2018 at project 17-3006 (Kuhn Road box beam bridge)

Test dates:
April 30, 2018 (5 days)
May 2, 2018 (7 days)
May 9, 2018 (14 days)
May 23, 2018 (28 days)

5-day field cured 4X8 cylinders	8,045 psi	7,440 psi		Average = 7,743 psi
7-day field cured 4X8 cylinders	8,305 psi	7,990 psi		Average = 8,148 psi
7-day lab cured 4x8 cylinders	8,140 psi	8,365 psi	8,240 psi	Average = 8,248 psi
7-day field cured 3X6 cylinders	8,698 psi	8,859 psi		Average = 8,779 psi
7-day lab cured 3X6 cylinders	8,455 psi	8,554 psi		Average = 8,505 psi
14-day lab cured 4x8 cylinders	8,993 psi	9,140 psi		Average = 9067 psi
28-day lab cured 4x8 cylinders	9,140 psi	9,480 psi		Average = 9,310 psi
28- day lab cured 3x6 cylinders	10,545 psi	10, 488 psi		Average = 10,517 psi

J.8 Inspections of the Bridge After Being Open to Traffic

The bridge was open to traffic by the time the next inspection was done on May 19, 2018. The top surface of the asphalt concrete of the bridge after it was open to traffic is shown in Fig. J.10. The bridge was again inspected in October 2018, just prior to the submission of the final report.

J.9 Summary

The research findings from this project were successfully implemented in a concrete bridge (RIC-CR184-2.17, SFN 7030013) over Kuhn Road in Shelby, Ohio. No visible cracks were detected on the surface of the bridge at the longitudinal joints between the adjacent box beams of the bridge six months after the bridge construction. The outcome of the implementation of the modified specifications and key way details is considered a success.

Fig. J.8 Membrane Over Adjacent Beams That were not Level

Fig. J.9 Deck Top Surface after Membrane Installation

Fig. J.10 Bridge Surface After Being Opened to Traffic